THE EFFECTS OF VARIOUS PROCESSING CONDITIONS ON THE PROPERTIES OF HYDROXYAPATITE

TEH YEE CHING

FACULTY OF ENGINEERING
UNIVERSITY OF MALAYA
KUALA LUMPUR

2017

THE EFFECTS OF VARIOUS PROCESSING CONDITIONS ON THE PROPERTIES OF HYDROXYAPATITE

TEH YEE CHING

THESIS SUBMITTED IN FULFILMENT OF THE REQUIREMENTS FOR THE DEGREE OF DOCTOR OF PHILOSOPHY

FACULTY OF ENGINEERING
UNIVERSITY OF MALAYA
KUALA LUMPUR

2017

UNIVERSITY OF MALAYA

ORIGINAL LITERARY WORK DECLARATION

Name of Candidate: **TEH YEE CHING** (I.C/Passport No: [redacted])

Registration/Matric No: **KHA 120096**

Name of Degree: **DOCTOR OF PHILOSOPHY**

Title of Project Paper/Research Report/Dissertation/Thesis ("this Work"):

THE EFFECTS OF VARIOUS PROCESSING CONDITIONS ON THE PROPERTIES OF HYDROXYAPATITE

Field of Study: **MECHANICAL ENGINEERING**

I do solemnly and sincerely declare that:

(1) I am the sole author/writer of this Work;
(2) This Work is original;
(3) Any use of any work in which copyright exists was done by way of fair dealing and for permitted purposes and any excerpt or extract from, or reference to or reproduction of any copyright work has been disclosed expressly and sufficiently and the title of the Work and its authorship have been acknowledged in this Work;
(4) I do not have any actual knowledge nor do I ought reasonably to know that the making of this work constitutes an infringement of any copyright work;
(5) I hereby assign all and every rights in the copyright to this Work to the University of Malaya ("UM"), who henceforth shall be owner of the copyright in this Work and that any reproduction or use in any form or by any means whatsoever is prohibited without the written consent of UM having been first had and obtained;
(6) I am fully aware that if in the course of making this Work I have infringed any copyright whether intentionally or otherwise, I may be subject to legal action or any other action as may be determined by UM.

Candidate's Signature Date:

Subscribed and solemnly declared before,

Witness's Signature Date:

Name:

Designation:

ABSTRACT

The sintering behavior of hydroxyapatite (HA) powder produced by wet chemical precipitation method via three different drying methods, i.e. freeze drying (FD-HA), microwave drying (MD-HA) and oven drying (OD-HA) were investigated over the temperature range of 1050 ℃ to 1350 ℃. The characterization of HA was assessed in terms of powder morphology, powder element analysis, phase stability, bulk density, microstructure, grain size, Vickers hardness and fracture toughness. Based on these results, the HA powder that demonstrated the optimum properties was chosen for further studies to investigate the effects of microwave sintering on the sinterability of the chosen HA. The microwave sintering carried out in temperature ranging from 950 ℃ to 1250 ℃. The sinterability of microwave sintered HA was compared to that of conventional pressureless sintered HA. Subsequently, the effects of adding zinc oxide (ZnO) ranging from 0.1 wt% to 1.0 wt% on the sinterability of HA when sintered between 1100 ℃ to 1300 ℃ via conventional pressureless sintering were also evaluated.

In the present study, the use of microwave drying accelerates the manufacturing of HA powder as only 15 minutes were required to dry the HA powder (MD-HA) while at least 16 hours and 36 hours drying time were required for conventional oven drying (OD-HA) and freeze drying (FD-HA), respectively. It has been revealed that MD-HA possess overall better sinterability and mechanical properties than OD-HA and FD-HA. The optimum sintering temperature for the synthesized MD-HA was 1200 ℃ with the following properties being recorded: relative density of 97.5%, Vickers hardness of 5.04 GPa and fracture toughness of 1.15 $MPam^{1/2}$. Besides, decomposition of MD-HA phase upon sintering was not observed in the present work but small amount of tricalcium phosphate was observed in OD-HA when sintered at 1350 ℃.

The current study also revealed that microwave sintering played an important role in enhancing the mechanical properties of HA matrix particularly at low sintering temperature. HA with high fracture toughness value of ~1.85 $MPam^{1/2}$ was produced at 1050 ℃ via microwave sintering. In addition, the addition of 0.5 wt% of ZnO was found to be beneficial in improving the fracture toughness of HA powder. The results indicated that that the resulting 0.5 wt% ZnO-doped HA sintered body exhibited an increased toughness of to 1.37 $MPam^{1/2}$ and hardness value to 5.63 GPa when compared to the undoped body (1.16 $MPam^{1/2}$ for fracture toughness and 4.75 GPa for hardness) at 1150 ℃ via conventional sintering.

The main advantageous of this research is the economical and rapid production of HA that exhibited enhanced sinterability at low temperatures that is suitable for the production of biomedical devices without compromising the phase stability and biocompatibility nature of the HA.

Abstrak

Sifat persinteran HA dihasilkan daripada pemendakan kimia basah melalui tiga kaedah yang berbeza iaitu pegeringan melalui pembekuan (FD-HA), pergeringan melalui gelombang microwave (MD-HA) dan pegeringan melalui ketuhar (OD-HA) telah disiasat dalam lingkugan suhu persinteran 1050 ℃ hingga 1350 ℃. Pencirian HA dinilai dari segi morfologi serbuk, analisis unsur serbuk, kestabilan fasa, ketumpatan pukal, mikrostruktur, saiz butiran, kekerasan Vickers dan keliatan patah.

Berdasarkan keputusan ini, serbuk HA yang menunjukkan ciri-ciri yang terbaik akan dipilih untuk melanjutkan pelajaran untuk menyiasatkan kesan persinteran gelombang mikrowave atas sifat persinteran HA. Suhu ketuhar gelombang mikro persinteran adalah dari 950 ℃ hingga 1250 ℃. Sifat persinteran HA melalui gelombang microwave dibandingkan dengan HA yang disinterkan melalui pensinteran konvensional tanpa tekanan. Selepas itu, kesan penambahan ZnO antara 0.1 % berat hingga 1 % berat atas sifat persinteran HA melalui persinteran konvensional dan ketuhar gelombang mikro dalam lingkungan suhu 1100 ℃ hingga 1300 ℃ telah dikaji.

Dalam kajian ini, penggunaan pengeringan ketuhar gelombang mikro mempercepatkan pembuatan serbuk HA kerana hanya 15 minit dikehendaki untuk mengeringkan serbuk HA manakala sekurang-kurangnya 16 jam masa pengeringan dikehendaki untuk pengeringan ketuhar konvensional dan 36 jam untuk pengeringan pembekuan. Kajian ini membuktikan MD-HA telah didapati mempunyai sifat persinteran dan sifat-sifat mekanikal yang lebih baik daripada OD-HA dan FD-HA. Suhu pensinteran optimum untuk MD-HA disinter adalah 1200 ℃ dengan sifat-sifat berikut direkodkan: ketumpatan pukal relatif 97.5% , Vickers kekerasan 5.04 GPa dan patah keliatan 1.15 $MPam^{1/2}$. Selain itu, tiada kesan decomposition fasa MD-HA bila disinterkan tetapi sedikit trikalsium fosfat dikesan dalam OD-HA apabila disinter pada

1350 ℃. Kajian ini juga mendedahkan bahawa pensinteran microwave memainkan peranan penting dalam meningkatkan sifat-sifat mekanik matriks HA pada suhu pensinteran rendah. HA dengan nilai keliatan patah yang tinggi ~ 1.85 $MPam^{1/2}$ telah dihasilkan pada suhu 1050 ℃ melalui persinteran microwave. Di samping itu,penambahan 0.5 wt% ZnO membawa kebaikan dalam meningkatkan keliatan pepatahan HA. Keputusan menunjukkan bahawa 0.5 wt% ZnO dop HA menunjukkan perningkatan dalam keliatan pepatahan ke 1.37 $MPam^{1/2}$ dan kekerasan ke 5.63 GPa apabila berbanding kepada HA tanpa ZnO (1.16 $MPam^{1/2}$ keliatan pepatahan dan 4.75 GPa kekerasan) pada 1150 ℃ melalui persinteran konvensional.

Faedah utama kajian ini adalah menghasilkan HA yang dengan cara yang murah dan cepat selain mempamerkan sifat persinteran yang tinggi pada suhu persinteran yang rendah dan sesuai sebagai peranti bioperubatan tanpa mengorbankan kestabilan fasa dan bioserasi HA.

ACKNOWLEDGEMENTS

I would like to express my sincere appreciation to the following individuals that have constantly guided and supported me throughout the course of my PhD research:

- My project supervisor, Prof. Ir. Dr. Ramesh Singh for his vital encouragement, support, knowledge transfer and constructive suggestions throughout the research and the thesis writing.
- My Co-supervisor, Assoc. Prof. Dr. Tan Chou Yong for his assistance, continuous guidance, advices and correction throughout the course of this research and the thesis writing.
- The Surface Engineering, Advanced Material Processing Laboratories and High Impact Research (HIR) of University of Malaya for providing facilities and instrument support.
- My colleagues and lab instructors at University of Malaya for their immeasurable guidance and advices.
- Geran Penyelidikan Universiti Malaya (UMRG) Grant No. RP011B-13AET, Fundamental Research and Grant Scheme (FRGS) Grant No. FP029-2013A and Postgraduate Research Grant (PPP) Grant No. PG080-2013A for the financial support.

Lastly, I would like to thank my family members and friends for their unconditional support, understanding, patience and encouragement.

TABLE OF CONTENTS

LIST OF FIGURES

LIST OF TABLES

LIST OF SYMBOLS AND ABBREVIATIONS

ρ	:	Bulk Density
α-TCP	:	Alpha-Tricalcium Phosphate
Al_2O_3	:	Alumina
BET	:	Brunauer-Emmett-Teller
C_4P	:	Tetracalcium Phosphate
$Ca(OH)_2$	:	Calcium Hydroxide
Ca/P	:	Calcium to Phosphorous Ratio
$Ca_{10}(PO_4)_6(OH)_2$	:	Calcium Phosphate Tribasic / Hydroxyapatite
$Ca_3(PO_4)_2$	:	β-tricalcium Phosphate
$CaCO_3$	:	Calcium Carbonate
CaO	:	Calcium Oxide
CIP	:	Cold Isostatic Press
EDX	:	Energy Dispersive X-Ray
FE-SEM	:	Field Emission Scanning Electron Microscope
FD-HA	:	Freeze Dried Hydroxyapatite
FTIR	:	Fourier Transform Infrared
H_3PO_4	:	Orthophosphoric Acid
HA	:	Hydroxyapatite
HDPE	:	High Density Polyethylene
H_v	:	Vickers Hardness
ICDD	:	International Center for Diffraction Data
JCPDS	:	Joint Committee of Powder Diffraction Standard
K_{Ic}	:	Fracture Toughness
MD-HA	:	Microwave Dried Hydroxyapatite

MTT	:	3-(4,5-Dimethylthiazol-2-yl)-2,5-Diphenyltetrazolium Bromide
MWS	:	Microwave Sintering
NH_3	:	Ammonia
NH_4OH	:	Ammonium Hydroxide
OH	:	Hydroxyl
OD-HA	:	Oven Dried Hydroxyapatite
SBF	:	Simulated Body Fluid
SEM	:	Scanning Electron Microscope
SiC	:	Silicon Carbide
TCP	:	Tricalcium Phosphate
TEM	:	Transmission Electron Microscope
TTCP	:	Tetracalcium Phosphate
XRD	:	X-Ray Diffraction
ZnO	:	Zinc Oxide
β-TCP	:	Beta-Tricalcium Phosphate

LIST OF APPENDICES

CHAPTER 1: INTRODUCTION

1.1 Background of the Study

The bones in the human body play important roles such as providing structural support, protecting bodily organs and serving calcium phosphorus for the blood cell formation (Karin, 2005). Unfortunately, bone is susceptible to fractures due to injuries, degenerative diseases and aging where the hard tissue loss gradually in their biological system (Best *et al*., 2008). An estimated 1.7 million hip fractures occur annually around the world, with one third happened in Asia. This problem is rapidly emerging in Asia as statistics show that more than half of all osteoporotic hip fractures expected in Asia by the year of 2050 (Lau *et al*., 1997). Therefore, medical treatment is eagerly needed to heal or replace the damaged hard tissue or bones.

In early stage, transplantation such as autograft or allograft was a promising method to replace damaged hard tissue or bones. However, it was later found to be unsuitable for medical purpose due to the scarcity of suitable donor tissues, risk of disease transmission, risk of tissue rejection and low success rate (Karin, 2005). This fact leads to the exigency research and development of advanced synthetic materials for the fabrication of replacement implants. Metallic biomaterials used in orthopaedic have drawbacks due to corrosion, wear and negative tissue reaction which lead to loosening of the implant (Hench, 1991). Therefore, an ideal implant material must show biocompatibility. An interpretation of the word "biocompatibility" has been based upon the interaction(s) between synthetic substances to the local tissues. In this respect, interactions have been correlated with conditions of minimal harm or change, either to the host or to the implants (Doremus, 1992; Lemons, 1996). A material that exhibits excellent biocompatibility is non-immunogenic, non-toxic, non-irritant, has no mutagenic effects on the biological system and stable under extreme physical and chemical conditions in the living body (Suchanek & Yoshimura, 1998; Williams, 2008).

Therefore, great demands have been placed on the use of ceramics as implant materials as they possess favourable properties such as ease of processing and cause no toxic response in human body (Katti, 2004; Fathi, 2008) in addition to their good biocompatibility; the ability to stay in body without giving adverse effects (Hench, 1998). These ceramics are subsequently termed as 'Bioceramics'. Besides, bioceramics are non-toxic, have thermal and chemical stability; high wear resistance and have wonderful durability. These excellent properties all contribute to make them as good candidate material for surgical implants (Jayaswal *et al.*, 2010).

Amongst all the bioceramics, calcium phosphate family ceramics, particularly hydroxyapatite [$Ca_{10}(PO_4)_6(OH)_2$, HA] (Liu *et al.*, 1997) has been widely employed as medical implant and hard tissue replacement because it is chemically similar with the inorganic component of hard tissue of human bones and teeth (Best *et al.*, 2008; Irma *et al.*, 2006; Hench, 1998). Furthermore, HA is a bioactive material, having excellent biocompatibility which denotes that it does not exhibit any rejection by the human body (Suchanek and Yoshimura, 1998). Therefore, a great deal of different synthesising methods to produce HA powder has been established such as wet chemical precipitation (Loo *et al.*, 2008; Sung *et al.*, 2004), mechanochemical (Mochales *et al.*, 2004; Nasiri-Tabrizi *et al.*, 2009) and sol-gel (Han *et al.*, 2004; Rajabi-Zamani *et al.*, 2008).

The wet chemical precipitation method is one of many novel methods found to be simple and cost effective (Kong *et al.*, 2007; Verwilghen *et al.*, 2007). The earlier work showed that powder synthesised through the wet chemical precipitation method is homogenous, with good crystallinity, physiologically stable, morphologically similar to hard tissue and has high relative density (Kothapalli *et al.*, 2004; Donadel *et al.*, 2005; Tolouei *et al.*, 2012). In wet chemical method, drying of the precipitate is one of the crucial steps. Drying is divided into heating and non-heating method. Conventional

oven drying is categorized under heating method as it involves convective, conductive and radiation drying by external heat sources. It is the most commonly used drying method in wet chemical due to its simplicity and low cost. However, oven drying usually takes a very long drying hour for the precipitate to dry thoroughly which is not practical for mass production and may lead to serious agglomeration of the synthesized powder (Yu *et al*., 2010). Freeze drying on the other hand is a widely used non-heating drying in wet chemical method (Lu *et al*., 1998; Stanley & Nesaraj, 2014; Yoruc & Koca, 2009). In freeze drying, the initial liquid suspension is frozen and the pressure above the frozen states is reduced and the water is removed by sublimation. This drying method produces homogenous and uniform fine-grained powders (Lu *et al*., 1998; Wang & Lloyd, 1991). Nonetheless, there are a few drawbacks of freeze drying method such as high equipment cost, complex operations and procedures as well as long drying time. Therefore, there is a need to search for an alternative drying method that would significantly reduce the drying hours of HA precipitate while eliminating the serious powder agglomeration problem.

Microwave drying has been identified as one of the alternative drying method of HA precipitate as this drying method offers several advantages including shorten the drying times, provides reduction of energy requirements in synthesizing, improve the quality of products and lower operating cost (Atong *et al*., 2006; Feng at al., 2012; Yu *et al*., 2010; Abd Rahman *et al*., 2009; Tonanon *et al*., 2006; Hart *et al*., 2007). Microwaves are electromagnetic waves with wavelengths range 1 mm to 1 m; having frequencies lies between 300 MHz to 300 GHz (Sun *et al*., 1994). The range of wavelengths and frequencies allows microwaves penetrate into the wet product effectively that the heat is generated uniformly within the material. Microwaves are very specific to small polar molecules such as water which makes it suitable to be used in the drying of wet HA precipitate as water is the only by product of the wet chemical

method. Due to the dipolar nature, water molecules randomly oriented in the materials if there is no microwave field exists (Das *et al*., 2009). With the presence of the alternating microwave fields, water molecules tend to follow the electric field associated with the electromagnetic radiation by oscillating at high frequencies (many millions times per second). This high frequency oscillations produce molecular friction results in the generation of the instantaneous heat within the material. The repeated movement of water molecules due to the flip flopping electrical field causes the material to gain more energy and heat up. This heat generation creates a temperature gradient between the core and the surface of the material. The high temperature in the core drives the evaporating liquid to the surface of the material (lower temperature) which enables the water movement and its subsequent removal from the material. The heating of water occurs selectively due to the greater dielectric loss of water as compared to the material to be dried. Therefore, further drying or the danger of overheating could be avoided once the water is removed. Hence, microwave drying has a great potential in producing high quality HA powders coupled with enhanced mechanical properties of the sintered samples with shorter processing time.

To be an ideal implant, the simultaneous achievement of bioactivity and a match of the mechanical properties of the implant with the bone are required to guarantee clinical success. Therefore, numerous research has been done to produce dense HA ceramics through powder compaction followed by time consuming conventional sintering to improve the mechanical properties of HA. However, the use of HA is still limited in load bearing applications because of its low fracture toughness, thus, is prone to mechanical failure (Rodr ́guez-Lorenzo *et al.*, 2002). The low mechanical properties of HA could be attributed to the conventional sintering method as it regularly calls for high sintering temperature and lengthier sintering schedule (approximately 18–24 hours) which propagate rough grained microstructure, resulting poor mechanical properties

(Ramesh *et al*., 2007). Microwave energy has been very popular and reported to produce ceramics such as alumina (Fang *et al*., 2004; Cheng *et al*., 2000), zirconia (Binner *et al*., 2008), zinc oxide (Gunnewiek & Kiminami, 2014; Savary *et al*., 2011) and etc. (Oghbaei & Mirzaee, 2010) that possessed improved mechanical properties. Microwave sintering is fundamentally different from conventional sintering as it is fast and rapid. The heat is generated volumetrically by the electromagnetic energy (Das *et al*., 2009) within the material instead of being transferred from outer are of the material (Ramesh *et al*., 2007; Agrawal, 1998). As the microwave sintering is rapid, it could improve the mechanical properties of HA by suppressing the grain coarsening that occurred due to long sintering time. In short, microwave sintering offers shorter time of processing, uniform heating, enhanced material properties and suppressed grain coarsening that normally occurred in conventional sintering. Hence, it has great potential to produce HA ceramics with high mechanical properties.

Another economical technique to improve the mechanical properties of HA while maintaining its bioactivity is by incorporating appropriate low temperature sintering additives (Suchanek *et al*., 1997) Zinc oxide (ZnO) is of interest as sintering additives as zinc has proven to play an important role in proliferative effects on osteoblastic cells and the beneficial effects of zinc oxide (ZnO) on the bioactive properties of HA have been extensively studied (Ishikawa *et al*., 2002; Jallot *et al*., 2005). Besides, there are numerous works investigated the microwave sintering effects on the sinterability of pure HA (Ramesh *et al*., 2007; Yang *et al*., 2002; Vijayan & Varma, 2002; Nath *et al*., 2006; Bose *et al*., 2010). However, the sinterability of zinc oxide doped HA has not been systematically studied.

Hence, the effects of microwave drying, microwave sintering and the addition of ZnO on the sintering behavior of hydroxyapatite were investigated.

1.2 Scope of Research

The research is divided into three phases where the initial phase of the research was to prepare pure HA powder using novel wet chemical precipitation method (Ramesh, 2004) via freeze drying, microwave drying and conventional oven drying. Freeze drying of HA precipitate was carried out in a freeze dryer at temperature below - 45 ℃ and the vacuum below 0.049 mBar for 36 hours. On the other hand, microwave drying of the HA slurry was carried out in a household microwave oven at 900 watts for 15 minutes while oven drying was carried out in a conventional oven for 16 hours at 60 ℃ before sieving. The morphology, specific surface area, phase stability and elemental composition of the synthesized powders were examined and compared. Subsequently, the sintering behaviour of the three synthesized HA was compared in terms of HA phases stability, bulk density, hardness, fracture toughness and grain size. Optimisation studies were carried out at temperature ranging from 1050 ℃ to 1350 ℃ using a standard heating and cooling rate of 2 ℃/min and a holding time of 2 hours. The sintering was conducted in conventional electrical furnace.

Based on these results, the HA powder that demonstrated the optimum properties was chosen for further studies to investigate the effect of microwave sintering and sintering additives on the sinterability of HA. In the first part of second phase, the HA pellets were microwave sintered (MWS) in a microwave furnace at a constant power output of 2000 watts. The sintering regime employed was at temperature range of 950 ℃ - 1250 ℃. Then, the sinterability of microwave sintered HA was compared to that of conventional sintered HA samples.

The subsequent stage of the research was to reinforce zinc oxide (ZnO) into HA according to the different amount of weight percentage: 0.1 wt%, 0.3 wt%, 0.5 wt% and 1.0 wt% respectively. All the undoped and ZnO-doped HA samples were subjected to

conventional sintering at temperatures ranging from 1100 ℃ to 1300 ℃. The effects of sintering temperature and the influence of ZnO as dopants on the densification, microstructure, hardness, fracture toughness and phase stability of the sintered HA were evaluated. The flowchart of the research scope is shown in Figure 1.1.

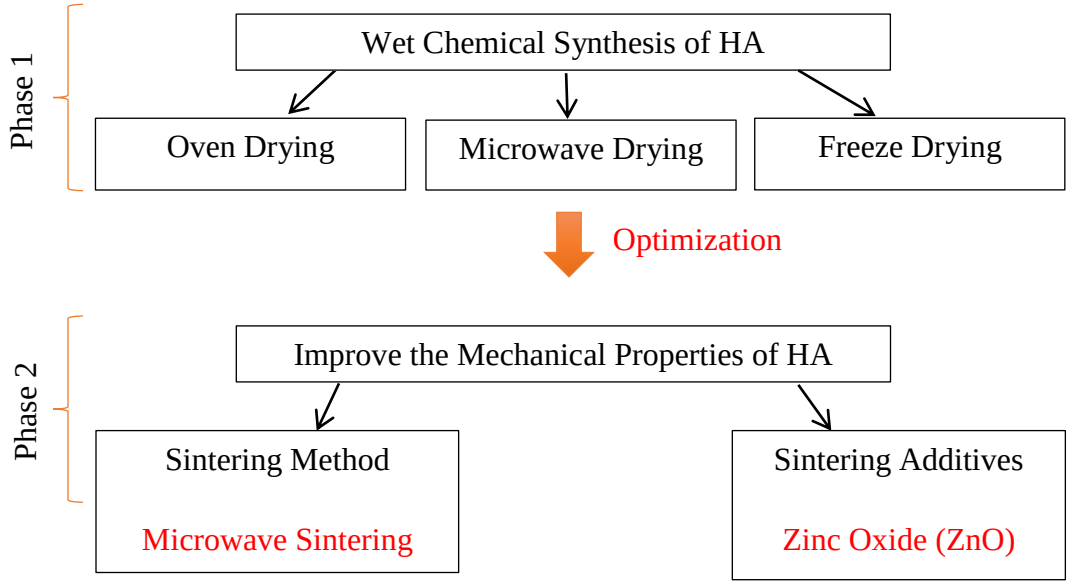

Figure 1.1: Flow chart of the research scope.

Hence, the ultimate goal of the present study is to fabricate and study the effects of drying methods, sintering methods and the ZnO addition on pure HA and to produce HA with high relative density (~97% theoretical) and enhanced fracture toughness via rapid and effective method.

1.3 Objectives of the Research

The objectives of the present research are as follows:

- To develop a simple, repeatable, and relatively rapid drying process to synthesize pure hydroxyapatite (HA) powder using a household microwave oven via wet chemical precipitation method.
- To produce nanostructured and submicron HA compacts those are suitable for clinical applications.

- To study and compare the phase stability, densification, microstructural differences and mechanical properties of the microwave and conventionally sintered HA.
- To enhance the fracture toughness of HA through the addition of sintering additives
- To evaluate the mechanical properties of the engineered HA.

1.4 Structure of the Thesis

In chapter 2, literature review on bioceramics and their classification are addressed. Subsequently, a general literature on hydroxyapatite (HA) and its importance are presented. Types of the synthesis methods of HA and the synthesis parameters involved in wet chemical method are extensively discussed. Besides that, the microwave theories and introduction to the potential usage of microwave drying on HA have been reviewed.

Chapter 3 presents the significant parameters that affect the sinterability of HA such as sintering temperature, sintering time, sintering ramp rate, powder consolidation techniques and sintering additives that have been reported by various researchers. At the end of the chapter, the potential of ZnO as sintering additives on ceramics are presented. This chapter provides a framework for a better perceptive of factors controlling the physical and mechanical properties of HA ceramics.

A detailed description of the experimental techniques such as drying process, synthesis process, ultrasonic process, ball milling process, uniaxial pressing, cold isostatic pressing, sintering process, polishing and the usage of several apparatus used in this research are documented in Chapter 4. In addition, powders and sintered samples characterization such as X-Ray Diffraction (XRD), Scanning Electron Microscope (SEM), Energy Dispersive X-Ray (EDX), Field Emission Scanning Electron Microscope (FE-SEM), Brunauer-Emmett-Teller (BET) method, Transmission Electron

Microscope (TEM), Fourier Transform Infrared (FTIR), density measurement, hardness and fracture toughness measurement are further discussed in this chapter.

The experimental findings and discussion are explored and comprehended in Chapter 5 and 6. In chapter 5, discussion mainly focused on the comparison between HA powders synthesized via three different drying methods, i.e. microwave drying, freeze drying and oven drying in terms of powder characteristics and sintering behaviour. Based on the result of this study, the powder that exhibited the overall best sintering properties is selected for further studies. In Chapter 6, the effect of microwave sintering on the sinterability of the selected pure HA powder is deliberated. Additionally, the sinterability of the ZnO-doped HA and pure HA in conventional sintering are compared and discussed with regards to phase stability, bulk density, hardness and fracture toughness.

Lastly, Chapter 7 emphasizes on the suggestion for future work and conclusion drawn from the current research findings. The appendices, documented the pictures of equipment used, water density table and the JCPDS files.

CHAPTER 2: SYNTHESIS METHODS OF HYDROXYAPATITE

2.1 Introduction to Hydroxyapatite

Hydroxyapatite (HA) is a hydrated calcium phosphate mineral and is the hydroxyl end member of the complex apatite group (Myoui *et al*, 2003).The chemical formula of HA is $Ca_{10}(PO_4)_6(OH)_2$ and it is a natural occurring phosphate on earth. HA is also known as hydroxylapatite, apatite and calcium hydroxyapatite (Chou *et al.*, 1999; DeGroot *et al*., 1987). Pure HA has the theoretical composition of 39.68 wt% Ca, 18.45 wt% P and a set of crystallographic properties which have close resemblance of that hard tissue. Due to its similarity with the inorganic component of human bone and teeth as shown in Table 2.1 (Hench, 1998; LeGeros & LeGerous, 1993), hydroxyapatite (HA) has drawn great interest from researchers to be used clinically in different applications.

Table 2.1: Comparison between composition and physical properties of human enamel, bone and HA ceramic (Hench, 1998; LeGeros & LeGeros, 1993).

Composition (wt%)	Enamel	Bone	HA
Calcium, Ca^{2+}	36	24.5	39.68
Phosphorus, P	17.7	11.5	18.45
Ca/P molar ratio	1.62	1.65	1.667
Sodium, Na^{+}	0.5	0.7	-
Potassium, K^{+}	0.08	0.03	-
Magnesium, Mg^{2+}	0.44	0.55	-
Carbonate as CO_3^{2-}	3.5	7.4	-
Fluoride, F^{-}	0.01	0.02	-
Chloride, Cl^{-}	0.30	0.10	-
Total inorganic (mineral)	97	65	100
Total organic	1	25	-
Absorbed H_2O	1.5	9.7	-
Crystallographic Properties			
Lattice Parameters (± 0.003 Å)			
a-xis	9.441	9.419	9.422
c-axis	6.882	6.880	6.880
Crystallinity index	70 – 75	33 – 37	100
Average crystallite size	1300 × 300	250 × 30	-
Ignition products @ 800 ℃ - 950 ℃	β-TCP + HA	HA + CaO	HA

The similarities of HA to the hard tissues' mineral phase promote osseointegration process and integrate well with the surrounding host bone and promote new bone formation without showing any adverse effects like toxicity, inflammatory and immunogenic (Wang *et al.*, 2007; Murugan & Ramakrishna, 2005). Hence it has been widely used for hard tissue repairs include bone and tooth defect fillers, alveolar ridge augmentations and reconstruction, small and unloaded ear implants, repair of periodontal bony defects, dental implant, biocompatible and bioactive coatings on metallic implants for dental implants and hip joint prosthesis (Dorozhkin, 2009; Xia *et al.*, 2013; Valletregi, 2004; Yang & Chang, 2005; Saiz *et al.*, 2007; Dorozhkin, 2010).

Its biocompatibility and ability to bond with surrounding tissues/bone has been experimentally proven to be superior by *in vitro* and *in vivo* methods (Akao *et al.*, 1993; Cao & Hench, 1996; Sinha *et al.*, 2001). *In vitro* test is known as cell culture test where the bioactivity of biomaterials is estimated by a simulation environment (Sun *et al.*, 2006; Banerjee *et al.*, 2007) such as the simulated body fluid (SBF). SBF has ions and ion concentration close to human blood plasma as shown in Table 2.2 (Oréfice *et al.*, 2000).

Table 2.2: Ionic concentration (mmol/dm^3) of SBF and human blood plasma (Oréfice *et al.*, 2000).

Ion	SBF	Blood Plasma
Na^+	142.0	142.0
K^+	5.0	5.0
Mg^{2+}	1.5	1.5
Ca^{2+}	2.5	2.5
Cl^-	147.8	103.0
HCO^{3-}	4.2	27.0
HPO_4^{2-}	1.0	1.0
SO_4^{2-}	0.5	0.5

The growth rate of the apatite layer on the surfaces of the material immersed in SBF can be used to estimate the bioactivity of the material. In the experiment conducted by Sun *et al*. (2006), HA powder particles sintered at 900 ℃ was soaked in SBF and was found to possess high bioactivity as apatite layer formed in short period on the HA particles surface. Kim *et al*. (2005) reported that apatite with sharp needle-like morphology grew on the surface of dense HA sample after its immersion in SBF for a short period of time. On the other hand, study indicated that HA is non-cytotoxic as human osteoblast derived from human bone tissue and cells attached well on dense HA surfaces (Banerjee *et al*., 2007). In 2010, Catros *et al*. (2010) did an *in vitro* characterization of HA powder by observing cell proliferation using MTT assay. The result showed that HA was biocompatible with osteoblastic MG63 cells and the formation of mature bone tissue was observed. The biological performance of HA is important in the field of tissue engineering.

In vivo test on the other hand, involves the implantation of the material in body. The samples were implanted in a living organism to access the bioactivity, biocompatibility and cytotoxicity of the material. Early in 1993, Tatsuo *et al*. (1993) implanted HA into the tibias of male rats for a month. The authors observed a 100% contact between HA and the natural bone of the young rats. Another *in vivo* test has been done on eight mice on the calvarial bone (Catros *et al*., 2010). HA demonstrated osteoconductive properties after 1 month healing as there is no foreign body reaction detected around the implanted HA crystallite. This finding proved that HA composite has extraordinary biocompatibility and could integrate with bone without forming fibrous tissue. There are many more *in vivo* studies of HA implanted in other animals like sheep (Liu *et al.*, 2000; Gatti *et al.*, 1990), dogs (Xue *et al.*, 2004), rats (Okamoto *et al.*, 2006) and rabbits (Chu *et al.*, 2006; Darimont *et al.*, 2002). All these studies draw the same conclusion that the HA bond chemically with the bone after a certain period of implantation.

Aside from implantation in animals, there are researchers conducted to access the biocompatibility of HA in human hard tissue. Van Blitterswijk *et al*. (1985) have shown great biocompatibility of HA ceramics when implanted in human middle ear for a studied duration of 4 – 40 months. Further to that, Oguchi *et al*. (1995) reported that HA appeared to bond directly to human bones without causing damages to the fibrous tissue after an implantation period of 3.5 to 9 years. Besides, Sires and Benda (2000) have carried out the histological findings of HA orbital implant after 5.5 years of implantation in a 17 years old female patient in which the authors concluded that bone may integrate throughout the pores of HA orbital implants.

The practical potential applications of HA stem primarily from the nature of the HA structure. HA is a compound of a definite composition, $Ca_{10}(PO_4)_6(OH)_2$ and a definite crystallographic structure. Stoichiometric HA has a Ca/P ratio of 1.67 and a crystal structure of hexagonal system with space group $P6_3/m$ with lattice parameters of a=b= 9.42, c= 6.88 Å and $\gamma = 120^{\circ}$ (LeGeros & LeGeros, 1993). Besides that, HA can be easily obtained from solid solutions via chemical reactions with various kinds of metal oxides, halides and carbonates. Ca^{2+} can be substituted to some extent with monovalent (Na^{+}, K^{+}), divalent (Sr^{2+}, Ba^{2+}, Pb^{2+}) and trivalent (Y^{3+}) cations, while the OH^{-} can be substituted by fluoride, chloride or carbonate ions (Barralet *et al*., 1995; Jha *et al*., 1997). The substitutions in the apatite structure for (Ca), (PO_4) or (OH) group result in changes in properties such as lattice parameter, morphology and solubility without significantly changing the hexagonal symmetry as described in great detail by Elliott *et al*. (1973).

In terms of phase stability, HA is the most stable calcium phosphate at normal temperature and pH between 4 to 12 (Koutsopoulous, 2002). However, at higher temperature, phases such as $Ca_3(PO_4)_2$ (β-tricalcium phosphate, C_3P, TCP) and $Ca_4P_2O_9$ (tetracalcium phosphate, C_4P) are present. As shown in the phase diagram (Figure 2.1),

the phase equilibrium of HA depends on both the temperature and the partial pressure of water (p_{H_2O}) in the sintering atmosphere. When the water is present, HA can be formed and is stable up to 1360 ℃ for CaO and P_2O_5. Without water, C_4P and C_3P are the stable phases (DeGroot *et al*., 1990). It is also noteworthy that OH^- ions remain stable in the HA structure even at high temperatures up to 1350 ℃ (Jha *et al*., 1997).

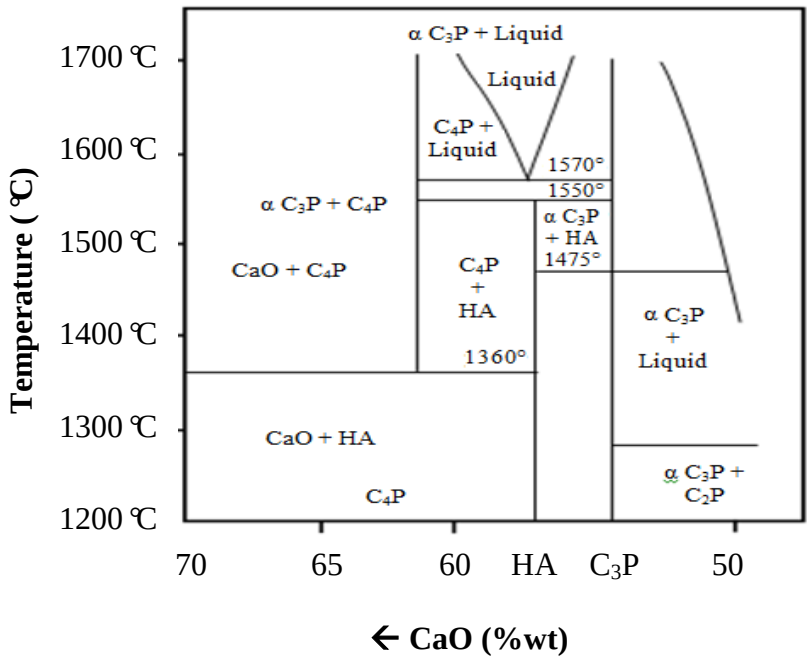

Figure 2.1: Calcium phosphate phase equilibrium diagram at 66 kPa (DeGroot *et al*., 1990).

In general, HA exists in various forms and has found numerous uses in biomedical application including fully dense sintered implant (Banerjee *et al*., 2007), coatings of orthopedic and dental implants (Yang & Chang, 2005), porous form for alveolar ridge augmentation and scaffolds for bone growth (Saiz *et al*., 2007) and as powders in total hip and knee surgery (Hench, 1991). Different phases of calcium phosphate ceramics are used in biomedical application depending upon whether a resorbable/biodegradable or bioactive material is desired.

Besides hard tissue repair, HA is considered as potential material as a temporary scaffold for bone tissue engineering applications, allowing subsequent bone tissue regeneration after implantation *in vivo* (Oh *et al*., 2006; Zhou & Lee, 2011). HA can also be served as drug carrier for controlled drug/protein delivery to the site of infection in body. It is worth mentioning that it suppresses inflammation process in the infection part, has low toxicity, has inertia to microbial degradation and excellent storage ability (Li *et al*., 2010; Rodriguez-Ruiz *et al*., 2013; Lin *et al*., 2013; Wu *et al*., 2011).

The other applications of HA include soft tissue repairs where HA can activate the fibroblasts to support the skin wounds healing (Okabaysahi *et al*., 2009), applications in cell targeting, bioimaging and diagnosis (Kozlova *et al*., 2012; Chen *et al*., 2012; Ashokan *et al*., 2010) where mono-dispersed nano-sized HA enhanced the simultaneous contrast of magnetic resonance imaging (MRI) and near-infrared (NIR) fluorescence imaging and also as purification agent in chromatography for the separation of nuclei acid, proteins and antibodies (Akkaya, 2013; Morrison *et al*., 2011).

As reported in the previous section, HA is known to be bioactive where bone growth is supported directly on the surface of the material when implanted next to bone. This bioactive response leads HA to be used in clinical applications in both powder and bulk form as mentioned above. However, there is concern with regards to its mechanical properties. It has relatively low fracture toughness, i.e. 0.7 – 1.2 $MPam^{1/2}$ as compared to 2.2 – 4.6 $MPam^{1/2}$ for natural bone (Table 2.3). Consequently, the usage of HA is limited to non-load bearing applications (Ruys *et al*., 1995; Muralithran & Ramesh, 2000; Ramesh *et al*, 2007) such as artificial hip joint, knee joint, etc. (Suchanek & Yoshimura, 1998). Table 2.3 compares the mechanical properties of sintered HA with human hard tissue (LeGeros & LeGeros, 1993). In view to this limitation, parameters

controlling the sinterability of HA and methods to improve the mechanical properties of sintered HA must be identified and deliberated in Chapter 3.

Table 2.3: Comparison of mechanical properties of sintered HA with human hard tissue (LeGeros & LeGeros, 1993).

	Enamel	Bone	HA
Density (g/cm^3)	2.9 – 3.0	1.5 – 2.2	3.156
Relative Density (%)	-	-	95 – 99.8
Grain Size (μm)	-	-	0.2 – 25
Compressive Strength (MPa)	250 – 400	140 – 300	270 – 900
Bending Strength (MPa)	-	100 – 200	80 – 250
Tensile Strength (MPa)	-	20 – 114	90 – 120
Young's Modulus (GPa)	40 – 84	10 – 22	35 – 120
Fracture Toughness ($MPam^{1/2}$)	-	2.2 – 4.6	0.7 – 1.2
Hardness (GPa)	3.4 – 3.7	0.4 – 0.7	3.0 – 7.0

2.2 Synthesis Method of Hydroxyapatite (HA) Powders

High demand has been placed on producing HA powder due to the advantages and clinical potential of HA. Therefore, several techniques have been developed for the synthesis of HA powders such as wet chemical, hydrothermal, sol-gel, mechanochemical (solid state reaction) etc. Synthesis methods of HA can have significant effects on the morphology, stoichiometry, specific surface and sinterability of HA powders (Orlovskii *et al*., 2002; Suchanek & Yoshimura, 1998; Pretto *et al*., 2003). The subsequent sections provide a brief account of some main synthesis technique that has been reported in the literature for the production of hydroxyapatite powder.

2.2.1 Wet Chemical Method

Wet chemical method, also known as wet precipitation method is most widespread, common and simplest route to produce HA powder (Pattanayak *et al*., 2007; Adamopoulus & Papadopoulus, 2007) due to the minimal operating cost (Santos *et al*.,

2004), inexpensive raw materials, low probability of contamination (Afshar *et al*., 2003) and it can be easily carried out at low temperature ranging from room temperature to 100 ℃ (Kumar *et al*., 2004). Generally, steps involved in the wet chemical method of HA include:

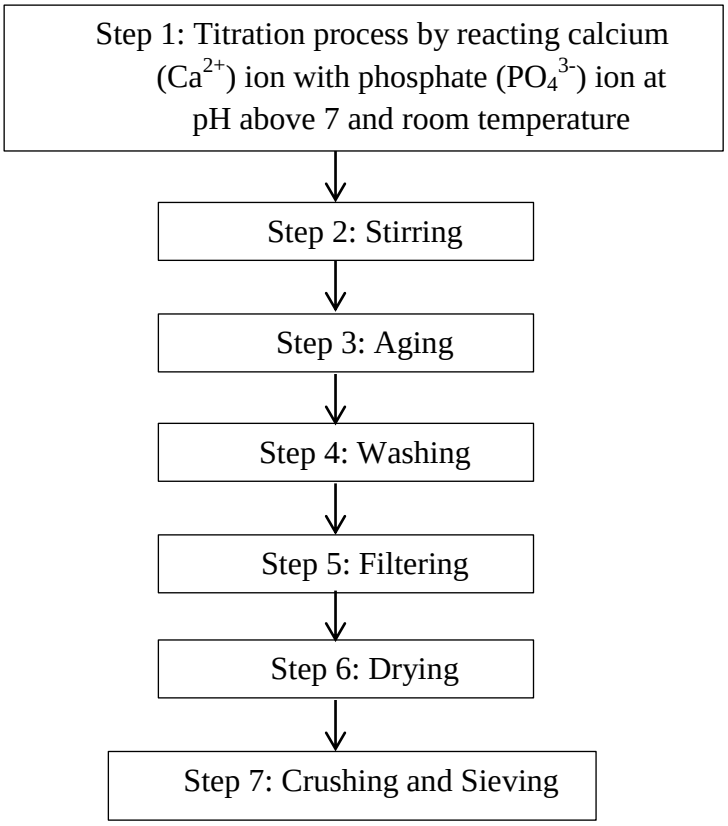

Figure 2.2: General procedures involved in wet chemical method.

HA powder synthesized through this method is homogenous, has high purity and is morphologically similar to hard tissue (Donadel *et al*., 2005; Kothapalli *et al*., 2004). However, the shortcomings of this method are the resulting powder is poorly crystallized without regular shape and the powder quality is greatly affected even by a slight difference in the reaction/process variables (Kumta *et al*., 2005). Therefore, it is indispensible to study the effects of the process variable associated with the wet chemical method; in relation to the impacts they imposed on the HA powder properties and sinterability.

2.2.1.1 Starting Precursors

A variety of starting precursors can be selected such as calcium nitrate ($Ca(NO_3)_2$), calcium chloride ($CaCl_2$), calcium carbonate ($CaCO_3$), calcium hydroxide ($Ca(OH)_2$), calcium sulphate ($CaSO_4$) as calcium ions and ammonium phosphate ($NH_4H_2PO_4$), phosphoric acid (H_3PO_4), potassium phosphate (K_3PO_4), and diammonium phosphate ($(NH_4)_2HPO_4$) as phosphate ions source (Sadat-Shojai *et al*., 2013).

Initially, calcium nitrate ($Ca(NO_3)_2$) and diammonium phosphate ($(NH_4)_2HPO_4$) was used as starting precursors by Hayek and Stadlman (1955) via the following equation:

$$10Ca(NO_3)_2 + 6(NH_4)_2HPO_4 + 8NH_4OH \Rightarrow$$

$$Ca_{10}(PO_4)_6(OH)_2 + 6H_2O + 20NH_4NO_3 \qquad (2.1)$$

Later, various researchers (Sung *et al*., 2004; Bianco *et al*., 2007; Mobasherpour, 2007; Pattanayak *et al*., 2007; Monmaturapoj; 2008) used calcium nitrate tetrahydrate ($Ca(NO_3)_2 \cdot 4H_2O$) to produce HA based on the following equation:

$$10\ Ca(NO_3)_2 \cdot 4H_2O + 6(NH_4)_2HPO_4 + 8NH_4OH \Rightarrow$$

$$Ca_{10}(PO_4)_6(OH)_2 + 20H_2O + 20NH_4NO_3 \qquad (2.2)$$

These authors reported that the synthesized HA powders have particle size ranging from nanometer to micrometer and have Ca/P ratio in the range of 1.25 to 1.70.

Akao *et al*. (1981) on the other hand, proposed that calcium hydroxide ($Ca(OH)_2$) and orthophosphoric acid (H_3PO_4) to be used as starting materials. HA powders with a Ca/P ratio of 1.69 were successfully synthesized. The reaction follows the formula:

$$10Ca(OH)_2 + 6H_3PO_4 => Ca_{10}(PO_4)_6(OH)_2 + 18H_2O \qquad (2.3)$$

The byproduct contains only water which makes this reaction favorable to the researchers. Osaka *et al*. (1991), Tampieri *et al*. (2000), Afshar *et al*. (2003), Ramesh *et al*. (2008) and Teh *et al*. (2014) have also adopted this method. These authors attained HA powders in the nanometer to submicron range with Ca/P ratio ranging from 1.5 to 1.9.

There are studies on deriving calcium precursors from natural resources and bio-waste such as eggshells, seashells and snail shells and they appear to be a promising source of calcium for the preparation of hydroxyapatite. Adak *et al*. (2011) extracted calcium source from dead snail shells. The dead snail shells were washed and heated at 1000 ℃ to decompose the organic matters and converted to calcium oxide which in turn on exposure to atmosphere forms calcium hydroxide. Pure HA powder with high thermal stability (no secondary phases were detected at 1200 ℃) was then produced via chemical route. The HA particle exhibited spherical shape with average particle size of 60 – 80 nm.

Using the similar extraction method, Kamalanathan *et al*. (2014) obtained calcium hydroxide from raw eggshells as calcium precursor. HA was then synthesized using the $Ca(OH)_2$ and H_3PO_4 via wet chemical method. XRD results indicated the synthesis of single phase and nanocrystalline (35.3 nm) HA was produced in the work. Furthermore, phase pure HA was obtained and remained stable after albeit sintered at 1250 ℃. Similar to the abovementioned methods, CaO was derived from sea shells as starting material which was converted to calcium hydroxide ($Ca(OH)_2$) and subsequently reacted with phosphoric acid by wet chemical reaction (Santhosh *et al*., 2013). The synthesized powder was pure HA in rod-shape, having crystallite size about 101 nm with Ca/P ratio of 1.8.

2.2.1.2 Synthesis Temperature

In 2007, Bianco *et al*. (2007) compared wet chemical synthesized HA powder produced at 40 ℃ and 70 ℃. Both synthesis temperatures produce needle-like HA particle which is not in agreement with the study conducted by Bouyer *et al*. (2000). As shown in Figure 2.3, low synthesis temperature gives needle shape nanoparticle while increasing the reaction temperature leads to particle of a more regular shape close to circular (Figure 2.3). Thus, it can be observed that the shape factor (particle length divided by particle width) of the HA particle decrease with an increase of the synthesis temperature.

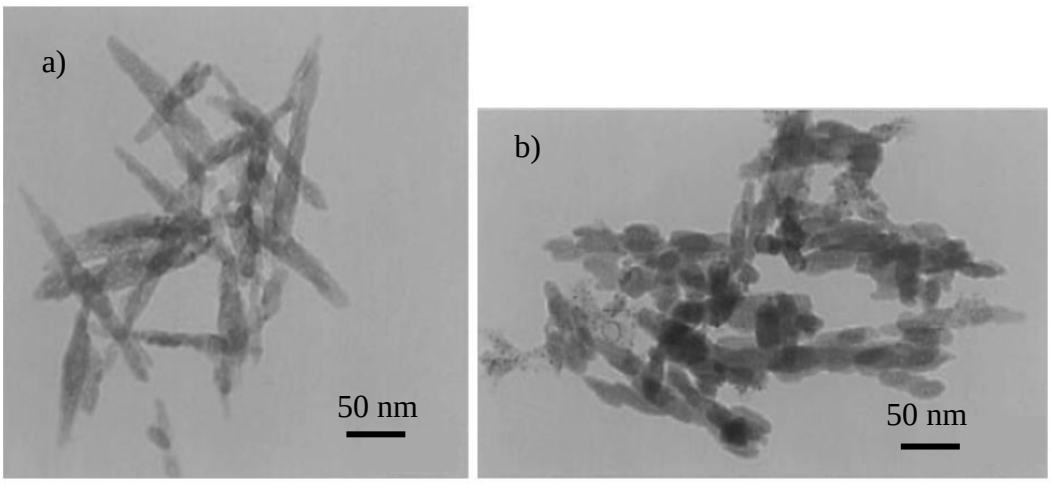

Figure 2.3: TEM picures of as-synthesized HA nanocrystal at different synthesis temperature: (a) 35 ℃; (b) 85 ℃ (Bouyer *et al*., 2000).

Besides affecting the morphology of the HA particles, reaction temperature was found to affect the crystallinity but not the phase purity of the synthesized HA as shown in Figure 2.4 (Pham *et al*., 2013). The XRD spectra (Figure 2.4) shows that all the HA has characteristics peaks of pure HA while but the crystallinity increased with increasing synthesis temperature as the peaks get sharper at higher temperature.

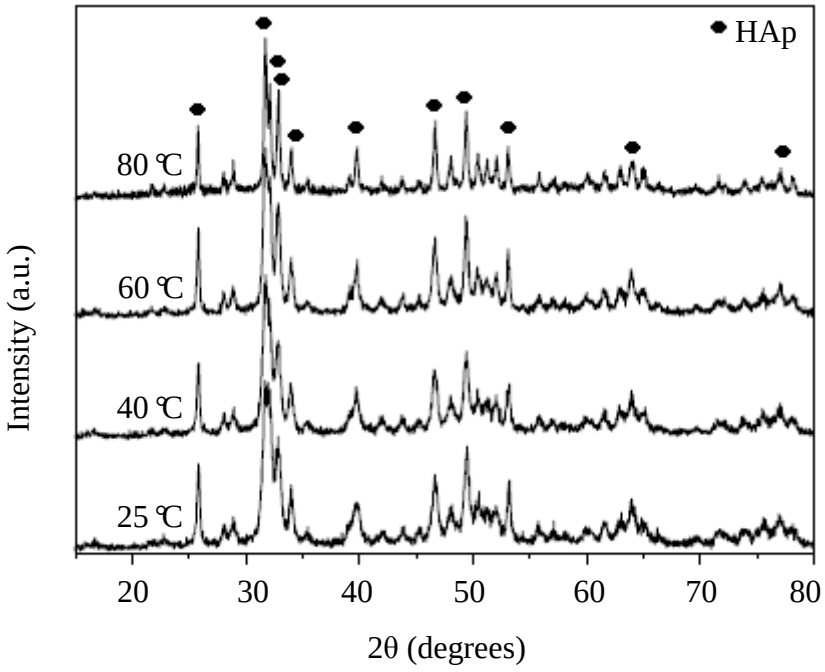

Figure 2.4: XRD spectra of HA powder synthesized at different temperatures (Pham *et al*., 2013).

2.2.1.3 Reaction pH

Proper control of the reaction pH is indispensible in wet chemical process as improper control of the pH can affect the phase purity, microstructural configuration, crystallite size, mechanical properties etc (Sadat-Shojai *et al*., 2013). The pH of the solution is usually adjusted by using ammonium hydroxide (NH_4OH) or sodium hydroxide (NaOH) (Orlovskii *et al*., 2002) to provide an alkaline medium.

Wang *et al*. (2010) pointed out that pH values equal or higher than 10 is required to produce pure HA powder as shown in Figure 2.5. HA synthesized at pH 11 and 10 revealed pure HA peaks with slight difference in degree of crystallinity as shown in Figure 2.5. As observed from Figure 2.5, the HA prepared at pH 9 was proved to be the mixture of β-TCP and HA where the diffraction of β-TCP was very weak while the phase of HA prepared at pH 8 was most of β-TCP.

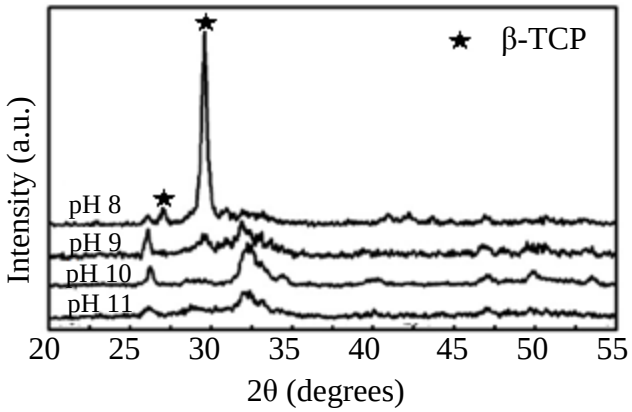

Figure 2.5: XRD patterns of HA samples.

Besides that, Inthong *et al*., (2013) claimed that the reaction pH has effects on HA particle as increasing the pH value would increase the formation of particle agglomeration but reduce the particle size of the HA powder as shown in Figure 2.6.

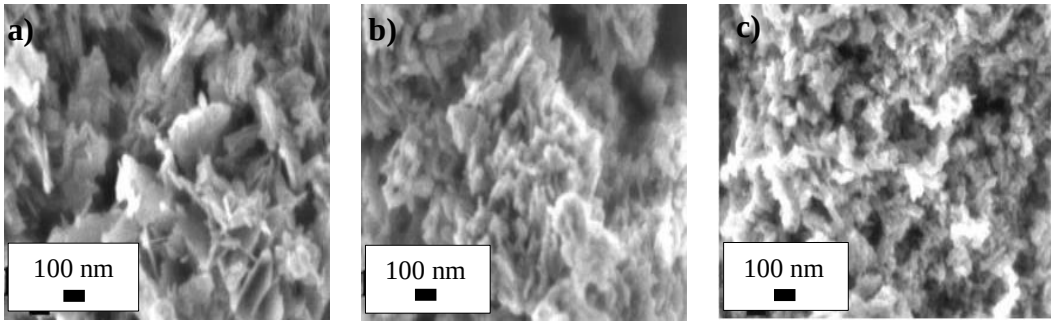

Figure 2.6: SEM micrographs of HA nanoparticles synthesized at (a) pH 5 (acidic), (b) pH 7, and pH 11 (alkaline) (Inthong *et al*., 2013).

In the same study, reaction pH value has direct effect on the grain size and mechanical properties of HA. It is perceived that HA synthesized at pH value of 9 shows the highest density and hardness value as shown in Table 2.4. Low reaction pH value (5 – 7) results in lower density and hardness value compared to those synthesized at high pH value (8 – 11).

Table 2.4: Mechanical properties of HA prepared with different pH values (Inthong *et al*., 2013).

pH value	Density (g/cm^3)	Grain Size (μm)	Hardness (GPa)
5	2.75	2.19	3.12
6	2.82	1.64	3.39
7	2.83	1.72	3.50
8	3.00	5.97	4.63
9	3.04	6.81	6.06
10	2.98	4.34	4.68
11	3.02	2.38	4.67

2.2.1.4 Ca/P Ratio

Pham *et al*. (2013) studied the effect of various Ca/P ratio (3/2, 10/6 and 10/3) on the properties of HA powder and Ca/P ratio did not affect the purity of HA as all the HA powder revealed XRD peaks corresponding to pure HA without any presence of secondary phases. This result is different from those reported by Raynaud *et al.* (2002). According to Raynaud *et al.* (2002), powders having a Ca/P molar ratio of 1.667 and composed of single HA phase could only be synthesized with a high reproducibility provided that the Ca/P ratio of the initial reagents were fixed at 1.667. Any Ca/P ratio lower or higher than 1.667 would lead to phase decomposition as shown in Table 2.5. Furthermore, Adak *et al*. (2011) stated that HA of Ca/P = 1.67 has better densification and finer particle size.

Table 2.5: Phase composition of HA prepared with different Ca/P ratio (Raynaud *et al*., 2002).

Ca/P (Molar Ratio)	Phase Composition (wt%)
< 1.50	β-TCP + β-$Ca_2P_2O_7$ (minor phase ~ 10 wt %)
1.511 ± 0.001	93% β-TCP + 7% HA
1.535 ± 0.004	78% β-TCP + 22% HA
1.631 ± 0.004	80% HA + 20% β-TCP
1.643 ± 0.003	87% HA + 13% β-TCP
1.655 ± 0.002	93.5% HA + 6.5% β-TCP

Table 2.5, continued.

1.663 ± 0.001	98% HA + 2% β-TCP
1.667 ± 0.005	> 99.5% HA
1.71 ± 0.01	98.5% HA + 1.5% CaO

2.2.1.5 Drying Methods

Drying can be defined as a process of removal of water as vapor from the material surface (Abd Rahman *et al*., 2009). It is one of the crucial steps in the wet chemical synthesis of HA powder. A few drying methods such as oven drying, freeze drying, spray drying and microwave drying have been utilized in wet chemical synthesis of HA powders.

(a) ***Oven Drying***

Majority of the research employed oven drying on the HA slurry at drying temperature ranging between 65 – 105 ℃ to obtain HA powder (Lazic *et al*., 2001; Saeri *et al*., 2003; Smiciklas *et al*., 2005; Markovic *et al*., 2004; Ramesh *et al*., 2007). Oven drying involves heating of the surface and the heat transferred into the material by the means of convective, conductive and radiation (Singh *et al*., 2015) and it usually takes a very long drying hours (16 – 48 hours). Zhang and Yokogawa (2008) studied the effect of drying conditions during HA powder synthesis on the properties of the HA powders. The HA slurry was dried at temperature ranging from 60 – 150 ℃ for 3 – 21 days, respectively. In this study, the author noticed that the drying period had no effects on the phase stability, Ca/P molar ratio and particle shape of the HA powders. However, they found that HA powder particle sizes decreased with the drying time (Figure 2.7) but independent of the drying temperature. They also found that the longer the drying period, the larger the powder agglomeration as evidence from the TEM micrographs (Figure 2.8) of HA powder.

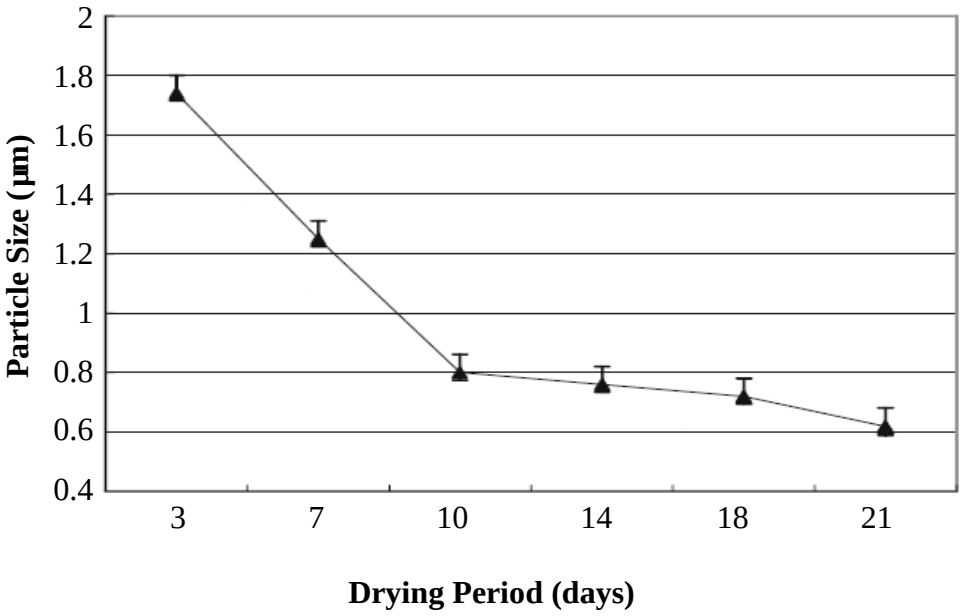

Figure 2.7: Relation between drying period and the particle size of HA powder dried at 60 ℃ (Zhang & Yogokawa, 2008).

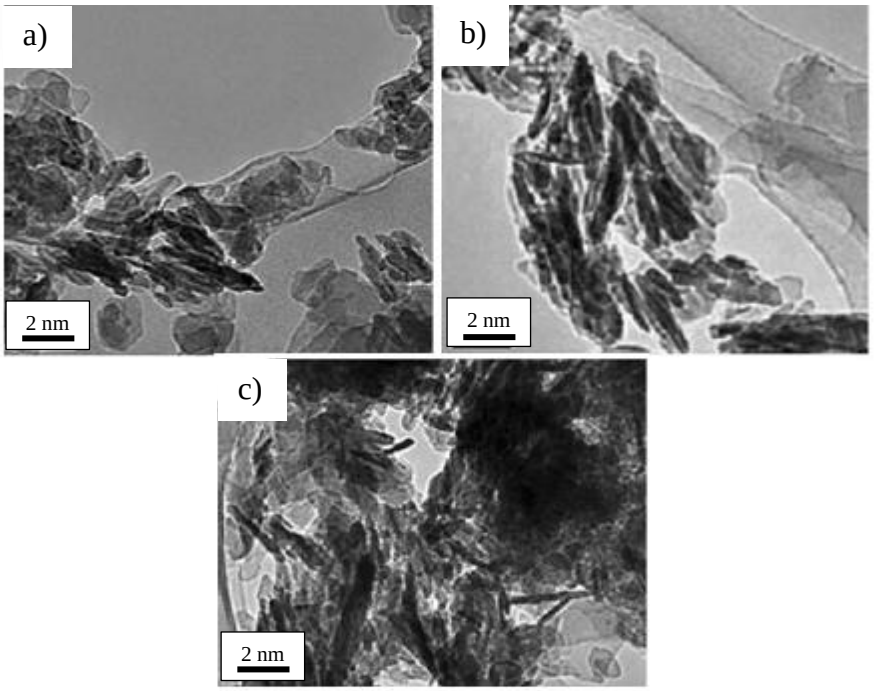

Figure 2.8: TEM photos of HA powders dried at 60 ℃ for (a) 3, (b) 10 and (c) 18 days (Zhang & Yogokawa, 2008).

The severe powder agglomeration of HA powders produced via wet chemical methods is in agreement with various studies (Lu *et al*., 1998; Hsu & Chiou, 2011;

Yu *et al*., 2010). Although oven drying is economic and simple but it is also well known that wet chemical synthesized HA powders dried by the means of conventional oven drying are invariably agglomerated often with several levels of porosity Hence, drying methods such as freeze drying and spray drying were introduced to dry the HA precipitate while microwave drying was found to be potential alternative to those drying methods. The comparison studies between oven dried HA powders with the HA dried by the alternative drying methods are discussed in the next sections.

(b) ***Freeze Drying***

Freeze drying has been reported as an efficient way to eliminate the powder agglomerations problem (Girija *et al*., 2012) and preparing uniform fine-grained powders which can be sintered to very high density (Lu *et al*., 1998; Chesnaud *et al*., 2007; Shlyakhtin *et al*., 2000; Wang *et al*., 1992). Hence, it has become a popular drying method in the wet chemical synthesis of hydroxyapatite (Lu *et al*., 1998; Girija *et al*., 2012, Wang *et al*., 2010).

Firstly, the HA slurry is frozen to solid state (Chen & Wang, 2007) which can be carried out by immersing the slurry in liquid nitrogen (fast freezing) or in an industrial deep freezer (slow freezing). Fast freezing rate is desirable to prevent aggregation and recombination of the particles but it usually requires special equipment and there are risks in handling liquid nitrogen. After freezing, the frozen HA slurry, mostly in ice form is sublimated by reducing the pressure below the triple point (Figure 2.9) of the water through vacuum pump. Therefore, in freeze drying, the frozen HA precipitate directly transformed into a gaseous form without passing through a liquid phase and high temperature is not required.

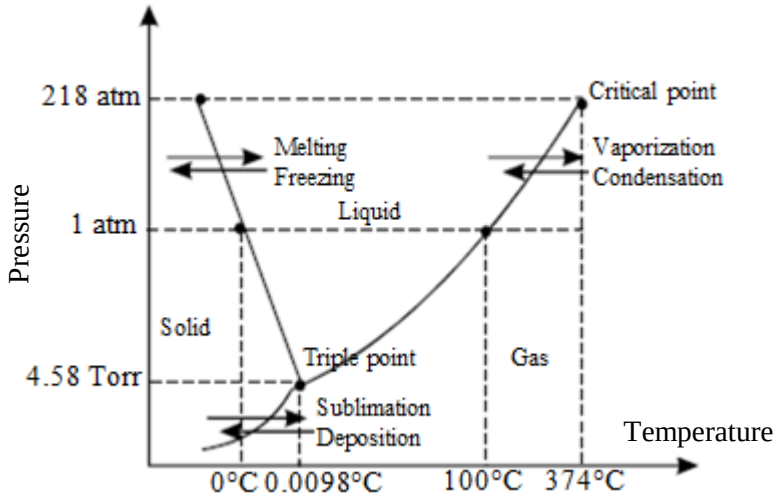

Figure 2.9: Schematic diagram for the triple phases of water (Yu *et al*., 2011).

A systematic study on the effects of freeze drying on the powder properties and sinterability of hydroxyapatite was reported by Lu *et al*. (1998). In their work, HA precipitate mixture was rapidly frozen with liquid nitrogen and subsequently brought into freezing drying apparatus for about 36 – 70 hours to get HA powder form, hereafter known as FD-HA. The authors confirmed that as-synthesized FD-HA powder is pure and has ideal stoichiometry (Ca/P = 1.67). However, it was found that the FD-HA powder decompose to β-TCP at sintering temperature of 1300 ℃. A similar decomposition temperature was found on the conventional oven dried HA powder indicated that freeze drying has no negative impact on the thermal stability of the HA powder.

TEM images show that the powder particle size of FD-HA (33 nm) was smaller than oven dried HA powder (40 nm) and the FD-HA powders are homogenous while oven dried HA is in the form of large agglomerates (Figure 2.10). This could be the reason that the density of sintered FD-HA is always higher than the oven dried HA throughout the sintering regime as Lin *et al*. (2007) reported that smaller particle

size with less agglomerates provides higher driving force for the densification of ceramics during sintering (Lin *et al*., 2007).

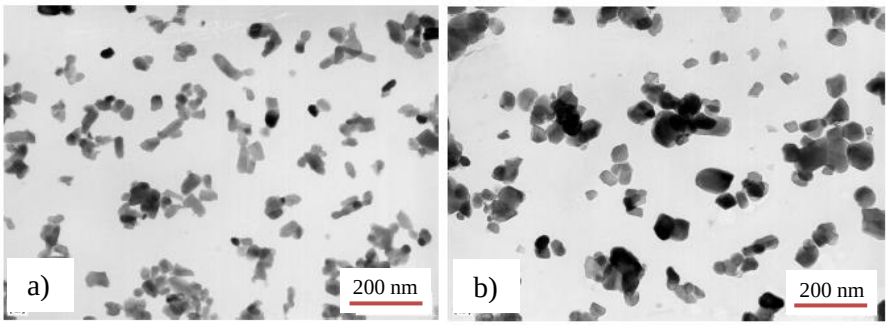

Figure 2.10: Transmission electron micrographs of HA powders after calcining at 800 ℃ for 3 hours: (a) freeze dried HA, (b) oven dried HA (Lu *et al*., 1998).

A maximum density of ~99% was obtained from FD-HA at 1350 ℃ and the maximum hardness for the FD-HA is 820 MPa, compared to 670 MPa for the oven dried HA. The high hardness of FD-HA is due to the simultaneous effects of the high density coupled with small and uniform grain size of the sintered FD-HA as shown in Figure 2.11.

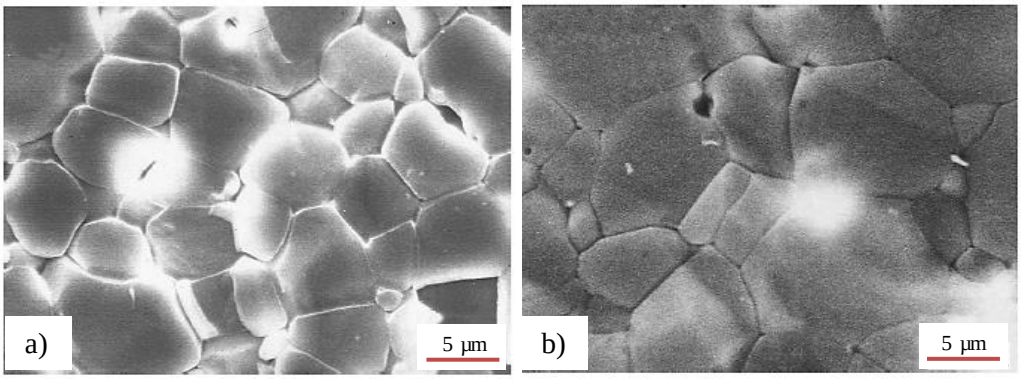

Figure 2.11: SEM micrographs of etched fracture surface of (a) freeze dried HA, (b) oven dried HA, sintered for 3 hours at 1350 ℃ (Lu *et al*., 1998).

The beneficial effects of freeze drying were supported by Girija *et al*. (2012). In their work, HA precipitate was subjected to pre-freezing at –5 ℃. This pre-frozen

product was dried in a vacuum freeze dryer at –50 ℃. The freeze dried HA has higher thermal stability compared to oven dried HA where decomposition to β-TCP took place at sintering temperature of 900 ℃ and subsequently transform to α-TCP at 1100 ℃ for oven dried HA while pure HA phase remained for HA synthesized by freeze drying at all sintering temperature. Moreover, the sintered freeze dried HA was found to have homogenous grain and highly densified compared to sintered oven dried HA. The author proposed that the formation of tri-calcium phosphate and pores in oven dried HA leads to less shrinkage and hence less densification and higher porosity of the sample.

(c) ***Spray Drying***

The spray drying is a continuous process of drying liquid or slurry into a free flowing powder material (Murtaza *et al*., 2012). The slurry of the material is sprayed as a fine spray or mist into a chamber with heated air to produce spherical powder agglomerates of relative homogeneity. It offers several advantages such as the ability to control particle size, particle size distribution, bulk and particle density with careful choice of spray dryer operating parameters (Bertrand *et al*., 2005), can be scaled up to ton quantities (Iskandar *et al*., 2003), low heat and short processing time. Hence, spray drying is introduced in the synthesis of HA to produce HA with homogenous morphology (Luo *et al*., 1999; Murtaza, 2012; Wang *et al*., 2009).

Wang *et al*. (2009) synthesized hydroxyapatite slurry via wet method and spray drying. The spray dried HA powder has low crystallinity and possessed XRD peaks that match perfectly to the HA standard peaks without impurities such as TCP and CaO. Under the examination of SEM, the shape of the spray dried HA powder particle is smooth and uniform; having microspheres morphology with broad size distribution.

On the other hand, Murtaza *et al*. (2012) successfully produced uniform HA particles with solid spherical shape via spray drying which is consistent with the reported study from Wang *et al*. (2009). However, Murtaza *et al*. (2012) obtained powders with narrow particle size distribution which is opposed to the results published by Wang *et al*. (2009). This could be due to different starting precursors were used in their experiments. Both studies emphasized that by manipulating process parameters like liquid feed rate, slurry viscosity, inlet air temperature and compressed air flow rate can affect the HA properties such as specific surface area, particle size, particle size distribution and powder morphology.

(d) ***Microwave Drying***

In the past 30 years, the research on microwaves has been popular in the food related field, treatment of biomass and biosolids, mineral processing, materials processing etc. (Decareau, 1985; Dorantes -Alvarez *et al*., 2000; Rodr ́guez *et al*., 2003; Yongsawatdigul & Gunasekaran, 1996; Lefeuvre, 1981; Moller & Linn, 2001; Shyju, 2010) due to its numerous advantages over the conventional method such as fast and rapid for extreme time and energy savings, material can be dried completely due to volumetric heating, it provides uniform energy distribution, it is specific only to certain substance (ie. water), it is environmental friendly as no harmful greenhouse gas emissions from the heat source (Srogi, 2006; Moller & Linn, 2001; Abd Rahman *et al*., 2009). Due to the abovementioned benefits, microwave is termed as potential alternative drying method to the conventional oven drying.

In conventional drying methods, the heat required to evaporate the moisture has to be transmitted inward through the moist material from the surface where this process is very time consuming (Venkatesh & Raghavan, 2004). This hurdle is eliminated in microwave drying, where internal heat generation phenomenon is the

source of drying. Microwave is an electromagnetic waves falls in the frequency range of 300 MHz to 300 GHz (Sun *et al*., 1994) that acts specifically on polar molecules like water. The charged portions of the water molecules move with respect to the rapid oscillating electric field of the electromagnetic waves. This rapid movement is realized as molecular vibrations that result in local kinetic heating in the core of the material in a very short period of time. The high temperature/heat in the core drives the evaporating liquid to the surface of the material, enabling the water movement and its subsequent removal from the material rapidly. This phenomenon is known as volumetric heating (Strumillo & Kudra,1986). The difference of microwave drying and conventional drying in terms of temperature profile is shown in Figure 2.12.

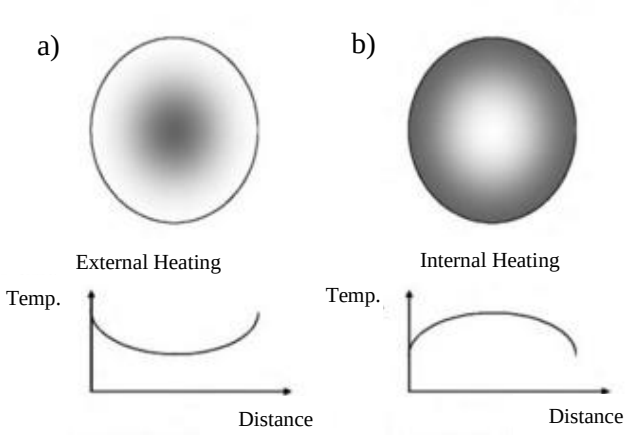

Figure 2.12: Temperature profile inside sample of (a) conventional drying (b) microwave drying (Hui, 2008).

Due to the advantages offered by microwave drying, it has been utilized in the drying of ceramics. Thevi *et al*. (2009) reported that milled mixture of β-TCP and $CaCO_3$ was rapidly dried using microwave oven for 60 – 70 minutes and followed by conventional sintering to form porous HA scaffolds. The sintered HA is highly crystalline and the elements exist are mainly calcium phosphorus coupled with a Ca/P ratio ranging from 1.62 – 1.69 which was confirmed by ICP-AES analysis. On

the other hand, Sundaram *et al*. (2008) showed that gelatin-starch with nano HA composite has been successfully fabricated via microwave drying for 40 – 45 minutes.

Most of the studies were focused on the use of microwave drying in fabricating porous HA scaffolds composite as stated above. Literature reports on the use of microwave in drying pure HA and the effects of microwave drying on the properties of the HA powder are limited. The only available study was done by Santhosh and Prabu (2012) who compared HA powders that dried in electric furnace at 80 ℃ for 8 hours with HA powder dried in domestic microwave oven at 480 W for 25 minutes. There was evident from their XRD analysis that no significant change in phase formation had occurred due to microwave drying. However, the size of HA crystallites produced by microwave drying were bigger than those produced by furnace drying. Microwave dried HA had crystallite size in the range of 34 – 102 nm as compared to 7 – 34 nm of the furnace dried HA. This was due to fact that ion-covalent materials such as HA is microwave sensitive which absorb the microwave power rapidly, causing the grain coarsening.

Besides bioceramics, microwave drying has been applied on engineering ceramics such as alumina and zinc oxide. Abd Rahman *et al*. (2009) have discussed the effects of microwave drying on the properties of alumina-zeolite foam. The ceramic slurry was obtained by mixing commercial alumina powder and zeolite with water and then underwent microwave drying in a common domestic microwave oven at 800 watts. It is worth mentioning that 7 minutes is sufficient to remove all the free and bound water from the material. The dried green bodies were subsequently sintered at 1350 ℃. In comparison to conventional oven drying, the linear shrinkage of the microwave dried foam is lower. In terms of flexural strength,

microwave drying shows significant improvement (2.11 MPa) compared to oven dried foam (0.76 MPa). The higher flexural strength of the microwave dried foam is attributed to its finer and smaller grains as evident in Figure 2.13.

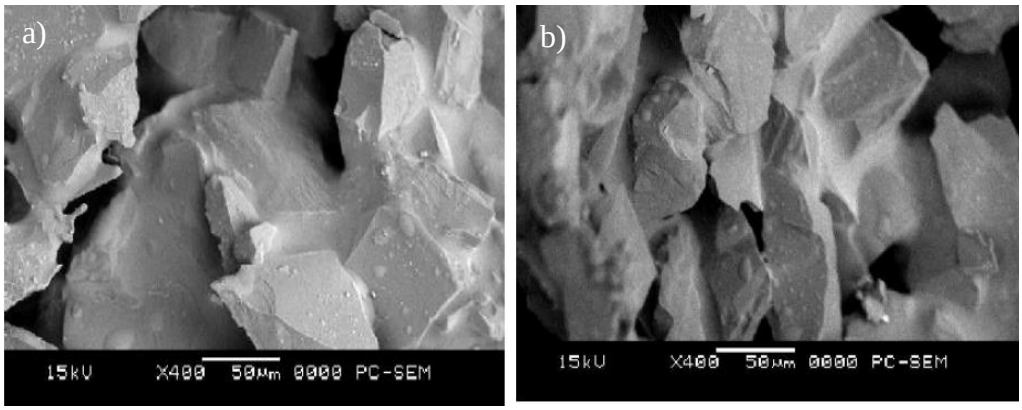

Figure 2.13: SEM micrographs of sintered foam from (a) conventional drying and (b) microwave drying (Abd Rahman *et al*., 2009).

On the other hand, Shirai *et al*. (2006) applied a rapid microwave drying technique on ZnO ceramic and the characteristics of the ceramic bodies were compared with those dried by conventional drying techniques. In their study, commercially available ZnO powder was dispersed in 60 vol% distilled water with 0.32 mass% of ammonium poly acrylilate dispersant and subjected to ball milling for 12 hours to obtain the ZnO slurry. After that, a batch of green bodies was dried at oven at 80℃ for at least 24 hours while another batch was dried in a microwave oven for 30 minutes. Upon drying, the green bodies were sintered in a conventional furnace at 1000℃. The authors noticed that only 30 minutes are required to eliminate all the water contents from the green bodies via microwave drying while in oven drying, 5 hours is necessary to remove all free and bound waters. Moreover, Shirai *et al*. (2006) reported that microwave drying produce sintered ceramic bodies with relative density that significantly higher than that of oven dried ceramic bodies.

In conclusion, microwave drying has shown promising results in enhancing the powder properties, densification and mechanical properties of ceramics within a short period of time. Hence, it has a great potential to be incorporated in the wet chemical synthesis of hydroxyapatite powder.

2.2.1.6 Other Synthesis Parameters

Besides the staring precursors, synthesis temperature, reaction pH, Ca/P ratio and drying methods, the effects of other synthesis parameters such as solvent used for the precipitation, the acid addition rate, the stirring and aging time were investigated by researchers too. The solvent/medium used for the precipitation process affects the morphology and particle size of the synthesized HA (Alobeedallah *et al*., 2011). Alobeedallah *et al*. (2011) found that HA particles formed from ethanol solution were rod like shape crystals while those synthesized in water had irregular to spherical shape particle. Besides, the HA crystal formed in ethanol was smaller than those prepare in water system.

The acid addition rate was found to have effects on the size of the formed HA crystal. Pham *et al*. (2013) conducted a study to investigate the effects of acid addition rate on the crystal size and phase of HA. The results concluded that the increase of acid addition rate could lead to the increasing HA crystal length. According to Pham *et al*. (2013), the faster the acid adding rate, the greater the frequency of reactant collisions, so larger HA crystals were created. In general, all the FTIR spectra with different dropping rates have similar shape and specific peaks corresponding to functional groups of HA (Figure 2.14). XRD results in Figure 2.15 confirmed that pure HA was synthesized regardless of acid addition rates.

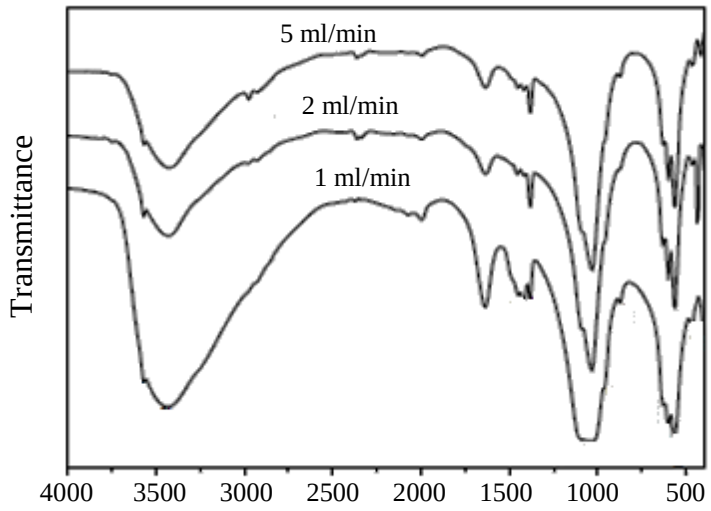

Figure 2.14: FTIR spectra of HA powder synthesized at different acid addition rate: 1, 2 and 5 ml min^{-1} (Pham *et al*., 2013).

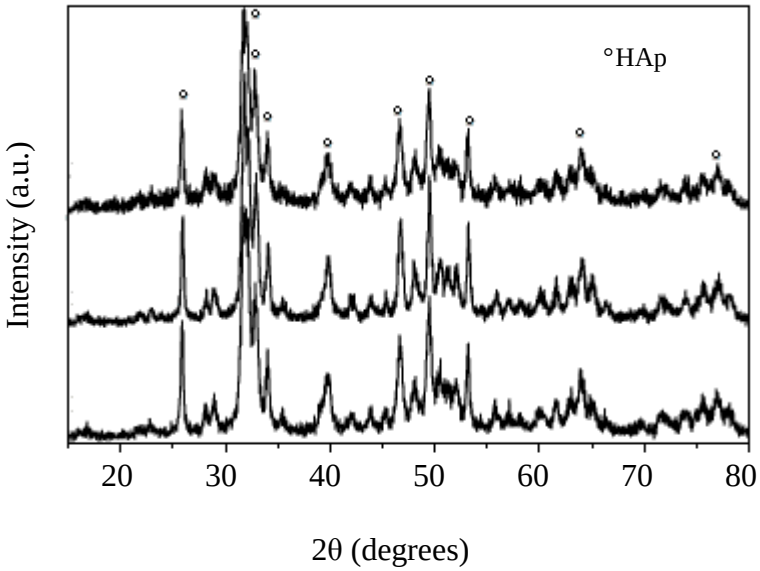

Figure 2.15: XRD spectra of HA powder synthesized at different acid addition rate: 1, 2 and 5 ml min^{-1} (Pham *et al*., 2013).

Stirring during the precipitation has found to have effects on the HA powder properties. Jarcho *et al*. (1976) reported that stirring of 24 hours or more gives the solution a Ca/P ratio close to the stoichiometric hydroxyapatite 1.67. In the study conducted by Santos *et al*. (2004), they claimed pure HA produced under vigorous stirring while biphasic HA/TCP was obtained under slow stirring. Moreover, a powerful

and high speed stirring would yield a good homogenous medium for the precipitation of HA (Afshar *et al*., 2003).

In terms of aging or settling time, Pham *et al*. (2013) investigated the effects of various settling time (0, 2, 15, 21 and 24 hours) on the HA powder properties. It was found that all the synthesized HA are pure HA with cylinder shape morphology regardless of the settling time. However, it does have effects on the particle size. The particle size reduced when the settling time increased from 0 to 15 hours and increased continuously up to 21 and 24 hours. Thus, the authors concluded that 15 hours is the optimal settling time to get the smallest HA particles powder.

2.2.2 Hydrothermal

The synthesis of HA powder through hydrothermal process involves the reaction of chemicals in an aqueous solution at elevated temperature (typically above water's boiling point) in a sealed vessel (pressure exceeds the ambient pressure) (Zhang *et al*., 2011; Manafi & Rahimipour, 2011; Yoshimura & Byrappa, 2008). Besides producing high crystalline and high purity HA powder, it has been reported that hydrothermal offers advantages such as low cost reagents, short reaction time and post heat treatment on HA powder is not required (Guo and Xiao, 2006; Guo *et al*., 2005; Zhang & Vecchio, 2007). In addition, hydrothermal synthesis can produce powders with different morphologies such as nanowire, sphere, nanobelt and prism-like particles (Zhu *et al*., 2008).

Liu *et al.* (1997) reported a simplified hydrothermal process of synthesizing high quality HA powders by utilizing a pressurized cooking utensil. According to this method, reagent grade $Ca(H_2PO_4)_2.H_2O$ and $Ca(OH)_2$ powders were ball-milled and dried under an infrared lamp and subsequently mixed with 2 litres distilled water in a commercially available pressurized pot at pressure of ~ 0.125 MPa and ~ 109 ^{o}for 1 – 3

hours. The reaction product was filtered, washed and dried at 90 ℃ to obtain HA powder. Some researchers used different combination of starting precursors such as $CaCO_3$ and $NH_4H_2PO_4$ (Orlovskii *et al*., 2002), $Ca_2P_2O_7$ and CaO (Li *et al*., 1994) and etc (Andres-Verges *et al*., 1998; Guo & Xiao, 2006) to produce HA powder.

Although, the hydrothermal process is able to produce single phase HA, this process is very time consuming and requires equipment that must be corrosion resistant, able to with stand high pressures and high temperatures and hence expensive compared to other methods.

2.2.3 Sol-Gel Method

Sol-gel method is one of the preferred method to produce HA powder due to the low synthesis temperature, homogenous molecular mixing of starting materials and effective in producing nanophasic HA. It needs strict control process parameters (Balamurugan *et al*., 2006) as it involves the molecular level mixing of the calcium and phosphorus. It has been reported that sol gel synthesized HA has enhanced stability at the bone interfaces *in vitro* and *in vivo* (Li *et al*., 1994). Moreover, the HA powder obtained via sol-gel method has high purity and large surface area with small particle size (Fathi *et al*., 2008; Hsieh *et al*., 2001, Wang *et al*., 2007). In general, sol gel process involves the creation of a three-dimensional, interconnected network, termed a "gel", from a suspension of very small, colloidal particles, called a "sol" (Chen *et al*., 2011; Ioitescu *et al*., 2009). One of the major disadvantages of this method is the complicated and lengthy process includes the mixing of alkoxides in either aqueous or an organic phase, aging at room temperature, gelation, drying, stabilization and post heat treatment (calcination).

The aging of the solution necessitate more than 24 hours to stabilize the solution system to enable the formation of monophasic HA (Liu *et al*., 2001). The need of long

aging time is in agreement with the studies carried out by Chai *et al*. (1998) and Liu *et al*. (2002). Apart from that, the high cost of the raw materials especially alkoxide-based precursors is also a major discouragement to researchers (Kim & Kumta, 2004). Eshtiagh-Hosseini *et al*. (2007) and Jillavenkatesa and Condrate Sr. (1998) reported that the generation of secondary phase like calcium oxide (CaO) is always found in sol-gel derived HA. The formation of CaO is unfavorable as CaO adversely affects the biocompatibility of HA. Besides CaO, insufficient aging or uncontrolled gelation and heat treatment may cause the generation of various impurities such as $Ca_2P_2O_7$, $Ca_3(PO_4)_2$ and $CaCO_3$(Eshtiagh-Hosseini *et al*., 2007; Hsieh *et al*., 2001).

2.2.4 Mechanochemical (Solid State Reaction)

Mechanochemical powder synthesis takes advantage of the perturbation of surface-bonded species by pressure to enhance thermodynamic and kinetic reactions between solids (Coreno *et al*., 2005; Mochales *et al*., 2004; Chen *et al*., 2004). This transformation is induced by mechanical milling of the precursors. During the process, the precursors subjected to the deep squeezing and crushing between the milling media or the milling media and the container wall while the molar ratio between the precursors is kept at the stoichiometric ratio. Phase transformations occur at room temperature as a high local heat is generated in the milling container during the milling process. The main processing variables include the following: (a) the type of milling equipment such as low energy ball mills, attrition mill, planetary and vibratory mills; (b) the type of milling medium; (c) the type and diameter of the milling balls; (d) the duration of the milling process; (e) the powder to ball mass ratio and (f) the type of starting precursors (Suchanek *et al*., 2002; Tian *et al*., 2008; Silva *et al*., 2004; Fathi & Mohammadi Zahrani, 2009; Honarmandi *et al*., 2010). Besides, mechanochemical method involves long heat-treatment times (post synthesis calcination) (Orlovskii *et al*., 2002; Suchanek *et al*., 1997; Naruporn Monmaturapoj & Chokchai, 2010). It offers advantages such as

simple, high productive, suitable for mass production and is cost effective (Pramanik *et al*., 2007). However, it has a few shortcomings such as long milling hours to ensure homogeneity of mixing materials, produces HA with low specific surface area and low sinterability (Suchanek &Yoshimura, 1998).

The commonly used starting precursors selected to prepare HA powder via this method includes dicalcium phosphate anhydrous ($CaHPO_4$), dicalcium phosphate dihydrate ($CaHPO_4.2H_2O$), monocalcium phosphate monohydrate ($Ca(H_2PO_4)_2.H_2O$), calcium pyrophosphate ($Ca_2P_2O_7$), calcium carbonate ($CaCO_3$), calcium oxide (CaO) and calcium hydroxide ($Ca(OH)_2$), etc. (Otsuka *et al.*, 1994; Chaikina, 1997; Rhee, 2002). Silva *et al*. (2003) carried out mechanochemical synthesis in planetary mill with different types of precursors combinations and they found out that the following reactions successfully produced single phase nano-sized HA powder.

$$3Ca_3(PO_4)_2.xH_2O + Ca(OH)_2 \Rightarrow Ca_{10}(PO_4)_6(OH)_2 + xH_2O \quad (2.4)$$

$$10Ca(OH)_2 + 3P_2O_5 \Rightarrow Ca_{10}(PO_4)_6(OH)_2 + 9H_2O \quad (2.5)$$

$$4CaCO_3 + gCaHPO_4 \Rightarrow Ca10(PO_4)_6(OH)_2 + 2H_2O + 4CO_2 \quad (2.6)$$

In order to find a suitable medium for mechanochemical, Rhee (2002) compared the results when either water or acetone was used as the medium. Rhee concluded that pure HA powder could be obtained after milling for 8 hours using water as milling medium while powders attained through acetone as milling medium revealed the presence of β-TCP. In another work, Yeong *et al*. (2001) used ethanol as the milling medium and the milling process has to be extended to 20 hours in order to produce pure HA powder. Thus, water is favourable in producing pure HA powder via mechanochemical reaction.

2.2.5 Other Processing Techniques

There are also alternative techniques for preparation of HA powder, such as spray-pyrolysis (An *et al.*, 2007; Cho *et al*., 2008; Itatani *et al*., 2010), electrocrystallization technique (Manso *et al*., 2000; Shirkhanzadeh, 1994), emulsion route (Zhang & Cooper, 2005; Yang *et al*., 2011; Jarudilokkul *et al*., 2007), self propagating combustion synthesis (Tas, 2000; Sasikumar *et al*., 2010), hydrolysis route (Shih *et al*., 2006; Monma & Kamiya, 1987) and microwave hydrothermal route (Pushpakanth *et al*., 2008; Han *et al*., 2006).

These methods have the ability to synthesize HA powder with varying degree of purity, crystallinity, morphology and stoichiometry. However, there are some major drawbacks of these methods such as time consuming and complex methodology, requires special and expensive equipment and high cost of starting precursors which make them unsuitable for mass production (Pushpakanth *et al*., 2008; Cao *et al*., 2005; Wang *et al*. 2007).

In summary, it is well established that the processing of ceramics is complicated by the number of steps typically required for manufacture and the need to optimize the processing steps. The processing of ceramics is extremely important because ceramics are basically flaw intolerant materials. As a result, minor chemical and physical defects can severely degrade properties. Proper selection of raw materials and processing conditions is especially important in ceramics because mistakes generally cannot be corrected during the firing and post-firing processes.

Thus, there is a great need for a simple, reliable and reproducible synthesis technique to manufacture a high purity and crystalline hydroxyapatite powder which has a good sinterability at low firing temperatures coupled with superior mechanical properties suitable for biomedical applications.

CHAPTER 3: THE SINTERING AND SINTERABILITY OF HYDROXYAPATITE

3.1 Powders Consolidation (Sintering) Techniques

One of the main methods to produce bulk hydroxyapatite (HA) is sintering process (Prokopiev & Sevostianov, 2006). Sintering process is a consolidation process that eliminates the intra- or inters- agglomerate pore of material and brings the individual particles together to form a solid body (Uhlmann *et al*., 1976). It has been reported that sintered HA has high density (Ramesh *et al*., 2007c) than non-sintered HA and can form tight bonds with bone tissue (Stea *et al*., 1995). To date, various consolidation techniques have been developed to sinter bulk HA such as conventional pressureless sintering (CPS), microwave sintering (MS), hot pressing sintering (HPS), spark plasma sintering (SPS) and two steps sintering (TSS).

3.1.1 Conventional Pressureless Sintering (CPS)

Conventional pressureless sintering (CPS) is performed in a conventional programmable furnace and it is a widely used consolidation method on hydroxyapatite (HA) owing to its practicability and simplicity (Wang & Chaki, 1993). However, the main problem associated with this method is the generation of thermal stress which leads to the formation of microcracks in the HA specimen (Prokopiev & Sevostianov, 2006). To avoid this problem, the employed ramp rate must be less than 5 ℃/min, and thus, makes CPS a very time consuming process. Furthermore, high sintering temperature and long holding time required in CPS not only lead to the production of large grain HA (Mazaheri *et al*., 2008), but also promote the decomposition of HA into secondary phases. The presence of secondary phases can hinder the mechanical properties of HA (Wang & Chaki, 1993). Due to these drawbacks, other alternatives such as MS, HPS, SPS and TSS are introduced.

3.1.2 Microwave Sintering (MS)

Microwave energy provides advantages in various industries such as fast and rapid, time and energy saving, complete drying of material and environmental friendly. In terms of sintering, microwave sintering (MS) serves as alternative to the common conventional pressureless sintering (CPS) and has been applied successfully to sinter various types of ceramics (Clark & Sutton, 1996; Agrawal, 1998; Leparoux *et al*., 2003). In MS, the density of the material can be enhanced to higher level than would be achieved in CPS at the same temperature (Agrawal, 2006; Wang *et al*., 2006). MS also requires less sintering time and less energy consumption. In addition, MS enhanced the microstructure and mechanical properties of ceramics by inhibiting the excessive grain growth (Ramesh *et al*., 2007a). Both CPS and MS provide heat to the material in order for them to densify. However, they work differently in terms of the heat transfer profile. Heat is transferred to the ceramics via conduction, convection and radiation from the surface into the interior of the ceramics in CPS (Figure 3.1 (a)). In contrast, MS demonstrates inverse temperature flow as electromagnetic radiations are transformed into heat inside the core of the ceramic and subsequently transported to the surface from the core as shown in Figure 3.1 (b).

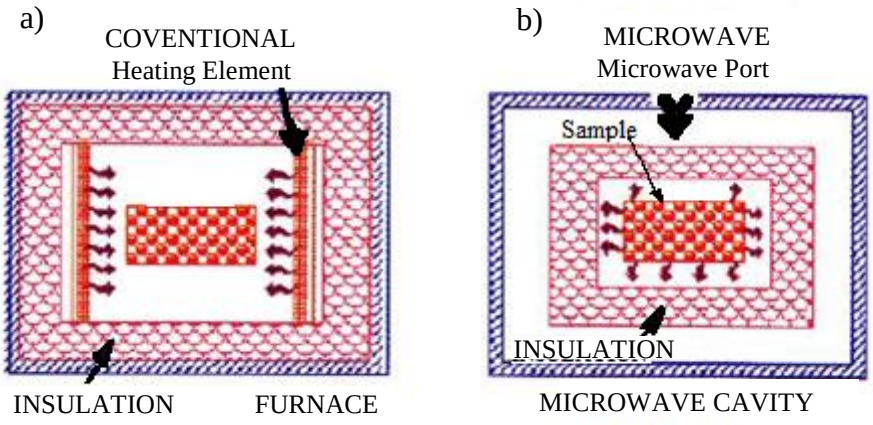

Figure 3.1: Comparison of heating procedure between (a) Conventional sintering and (b) Microwave sintering (Agrawal, 2006).

In Chapter 2, the application of microwave energy is mainly on drying which involved the use of domestic microwave oven where the water molecules are excited to generate heat. In microwave sintering, heat produced due to the interaction between the microwaves with the ceramics without the assist of water molecules. Unlike microwave drying, microwave sintering requires much higher temperature and higher heating rate.

Materials are divided into two main categories in terms of MS, namely conductive materials or resistive (dielectric) material (Vollmer, 2004). When microwave strike the interface of materials, some of the energy is reflected. Conductive materials such as metals reflect nearly all of the microwave energy and hence, metals are considered to be opaque to microwaves as shown in Figure 3.2 (a). On the other hand, most ceramics are dielectric (insulators) materials that contain atoms and molecules where the electrical charges are bound. They create dipole by slightly displaced from their original position. Therefore, dipole alignment is the primary mechanism in the conversion of microwave energy to heat energy (Groza, 2007). Basically, the molecular dipoles are said to be polarized when they tend to align themselves along the field lines when subjected to the uniform electric field. In slow oscillating field (few hundred hertz), the dipoles oscillate with the field but no significant heat was generated due to small amounts of friction (Grant & Halstead, 1998). However, when ceramics interact with a very fast oscillating field like microwave (2.45 GHz), the dipoles will reverse their orientation each time the field reverses (few billions times per second) and this energy dissipated from the electromagnetic field is converted into heat by dipoles molecular friction and collision. This is known as dielectric loss. If there is a sufficient dissipation of the energy as the electromagnetic waves travel through the material, the energy is absorbed (Figure 3.2 (b)) and dielectric heating occurs just like the case in ceramic materials (Lidström *et al.*, 2001).

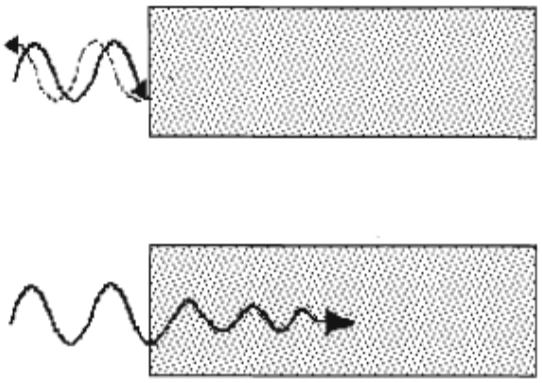

Figure 3.2: Schematic diagram of the main ways that microwaves can interact with materials (Sutton, 1989).

Although MS is advantageous in various aspects, a major problem has been encountered in the MS of hydroxyapatite (HA) as HA lacked of microwave susceptibility at ambient temperature due to their loss factor and low thermal conductivity (Del Regno, 2006; Lasri *et al*., 2000). Below critical temperature, HA is poor absorber and it needs to be heated up to a critical temperature to become microwave absorbent (Edabzadeh & Valefi, 2008; Haung *et al*., 2009). This problem can be overcome by using an external susceptor to initiate the heating. Susceptor is an excellent microwave absorber and it supplies heat to HA by absorbing microwave up to a temperature high enough that HA starts to absorb the microwave and heat by itself (independent of suspector).

The most common susceptor materials used in the microwave sintering of HA are silicon carbide (SiC) and zirconia (ZrO_2) (Nath *et al*., 2006; Fang *et al*., 1994; Vijayan & Varma, 2002; Bose *et al*., 2010; Yang *et al*., 2002; Ramesh *et al*., 2008, Ramesh *et al*., 2007a). All these authors used either zirconia or SiC as susceptor to sinter the HA in microwave furnace. They found that MW has substantial effects on the densification,

microstructure, phase stability and mechanical properties on the sintered HA compared to CPS.

For instance, Ehsani *et al.* (2013) experimented sintering on HA using both MS and CPS technique. The authors reported that with MS, densification began at 900 ℃ which was 100 ℃ lower than for CPS. MS-HA obtained higher density than CPS-HA throughout the sintering regime and met plateau at temperature above 1300 ℃ as shown in Figure 3.3.

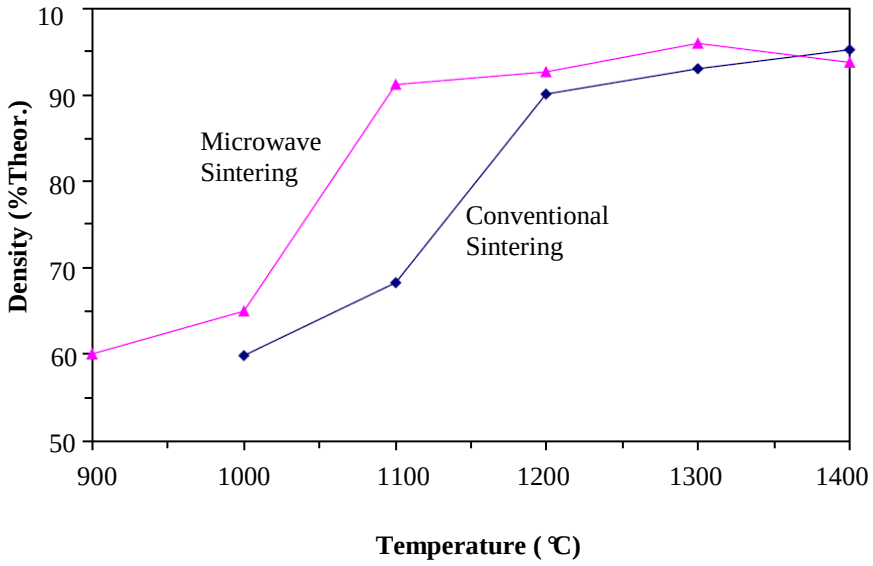

Figure 3.3: Comparative sintering curves for HA sintered by microwave and conventional heating (Ehsani *et al*., 2013).

The beneficial effect of MS in densification of HA is in agreement with the experiment carried out by Nath *et al*. (2006). In their study, the density of MS-HA was higher than that of CPS and maximum relative density of 99% was obtained by MS-HA at 1000 ℃ sintered for 30 minutes. At the similar temperature, CPS-HA could attain only 96.99% albeit being sintered for 3 hours. Although the density of MS-HA is higher, MS-HA sintered at 1100 ℃ has grain size of about ~20 – 30 μm, which significantly bigger than that of CPS-HA (5 – 10 μm) at the same temperature.

However, Ramesh *et al*. (2008) reported that the densification of CPS-HA was higher than MS-HA although the grain size was finer for the latter as shown in Table 3.1 and Figure 3.4, respectively.

Table 3.1: Total sintering time taken to achieve the respective sintered density based on the two different sintering techniques (Ramesh *et al*., 2008).

Sintering Temperature (℃)	CPS		MS	
	Relative density (%)	Time taken (min)	Relative density (%)	Time taken (min)
1000	96.8	1090	90.8	29.4
1050	98.4	1140	95.2	30.4
1100	99.0	1190	96.5	31.4
1150	99.0	1240	96.7	32.4
1200	99.0	1290	96.6	33.4
1250	99.1	1340	97.0	34.4
1300	99.0	1390	98.0	35.4

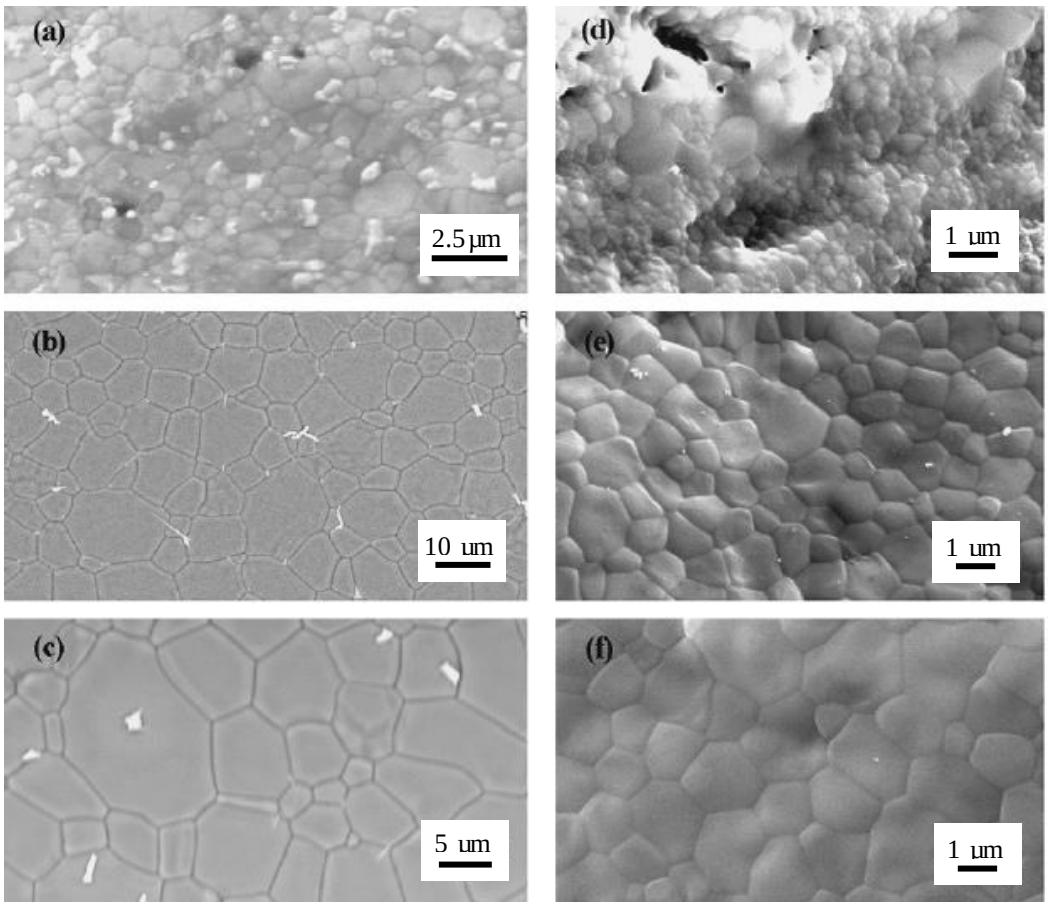

Figure 3.4: Microstructural evolution of CPS-HA (a-c) and MS-HA (d-f) when sintered at 1150 ℃ (a,d), 1250 ℃ (b,e) and 1300 ℃ (c,d) (Ramesh *et al*., 2008).

The fine and smaller grain size of MS-HA was the main factor contributed to the high fracture toughness of MS-HA. Overall, throughout the sintering regime, MS-HA obtained fracture toughness higher than CPS-HA, ranging from 1.24 $MPam^{1/2}$ to 1.45 $MPam^{1/2}$ while CPS-HA attained value from 0.91 to 1.22 $MPam^{1/2}$. The author concluded that MS not only improved the toughness and microstructure of HA, it significantly reduced the time taken to sinter the samples as shown in Table 3.1.

In terms of phase stability, Harabi *et al*. (2010) found that HA starts to decompose into TCP when microwave sintered at 1050 ℃ and the percentage of this phase was increased from 46% to 61% when the sintering temperature increases from 1050 ℃ to 1100 ℃, respectively. For samples sintered at 1150 ℃ and above, the TCP slowly

transformed into α-TCP. The XRD pattern of the microwave sintered HA at various sintering temperature is presented in Figure 3.5. The author claimed that this decomposition is due to the higher heating efficiency of microwave heating. This work is in contrary to research carried out by previous workers (Yang *et al*., 2002; Ramesh *et al*., 2008; Ramesh *et al*., 2007a) as they did not found a significant HA decomposition.

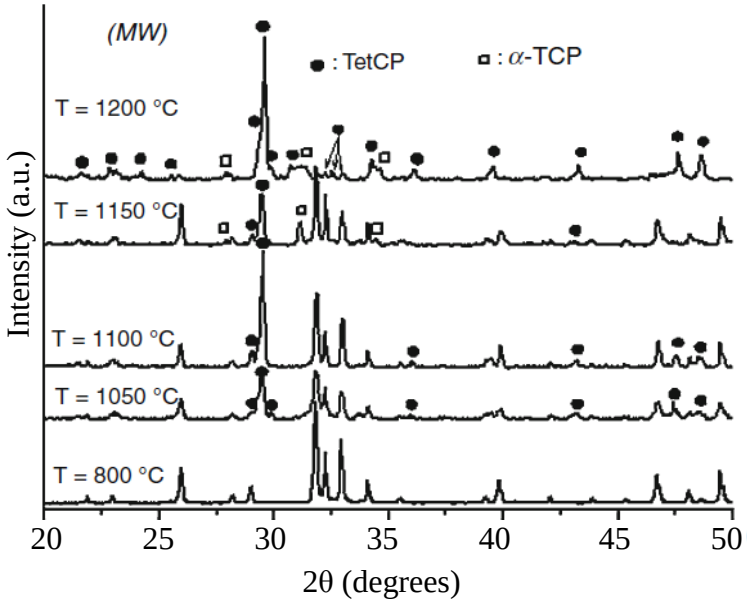

Figure 3.5: XRD of HA sintered at different temperatures for 15 minutes, using MS (Harabi *et al*., 2010).

In summary, MS has beneficial effects on the sinterability of HA (Vijayan & Varma, 2002; Bose *et al*., 2010; Ramesh *et al*., 2007a; Dasgupta *et al*., 2013; Mangkonsu *et al*., 2016). It can be concluded that HA compacts of certain green density can be sintered by microwave irradiation to high densities (> 96% of theoretical density), high hardness (> 4.19 GPa), high fracture toughness (> 1.3 $MPam^{1/2}$) and fine grain size (nano to micron size) within a short period of time (5 – 30 minutes). Besides that, in most of the studies, MS also did not alter the phase stability of the sintered HA throughout the employed sintering profile. In all cases, pure HA is recorded and no sign of the presence of TCP or any other phases is observed.

3.1.3 Spark Plasma Sintering (SPS)

Spark plasma sintering (SPS) is a rapid sintering method that uses self-heating phenomena of the ceramic powder where green compacts are subjected to arc discharges produced by a high energized electric current. Xu *et al*. (2007) studied the sintering behaviour of HA prepared by CPS and SPS. With CPS at 1200 ℃ for 5 hours and 10 ℃/min heating rate, relative density of 90.6% was obtained whereas a relative density as high as ~96.3% was successfully attained by employing SPS at 1100 ℃ for only 3 minutes with 100 ℃/min heating rate. Gu *et al*. (2002) on the other hand managed to obtain HA with high relative density (~99.5%) and high fracture toughness (1.25 $MPam^{1/2}$) at 950 ℃ in 5 minutes using SPS technique. However, HA decomposed into β-TCP at temperature beyond 1000 ℃. The low thermal stability of SPS-HA is in agreement with the research by Cuccu *et al*. (2015). They reported that SPS accelerated the decomposition of HA at 800 ℃ where the phase transformed drastically from biphasic HA-TCP into β-TCP phase and at 1200 ℃, the main phase was β-TCP rather than HA as shown in Figure 3.6.

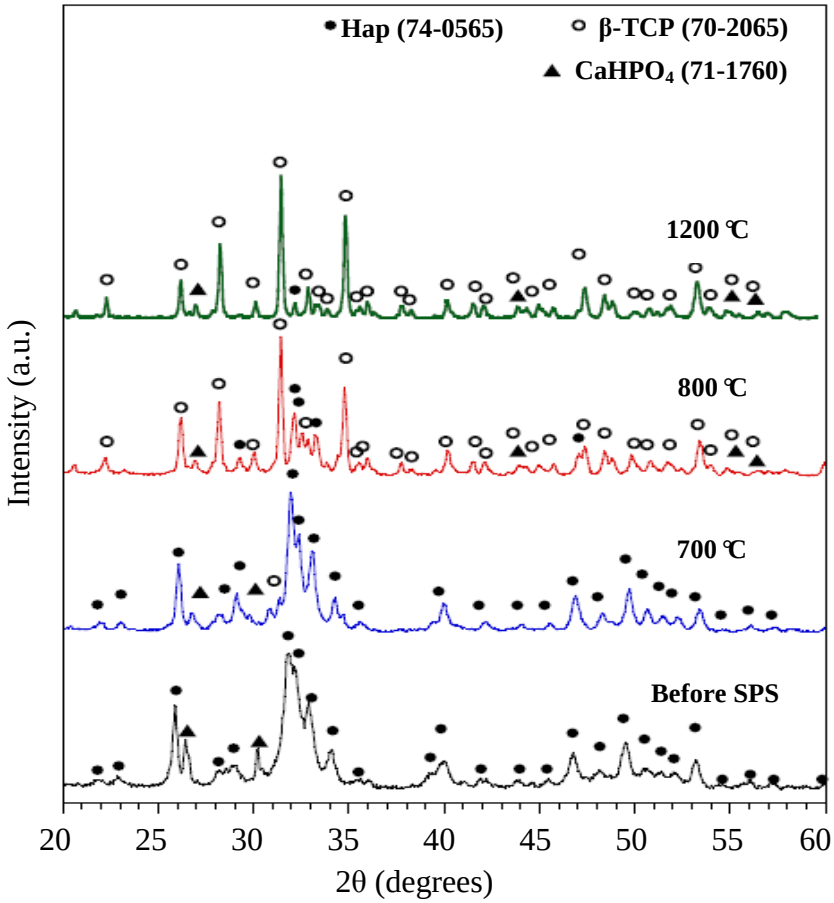

Figure 3.6: Comparison of XRD patterns before and after consolidation by SPS at 75 ℃/min (Cuccu *et al*., 2015).

It has been well known that SPS successfully sintered HA with higher density in a significantly shorter sintering time and lower sintering temperature compared to CPS. In spite of these advantages, sophisticated and expensive equipment is required for SPS which cast a shadow on the mass production of this method (Mazaheri *et al*., 2009).

3.1.4 Hot Pressing Sintering (HPS)

Hot pressing is one of the pressure assisted sintering method that can enhance the densification of HA while limiting grain growth. Veljović *et al*. (2008) made comparison study between HPS and CPS of HA. Dense HA ceramics with fine grain size (ranging from 50 nm to 380 nm) were produced by hot pressing HA green compacts at 20 MPa and temperature of 950 ℃ and 1000 ℃ for 2 hours.

On the other hand, CPS of HA at 1000 ℃, 1050 ℃, and 1100 ℃ resulted in compacts having porous microstructure. Moreover, the fracture toughness and microhardness of HA attained through CPS was only 0.28 $MPam^{1/2}$ and 2.39 GPa, respectively. For the HPS-HA, both fracture toughness and microhardness were greatly higher, marked at 1.52 $MPam^{1/2}$ and 4.30 GPa. The authors also found that HPS did not affect the phase stability of HA as no decomposition was observed.

This result was in agreement with the study carried out by Rapacz-Kmita *et al*. (2005) who noticed that no decomposition into secondary phases occurred for HA samples sintered through neither HPS nor CPS. Nonetheless, dehydroxylation was observed from CPS-HA sintered at 1300 ℃ where OH^- groups in the HA structure, correspond to the band at 635 cm^{-1} is missing as shown in Figure 3.7 (b) as compared to the hot pressed HA (Figure 3.7 (a))

(a)

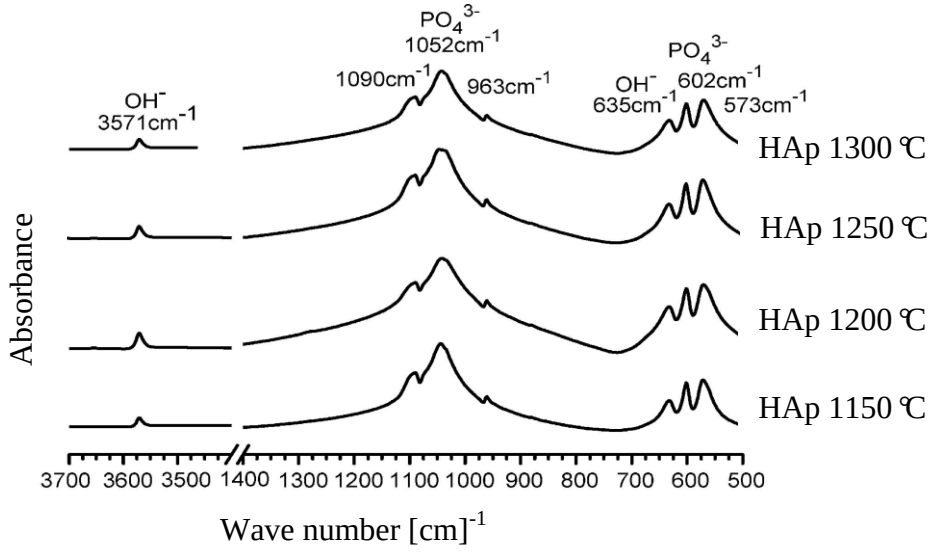

(b)

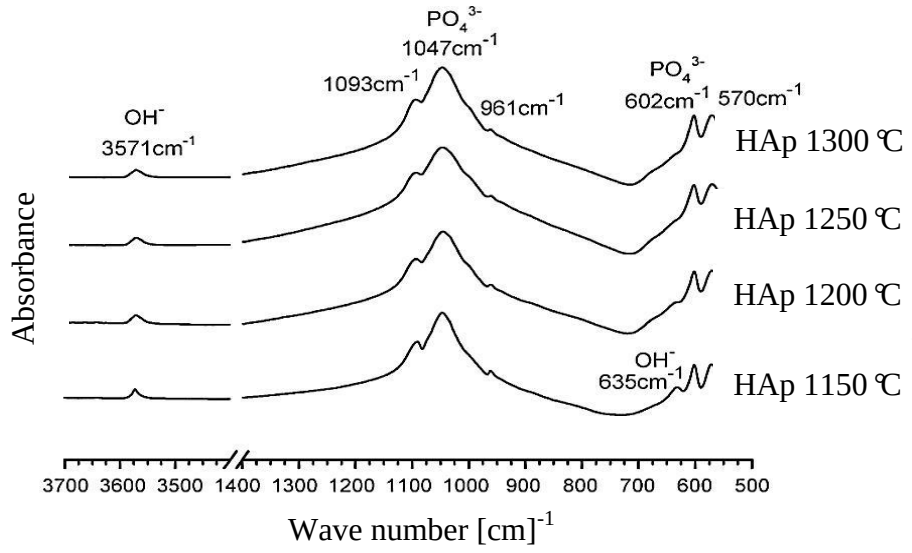

Figure 3.7: Comparison between FTIR spectra of (a) hot pressed and (b) pressureless sintered HA samples at various sintering temperatures (Rapacz-Kmita *et al*., 2005).

3.1.5 Two Steps Sintering (TSS)

Another novel method to control the grain growth of HA especially at the final stage of sintering is called two steps sintering (TSS) which was first proposed by Chen and Wang (2000). This is a modified pressureless sintering technique which suppresses the grain boundary migration that responsible for grain growth while keeping grain boundary diffusion for densification. This method modifies sintering regimes as followed: high temperature (T_1) sintering that could sinter the sample to a critical relative density of ~70% and followed by rapid cooling at lower temperature (T_2) until the densification is completed. This method was also applied by Mazaheri *et al*. (2009) to control the exaggerated grain growth of HA nanopowder compacts. In order to achieve dense HA specimen, CPS requires sintering temperature higher than 1100 ℃ while TSS requires only 900 ℃ for T_1 and 800 ℃ for T_2 to obtain full dense HA samples (>98%). The densification, grain growth and mechanical properties of CPS-HA and TSS-HA are compared and tabulated in Table 3.2. The high fracture toughness of TSS-

HA was due to the effectiveness of TSS in supressing the grain growth compared to CPS as shown in Table 3.2. Regarding the reduction of the grain size from 1.7 μm (CPS) to 190 nm (TSS), the fracture toughness increased from 0.98 ± 0.12 $MPam^{1/2}$ to 1.92 ± 0.20 $MPam^{1/2}$ which is almost 95% of increment.

Table 3.2: Mechanical properties of HA sintered via CPS and TSS (Mazaheri *et al*., 2009).

	CPS	TSS
Fractional Density (%)	98.3	98.8
Grain Size (μm)	1.7	0.19
Hardness (GPa)	7.06 ± 0.27	7.8 ± 0.41
Fracture Toughness ($MPam^{1/2}$)	0.98 ± 0.12	1.92 ± 0.20

The considerable grain size reduction can also be observed in the SEM micrograph of the TSS-HA in Figure 3.8 (a) while a coarse grained microstructure was obtained by the CPS-HA as shown in Figure 3.8 (b).

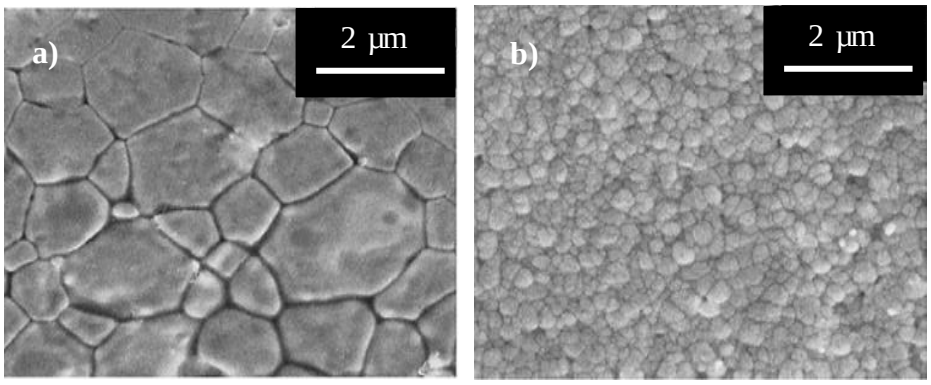

Figure 3.8: SEM micrographs of HA compacts sintered under (a) CPS at 1100 ℃ and (b) TSS at T_1 = 900 ℃ and T_2 = 800 ℃ (Mazaheri *et al*., 2009).

3.2 Sintering Temperature

Sintering temperature is reportedly able to develop densification by providing activation energy for consolidation of materials (Lu, 2008). Green bodies need to be sintered up to a certain temperature to initiate the densification process. Nonethelss,

when surplus activation (due to elevated sintering temperature) supplied to material, severe grain enlargement or decomposition of material began (Muralithran & Ramesh, 2000).

Petrakova *et al*. (2013) investigated the sinterability of HA at temperature range from 900 ℃ to 1400 ℃. It was observed that the porosity of the samples decreased with increasing temperature but to the detriment of grain growth as perceived in Figure 3.9. However, the relative density and microhardness increased proportionally to the sintering temperature as shown in Figure 3.10. The authors hence concluded that the strength of HA was dependent on the porosity and density of the samples rather than the grain size.

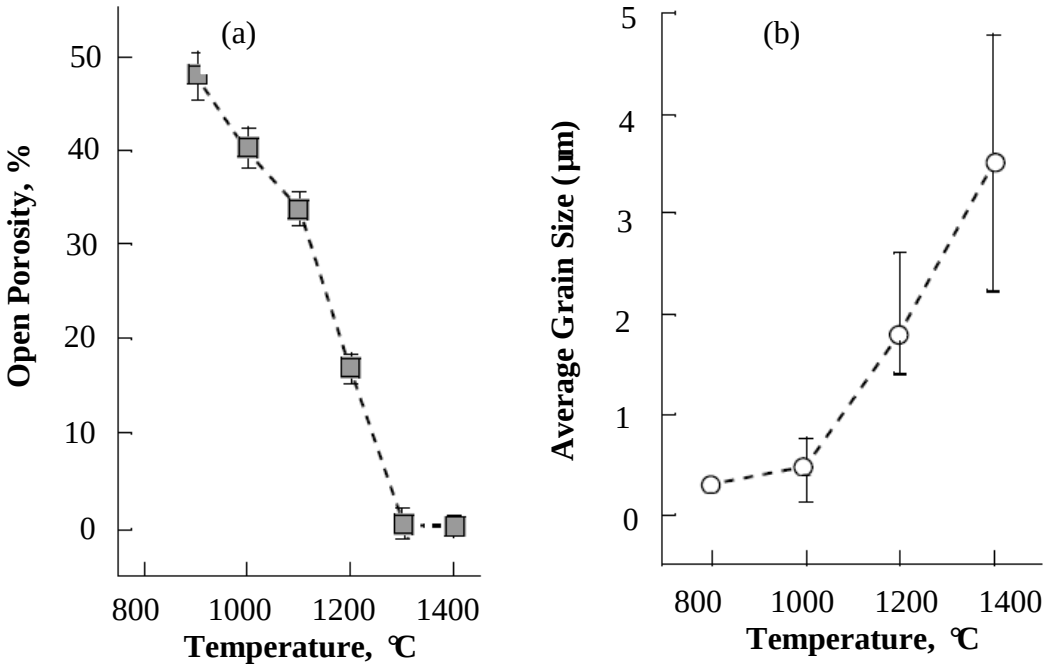

Figure 3.9: Temperature dependence of (a) open porosity and (b) average grain size of hydroxyapatite (Petrakova *et al*., 2013).

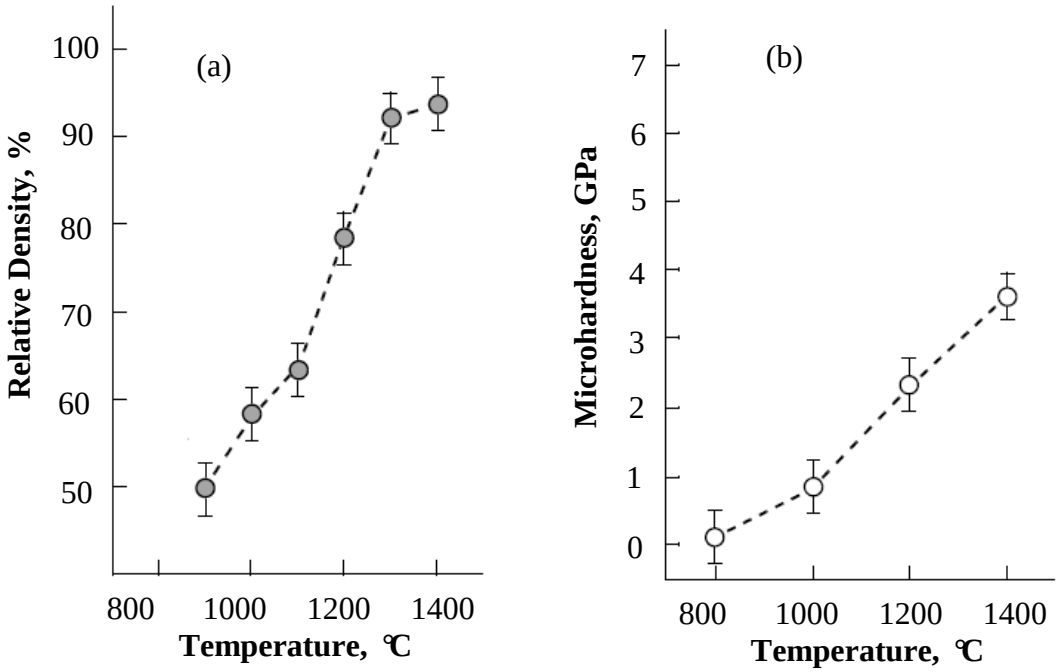

Figure 3.10: Temperature dependence of (a) relative density and (b) microhardness (Petrakova *et al*. 2013).

However, Muralithran and Ramesh (2000) had different findings in terms of the relationship between the hardness, density and grain size. The author reported that below ~ 2 μm, the hardness trend correlated well with the change in relative density i.e. hardness increases steadily with relative density (Figure 3.11). However, above 2 μm, the variation in hardness seem not be in agreement with the density curve as the relative density was found to remain constant at ~98% while the hardness gradually decreased with increasing grain size. Hence, it is hypothesised that below some critical grain size, the hardness is governed by density and grain size is the controlling parameter when the grain size is above the critical grain size.

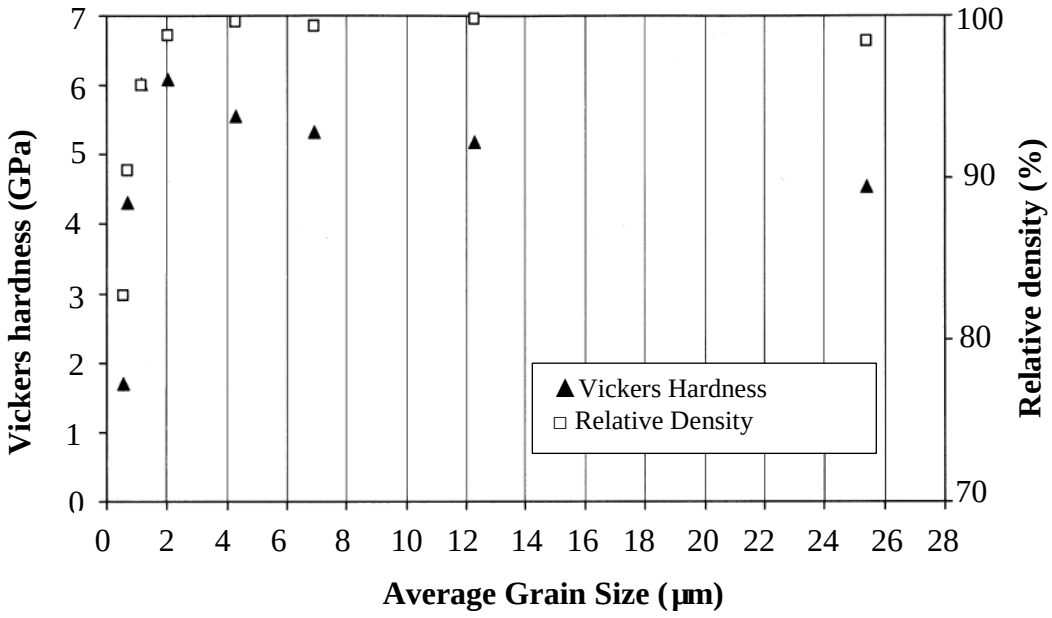

Figure 3.11: Variation of Vickers hardness and relative density as a function of average grain size (Muralithran & Ramesh, 2000).

The author concluded that the optimum sintering temperature was at 1250 ℃; having relative density of > 99% and microhardness of ~ 6 GPa. SEM examination of HA samples sintered below 1200 ℃ showed the presence of large pores which explained the low bulk density of these samples at low temperature. Besides, the author found that high sintering temperature can disrupt the phase stability of HA as decomposition of HA into TCP was detected at 1400 ℃. Similarly, Zhou *et al*. (1993) reported that sintering HA at elevated temperature has the tendency to results in the decomposition of HA phase. They reported that the dehydroxylation of HA starts at sintering temperature between 1200 ℃ to 1400 ℃ as OH^- were depleted gradually. The thermal dehydroxylation and decomposition of HA results correlated well with the findings reported by Ramesh *et al*. (2016) as shown in Figure 3.12 where α-TCP and TTCP was detected at 1300 ℃.

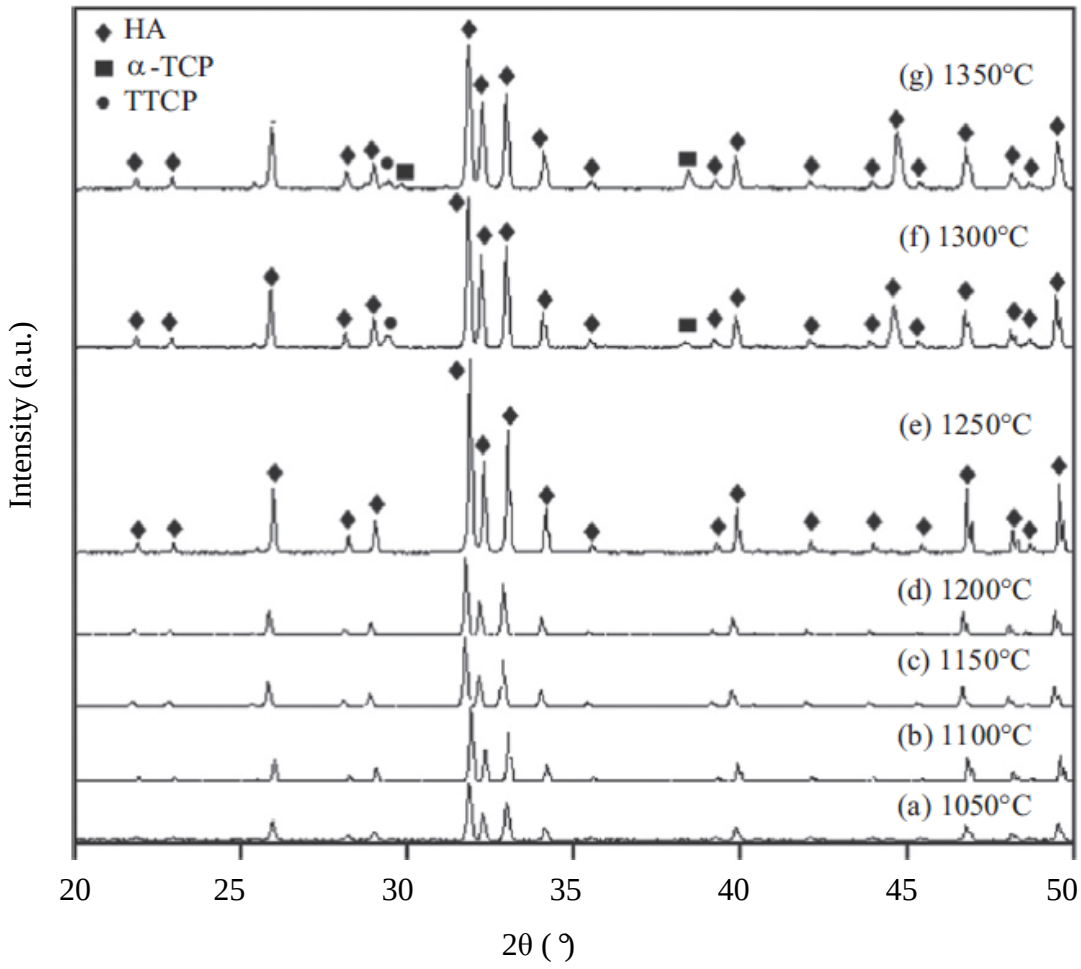

Figure 3.12: XRD patterns of HA derived from eggshells sintered at temperatures ranging from 1050 ℃ to 1350 ℃ (Ramesh *et al.*, 2016).

Besides densification and hardness, sintering temperature has great influence on the toughness of HA. Kamalanathan *et al*. (2014) found that sintering temperature has effects on the fracture toughness of HA as shown in Figure 3.13.

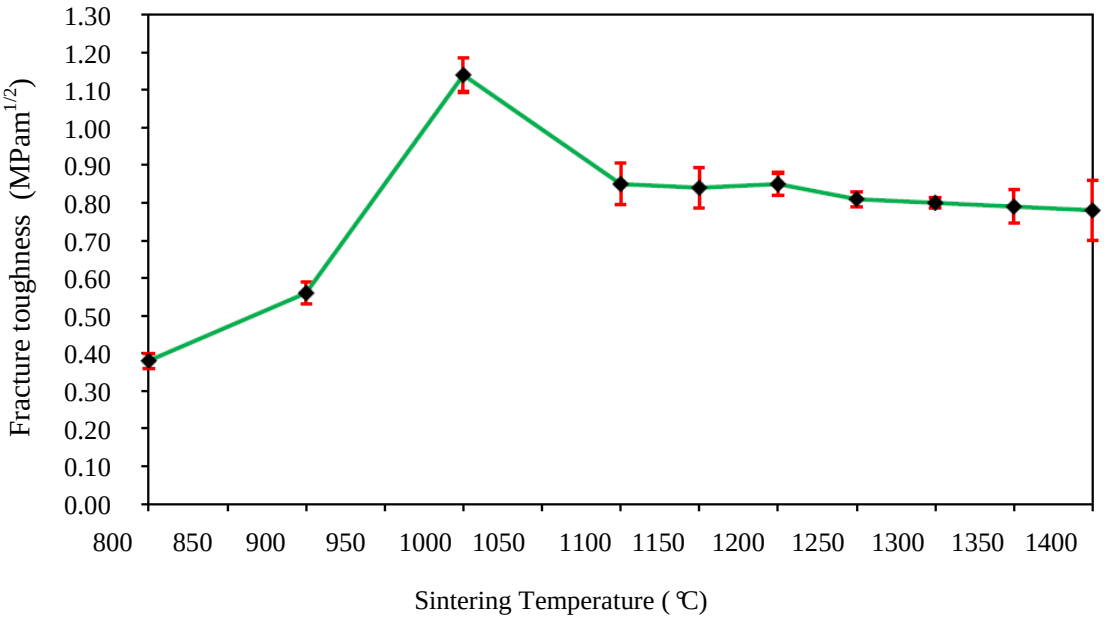

Figure 3.13: The variation of fracture toughness of conventional pressureless sintered EHA as a function of sintering temperature (Kamalanathan *et al*., 2014).

The authors noted a trend where the fracture toughness increased with sintering temperature and peaked at 1.14 $MPam^{1/2}$ at 1000 ℃ and then decreased with further increase in temperature as shown in Figure 3.13. At 800 ℃ and 900 ℃, the fracture toughness values were low at 0.38 $MPam^{1/2}$ and 0.56 $MPam^{1/2}$ respectively. This low value at such low temperatures could be attributed to the weak grain boundaries of the HA matrix. The author inferred that the variation of the fracture toughness with sintering temperature was due to the grain size as toughness increased with an increase in grain size as temperature rises. Small grain size reduces the inherent flaw size of the sintered microstructure which then improves the mechanical property of HA (Wang & Shaw, 2009). In a view of the above study, it can be concluded that further rising in the sintering temperature gave adverse effects on the mechanical properties of HA by the virtue of serious grain growth.

3.3 Sintering Time

The nominal sintering time chosen is critical to ensure favourable densification of ceramic body is achieved. Tolouei *et al*. (2011) carried out sintering of HA using dwell times of 1 minute and 120 minutes. They found that at lower sintering temperature like 1000 ℃, long holding time (120 minutes) produced HA with higher density than short holding time (1 minutes). However, at sintering temperature above 1000 ℃, both 120 minutes and 1 minute holding time produced HA samples with almost equivalent densities. Besides, the fracture toughness of HA sintered with short holding time was higher than those sintered at long holding time. This is because shorter holding time reduced the jeopardy of extreme grain growth which tends to deteriorate the toughness of HA. The use of short holding time is contradict to experiment conducted by Liu *et al*. (1997) who stated that the HA samples could attained relative density of more than 98% at 1200 ℃ for 2 hours. The need for 2 hours of holding time is supported by Veljović *et al*. (2009) as they claimed that samples sintered for 45 minutes exhibited porous microstructure (Figure 3.14 (a)). By prolonging the dwell time to 2 hours, porosity decreased as shown in Figure 3.14 (b). However, HA samples showed sign of fracture when sintering time prolonged to 8 hours.

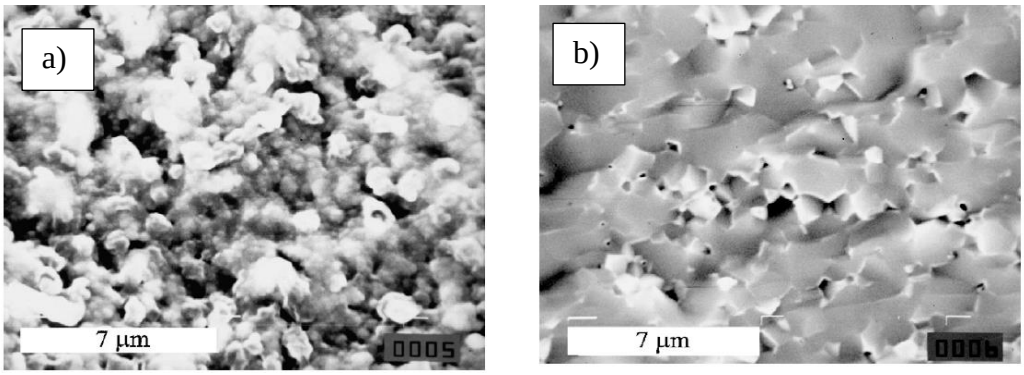

Figure 3.14: SEM micrograph of sample sintered at 1050 ℃ for (a) 45 minutes and (b) 2 hours (Veljović *et al.*, 2014).

3.4 Sintering Ramp Rate

Sintering ramp rate is another intrinsic part of sintering that could affect the microstructural condition of the sintered HA as heat transferred to ceramics body due to thermal gradient (Chu *et al*., 1991). Some researchers reported that higher ramp rate have positive effects in retaining relatively fine microstructure at high sintered densities (Brook, 1982; Johnson, 1984). Controversial discussion performed by Ramesh *et al*. (2007c) and Prokopiev & Sevostianov (2006). These authors recommended that the heating rate mustn't be too high above as excessive heating rate leads to thermal stress. This thermal residual stress will propagate microcracks and slowly to macro-cracks in sintered bodies (Pramanik *et al*., 2007). This is in agreement with the study carried out by Samuel *et al*. (2012) who reported that HA decomposition in their work is due to the thermal stresses generated by accelerated ramp rates. They found that at high temperature of 1300 ℃, HA sample sintered with a low ramp rate (2 ℃/min) maintain pure HA phase as shown in Figure 3.15 (a) while HA decomposition to β-TCP was confirmed in the HA sample sintered with ramp rate of 5 ℃/min as presented in Figure 3.15 (b). A further increase in ramp rate (10 ℃/min) resulted in the transition of β-TCP into α-TCP as shown in Figure 3.15 (c). Gibson *et al*. (2001) supported this finding by highlighting the decomposition of HA was associated with partial dehydroxylation due to the rapid heating rate, resulting in partial decomposition of the HA to TCP.

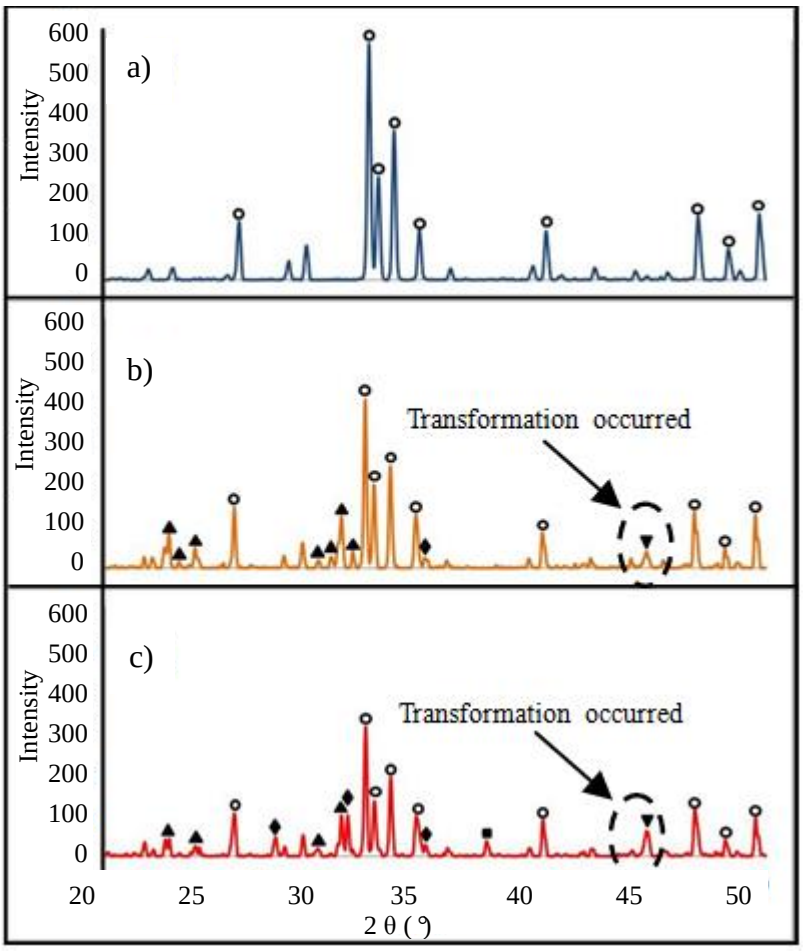

Figure 3.15: XRD patterns of HA sintered at 1250 ℃ with ramp rate of (a) 2 ℃/min, (b) 5 ℃/min and (c) 10 ℃/min (Keys: ○ = HA, ▲ = α-TCP, ▼= β-TCP ♦ = TTCP and ■ = CaO) (Samuel *et al.*, 2012).

3.5 Sintering Additives

As discussed in the previous sections, the sinterability of HA can be enhanced by unconventional sintering methods. Besides these, adding sintering additives (also known as dopants) was reported to be cost effective and have beneficial effects on the sinterability of HA (Suchanek *et al.*, 1997; Oktar *et al.*, 2007; Ramesh *et al.*, 2007b). The sintering additives should significantly enhance the densification without decomposition of HA, prohibit abnormal grain growth of HA grains and hence improve the toughness of HA ceramics.

The decomposition of HA into secondary phase such as CaO is unfavourable as it would affect the biological performance of HA. Hence, various studies have been carried out to study the effects of different sintering additives on the phase stability of HA especially upon sintering. Suchanek *et al*. (1997) have doped HA with the 5 wt% of the selected sintering additives such as K-, Na-, Li-, Mg-, Ca-, Al-, Si- Li- oxides, K-chlorides and silicon. All the doped HA samples were subsequently sintered at 1000 ℃ – 1100 ℃. Exaggerated grain growth was not observed in the samples studied. The addition of K_2CO_3, Na_2CO_3, KF and all sodium phosphates was found to improve the sinterability of HA. The authors further revealed that other than the undoped HA, KCL and β-$NaCaPO_4$, all other additives investigated caused either decomposition of HA into β-TCP or formation of CaO throughout the sintering regime employed. These secondary phases should be avoided as it increases the biodegradability of the HA ceramics. The authors concluded that β-$NaCaPO_4$ would be an effective sintering agent as it significantly enhances densification without affecting the HA phase stability.

It was found that the amount of the dopant addition has effects on the phase stability of HA. Tolouei *et al*. (2011) noticed that the doping HA by nano-silica of 0.8 wt% or higher resulted in the formation of secondary phases such as β-TCP when sintered at 1250 ℃ and the percentage of β-TCP formation increased when the amount of nano-silica increased. The decomposition of HA into β-TCP was found to hinder the densification and mechanical properties of HA as the density and hardness achieved for doped-HA was greatly lower than the pure HA. This is attributed to the differential shrinkage between HA and the secondary phases formed at the sintering temperature (Rao & Kannan; 1999). The findings correlate well with the findings carried out by Xu and Khor (2007) who reported that the apatite structure became less stable and a secondary phases of β-TCP was detected in all the samples doped with silica. Similarly, Kutty and Singh (2001) found that the HA phase decreases with increasing Y-TZP

content in the system regardless of sintering temperature employed. The presence of α-TCP, β-TCP and CaO peaks were detected, indicating that HA phase was disrupted by the addition of Y-TZP.

The addition of dopants not only affects the thermal stability of HA but it influences the mechanical properties of the ceramic. The influences of additives on the microstructure and sinterability of HA using 0.05 wt% to 1 wt% manganese oxide (MnO_2) had been studied by Ramesh *et al*. (2007b). According to Ramesh *et al*. (2007b), the doping of 0.05 wt% MnO_2 was proven to obtain a hardness of 7.58 GPa and fracture toughness of 1.65 $MPam^{1/2}$ as compared to 5.72 GPa and 1.22 $MPam^{1/2}$ for undoped HA. It was found that the hardness of HA was closely related to the grain size. The hardness of the HA increase with grain size and reached a maximum at a certain grain size limit before decreasing as shown in Table 3.3. It was seen that 0.05 wt% doped HA sample had the smallest grain size and hence highest hardness and fracture toughness. Besides, the authors found that the addition of 1 wt% MnO_2 was found to be detrimental to hardness of the sample as the hardness marked the lowest value at 5.32 GPa.

Table 3.3: Grain size at which maximum hardness were measured for undoped and MnO_2-doped HA (Ramesh *et al*., 2007b).

MnO_2 Content (wt%)	Grain Size (μm)	Maximum Vickers Hardness (GPa)
0 (undoped)	0.50	7.21
0.05	0.47	7.58
0.10	0.58	7.00
0.30	0.52	7.30
0.50	1.03	7.04
1.00	1.56	5.32

On the other hand, Oktar *et al*. (2007) did a study on the sinterability of HA when doped with a variety of dopants. In this experiment, with the objective of improving the sinterability and mechanical properties of HA, it was doped with 5 wt% and 10 wt% of

SiO_2, MgO, Al_2O_3 and ZrO_2. The presences of these oxides in HA are encouraging as they can act as crack arresters which will directly reduce the brittleness of HA. From their work, doping HA with 5 wt% MgO gave the best sintering result because it possessed denser HA compared to other dopants while the addition of SiO_2 caused a collapse in the hardness and density of HA. The additions of Al_2O_3 and ZrO_2 did not exhibit significant improvement in mechanical strength of HA.

The beneficial effects of the addition of MgO was supported by Tan *et al*. (2013). As presented in Figure 3.16 (a), doping of pure HA with different amount of MgO noticeably enhanced the fracture toughness with the highest value recorded at 1.48 $MPam^{1/2}$ for 1.0 wt% MgO-doped HA as compared to 1.08 ± 0.05 $MPam^{1/2}$ measured for the undoped HA when sintered at 1150 ℃. This value is encouraging as other researchers who doped HA with different additives such as zirconia (Kim *et al*, 2003), alumina (Champion *et al*., 1996) and titania (Manjubala and Kumar, 2000) obtained fracture toughness ranging between 1.0-1.4 $MPam^{1/2}$. Moreover, there are reports indicating that decomposition would occur when HA is doped with these dopants. However, in their study, the phase stability of HA was not disrupted by the addition of MgO as pure HA phase remained for all the doped and undoped samples throughout the sintering regime. Furthermore, hardness and relative density have greatly increased in HA with the reinforcement of MgO in the HA matrix. With the addition of MgO, the hardness of HA maintained in a high range of ~6 GPa to 7.52 GPa even at considerably low sintering temperatures as shown in Figure 3.16 (b).

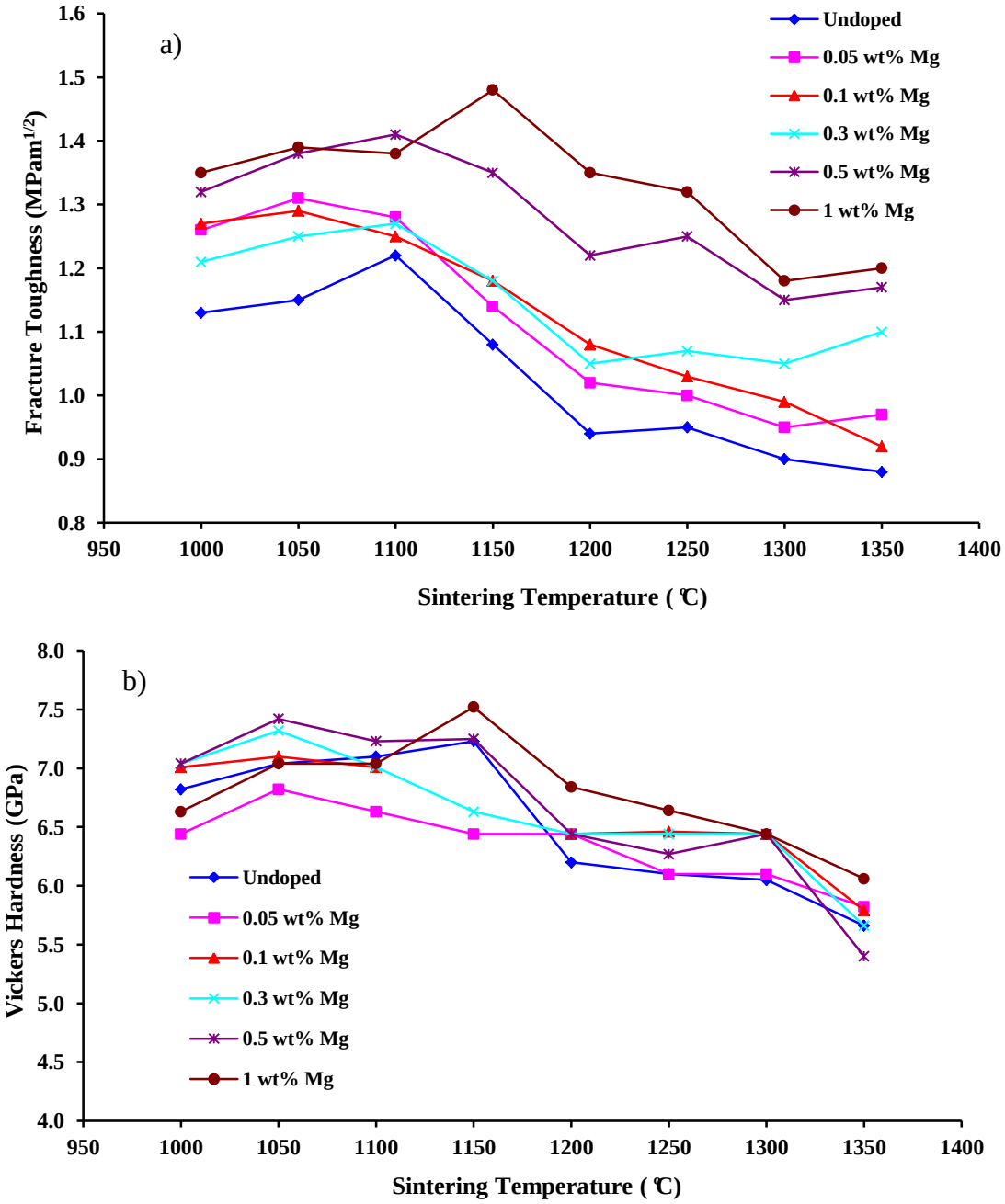

Figure 3.16: Fracture toughness and Vickers hardness of MgO-doped and undoped HA (Tan *et al*., 2013).

3.5.1 Zinc Oxide as Sintering Additives

In short, it is clear that the mechanical properties of HA depend on the type and the amount of sintering additives. It should be aware that the dopants added into HA matrix should enhance the sinterability of HA without compromising the biocompatibility of HA to ensure the reliability of HA as an effective implant material. Therefore, it is

important to choose a suitable dopant with adequate quantity of addition to ensure the stability of the dopant within the HA matrix.

Zinc oxide (ZnO) was found to be a potential sintering additive to be doped into HA matrix as zinc is an essential trace element in human bone. It presents in a small amount in the enamel of human teeth and bone (Bandyopadhyay *et al*., 2006). Moreover, zinc promotes bone growth (Yamaguchi *et al*., 1987), inhibits bone resorption (Moonga & Dempster, 1995) and offers antimicrobial resistance (Hernández-Sierra *et al*., 2008) which is indispensible for bone implant materials. In the study carried out by Yu *et al*. (2014), HAP/ZnO biocomposite has significant antibacterial efficacy against various microorganisms, indicate enormous potential for its use in anti-inflammatory application as maxillofacial bone repair biomaterial. Additionally, zinc oxide has been doped into beta-tricalcium phosphate (β-TCP) to develop zinc-releasing biomaterials and it has been proved to promote bone formation (Ito *et al*., 2000). The positive effect of ZnO in biological properties of calcium phosphate is supported by Kawamura *et al*. (2000) as zinc promotes excellent bioactivity than the undoped calcium phosphate. Stimulated bone formation was observed around ZnO containing calcium phosphate ceramics implanted in rabbit femora. The bioactive properties of ZnO-doped HA have also been extensively studied (Ishikawa *et al*., 2002; Jallot *et al*., 2005). Although small addition of ZnO is advantageous to the host material, but a high zinc concentration can have serious toxic side effects on human cells (Bettger & O'dell, 1993). In addition, Ito *et al*. (2000) have also reported that the addition of ZnO higher than 1.2 wt% in TCP could release zinc and subsequently cause cytotoxicity effects in human body. This is in agreement with the cell culture study by Bandyopadhyaya *et al*. (2007) where the cell material interaction shows that ZnO addition on calcium phosphate ceramic was non-toxic at the initial stage. However, as the ZnO content increased, the cell spreading and cell-cell interactions in both TCP and HA decreased. It can be concluded that good cell

attachment is up to 1.5 wt% ZnO doping and addition of ZnO more than 1.5 wt% limited the cell spreading and growth on the HA surface. Therefore, the ZnO content in the doped ceramic has to be less than 1.2 – 1.5 wt%.

To be a reliable human implant, the ZnO-doped HA ceramics should have a harmonious balance between biocompatibility and mechanical properties. Hence, the ZnO addition should also enhance the mechanical properties of HA ceramics. Bandyopadhyay *et al.* (2007) have proved that the addition of ZnO improved the sintered density and microhardness of HA as shown in Table 3.4.

Table 3.4: Properties of HA containing varying amounts of ZnO (Bandyopadhyay *et al.*, 2007).

HA (wt %)	ZnO (wt %)	Linear Shrinkage (%)	Sintered Relative Density (%)	Microhardness (MPa)
100	0.0	47.3	81	3696
98.5	1.5	51.7	88	4781
97.5	2.5	51.1	89	4797
96.5	3.5	51.4	92	4540

Further to that, interconnected porous β-TCP scaffolds improved by ZnO were successfully prepared by Feng *et al*. (2014). It was found that the addition of ZnO improved the densification of the strut of β-TCP scaffolds. Moreover, the addition of ZnO could improve the mechanical properties such as fracture toughness, stiffness and hardness of the scaffolds as presented in Figure 3.17. In vitro cell tests showed that the scaffold with ZnO doping exhibited a good cellular viability as well as cellular proliferation. The formation of a new bone like apatite layer indicated that the scaffold demonstrated better bioactivity.

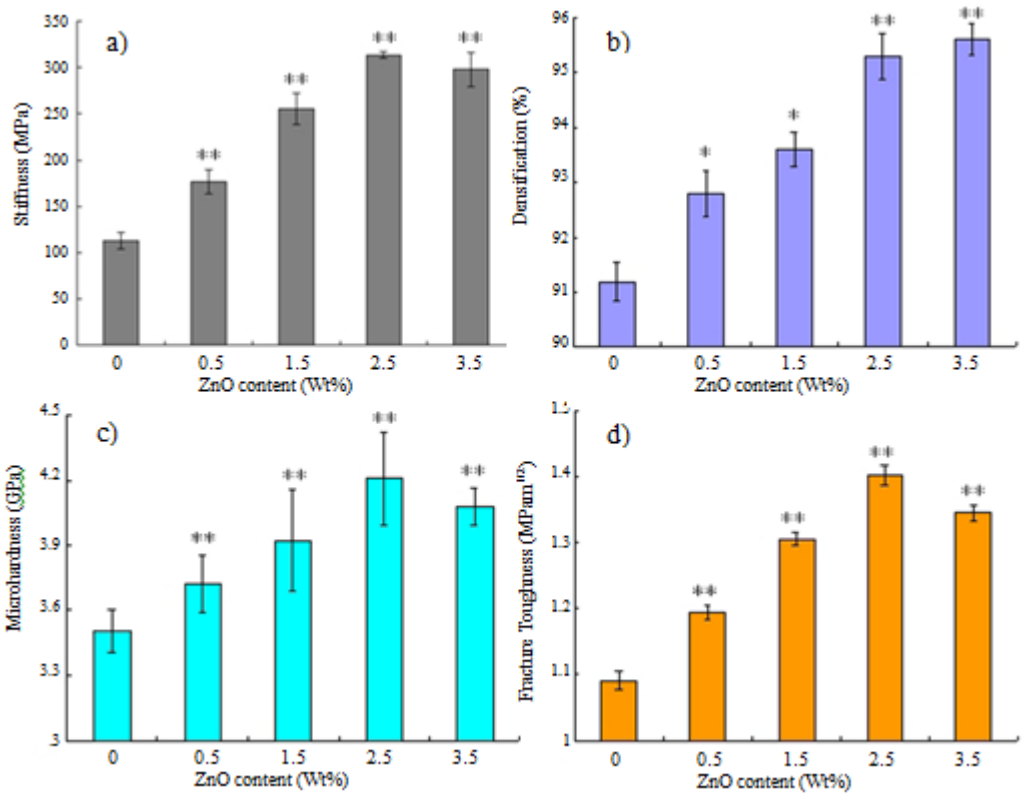

Figure 3.17: Effect of ZnO contents on the (a) stiffness, (b) densification, (c) microhardness and (d) fracture toughness of the strut (Feng *et al*., 2014).

Researchers have also done investigation on the effects of ZnO addition on the sinterability of other ceramics such as ceria based material, SnO_2 based ceramic and Tin-doped indium oxide. With the addition of ZnO, the relative density, grain size and microstructure of these host materials have improved without affecting the phase stability (Liu *et al*., 2014; He *et al*., 2012; Chen *et al*., 2014). Hence, ZnO is a potential sintering additives to improve the mechanical properties of HA without compromising the phase stability and biological performance of HA.

In summary, this chapter has provided a brief overview of the various parameters that governs the sinterability of hydroxyapatite ceramics such as powder consolidation technique, sintering temperature, sintering time and heating rates and sintering additives. Therefore, particular attention has to be paid to optimize these parameters in the quest to improve the sinterability of the hydroxyapatite powders.

CHAPTER 4: EXPERIMENTAL TECHNIQUES

4.1 Synthesis of HA Powder via Wet Chemical Method

The hydroxyapatite (HA) powder used in the present work was prepared according to a novel wet chemical method comprising precipitation from aqueous medium via a titration process by reacting calcium ion with phosphate ion based on a molar ratio of Ca/P = 1.67 and maintained at a pH of about 10-12 by the addition of small amounts of ammonium (NH_3) solution (25% concentration) (Ramesh, 2004). The starting precursors used were commercially available calcium hydroxide $Ca(OH)_2$ (98% purity, RNM) and orthophosphoric acid H_3PO_4 (85% purity, Merck) following the chemical reaction:

$$10Ca(OH)_2 + 6H_3PO_4 \Rightarrow Ca_{10}(PO_4)_6(OH)_2 + 18\ H_2O \qquad (4.1)$$

In general, the synthesis process involved the preparation of H_3PO_4 and $Ca(OH)_2$ solution. To prepare the H_3PO_4 solution, the required amount of H_3PO_4 was diluted in distilled water, stirred for 10 minutes and subsequently contained in a titration funnel. The pH of the prepared acid solution was about 1. A similar procedure was employed to prepare the $Ca(OH)_2$ solution under stirring condition. The pH of the prepared $Ca(OH)_2$ solution was about 12. The beaker containing the $Ca(OH)_2$ solution was covered with a cling film to minimize contamination as well as any reaction between carbon dioxide in air with the mixture.

The prepared H_3PO_4 solution was then added dropwise into the stirring suspension of $Ca(OH)_2$ in distilled water. The titration process normally takes about 3 hours. Throughout the titration process, the pH of the mixture was monitored and kept above 10.5 by the addition of NH_3 solution. Stirring process was continued after the titration process for another 6 hours and the precipitate was allowed to settle down overnight before filtration. For the filtration process, the aged HA solution was poured into the

prepared funnel connected to the pump and layered with 2 filter papers. The filtered precipitate (HA slurry) was rinsed three times using distilled water and placed in ceramic bowls to be dried. In this experiment, three different drying methods were applied, namely conventional oven drying, microwave drying and freeze drying.

4.1.1 HA Powder Prepared via Oven Drying

The rinsed precipitate (HA slurry) was placed in a ceramic bowl and dried in an oven (Memmert UF30, Germany) at about 60°C. The slurry was weighed at hourly intervals throughout the drying process until the water has been completely removed (constant weight was obtained). It was found that 16 hours of oven drying period is sufficient to remove all the water as there was no change in the slurry's weight after 16 hours of drying. The dried HA slurry was crushed using mortar and pestle and then hand sieved (212 μm) to obtain HA powder, hereafter named OHA. The flow sheet of this method is shown in Figure 4.1.

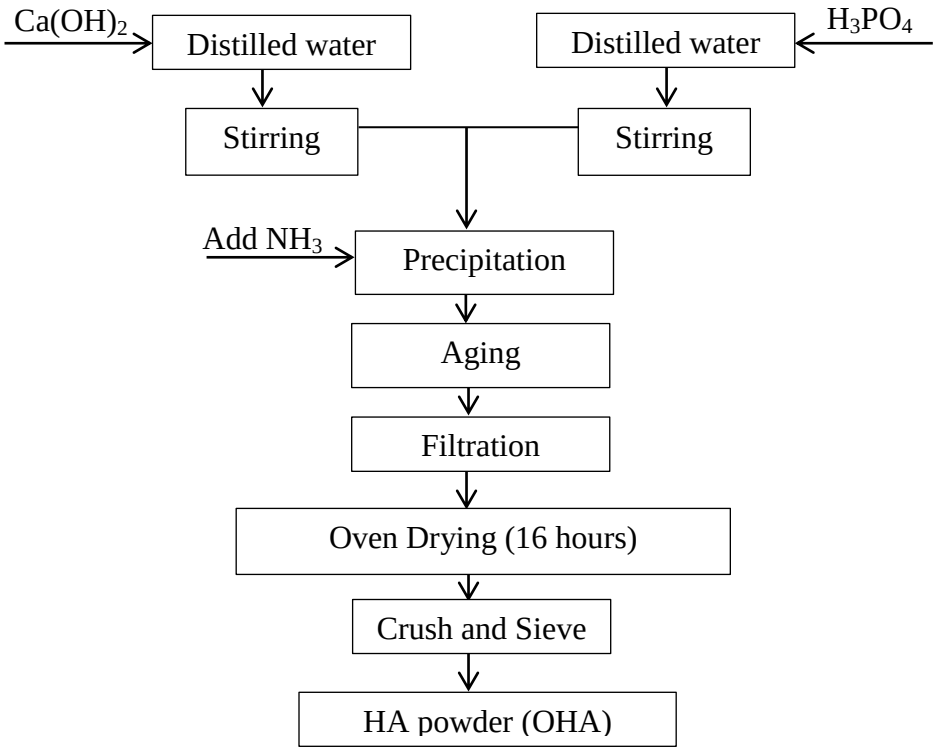

Figure 4.1: OHA wet chemical method flow sheet.

4.1.2 HA Powder Prepared via Microwave Drying

In terms of microwave drying, the rinsed HA precipitate was placed in a ceramic bowl and then subjected to microwave irradiation in a household microwave oven (Sharp, R-898M, 900 W power).The specifications of the microwave oven are shown in Table 4.1.

Table 4.1: Specifications of Sharp R-898M Microwave Oven.

Specifications	Details
Microwave Power Consumption	1400 watt
Heater Power Consumption	1700 watt
Microwave Output	900 watt
Heater Output	1600 watt
Outside Dimension	520 mm (W) x 309 mm (H) x 486 mm (D)
Cavity Dimension	343 mm (W) x 209 mm (H) x 357 mm (D)
Microwave Frequency	2450 MHz

The precipitate was dried in the microwave oven at 100% power (900 watt) to remove the water content completely. The temperature and rate of heating were not controlled as those parameters were fixed for this microwave oven. Under microwave drying, the precipitate was removed periodically from the microwave oven for every 1 minute. This procedure was repeated to reach the case of no change in precipitate weight. The time taken for the samples to reach constant weight was 15 minutes. The microwave dried HA cake was crushed and sieved to obtain HA powder, hereafter named MD-HA. The flow sheet of this method is shown in Figure 4.2.

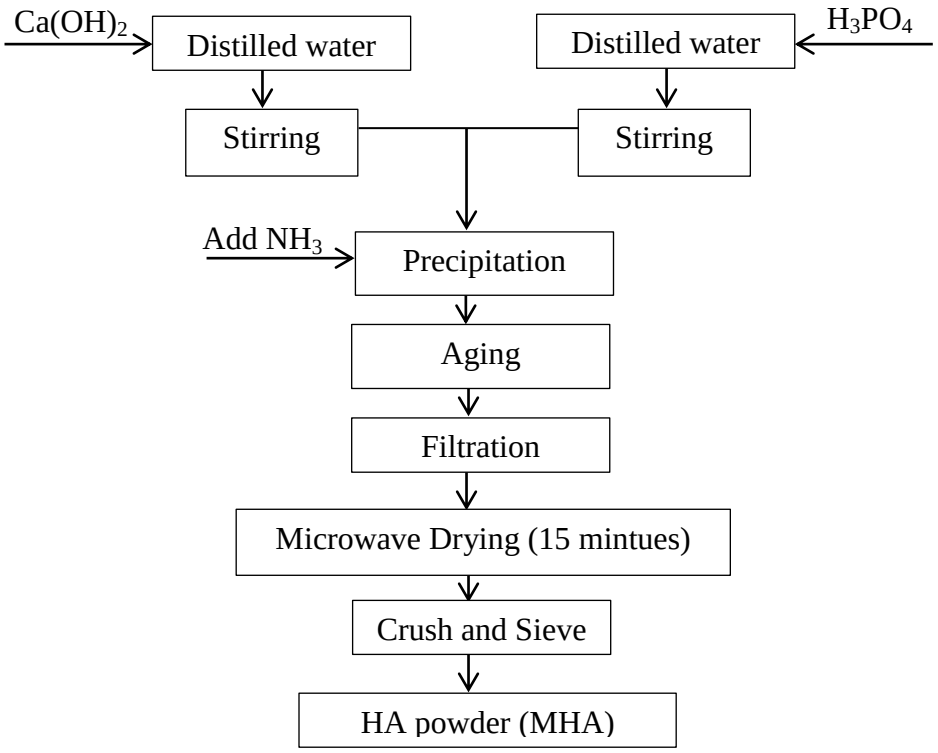

Figure 4.2: HA wet chemical method with microwave drying flow sheet.

4.1.3 HA Powder Prepared via Freeze Drying

As for freeze drying, the rinsed HA precipitate was transferred into a specific freeze dry container. The amount of precipitate was about 1/3 of the container's capacity to ensure the high evaporation efficiency throughout the freeze drying process. The freeze dry container was immediately transferred into a freezer (Telstar, Igloo, Netherlands); deep freeze at –80°C for 24 hours to solidify the water and induce solid liquid phase separation. On the other hand, the freeze dryer (FDU-1200, Japan) was pre-set at –45°C and was evacuated by means of vacuum pump (60L/min, 0.049 mBar). After 24 hours, the frozen sample was removed from freezer and quickly taken to the freeze dryer. By maintaining the temperature of the HA sample below –45°C and the vacuum below 0.049 mBar, water was removed by sublimation in the freeze dryer. The weight of the HA precipitate was not recorded periodically as removing the sample from the freeze dryer could affect the temperature and pressure of the system. After 36 hours of freeze

drying, the HA sample was completely dried as no frost was observed on the surface of the freeze dry container. Crushing of HA is not required as a fluffy HA powder was obtained. The HA powder was sieved to obtain HA powder, hereafter named FD-HA. The flow sheet of this method is shown in Figure 4.3.

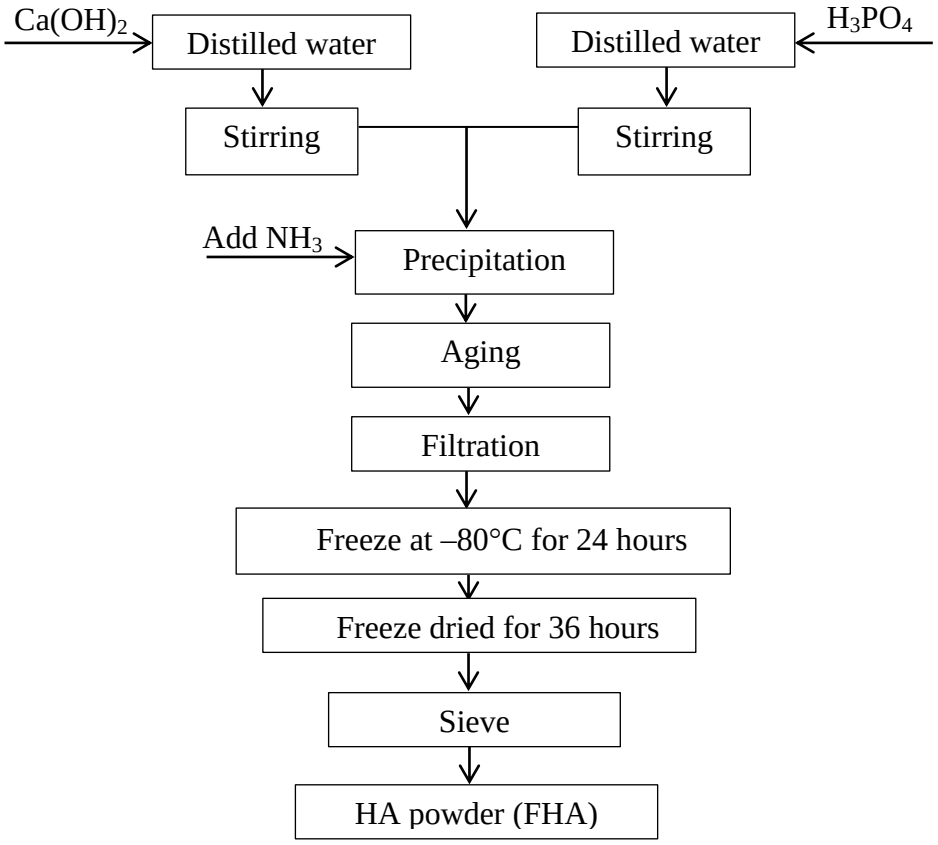

Figure 4.3: HA wet chemical method with freeze drying flow sheet.

4.2 ZnO-doped HA Powder Preparation

The starting zinc oxide (ZnO) powder used in the present research was of 99% purity (Systerm). The powder compositions, i.e. 0.1, 0.3, 0.5, 1.0 wt% ZnO-doped HA were prepared through a process involving ultrasonic and ball milling.

In a typical procedure, both powders (MD-HA powder and ZnO powder) were measured according to the respective ratio (composition) and put into a beaker

containing approximately 200 ml of ethanol. The solution underwent ultrasonic bath at 28–34 kHz for 22 minutes to improve dispersion of ZnO in the MD-HA powder. Upon the completion of the ultrasonic bath, the mixture was subsequently poured into a high-density polyethylene (HDPE) bottle (500 ml) followed by 3 mm diameter zirconia balls as the milling media. The mixture was ball-milled for 1 hour at rotating speed of 350 rpm.

During the ball milling process, the HDPE bottles were being shaked for every 15 minutes to ensure that the mixture mixed well. Immediately after the milling process, the slurry was separated from the milling media through a sieve and was dried overnight in oven at 60 ℃.The dried filtered cake was then crushed and sieved to obtain ready-to-press ZnO-doped HA powders. Throughout the powder preparation process, care was exercised to avoid contamination of the slurry by 'foreign' particles. The milling procedures were kept the same for all level of dopant to ensure a fair comparison of performance. A flow chart showing the powders prepared in the present work is shown in Figure 4.4.

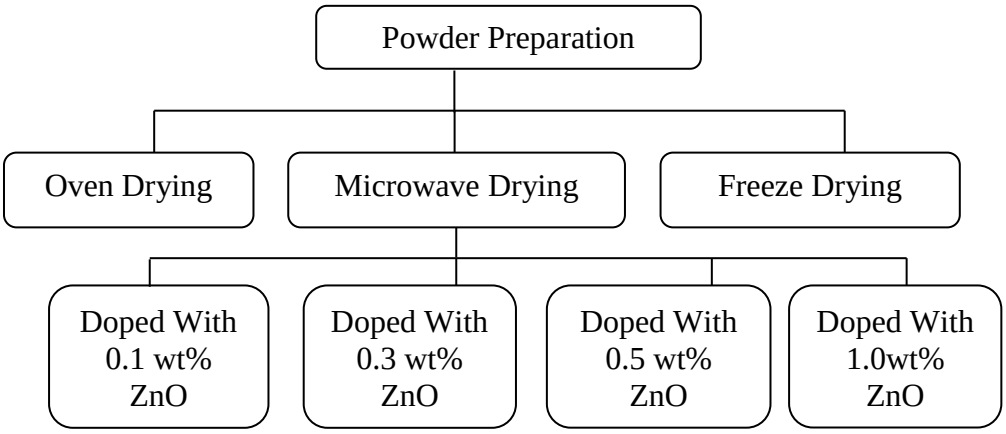

Figure 4.4: A flow chart showing the powders prepared in the present work.

4.3 Green Samples Preparation

The as prepared HA powders (OD-HA, MD-HA and FD-HA) as well as the ZnO-doped HA powder were uniaxial compacted at about 1.3 MPa to 2.5 MPa into discs (20 mm dia. 5 mm thickness) and into rectangular bars (32 x 13 x 6) mm using a hardened steel mould and die set. The cleanliness of the die was essential, so as not to contaminate the samples. The die used in conjunction with the sample preparation was cleaned with an oil-based liquid such as WD-40, in order to prevent powder lamination.

It is well established that the density variation in the green product will cause differential shrinkage and crack initiation upon sintering (Bortzmeyer, 1995; Satapathy, 1997). Thus, in order to avoid this, the green compacts were subsequently cold isostatically pressed (CIP) at a pressure of 200 MPa (Riken, Seiki, Japan) and hold at this pressure for about 1 minute. In CIP, pressure was applied on the as-pressed samples in all directions with the aid of hydraulic oil inside the cold isostatic pressing machine. Therefore, it produces more uniform density green samples. The green bodies with uniform density enable more uniform shrinkage during the sintering process and this prevents the samples from warping and cracking.

4.4 Sintering

4.4.1 Conventional Sintering

In the present research, sintering was achieved by by conventional pressureless sintering where the green compacts were sintered in air, using a standard rapid heating furnace (LT Furnace, Malaysia) at different temperatures; $1050^{o}C$–$1350^{o}C$ ($50^{o}C$ interval) for the OD-HA, MD-HA and FD-HA powder while temperature range of $1100^{o}C$–$1300^{o}C$ for ZnO-doped HA powder. A furnace ramp rate of $2^{o}C$/min (heating and cooling) and soaking time of 2 hours was used for each firing. In this method, the

duration of the sintering process ranges from between 15 to 24 hours depending on the sintering temperature. The sintering profile is shown in Figure 4.5.

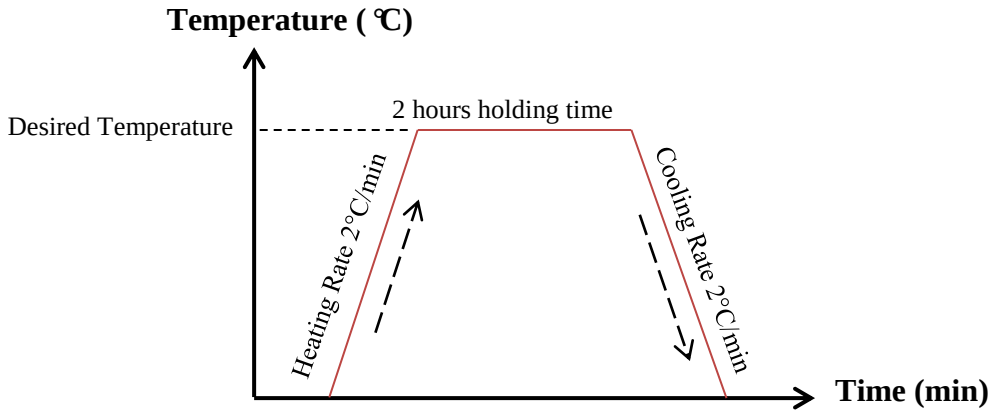

Figure 4.5: Sintering profile of conventional sintering.

4.4.2 Microwave Sintering

All the pressed HA pellets were microwave sintered (MS) in a microwave furnace (Delta MF, China) with an alumina fibre insulation box. A constant power output of 2000 watt was employed to sinter the HA samples at temperature of 950^{o}C–1250^{o}C. Figure 4.6 plots the sintering profile of the microwave sintered HA. A constant microwave power of 2000 watt at 2.45 GHz was maintained throughout the sintering process. The sintering rate for the first 250^{o}C was not controlled as this parameter was fixed for this microwave furnace; depending on the absorbance of the material. From 250^{o}C to 500^{o}C, the sintering rate was set as 15^{o}C/min to avoid thermal shock. Then, the samples were sintered at 30^{o}C/min to the desired temperatures (950^{o}C–1200^{o}C) with a holding time of 15 minutes to avoid excessive grain growth. Finally, the furnace was switched off and natural cooling of the sample was allowed. In this method, the duration of the sintering process ranges from between 5 to 6 hours depending on the sintering temperature.

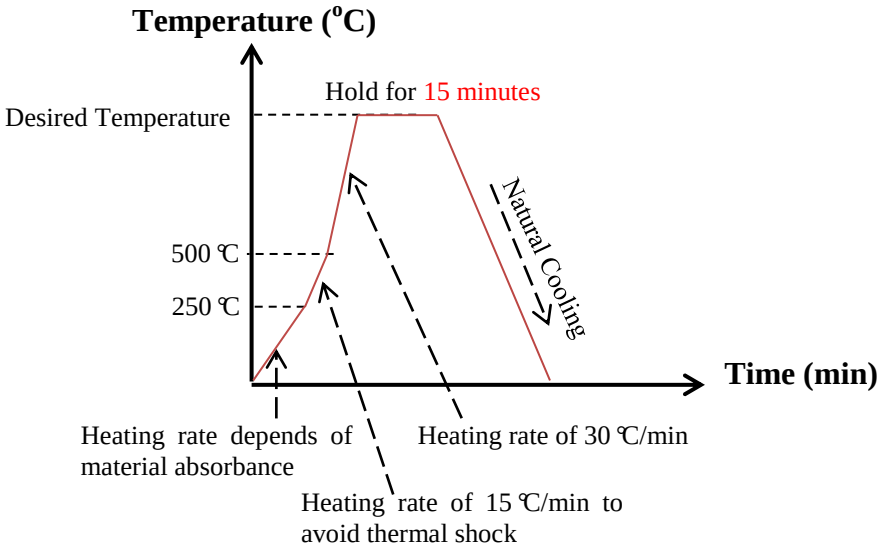

Figure 4.6: Sintering profile of microwave sintering.

4.4.2.1 Samples Arrangement

A variety of sample arrangements was tried, and it was found that disc shaped samples arranged as shown in Figure 4.7 gave the optimum results.

To initiate the microwave heating and minimize the thermal gradients, both silicon carbide (SiC) cylindrical and irregular shaped susceptor were used as auxiliary heating elements (hybrid heating). They were arranged as shown in Figure 4.7, where cylindrical SiC was placed right in front of the source of magnetron and the irregular shaped SiC was scattered around the insulation box. The insulation box is made from alumina fiber (not microwave susceptible) and was required to retain heat. At the same time, the samples were placed on top of pre-sintered zirconia plate. It was necessary to include zirconia plate in the arrangement in order to have sufficient load to achieve good coupling of the electromagnetic energy. The loss factor of the zirconia plate became sufficiently large to permit heating by microwave absorption, permitting more efficient microwave heating of the sample.

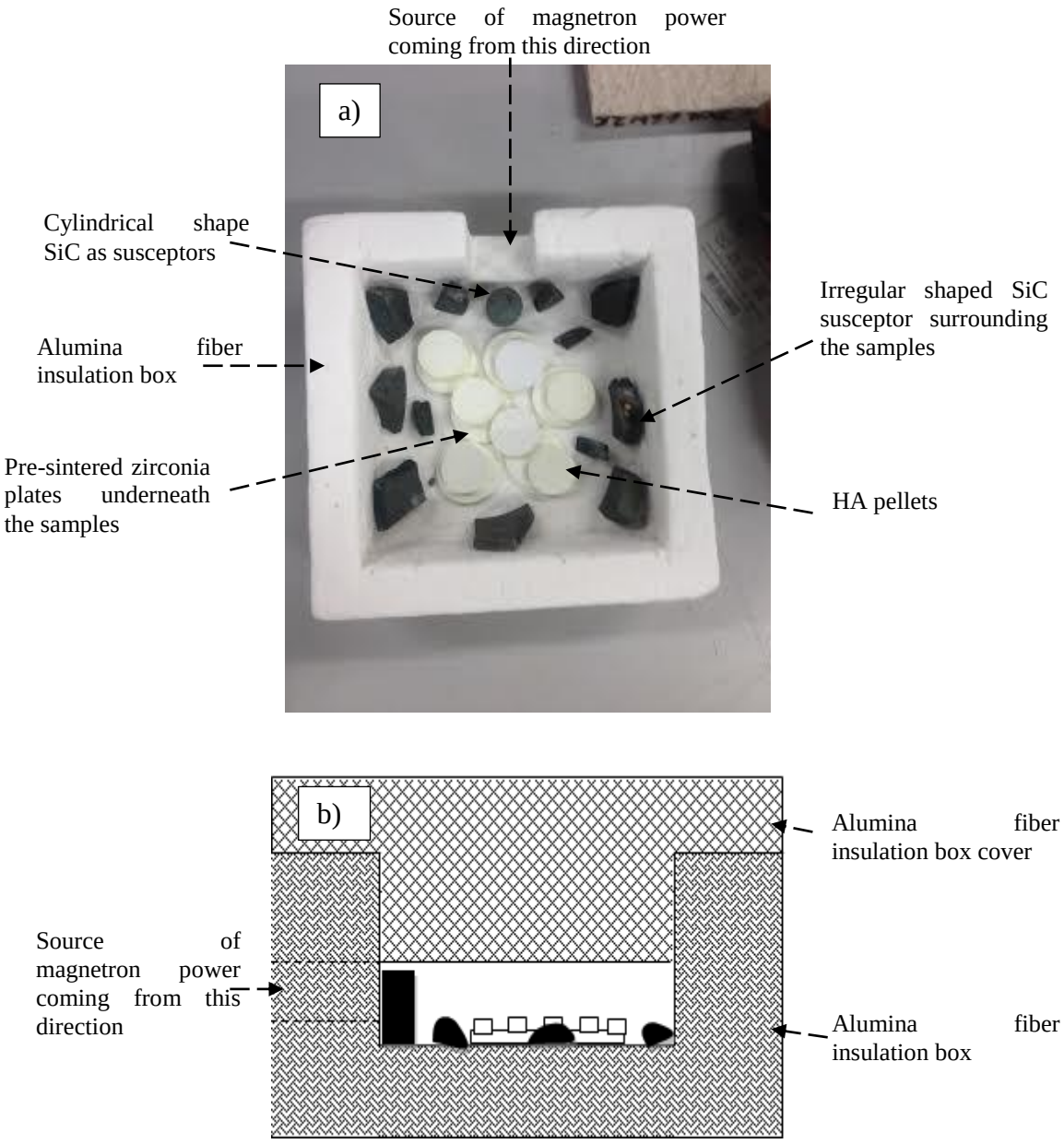

Figure 4.7: Samples arrangement in the microwave furnace: (a) plan view; (b) side view.

4.5 Grinding and Polishing

All the conventional and microwave sintered HA disc samples were firstly ground and then polished on one face prior to density measurement, phase analysis, Vickers hardness testing, fracture toughness evaluation and SEM investigation. Surface grinding and polishing was done manually using an Imtech Grinder-Polisher. The samples were

ground on SiC paper (600 grit-1200 grit) before being diamond polished to a 3 μm finish and subsequently to a 1 μm finish so as to obtain an optical reflective surface.

4.6 Characterization

The characterization process includes the specific surface area, crystallite size, Transmission Electron Microscopy (TEM) for HA powders; Fourier Transform Infrared (FTIR), X-Ray diffraction (XRD), Scanning Electron Microscopy (SEM) with Energy Dispersive X-Ray (EDX) analysis for both HA powders and HA sintered samples followed by grain size evaluation (SEM and Field Emission Scanning Electron Microscopy (FE-SEM)), bulk density measurement, Vickers hardness and fracture toughness examination for all the HA sintered samples.

4.6.1 Specific Surface Area and Crystallite Size

The specific surface area of the powder was measured by the Brunauer-Emmett-Teller (BET) method. Nitrogen gas adsorption analysis was performed on a physisorptionanalyser (ASAP 2020, Micromeritics, USA). Samples were outgassed at 150 ℃ for 30 minutes under vacuum.

The average crystallite size (d) can be estimated by measuring the broadening of a particular peak in a XRD diffraction pattern associated with a particular planar reflection from within the crystal unit cell based on Scherrer's formula (Cullity and Stock, 2001):

$$d = 0.9\lambda / B\cos\theta \qquad (4.2)$$

where λ is the wavelength of the X-ray which is 1.54056 Å for CuKα radiation, θ is the diffraction angle at 2θ = ~31.7 ° and ~25.7 ° and B (in radians) is the measured full width at the half maximum (FWHM) of a diffracting reflection.

4.6.2 Transmission Electron Microscopy (TEM) Analysis

The morphology of the as synthesized oven dried (OD-HA), microwave dried (MD-HA) and freeze dried (FD-HA) HA powder was analysed using TEM (JEOL, JEM-2100F, Japan) operated at an accelerating voltage of 120 kV. The particle size of the powder was measured from TEM micrographs. Prior to TEM observation, the as synthesized HA powder was dispersed in 1 – 2 ml of spectroscopic grade ethanol solution followed by ultrasonication for 1 hour to break up agglomerates. Approximately 50 µl of the OD-HA and MD-HA suspensions produced were deposited on a 200 mesh copper grid which was subsequently dried to remove the ethanol solvent. The deposited HA powder on the 200 mesh copper grid was then used in the TEM analysis.

4.6.3 Fourier Transformation Infrared (FTIR)

A Fourier transform infrared spectrometer (FTIR – Brukers IFS-66-VS, Germany) with a reflectance mode was used for qualitative analysis of the molecular radicals. Prior to testing, 40 mg of KBr is mixed with 0.4 mg of the tested powder. Subsequently, the powder is pressed into pellet of 13 mm in diameter. Advanced preparation is not required for the sintered samples. The possible structural variation and reactions in those samples were examined. The infrared spectrum with a resolution of 4 cm^{-1} and a scan number of 32 was adopted with a scan range 400 – 4000 cm^{-1}.

4.6.4 Scanning Electron Microscopy (SEM) and Energy Dispersive X-Ray Analysis (EDX)

The morphology, the Ca/P ratio and the distribution of elemental within the HA powder and sintered samples were examined on a phenom Pro-X microscope equipped with an energy dispersive X-Ray (Pro Suite & Elemental Analysis, Phenom).

Measurements were made in terms of atomic %, weight % and elemental spectra acquisition.

4.6.5 X-Ray Diffraction (XRD)

X-ray diffraction (XRD) provides information that relates to the crystal lattice of the material and can characterise the crystalline phases present. In the present work, the phases present in the powders as well as the sintered samples were determined at room temperature using X-Ray diffraction (Empyrean, PANalytical, Netherlands) operated at 35 kV and 15 mA with Cu-Kα as the radiation source. The X-ray scan speed and step scan were 0.5 °/min. and 0.02 °, respectively. The peaks obtained were compared to standard reference JCPDS-ICCD (Joint Committee of Powder Diffraction Standard – International Center for Diffraction Data) files for HA (PDF No. 74-566 for $Ca_{10}(PO_4)_6(OH)_2$, α-TCP (PDF No. 9-348), β-TCP (PDF No. 9-169), TTCP (PDF No. 25-1137) and CaO (PDF No. 37-1497). The files are attached in Appendix C.

4.6.6 Microstructural Examination

The microstructural evolution of the HA under various sintering temperature was examined by using the SEM (Pro-X, Phenom) and FE-SEM (JEOL, JSM7600F, Japan) both at an accelerating voltage of 10 kV and 15 kV. The sintered samples were firstly polished to a mirror like surface finished and then thermally etched to delineate the grain boundaries. The etching temperature employed was 50°C below the sintering temperature of the sample at a heating and cooling rate of 10°C/min, with a holding time of 30 minutes prior to cooling. In order to remove any contamination, the surface to be examined was cleaned in acetone and subsequently stuck on to an aluminium stub. The samples for SEM and FE-SEM examination were coated with platinum, which provides a conducting layer, to prevent charging from occurring in the microscope.

4.6.7 Grain Size Measurement

The grain size of sintered HA was determined on thermally etched specimens from scanning electron micrographs using the line intercept method. This technique requires measurements taken from polished sections. In a typical analysis, a known test line is drawn on a A4 size SEM micrograph of the selected polished section and the number of intercept between the test line and grain boundaries are counted. The test line should cover at least 50 grains and several lines are drawn and measured before average value is taken.

The average grain size is then calculated according to the equation proposed by Mendelson (1969):

$$\overline{D} = 1.56\overline{L} \tag{4.3}$$

where $\overline{D}$ is the average grain size and $\overline{L}$ is the measured average interception length over a large number of grains which can be represented by:

$$\overline{L} = \frac{C}{MN} \tag{4.4}$$

where *C*, *M* and *N* are the total length of the test line, the magnification of the SEM micrograph and the number of intercepts respectively.

The technique used to count the number of intersections was according to an international standard test method for intercept counting (ASTM E112-96, 2004). Essentially, the end points of a test line are not intersections and not counted unless the end appeared to exactly touch a grain boundary, when a ‘0.5’ intersection is scored. A tangential intersection with a grain boundary is scored as a ‘1’ intersection while for

intersection coinciding with the junction of 3 grains is scored as a ‘1.5’ intersection as shown in Figure 4.8.

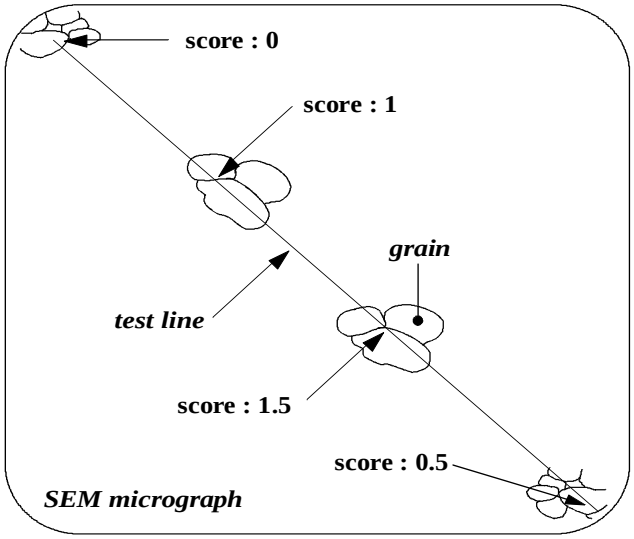

Figure 4.8: Diagram showing the score given for the type of intersections.

4.6.8 Bulk Density Measurement

The bulk densities of dense compacts (above 90% of theoretical density) were determined by the water immersion technique based on the Archimedes principle using a standard Mettler Toledo Balance AG204 Densi-meter. In the present research, distilled water was used as the immersion medium. The procedure to measure the bulk density can be summarized as follows:

(a) The dry weight of the sample is first measured.

(b) The sample is placed on a dish immersed in the distilled water after the electronic balance is zeroed. The weight of the sample in water is subsequently recorded. Extra care has to be taken, as any minor disturbance will incur vibration causing the readings to fluctuate.

The bulk density was calculated using equation (4.5) as followed:

$$\rho = \frac{W_a}{W_a - W_w} \rho_w \tag{4.5}$$

Where ρ is the bulk density of sample (g/cm^3), W_a is the weight of the sample in air (g), W_w is the weight of the sample in water (g) and ρ_w is the density of distilled water. The temperature effect on the density of distilled water was taken into consideration using the table provided in Appendix B. The relative density was calculated by taking the theoretical density of HA as 3.156 gcm^{-3}. However, for low-density samples (below 90% of theoretical density) the bulk density was obtained from the measurement of geometric dimensions and sample mass. This is because the former method allows water to penetrate the pores, resulting in an overestimate value of the sample's density.

4.6.9 Vickers Hardness and Fracture Toughness Evaluation

The Vickers hardness testing method was used to ascertain the hardness of the sintered HA. The indentations were made using a pyramidal diamond indenter (HMV series Shimadzu, Japan) with an applied load varying between 50 g to 200 g. In the Vickers test, the load is applied smoothly, without impact, and held in place for 10 seconds. The physical quality of the indenter and the accuracy of the applied load as defined clearly in ASTM E384-99 (1999) must be controlled to get the correct results. In general, the Vickers impression (Figure 4.9) appears to be square, and the two diagonals have almost similar lengths. After the load is removed, the impression diagonals as shown in Figure 4.9 are measured usually with a filarmicrometer built in the attached microscope on the Vickers machine, to the nearest 0.1 μm and the average value, *2a*, is obtained. The Vickers hardness (H_v) is calculated based on the surface area of the indent using equation (4.6):

$$H_V = \frac{1.854P}{(2a)^2} \tag{4.6}$$

Where *P* is the applied load and *2a* is the average diagonals. In the present work, five indentations were made for each sample and the average values were taken.

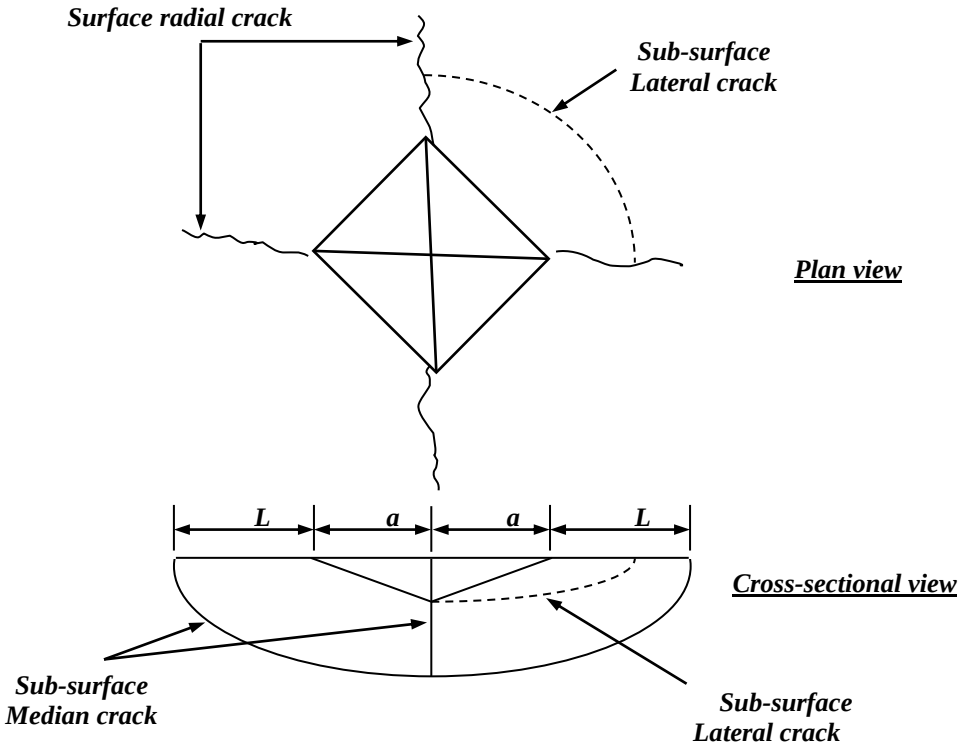

Figure 4.9: Schematic indentation fracture pattern of an idealized Vickers median (or half-penny) crack system (Niihara *et al*., 1982).

Using the same indentation image from Vickers hardness tester, fracture toughness (K_{Ic}) was determined from the equation derived by Niihara (1985):

$$K_{Ic} = 0.203\left(\frac{c}{a}\right)^{-1.5}(H_v)(a)^{0.5} \tag{4.7}$$

Where H_v is the Vickers hardness, c is the characteristics crack length (L+a), L is the average crack length and a is the half diagonal of indent.

CHAPTER 5: RESULTS AND DISCUSSIONS (PART 1)

5.1 HA Powder Characteristic

5.1.1 XRD Analysis and Crystallite Size

The wet chemical precipitated HA powders synthesized via three different drying methods, namely freeze drying (FD-HA), microwave drying (MD-HA) and oven drying (OD-HA) were subjected to X-ray diffraction (XRD) to examine the phase purity. The resulting XRD spectra for the synthesized HA are shown in Figure 5.1.

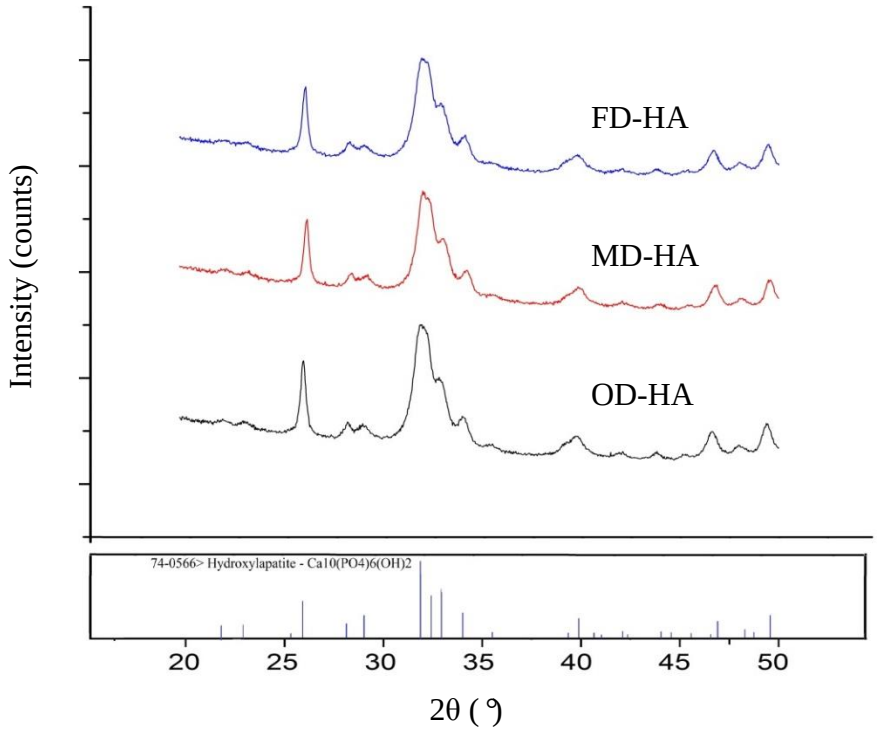

Figure 5.1: The XRD profiles of HA powder synthesized through wet precipitation method via three different drying methods.

All powders produced peaks correspond to the standard JCPDS card no: 74-0566 for stoichiometric HA with no significant evidence of secondary phases such as CaO, TTCO, β-TCP or α-TCP being detected. As illustrated in Figure 5.1, FD-HA, MD-HA and OD-HA produced nearly identical peaks with minimal difference in terms of the degree of crystallinity as MD-HA displayed slightly narrower diffraction at $2\theta = 31.9°$. The results proved that microwave drying has no adverse effects on the phase purity of

HA powders as supported by Santhosh & Prabu (2012) and Chanda *et al*. (2009). In general, broad diffraction peaks were observed for all the HA powders indicated that HA powders produced by the wet chemical method are poorly cystallined with a large amount of amorphous phase regardless of drying methods. The broad peaks of wet chemical produced HA powders could be resulted from the slow addition rate of the acid solution that gave the nanocrsytalline nature of the synthesized powders. This is in agreement with the study carried out by Santos *et al*. (2004), Angelescu *et al*. (2011) and Alobeedallah *et al*. (2011). Moreover, the broad diffraction peaks indicated that the HA crystal size were very small and the crystal size could be estimated from XRD data using Scherrer's equation (Pratihar *et al*., 2006; Tian *et al*., 2008) at prominent peak of HA such as (211) and (002) reflection as shown in Table 5.1.

Table 5.5.1: Estimate crystal size of HA particles based on the Scherrer's equation.

Sample	Crystal size (nm) based on XRD	
	(2 1 1) reflection @ $2\theta = \sim 31.9^{o}$	(0 0 2) reflection @ 2 $= \sim 25.7^{o}$
FD-HA	21.83	41.61
MD-HA	46.09	45.55
OD-HA	48.64	47.54

The results showed that all the HA powders has crystal size lie within nanometer range which is favorable for osseointegration due to large interfaces (Murugan & Ramakrishna, 2005) and HA with small crystal size exhibits higher bioactivity compared to coarse HA crystal (Mazaheri *et al*. 2008). From Table 5.1, FD-HA has smaller crystal size (21.83 nm) than MD-HA and OD-HA at (2 1 1) reflection while MD-HA and OD-HA recorded similar crystal size at 46.09 nm and 48.64 nm, respectively. OD-HA recorded the biggest crystal size at both (2 1 1) and (0 0 2) plane could be due to the aggregation of small particles as powder particles coalesce

during the long drying process where heat was constantly supplied to the HA slurry for 16 hours. The long drying hours allows the motion of molecules which increase the chance of molecules collision, hence, HA particle concentrated to form larger particles. This could explain the smaller crystal size of FD-HA as no heat was involved in the freeze drying process, eliminated the chance of particles to collide with each other and form large agglomerates. A similar finding was reported by Girija *et al*. (2012) who found that HA produced by freeze drying has smaller crystal size than that of oven dried HA powder. Besides, the OD-HA produced slightly bigger crystallite size than MD-HA is in disagreement to the study carried out by Santhosh & Prabu (2012). In their research, furnace dried HA had crystal size smaller than those produced by microwave drying. This contradict finding could be due to the shorter oven drying hour (80 ℃ for 8 hours) compared to the current research (60 ℃ for 16 hours), reduces the chance of particle coalescence.

5.1.2 FTIR Analysis of the Synthesized HA Powder

The phase purity of HA produced by three different drying methods was further examined by FTIR and the FTIR spectrum of the HA powders are shown in Figure 5.2. A comparison of the wave numbers for the functional groups of the HA produced by three different drying method and HA powder produced by Brundavanam *et al*. (2015) is tabulated in Table 5.2. From Figure 5.2, it can be deduced that all the HA powders displayed typical FTIR spectrum of pure HA powder. The characteristic bands corresponding to the (ν_3 and ν_1) PO_4^{3-} were clearly observed at ~1035cm^{-1} - 1038cm^{-1} and 962 cm^{-1}, respectively for all the HA powders. In addition, the characteristic bands attributed to the apatitic OH^- were observed at ~3567 cm^{-1} (stretching) for all the powders, proved that freeze drying and microwave drying did not alter the basic apatitic structure of HA powder.

Broad peaks assigned to chemically absorbed H_2O was observed at frequencies around 3341 cm^{-1} and 1632 cm^{-1} for FD-HA, 3360 cm^{-1} and 1643 cm^{-1} for MD-HA and 3345 cm^{-1} and 1640 cm^{-1} for OD-HA. It is worth mentioning that the chemically absorbed water peak was more obvious for MD-HA especially at 3345 cm^{-1} (stretching) compared to FD-HA and OD-HA. This indicated that OD-HA and FD-HA have lower water content than the MD-HA powder. The low water content of OD-HA could be due to the long oven drying hours (16 hours) which eliminated most of the water content from OD-HA. For FD-HA, liquid was not involved in the entire freeze drying process which lead to the narrow water peak in the FTIR as indicated in Figure 5.2.

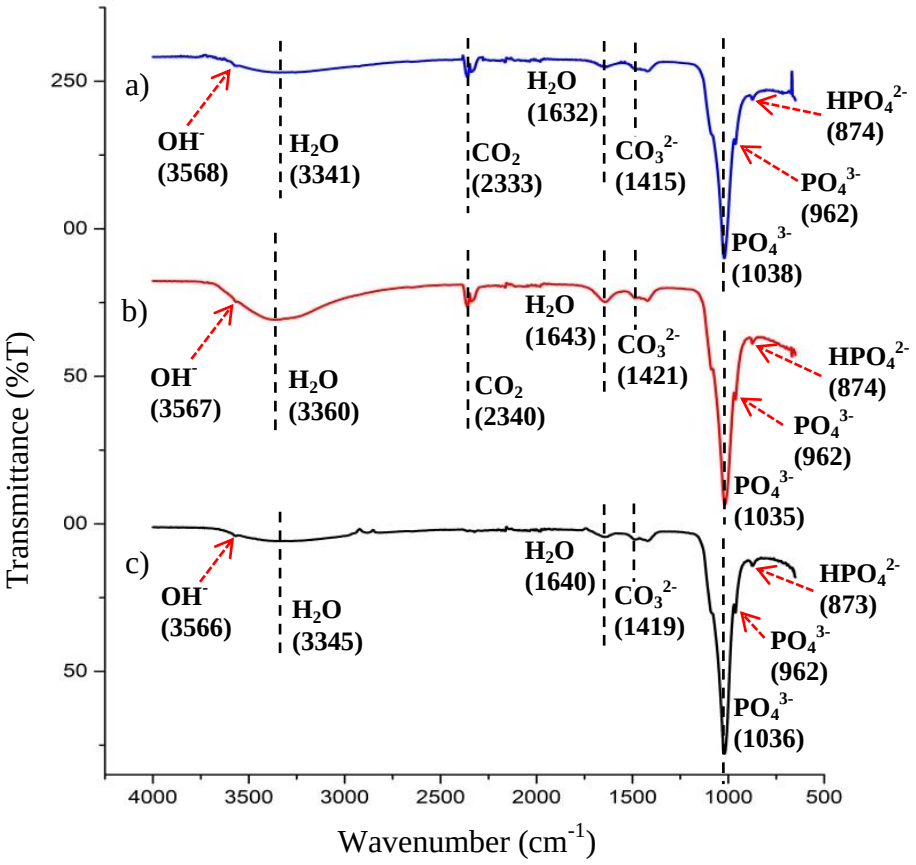

Figure 5.2: The FTIR spectrum of the synthesized HA powders: (a) FD-HA, (b) MD-HA and (c) OD-HA.

The characteristic peak corresponding to free CO_2 was detected from MD-HA (~2340 cm^{-1}) and FD-HA (2333 cm^{-1}) could be attributed to the atmospheric CO_2

concentration (Taquet *et al*. 2013). Similar CO_2 bond was also reported by Pretto *et al*. (2003) and Kamalanathan *et al*. (2014). Besides, the band at 1415 cm^{-1} (FD-HA), 1419 cm^{-1} (OD-HA) and 1421 cm^{-1} (MD-HA) suggesting the presence of B-type carbonate where the PO_4^{3-} in HA was substituted by CO_3^{2-}, similar to those reported in previous studies (Fuentes *et al*., 2008; Wu *et al*., 2013). The appearance of this band is due to carbonaceous impurities in ambient air or the interaction between the trace impurities in the starting precursors with the atmospheric CO_2 while some authors claimed that the presence of the B-type carbonate was due to the dissolution of atmospheric CO_2 in the alkaline medium during the powder synthesis process (Balamurugan *et al*., 2006; Vaidhyanathan & Rao, 1996; Alobeedallah *et al*., 2011; Sooksaen *et al*., 2010) as alkaline solution readily absorb CO_2 (Osaka *et al*., 1991). However, the B-type carbonate did not affect the purity of HA according to the XRD spectrum in Figure 5.1 and its appearance can be eliminated by subsequent sintering (Alobeedallah *et al*., 2011).

Table 5.2: Wave number for the functional groups of FD-HA, MD-HA, OD-HA and the comparison to the result obtained from previous study (Brundavanam *et al*., 2015).

Functional groups/bond	Associated FTIR wave number (cm^{-1})			
	FD-HA	MD-HA	OD-HA	(Brundavanam *et al*., 2015)
ν (OH^-)	3568	3567	3566	3569
ν_3 (PO_4^{3-})	1038	1035	1036	1024
ν_1 (PO_4^{3-})	962	962	962	964
ν_2 (H_2O absorbed)	1632	1643	1640	1654
ν_3 (CO_3^{2-})	1415	1421	1419	1415
ν_3 (CO_2)	2333	2340	-	-
H_2O absorbed	3341	3360	3345	3376
HPO_4^{2-}	874	874	873	880

5.1.3 EDX Analysis of the Synthesized HA Powder

Figure 5.3 - 5.5 show the energy-dispersive X-ray (EDX) spectrum and the mass percentage of all the detected elements of the FD-HA, MD-HA and OD-HA powders, respectively.

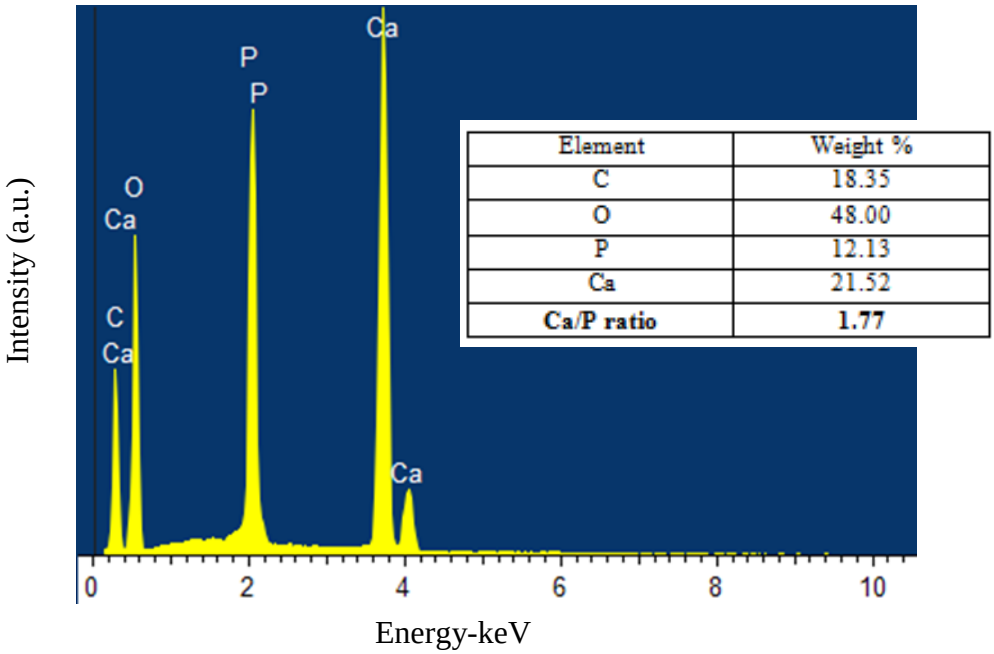

Element	Weight %
C	18.35
O	48.00
P	12.13
Ca	21.52
Ca/P ratio	**1.77**

Figure 5.3: The EDX spectrum and elemental composition of FD-HA.

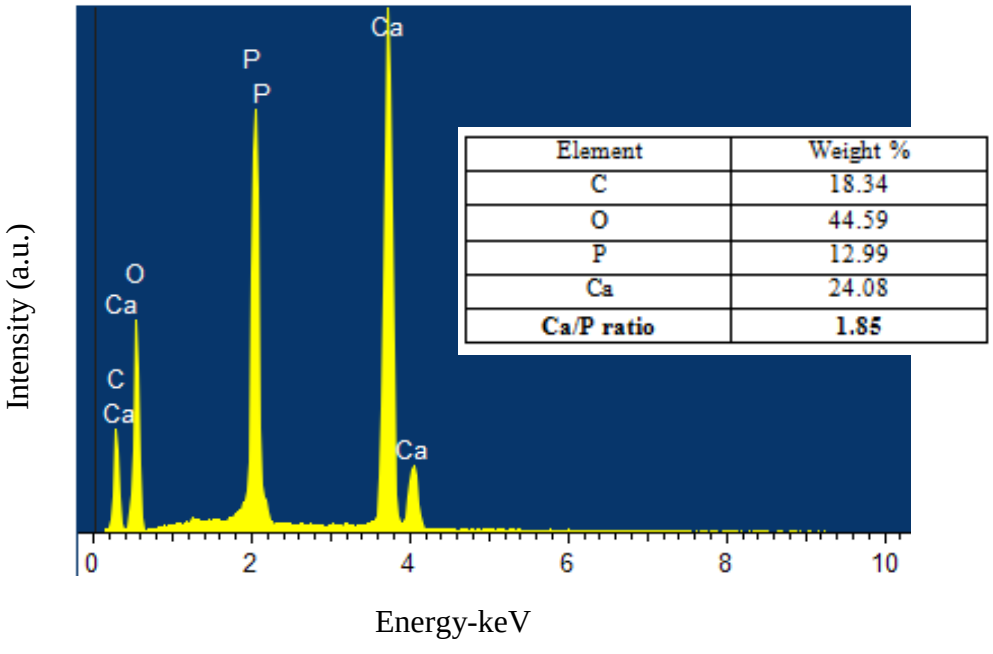

Element	Weight %
C	18.34
O	44.59
P	12.99
Ca	24.08
Ca/P ratio	**1.85**

Figure 5.4: The EDX spectrum and elemental composition of MD-HA.

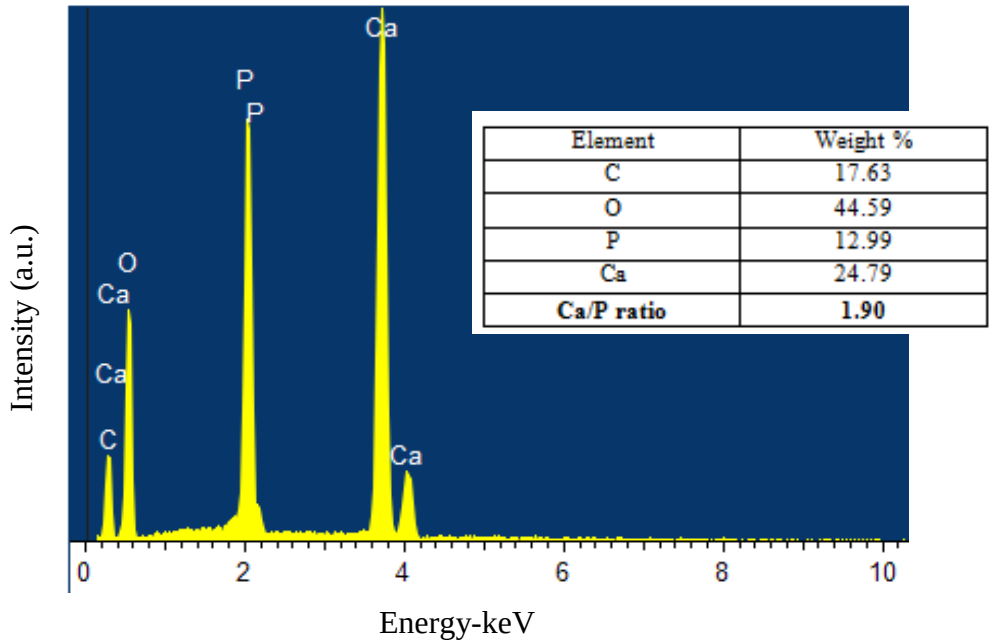

Element	Weight %
C	17.63
O	44.59
P	12.99
Ca	24.79
Ca/P ratio	**1.90**

Figure 5.5: The EDX spectrum and elemental composition of OD-HA.

According to the EDX spectrum (Figure 5.3 - 5.5), all the synthesized HA powders consist of main constituents of HA, where calcium, phosphorus and oxygen are present. From the results, it can be seen that all the HA powders, namely FD-HA, MD-HA and OD-HA have Ca/P ratio greater than the stoichiometric value of HA (1.667); recorded values of 1.77, 1.85 and 1.90, respectively. This is not in agreement with the findings from previous studies where Ca/P ratio of pure HA was close to 1.60 - 1.667 (Fanovich & Porto Lopez, 1998; Ramesh *et al*., 2012; Pattanayak *et al*., 2007; Lu *et al*., 1998). Apart from that, OD-HA recorded the highest Ca/P ratio of 1.90 compared to MD-HA and FD-HA which is in agreement with the study carried out by Santhosh *et al*. (2012) and Lu *et al*. (1998).

The high Ca/P ratio of the current study could be associated with the presence of B-type carbonate substitution as described in Figure 5.2 and Table 5.2. The substitution was believed to reduce the phosphorus content of HA, thus cause the higher value of Ca/P ratio (Boutinguiza *et al*., 2012). Moreover, it was reported that EDX results

represent the sample only at a microscopic level and hence the discrepancy between EDX data and the expected values have been frequently reported with some deviations (Kieswetter *et al*. 1994). Although the Ca/P ratio of all the synthesized powders are deviated from 1.667, it can be identified as HA because Ca/P ratio for HA could vary from 1.2 – 2.0 (Larsen & Widdowson, 1971). Liu *et al*. (2008) and Landi *et al*. (2000) stated that deviation from stoichiometric Ca/P ratio would affect the reactivity and phase stability of HA, however phase disruption was not observed in current study as evidence from XRD analysis (Figure 5.1).

5.1.4 FE-SEM Analysis of the Synthesized HA Powder

The FE-SEM micrographs of FD-HA, MD-HA and OD-HA are presented in Figure 5.6, Figure 5.7 and Figure 5.8, respectively. Generally, FD-HA (Figure 5.6) and MD-HA (Figure 5.7) consist of small to large size agglomerates made of small particles while OD-HA (Figure 5.8) consists of extremely large agglomerates. From Figure 5.6, the FD-HA powder was a loose agglomerates mixture of fine particle size. The distribution of HA particles was uniform and homogeneous. The agglomerates sizes are in the range from extremely small of 0.5 μm to a large size of 3 μm. Therefore, it can be deduced that the individual HA particle size is extremely small in nanometer range which is in agreement with the HA crystal size calculated from Scherrer's equation (Table 5.1). As for MD-HA, FE-SEM analysis revealed that the powder consists of a mixture of small and large agglomerates in size ranging from 0.4 μm to 4 μm. The larger particle appears to be large agglomerate of loosely packed smaller particles in nano regime. Conversely, the OD-HA powder as shown in Figure 5.8, consist of large and hard agglomerates, resulting in rougher surface. The smallest agglomerate of OD-HA is about 2 μm to as large as 10 μm. The powder seemed to be more compacted compared to FD-HA and MD-HA. It is well known that wet chemical synthesized HA powder dried by the means of conventional oven drying are accompanied by severe

agglomeration (Lu *et al*., 1998; Hsu & Chiou, 2011; Yu *et al*., 2010; Zhang & Yogokawa, 2008).

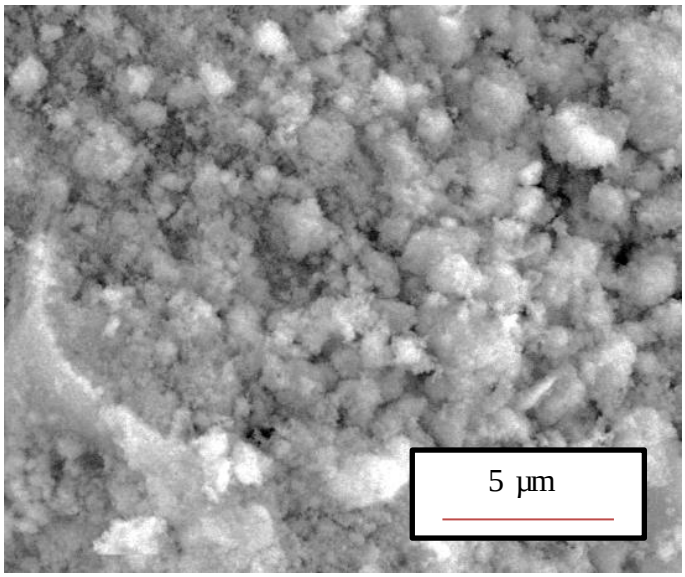

Figure 5.6: FE-SEM micrograph of synthesized FD-HA powder.

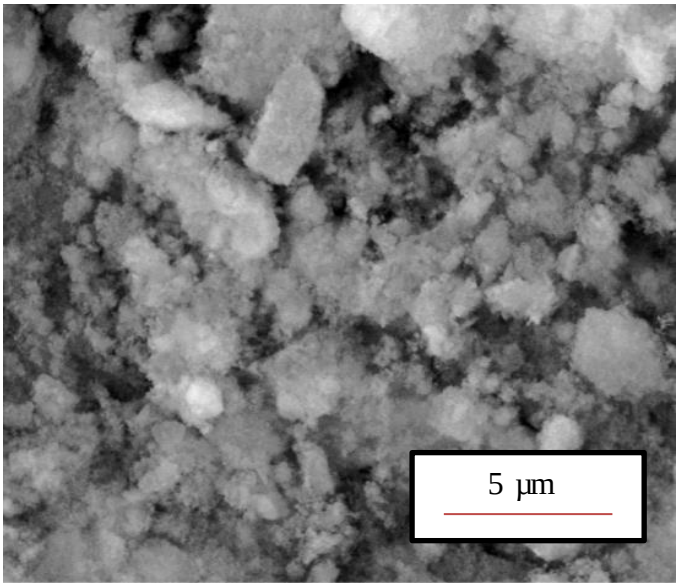

Figure 5.7: FE-SEM micrograph of synthesized MD-HA powder.

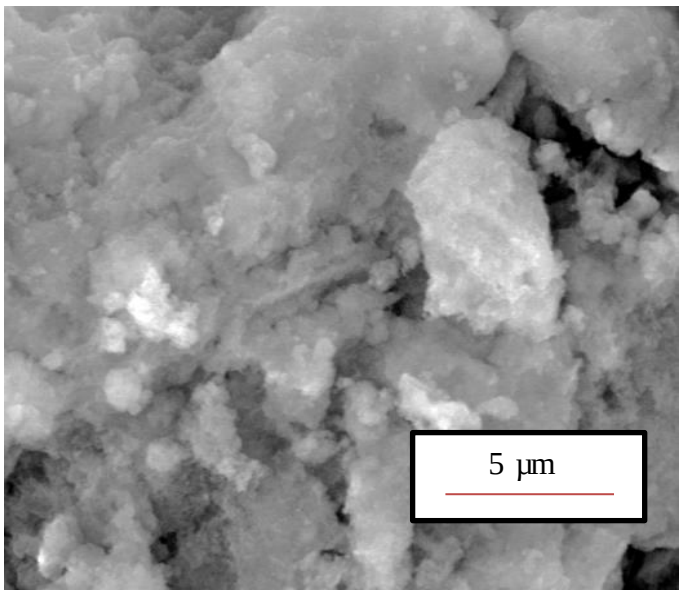

Figure 5.8: FE-SEM micrograph of synthesized OD-HA powder.

The small particle size of FD-HA is due to the fact that no heat was involved in the freeze drying process and hence crystal structure does not grow as there was no supply of heat energy. Microwave drying was found to produce HA powders with small particle size. During microwave drying, the internal and surface of the HA slurry was heated simultaneously. The water molecules within the HA slurry, being specific to microwave irradiation was heated instantly and triggered the quick expansion of vapor during the drying process. This rapid expansion of vapor caused the breakage of large aggregates into several tiny lumps, hence, small particle size (Qi *et al*., 2006). Oven drying removed water from the HA slurry via evaporation at an elevated temperature which promotes particles in close contact with each other. As the heat was supplied to the HA slurry constantly, solid particle bridging was formed between particles and lead to the formation of hard agglomerates (Yu *et al*., 2005). In conclusion, the drying method has significant effects on the powder particle and agglomerates size of the synthesized HA powders. It should be noted that the individual particles of all the powders could not be recognized due to their extremely small size and thus TEM analysis has to be carried out to further examine the particle sizes of all the powders.

5.1.5 TEM Analysis of the Synthesized HA Powder

The effects of different drying route on the morphology of the synthesized HA powder was determined via transmission electron microscopy (TEM) and the micrographs are shown in Figure 5.9. FD-HA (Figure 5.9 (a)) and OD-HA (Figure 5.9 (c)) resembled needle-like structure. The needle-like morphology was said to be similar to the bio-crystal found in human hard tissue (Nejati *et al*., 2009; Ferraz *et al*., 2004; Patel *et al*., 2001). Nevertheless, MD-HA was found to exhibited nano-rod structure and similar HA particle shape was reported by Santhosh & Prabu (2012) who synthesized HA via microwave drying. Siddharthan *et al*. (2006) claimed that the difference is HA particle shape was affected by the microwave power. They found that the shapes of HA changed from needle shape to rod/platelet shape as the microwave power increased from 175 W to 600 W. The resulting nano-rod shape could be explained as the consequence of high microwave power (800 W) applied in current research. Although MD-HA displayed different particle shape from FD-HA and OD-HA, it was found that all the powders are in nanometric range as tabulated in Table 5.3. Nano-size particles are desirable as they give better resorption and biological activity which promotes the adhesion and proliferation of bone cells (Le Geros, 1991; Pham *et al*., 2013). Moreover, nano-sized powders produced dense and nanocrystalline sintered ceramic that possesses superb mechanical properties by having higher driving force for the densification (Wang & Shaw, 2007). On the contrary, micro-sized powders caused exaggerated grain growth during sintering due to the agglomerated and irregular morphology (Groza & Dowding, 1996; Lin *et al*., 2007).

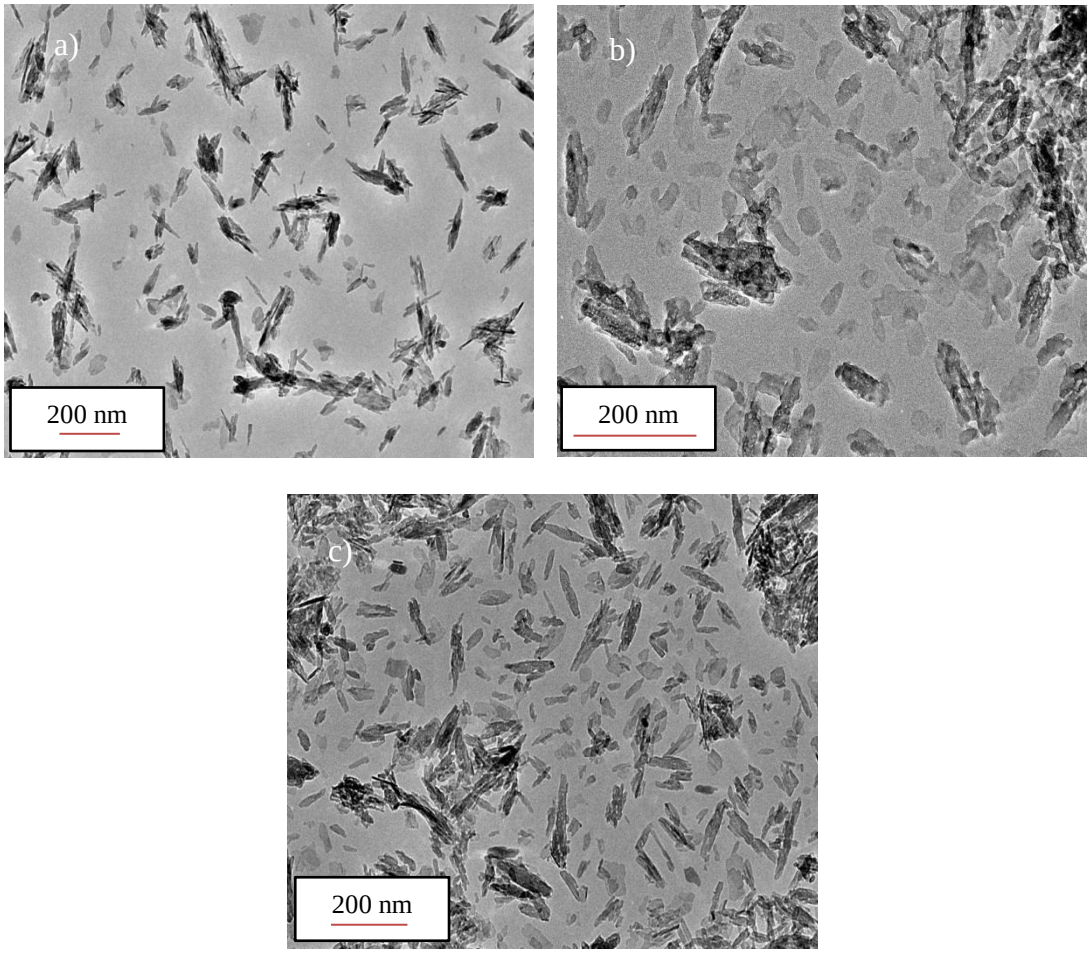

Figure 5.9: TEM micrographs of synthesized HA powder: (a) FD-HA, (b) MD-HA and (c) OD-HA.

Table 5.3: Summary of the average size of HA powder synthesized via different drying methods.

Sample	Particle size distribution	Average Particle Size (Length)	Average Particle Size (Width)
FD-HA	40 – 180 nm (Length) 10 – 50 nm (Width)	82.0 nm	24.8 nm
MD-HA	20 – 140 nm (Length) 10 – 40 nm (Width)	66.7 nm	23.6 nm
OD-HA	30 – 160 nm (Length) 10 – 30 nm (Width)	75.0 nm	21.4 nm

From Table 5.3, it can be seen that the particle size of FD-HA was slightly larger compared to MD-HA and OD-HA, having average particle size of 24.8 nm in width and 82.0 nm in length. Despite bigger particle size, the crystal particles show good

dispersibility with minimal agglomeration (Figure 5.9 (a)) compared to MD-HA and OD-HA which is consistent with the FE-SEM micrograph shown in Figure 5.6. Similarly, Wang *et al*. (2010), Bildstein *et al*. (2009) and Saluja *et al*. (2010) also reported that HA particle produced by freeze drying method displayed bigger particle size than other drying methods. However, this contradicts to the results reported by Lu *et al*. (1998) as they found that the particle size of FD-HA is smaller than that of normal heat dried HA powder. The dissimilarities in results might be due to the fact that the HA slurry was froze rapidly with liquid nitrogen in their work which fast cooling prevent ice nucleation which hinder the growing of large dendritic ice crystal and hence smaller particle size was produced (Kurapova *et al*., 2012). Similar to the previous study (Santhosh & Prabu, 2012), microwave drying manage to produce HA particles in nanometric range. However, the average particle sizes of MD-HA in the current study, recorded at 66.7 nm (length) and 23.6 nm (width) was bigger than that reported by Siddhartahn *et al*. (2006) at ~32 nm (length) and ~12 nm (width). The bigger HA particle size obtained from current study could be associated with the use of higher microwave power which favored the maturation of HA crystal growth. Although OD-HA has smaller particle size than FD-HA, the agglomeration of powders are rather serious compared to FD-HA. From Figure 5.9 (c), OD-HA shows agglomerated clusters with particles in needle shape. Lin *et al*. (2007) stated that the agglomerations in powder are detrimental to the densification of ceramics during sintering and should be avoided.

5.1.6 Specific Surface Area of the Synthesized HA Powder

The specific surface areas (SSA) of all the synthesized HA powder were determined via BET analysis and the finding is tabulated in Table 5.4.

Table 5.4: Summary of the average size of HA powder synthesized via different drying methods.

Sample	Specific Surface Area (m^2/g)
FD-HA	97.4
MD-HA	111.1
OD-HA	97.1

FD-HA and OD-HA obtained similar SSA of 97.4 m^2/g and 97.1 m^2/g, respectively while MD-HA exhibited high SSA of 111.1 m^2/g. Wang & Shaw (2007) claimed that high surface energy is stored in HA nano-rods as the side surface of nano-rods composed of the high energy prism planes of HA crystal. Therefore, it could be deduced that the high SSA of MD-HA compared to FD-HA and OD-HA was associated with the dissimilarities in HA particle shapes as shown in Figure 5.9 where MD-HA demonstrated nano-rod structure.

Nonetheless, the SSA of HA powders obtained in current study are generally higher than those reported in literature as most of them recorded SSA below 70 m^2/g (Wilson Jr & Hull, 2008; Saeri *et al*., 2003; Patel *et al*., 2001; Raynaud *et al*., 2002; Veljovic *et al*., 2009). The high SSA value attained in the current study is advantageous as high SSA induced higher driving force in enhancing densification processing kinetic and sintering activity (Lin *et al*., 2007) due to high surface energy stored in HA particle (Wang & Shaw, 2007). Therefore, it can be concluded that microwave drying is a promising method of manufacturing HA powder with higher SSA.

5.2 Sinterability of the HA Powder

5.2.1 HA Phase Stability

The HA powder synthesized via drying methods were subjected to sintering in air atmosphere and the phase stability was determined via XRD analysis. The phases

analysis of the sintered FD-HA, MD-HA and OD-HA are shown in Figure 5.10, Figure 5.11 and Figure 5.12, respectively.

The formation or secondary phases were not detected in FD-HA and MD-HA throughout the sintering regime as all the XRD peaks showed good correlation with the stoichiometric HA as shown in Figure 5.10 and Figure 5.11. However, β-TCP was observed in the OD-HA sintered at 1350 ℃ as shown in Figure 5.12. The results indicated that freeze drying and microwave drying can preserve the thermal stability of HA better than conventional oven drying method.

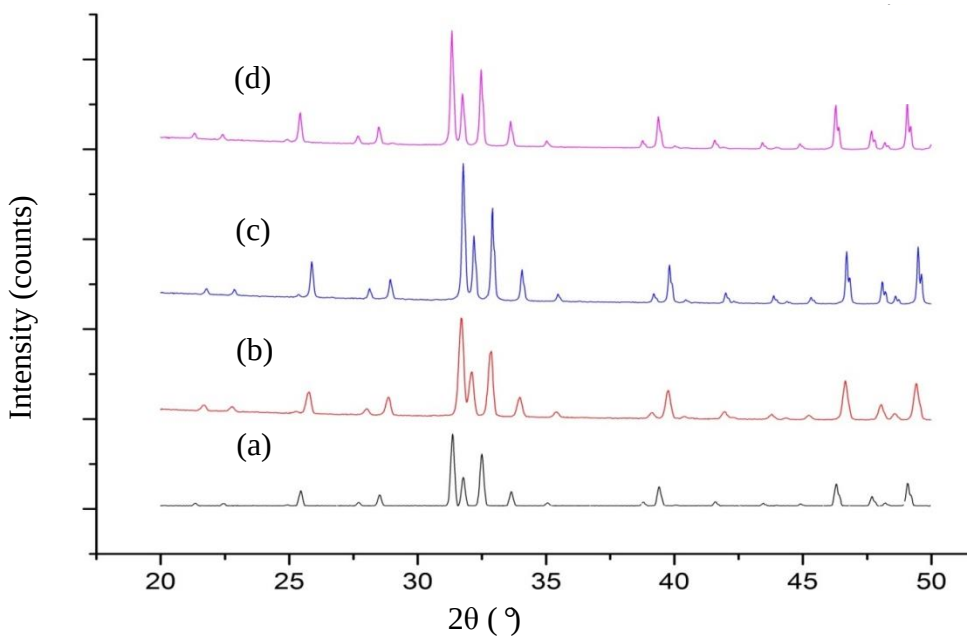

Figure 5.10: The XRD profiles of FD-HA sintered samples (a) 1050 ℃, (b) 1150 ℃, (c) 1250 ℃ and (d) 1350 ℃. All peaks belong to the HA phase.

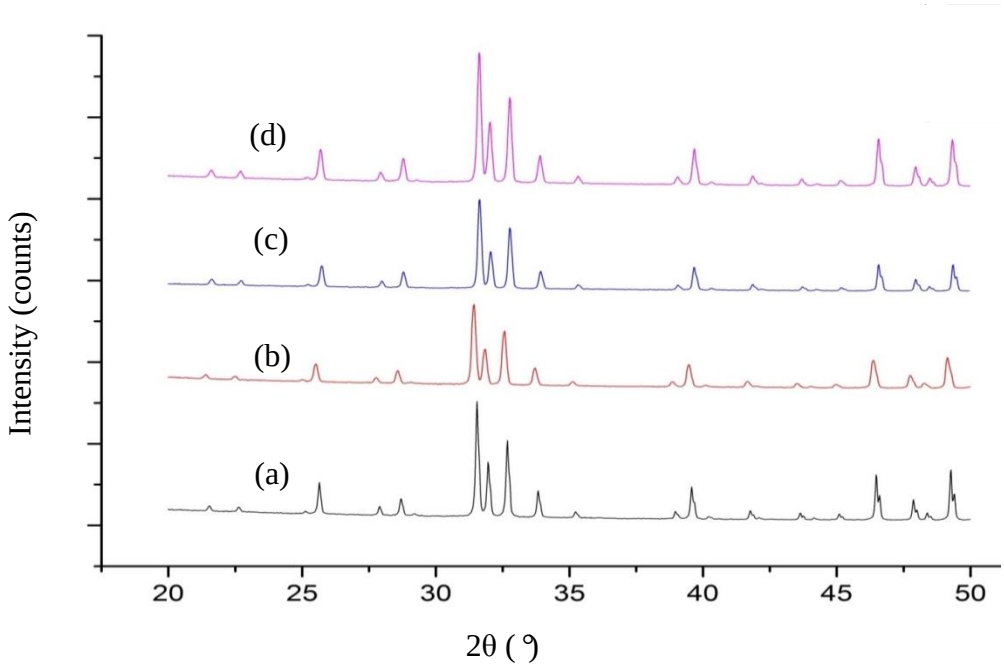

Figure 5.11: The XRD profiles of MD-HA sintered samples (a) 1050 ℃, (b) 1150 ℃, (c) 1250 ℃ and (d) 1350 ℃. All peaks belong to the HA phase.

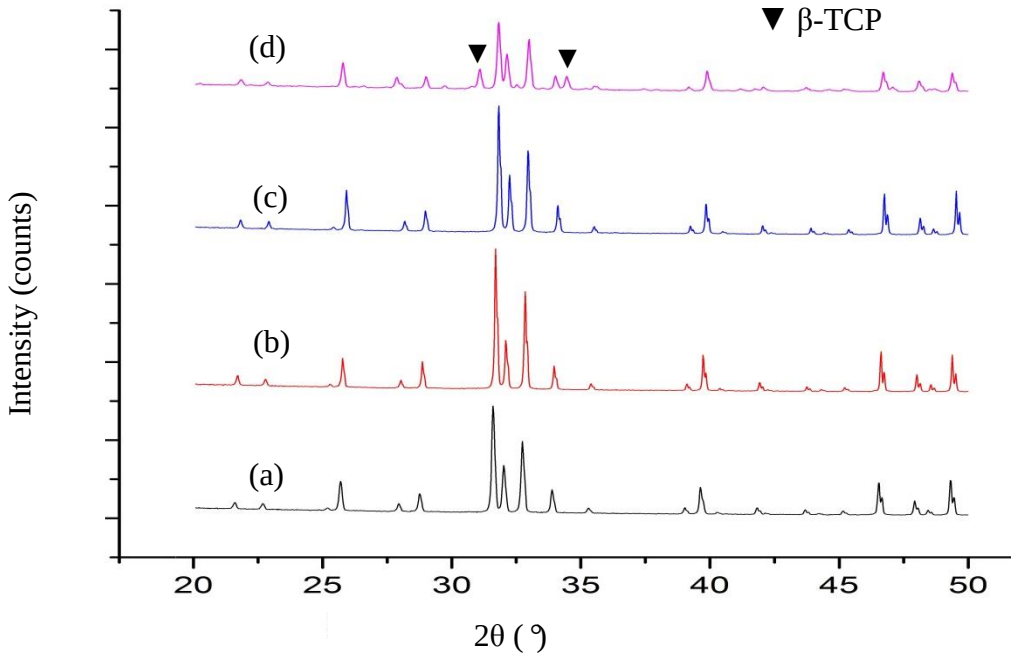

Figure 5.12: The XRD profiles of OD-HA sintered samples (a) 1050 ℃, (b) 1150 ℃, (c) 1250 ℃ and (d) 1350 ℃. The unmarked peaks belong to the HA phase.

Although the phase stability of FD-HA was not disrupted throughout the sintering regime, a small peak shift to lower diffraction angle was observed for sample sintered at 1350 ℃. This variation could be the consequence of dehydroxylation phenomenon due to water loss at high temperature (Lin *et al*., 2001; Wang & Chaki, 1993) or the loss of OH^- radial from HA lattice (Gu *et al*., 2002; Bianco *et al*., 2007). It was reported that thermal decomposition of HA occur in sequence of dehydroxylation (Slosarczyk *et al*., 1996; Wang *et al*., 2004). During dehydroxylation, HA will lose OH^- gradually and form oxyapatite according to the following equation (Zhou *et al*., 1993; Kijima & Tsutsumi, 1979; Trombe & Montel; 1978):

$$2OH \rightarrow O + H_2O \uparrow \quad (5.1)$$

$$Ca_{10}(OH)_2(PO_4)_6 \rightarrow Ca_{10}(PO_4)_6.O\square + H_2O \quad (5.2)$$

where □ is a vacancy and oxyapatite ,$Ca_{10}(PO_4)_6.O\square$ is also known as hydroxy-ion-deficient product. Accordingly, one of the lattice site was occupied by the two OH^- group in HA unit cell is now replaced by an oxygen atom while the other was left vacant. In addition to that, Zhou *et al*. (1993) reported that the oxyapatite phase is stable and will not cause phase transformation without further heating.

However, if sintering carried out at higher temperature, HA would decompose into tricalcium phosphate and tetracalcium phosphate in accordance to the following process:

$$Ca_{10}(OH)_2(PO_4)_6 \rightarrow 2Ca_3(PO_4)_2 + Ca_4P_2O_9 + H_2O \quad (5.3)$$

This phenomenon was observed from OD-HA sintered samples as illustrated in Figure 5.12. From the XRD profiles, HA phase was the main constituent phases present in these compacts at sintering temperature ranging from 1050 ℃ to 1250 ℃. However, the decomposition of HA into β-TCP was clearly observed from OD-HA sintered at

1350 ℃. The present results obtained for OD-HA samples contradicted the findings of Muralithran & Ramesh, 2000, Bianco *et al*., 2007 and Ramesh *et al*., 2008. In general, these authors reported that their HA powder which was synthesized using drying method as the present OD-HA showed that the transformation of HA into secondary phases only at sintering temperature beyond 1350 ℃. According to Muralitran & Ramesh (2000) and Arias *et al*. (1998), both dehydroxylation and decomposition reaction could be slow down by providing a high local humid furnace atmosphere during sintering as the dehydration of the OH^- from HA matrix could be prevent. Hence, it could be deduced that the differences in the findings could be attributed to the humidity, drying temperature and drying hours of the samples in the conventional oven.

It is worth mentioning that HA produced via microwave drying shows high thermal stability as no peak shifting nor decomposition were observed on MD-HA throughout the sintering profile. Since all of the HA sintered under the same sintering atmosphere, it could be confirmed that the high thermal stability of MD-HA compared to FD-HA and OD-HA was not due to the humidity of sintering atmosphere. The ability of MD-HA to preserve the phase stability at high temperature could be attributed to the significant amount of absorbed water remained in the structure of MD-HA compared to FD-HA and OD-HA as evidence from FTIR analysis of the HA powders (Figure 5.2).

In conclusion, the thermal stability of all the HA sintered samples (regardless of drying methods) are generally higher than most of the available literatures (Ruys *et al*., 1995; Finoli *et al*., 2010; Sanosh *et al*., 2010; Kothapalli *et al*., 2004; Kong *et al*., 2002). They produced HA with low thermal stability where the decomposition of HA started at sintering temperature lower than 1300 ℃. As such, the results obtained in the present work are encouraging and microwave drying was found to produce single phase HA stable up to 1350 ℃.

5.2.2 FTIR Analysis of Sintered HA Samples

Figure 5.13 shows the FTIR analysis of the FD-HA, MD-HA and OD-HA sintered at 1350 ℃ and the comparison with their respective as-synthesized powder. It was observed that the CO_3^{2-} band and the chemically absorbed H_2O bands are no longer visible in all the HA sintered at 1350 ℃ as indicated in Figure 5.13.

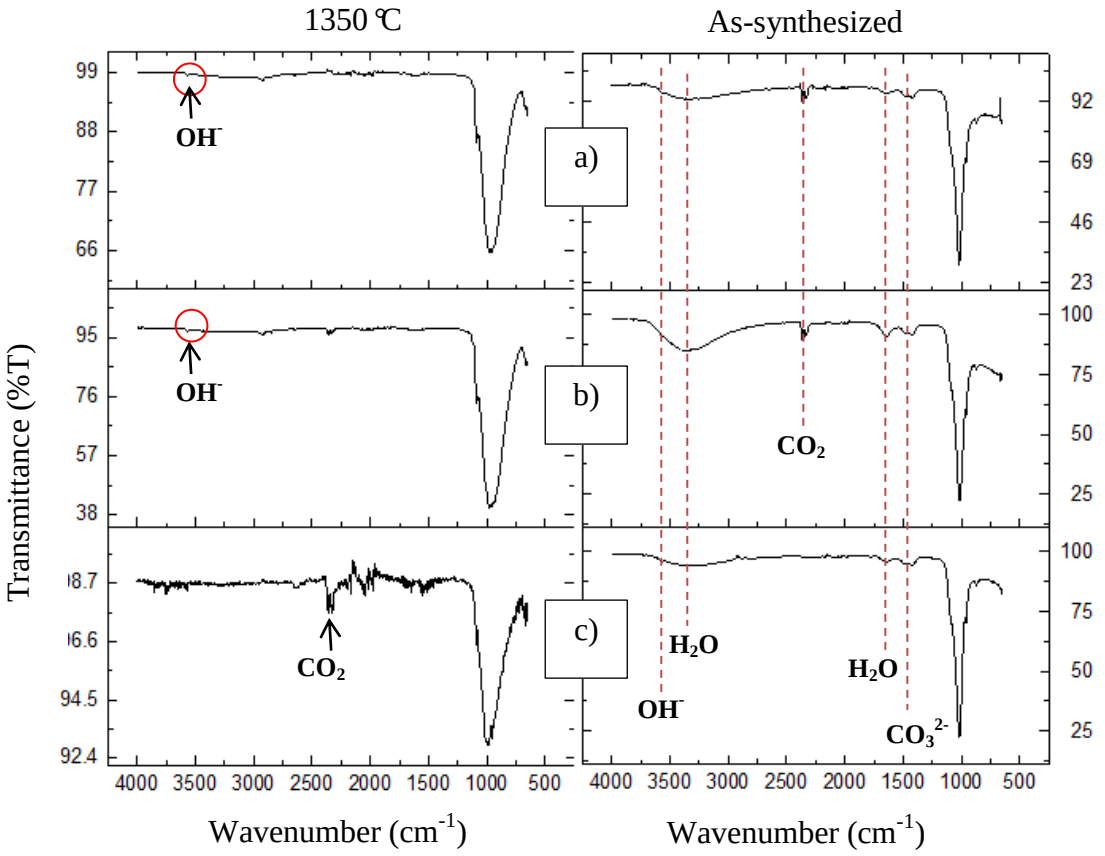

Figure 5.13: FTIR profiles of HA sintered at 1350 ℃ (left) with their respective as-synthesized powder (right): (a) FD-HA, (b) MD-HA and (c) OD-HA.

The intensity of peaks associated to the OH^- band of the sintered FD-HA and MD-HA are remarkably decreased as shown in Figure 5.13 (a) and (b). The weak OH^- band and the missing H_2O bands could be the primary factor that caused the dehydroxylation of FD-HA at 1350 ℃ as revealed by the aforementioned peak shifting in the XRD profile shown in Figure 5.10. Besides, the free CO_2 was previously appeared in the synthesized FD-HA and MD-HA are removed from the HA structure as the

corresponding peaks was not seen. The results showed that the sintering of FD-HA and MD-HA induced the elimination of combined water and carbonates without causing further decomposition of HA.

On the contrary, the FTIR peaks of OD-HA (Figure 5.13(c)) shows the appearance of CO_2 peak and the absence of the peaks corresponding to OH^- after sintering. The CO_2 could interrupt the HA phase and cause further decomposition while the absence of OH^- peak confirms its transformation into oxyapatite (Wang *et al.*, 2009). Hence, the decomposition of OD-HA at 1350 ℃ was due to the combined effects of the appearance of the CO_2 and absence of the OH^- peak.

5.2.3 Bulk Density

The variation of sintered density with sintering temperature for all HA samples synthesized via different drying methods are shown in Figure 5.14.

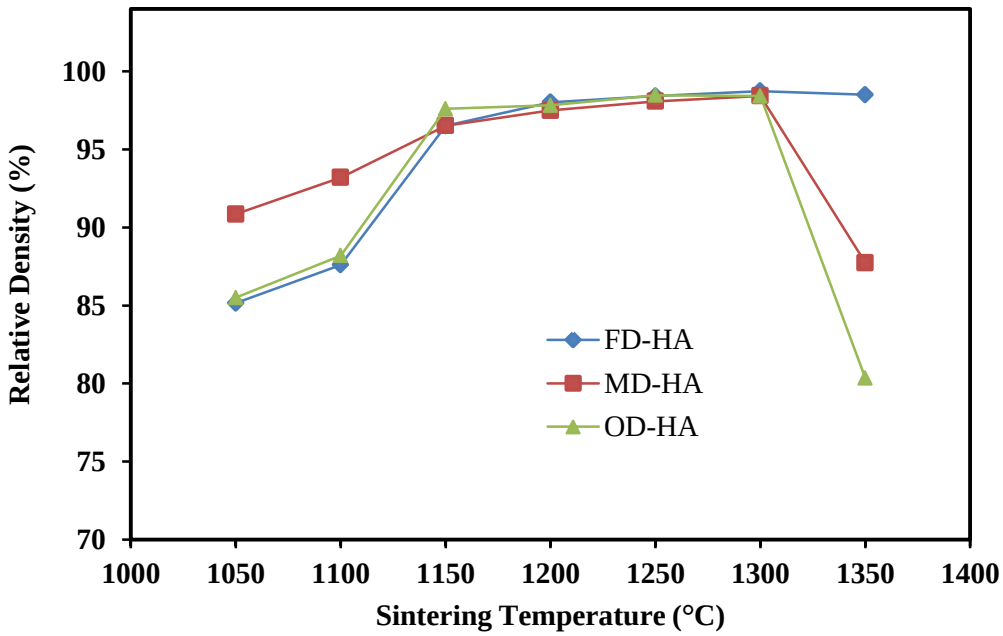

Figure 5.14: The effect of sintering temperature on the relative density of HA.

In general, the results proved that the relative density of the sintered HA increases when the sintering temperature increase and reach at plateau at 1300 ℃, irrespective of the different drying methods of the HA powders. A small increase in density is observed at 1050 ℃ to 1100 ℃ for FD-HA and OD-HA which corresponds to the first stage of sintering where necks forming into grains (Gibson *et al*., 2001). It could be seen that MD-HA has higher starting density than FD-HA and OD-HA. For example, MD-HA obtained high relative density of ~91% at 1050 ℃ compared to FD-HA and OD-HA which attained similar relative density of ~85% at 1050 ℃. The high starting density of MD-HA is due to the high specific surface area reported in earlier section which provides high surface energy for the densification process (Göller & Oktar, 2002). The second stage of sintering involved the onset of densification and the removal of porosity and this stage is indicated by a sharp increase in the sintered density. For both FD-HA and OD-HA, the sharp increment of relative density was between 1100 ℃ to 1150 ℃. Conversely, the onset of densification of MD-HA started at lowtemperature of 1050 ℃.

The MD-HA sintered samples exhibited densification of 93.2% at 1100 ℃ and achieved densification of >97.5% when sintered above 1200 ℃. Similar observation was reported by Gibson *et al*. (2001) and Rodriguez-Lorenzo (2001) that HA attained ~97% relative density at 1200 ℃. On the contrary, Mostafa (2005), Prokopiev & Sevostianov (2006), and Aminzarea *et al*. (2013) reported otherwise whereby their sintered HA samples achieved relative density less than 90% at 1200 ℃. At similar temperature of 1100 ℃, FD-HA and OD-HA attained only ~87.6% and 88.2% of theoretical density and both of them recorded relative density of ~98% at 1200 ℃ which is slightly higher than that of MD-HA. This is not in agreement with the findings of Van Landuyt *et al*. (1995), Thangamani *et al*. (2002) and Sanosh *et al*. (2010) as they found that sintering above 1300 ℃ was required to achieve ~98% of theoretical density. This difference in observation could be related to the different powder characteristics used.

Generally, all the HA samples achieved the maximum density at the same temperature of 1300 ℃. FD-HA attained the maximum density of 98.74% at 1300 ℃ and drop slightly to 98.5% at 1350 ℃. MD-HA recorded maximum density of 98.4% at 1300 ℃ and drop to 87.74% at 1350 ℃. On the other hand, OD-HA achieved the maximum density of 98.42% at 1300 ℃ and drop drastically to 80.3% at 1350 ℃. The sharp drop in relative density of OD-HA at 1350 ℃ is ascribed to the presence of secondary phase (β-TCP) in the sintered OD-HA as indicated in XRD data in Figure 5.12. Overall, MD-HA samples showed better densification than FD-HA and OD-HA as lower sintering temperature was required to achieve dense MD-HA samples of >90%. Moreover, as evident from the results in Figure 5.7 and Figure 5.9 (b), MD-HA powder was in nano-sized, homogenously distributed with small agglomerates and has high specific surface area. All these factors contribute to the MD-HA achieving higher densification than FD-HA and OD-HA at low temperatures (Patel *et al*., 2001; Xu *et al*., 2007; Göller & Oktar, 2002).

5.2.4 Microstructure Evolution and Grain Size

SEM analysis was carried out on FD-HA, MD-HA and OD-HA sintered samples to determine the microstructure and grain size of the samples. As shown in Figure 5.15 (b), MD-HA sintered at 1050 ℃ shows discrete grains with no visible formation of necking; corresponds to the second stage of sintering where densification has started and most of the porosities were removed. The dense microstructure with a few pores (0.1 μm to 0.4 μm) of MD-HA sintered at this temperature correlates well to the relative density results of ~91%. At similar temperature, large numbers of pores are remaining in the FD-HA and OD-HA samples as shown in Figure 5.15 (a) and 5.15 (c) respectively. The results showed that at 1050 ℃, the sintering was at the first stage for FD-HA where some necks formation were detected and large pores were observed. As for OD-HA, the sintering was at the end of first stage sintering as the interconnected pores started to from grains

and grain outline can be seen. This could explain the lower density (~85%) of both FD-HA and OD-HA at 1050 ℃.

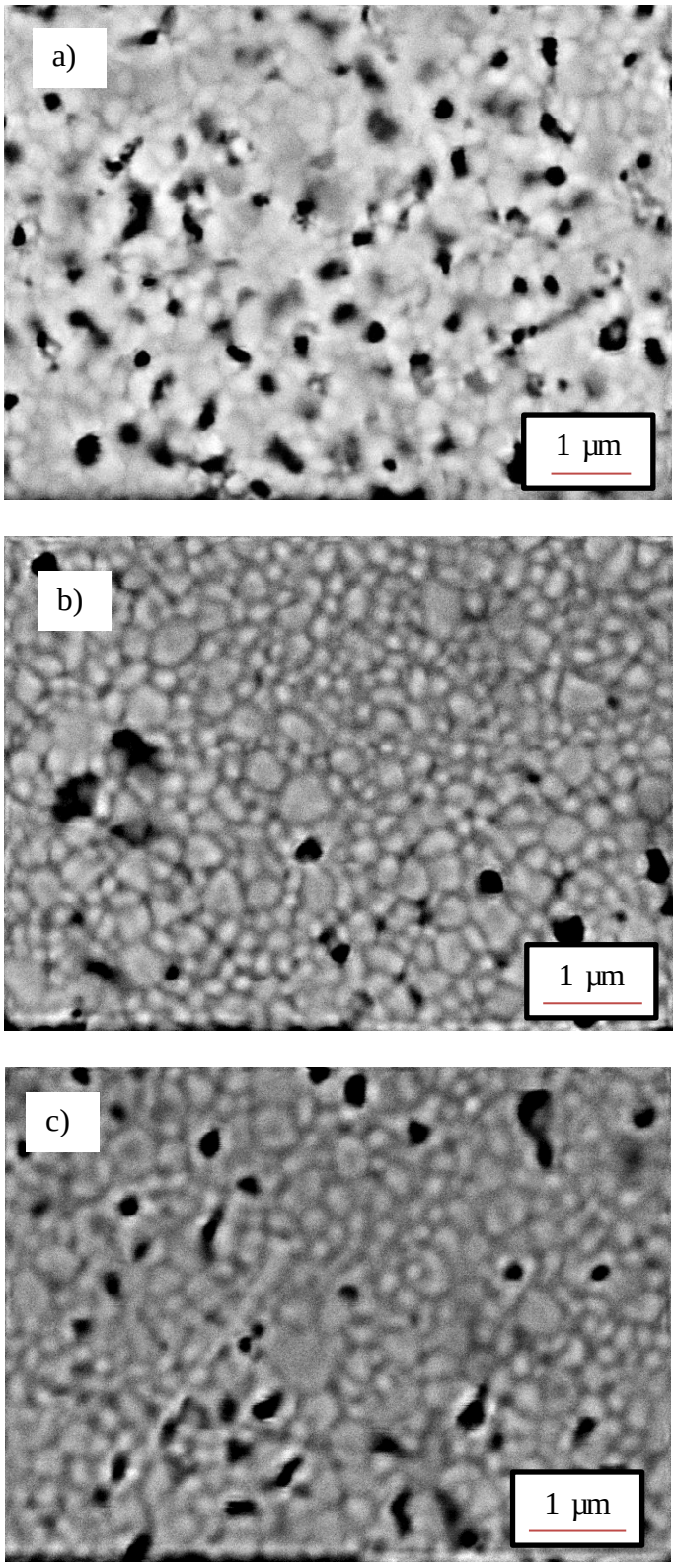

Figure 5.15: SEM images of (a) FD-HA, (b) MD-HA and (c) OD-HA sintered at 1050 ℃.

Subsequently, SEM images of samples sintered at 1150 ℃ Increase the sintering temperature could improve the densification and homogeneity of samples. At 1150 ℃, most of the pores were removed and denser microstructures were observed for all the samples; indicating that complete sintering has been achieved. These observations are in agreement with the relative density of the sintered HA samples whereby the FD-HA, MD-HA and OD-HA attained relative density of ~96.5%, ~96.52% and ~97.6%, respectively. In addition, the grain size of the FD-HA (Figure 5.16 (a)) and MD-HA (Figure 5.16 (b)) samples sintered at 1150 ℃ were observed to have a uniform distribution, having average grain size of 1.03 μm and 0.79 μm, respectively. Conversely, OD-HA attained an average grain size of 0.97 μm; accompanied by an uneven microstructure at the similar temperature as shown in Figure 5.16 (c). The recorded HA grain sizes are in agreement with most of the literatures as researchers reported that the grain size of HA sintered at 1150 ℃ is often less than 2 μm (Chaki & Wang, 1994; Veljovic *et al*., 2008; Mazaheri *et al*., 2009; Ramesh *et al*., 2007).

When sintering was carried out at 1200 ℃, all the HA samples exhibited dense microstructure where the grains are closely packed as shown in Figure 5.17. OD-HA samples sintered at 1200 ℃ shows better uniformity in terms of grain size distribution compared to those sintered 1150 ℃. Additionally, FD-HA, MD-HA and OD-HA attained average grain size of 1.73 μm, 1.34 μm and 1.67 μm, respectively at 1200 ℃.

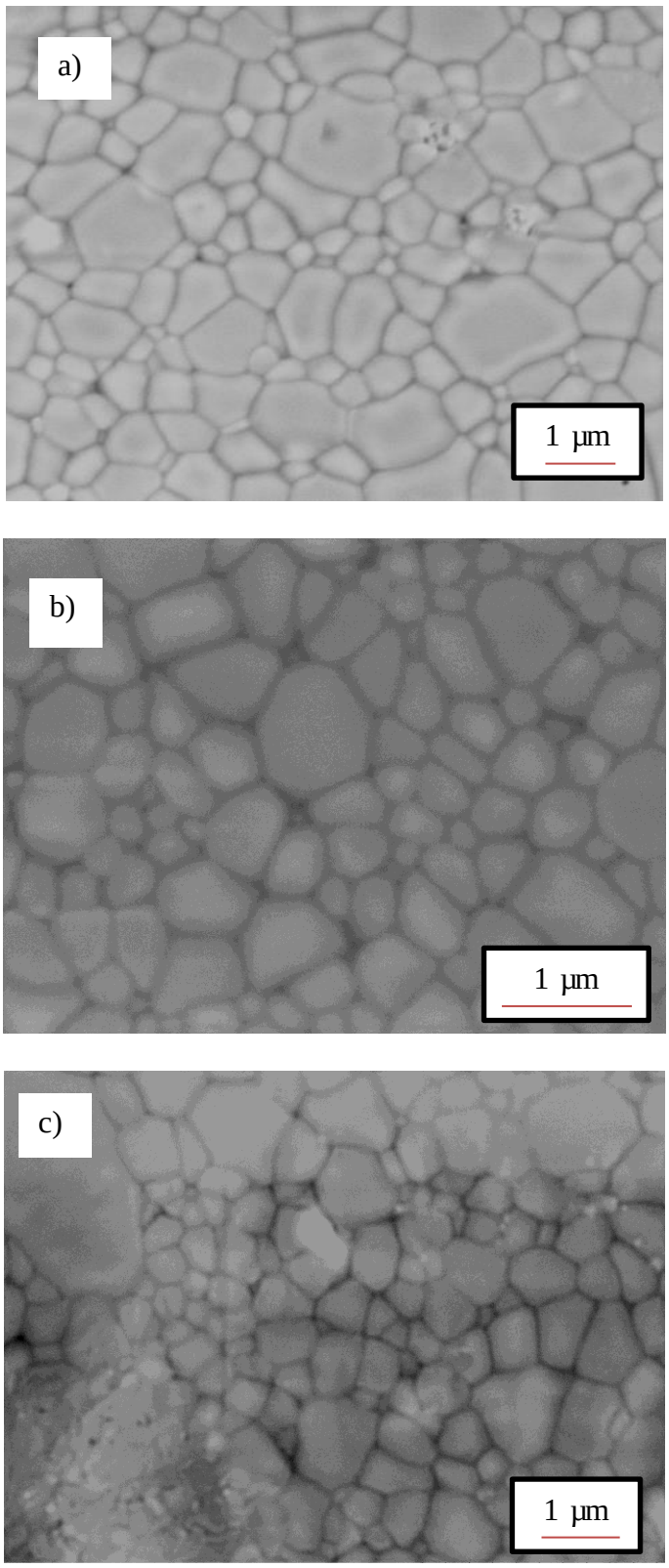

Figure 5.16: SEM images of (a) FD-HA, (b) MD-HA and (c) OD-HA sintered at 1150 ℃.

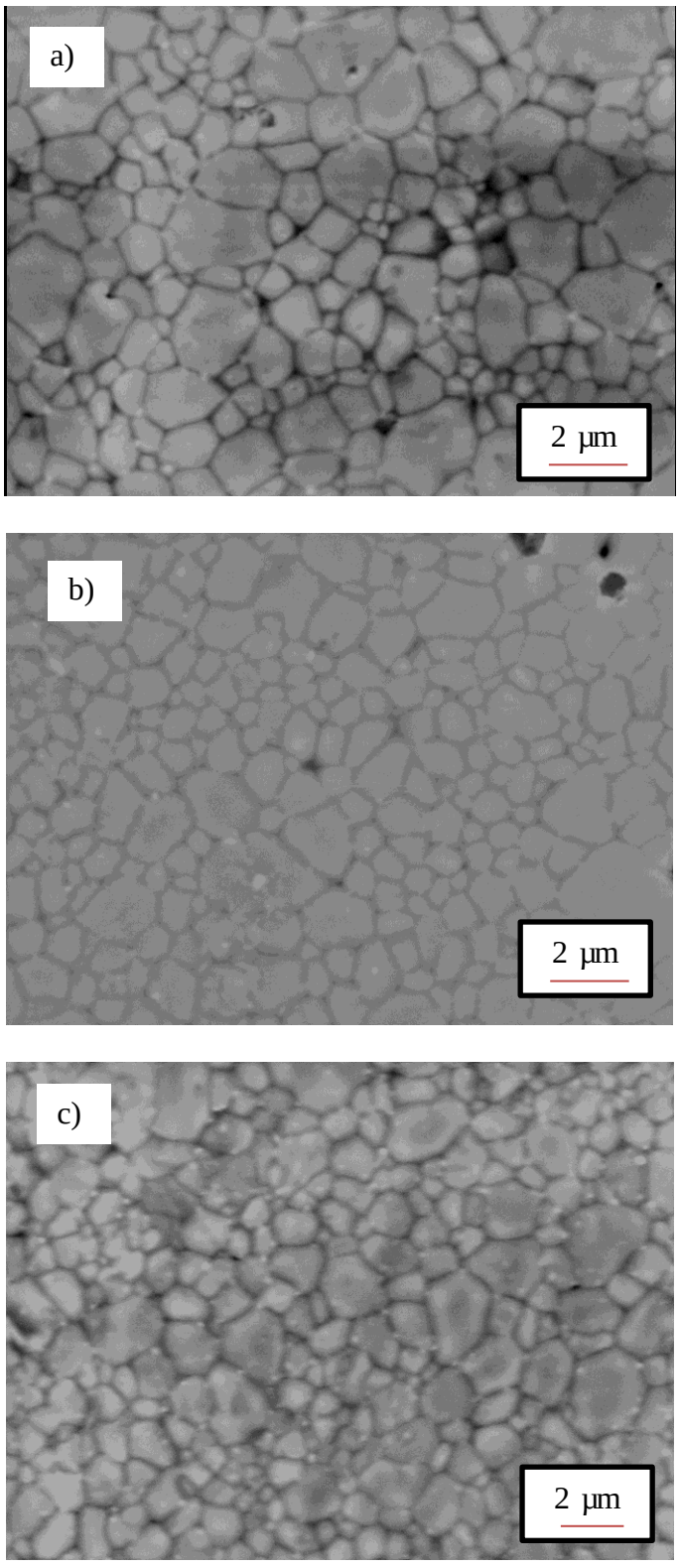

Figure 5.17: SEM images of (a) FD-HA, (b) MD-HA and (c) OD-HA sintered at 1200 ℃.

As sintering temperature goes up to 1350 ℃, FD-HA in Figure 5.18 (a) showed fully sintered microstructure with considerable grain growth which is in line with the relative

density of ~98.5%. Similarly, OD-HA in Figure 5.18 (c) was observed to display fully dense microstructure with minimal pores. Therefore, it could be deduced that the low density (80.34%) of OD-HA at 1350 ℃ was solely triggered by the presence of β-TCP in the OD-HA matrix. Unlike FD-HA and OD-HA, MD-HA presented fully sintered microstructure accompanied by the existence of several intergranular pores of ~2 μm at 1350 ℃ as shown in Figure 5.18 (b). The pores were believed to have contributed to the sudden drop in the relative density (to 87.74%) of MD-HA. These open pores were formed when the high internal pressure caused by the dehydration of HA at elevated temperature exceeds the strength of the closed pores (Ramesh *et al*., 2007).

Although the HA samples displayed different microstructure, the grain growth occurred for all the HA samples is significant with grains grew up to 8.9 μm - 10.9 μm as shown in Figure 5.18. This growth in the grain size due to the increase in sintering temperature was also observed by Kong *et al*. (2002), Mobasherpour *et al*. (2007), Kamalanathan *et al*. (2014), Ramesh *et al*. (2013) and Ramesh *et al*. (2016). This grain growth was due to the enhancement of homogeneity of the HA powder with increasing sintering temperature.

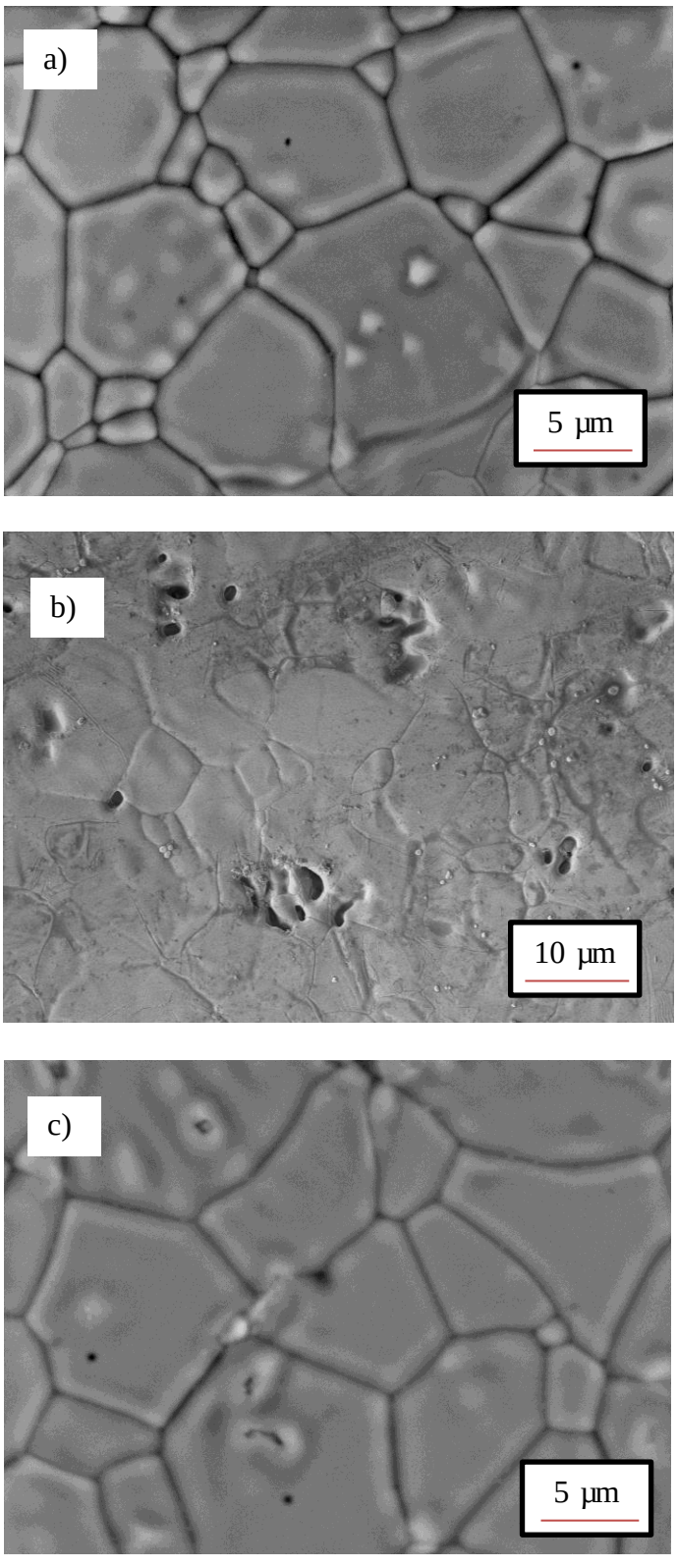

Figure 5.18: SEM images of (a) FD-HA, (b) MD-HA and (c) OD-HA sintered at 1350 ℃.

Under current study, the average grain sizes for all the synthesized HA with increasing sintering temperature are shown in Figure 5.19. All three HA samples demonstrated increasing grain size trend with increasing sintering temperature and MD-HA samples showed slower grain growth rate at 1050 ℃ - 1200 ℃ compared to FD-HA and OD-HA. However at an elevated sintering temperature of 1350 ℃, MD-HA recorded the highest grain size of 10.85 µm compared to FD-HA (8.9 µm) and OD-HA (9.3 µm).

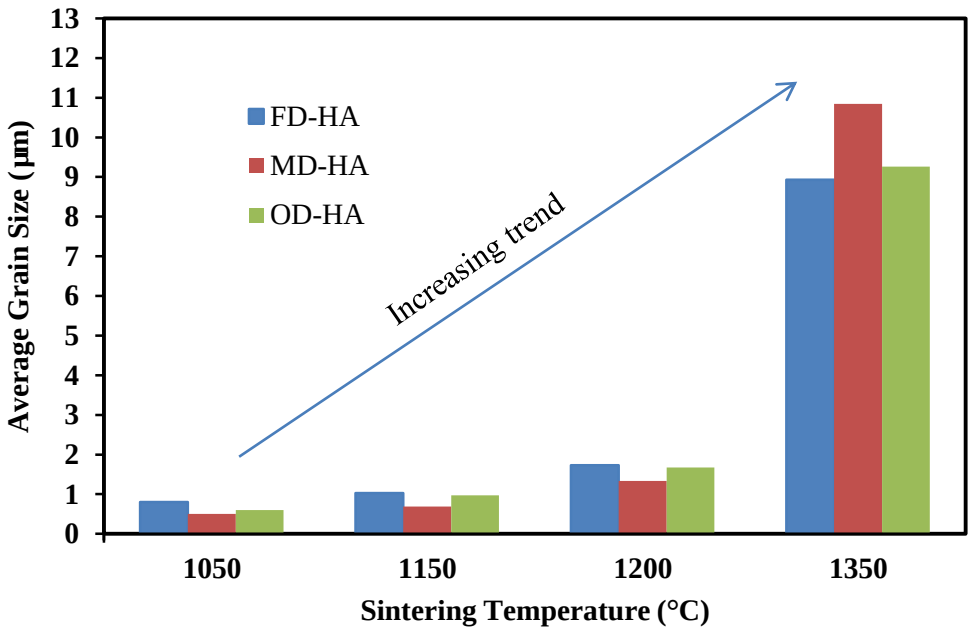

Figure 5.19: The effect of sintering temperature on the average grain size of sintered HA.

5.2.5 Vickers Hardness and Fracture Toughness

The dependence of hardness on the sintering temperature for all the sintered HA is shown in Figure 5.20. The results showed that hardness of FD-HA was at ~ 3 GPa when sintered at 1050 ℃ and obtained a maximum hardness of 5.3 GPa at 1150 ℃ followed by a decrease in hardness thereafter. The observed maximum hardness of FD-HA is close to 5.83 GPa obtained by Uysul *et al*. (2014) using similar freeze drying method. The increasing trend of the hardness of the FD-HA at temperature below 1150 ℃ was

attributed to the increase in density (Wang & Shaw, 2009; Niakan *et al*., 2015). However the hardness was found to decline as the sintering temperature increased from 1200 ℃ to 1350 ℃ despite the relative density was increasing from ~98% to ~98.5%. The decline of hardness at sintering temperature beyond 1150 ℃ was due to the increased of grain size (Hoepfner & Case, 2003; He at al., 2008; Veljovic *et al*., 2008; Ramesh *et al*., 2016). The effects of average grain size and relative density on the hardness of FD-HA are illustrated in Figure 5.21.

From Figure 5.20, the hardness results show that MD-HA exhibited similar increasing trend with increasing sintering temperature up to 1200 ℃. At temperature of 1050 ℃, the hardness value of MD-HA was at 3.5 GPa, slighter higher than that of FD-HA at the similar temperature. Subsequently, the hardness value of MD-HA reached a maximum value of 5.04 GPa at 1200 ℃ and then drop gradually to 4 GPa at 1350 ℃. Similar increasing trend was observed for OD-HA sintered sample where hardness value increased from 3.73 GPa at 1050 ℃ to a maximum of 5.12 GPa at 1150 ℃ and then declined almost linearly with the increasing of temperature. A sharp decrease to a hardness value of 3.02 GPa was observed for OD-HA sintered at 1350 ℃. It is believed that this decline in the hardness is associated to the simultaneous effects of low density and the decomposition of HA phase (Koutsopoulos, 2002; Aminzare *et al*., 2013) as confirmed by density curve and XRD analysis as shown in Figure 5.14 and Figure 5.12, respectively. The presence of secondary phases at high temperature creates volume changes and hence strains in the ceramic matrix which lowers the mechanical integrity of sintered body (Ruys *et al*., 1995).

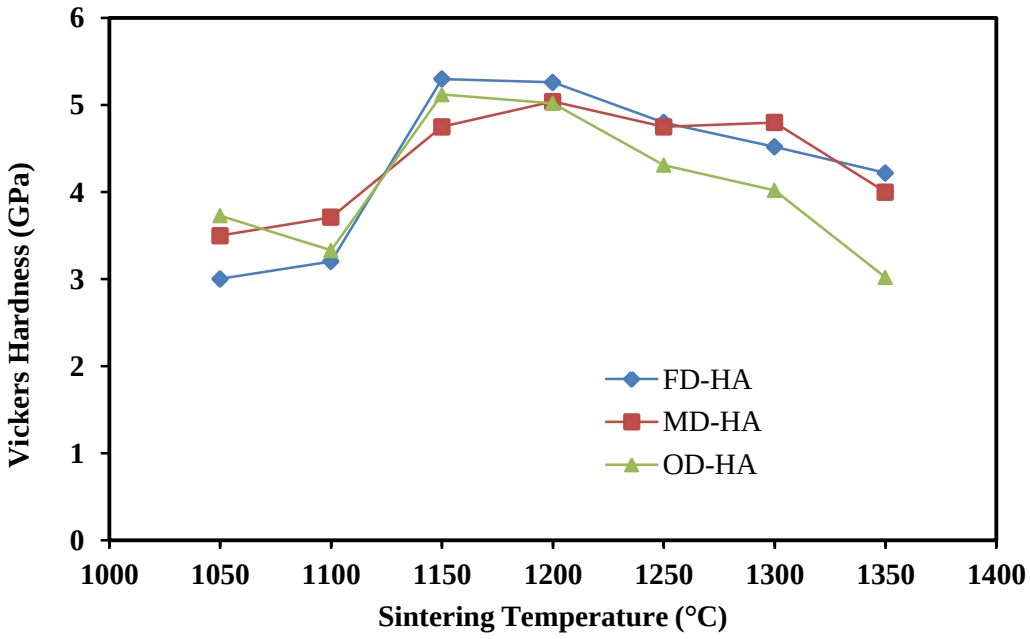

Figure 5.20: The effect of sintering temperature on the hardness of HA.

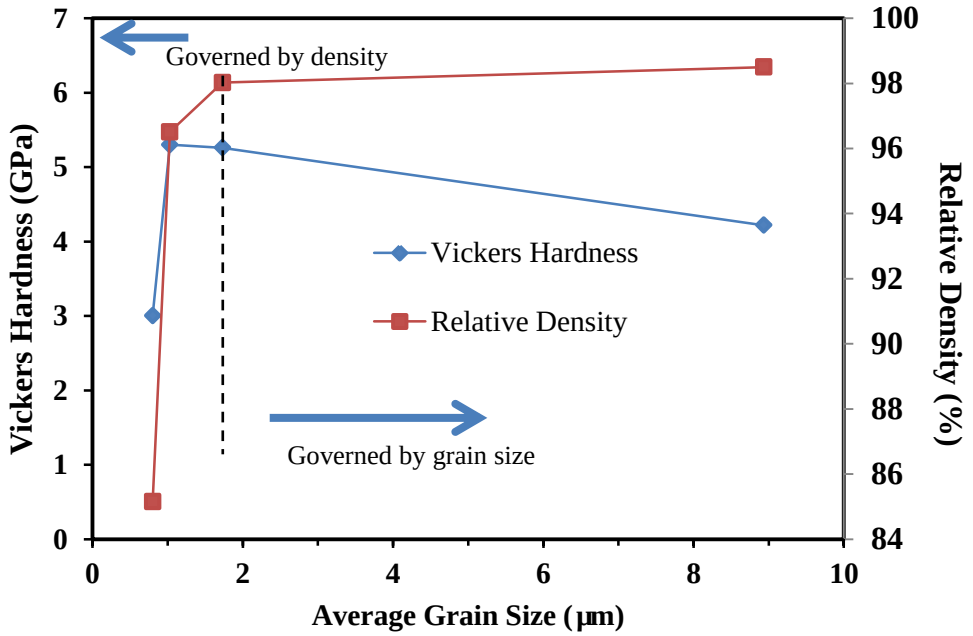

Figure 5.21: The variation of the relative density and hardness of sintered FD-HA as a function of average grain size.

In conclusion, the maximum hardness values for FD-HA, MD-HA and OD-HA were 5.3 GPa, 5.04 GPa and 5.12 GPa, respectively and these values are rather promising as

most of the previous studies recorded hardness lower than 5 GPa for conventional sintered HA (Aminzare *et al*., 2013; Bhattacharjee *et al*., 2011; Chen *et al*., 2008; Lin *et al*., 2012). Moreover, the hardness of sintered HA obtained from current study make them as a potential candidate for bone implant as the hardness is nearly 12 times higher than cortical bone (0.396 GPa) and cancellous bone (0.345 GPa) (Pramanik *et al*., 2005).

The effects of sintering temperature on the fracture toughness of the three different HA samples are shown in Figure 5.22. All the sintered HA exhibited similar trend where maximum fracture toughness obtained at certain temperature and sintering beyond that temperature caused the decline of fracture toughness. For example, the fracture toughness of MD-HA increased from 1.07 $MPam^{1/2}$ at 1050 ℃ to a maximum of 1.16 $MPam^{1/2}$ at 1150 ℃. Further heating to 1200 ℃ showed no improvement in fracture toughness and the value remained at 1.15 $MPam^{1/2}$. However, sintering MD-HA at temperature beyond 1200 ℃ showed signed of deterioration and lowest hardness value of 0.68 $MPam^{1/2}$ was obtained at 1350 ℃. Similarly, the FD-HA shows a maximum fracture toughness of 1.13 $MPam^{1/2}$ at the sintering temperature of 1150 ℃ and then decreased to 0.69 $MPam^{1/2}$ at 1350 ℃. This maximum value is slightly lower than that of MD-HA. On the other hand, OD-HA could only attain maximum fracture toughness value of 1.01 $MPam^{1/2}$ at 1200 ℃. Furthermore, any further increased in the sintering temperature caused severe deterioration of fracture toughness of the sintered OD-HA as fracture toughness was as low as 0.54 $MPam^{1/2}$ at 1350 ℃.

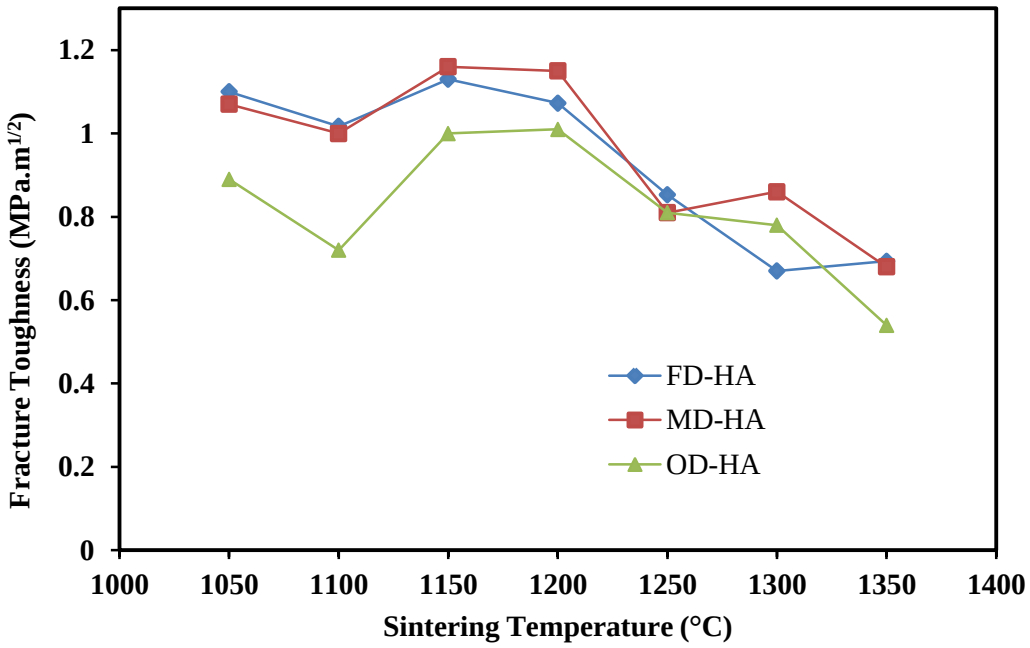

Figure 5.22: The effect of sintering temperature on the fracture toughness of HA.

Correspondingly, the fracture toughness of sintered HA samples is dependent on the grain size where fracture toughness increase with a decrease in grain size. The relationship of fracture toughness and grain size of the sintered HA is plotted in Figure 5.23. All the three HA demonstrated similar trend where critical grain size detected at 1150 ℃ whereby beyond this point, the fracture toughness is inversely proportional to the average grain size, i.e fracture toughness decrease with the increasing of grain size. A similar trend was observed in the previous literature by Tolouei *et al.* (2011), Wang & Shaw (2009), Kamalanathan *et al.* (2014), Ramesh *et al.* (2007). From Figure 5.23, it is clearly observed that smaller average grain size possess higher fracture toughness. The small grain size is favorable as small grain size lead to more grain boundaries per unit of volume that exist in the HA matrix, hence giving more limitation to the dislocations movement as grain boundary can stop dislocations. When the dislocations were effectively hindered, the permanent distortion of the sample can be prevented and hence giving the sintered sample higher fracture toughness.

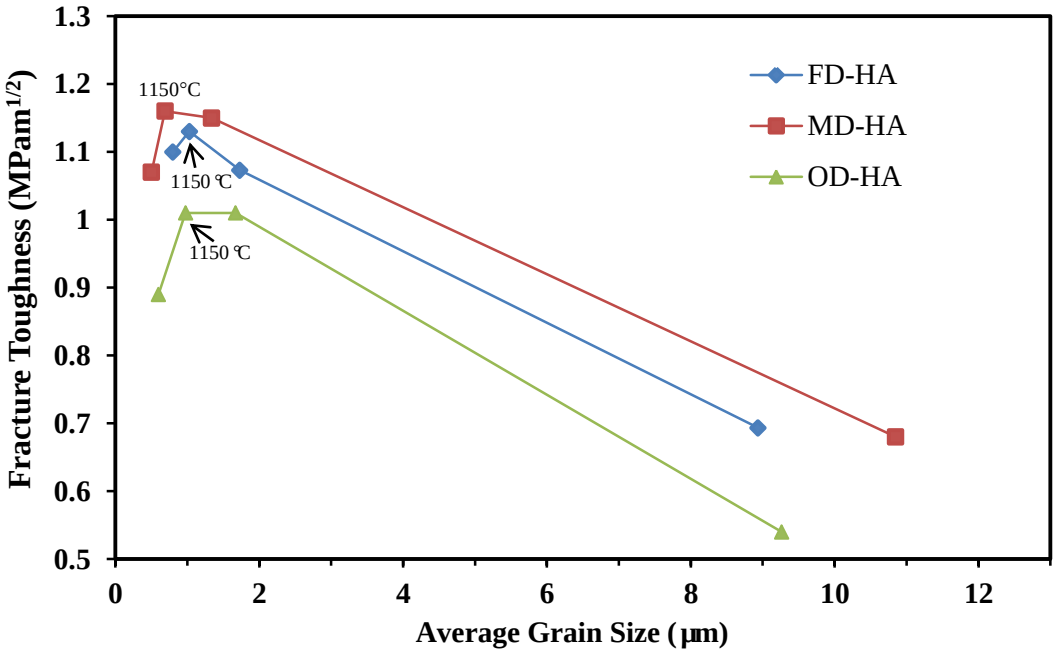

Figure 5.23: The effects of grain size on the fracture toughness of sintered HA.

Overall, the fracture toughness of MD-HA was noted to be superior when compared to FD-HA and OD-HA throughout the sintering regime. The highest fracture toughness value of 1.16 $MPam^{1/2}$ obtained from MD-HA was greater than pure sintered HA observed in the previous studies (Thangamani *et al.*, 2002; Ramesh *et al.*, 2011; Banerjee *et al.*, 2007; Wang & Shaw, 2009; Descamps *et al.*, 2013).

Although the mechanical properties of HA powders prepared by wet chemical method via microwave drying was found to be similar to those prepared by freeze drying and oven drying, the advantage of microwave drying can be viewed in the context of time consumed to obtain the respective hardness value and the high fracture toughness value. This advantage is clearly shown in Table 5.5 which compares the time taken to produce the MD-HA powders. The time taken to produce HA powders via microwave drying is significantly lower than the FD-HA and OD-HA. Hence, it can be concluded that microwave drying is a promising method to produce dense HA with high fracture toughness in a remarkably shorter time.

Table 5.5: Critical grain size for the sintered HA with their corresponding maximum hardness and fracture toughness.

Sample	Drying duration	Sintering Temperature (℃)	Critical Grain Size (μm)	Maximum Hardness (GPa)	Maximum Fracture Toughness ($MPam^{1/2}$)
FD-HA	36 hours	1150	1.023	5.3	1.13
MD-HA	15 minutes	1150	0.691	4.75	1.16
OD-HA	16 hours	1150	0.974	5.12	1.01

In summary, the current work proved that MD-HA exhibited slighter better sinterability compared to FD-HA and OD-HA and MD-HA requires significantly shorter synthesis time. Hence, MD-HA was chosen for further studies to investigate the effects of microwave sintering and sintering additives on the properties of MD-HA which will be discussed in the subsequent chapter.

CHAPTER 6: RESULTS AND DISCUSSIONS (PART 2)

6.1 Effect of Microwave Sintering on the Sinterability of MD-HA

In Chapter 5, the sinterability of the wet chemical synthesized HA produced by three different drying methods were investigated. From the results obtained, HA powder prepared by microwave drying demonstrated the overall optimum properties when sintered under conventional pressureless sintering (CPS). Microwave sintering has been widely applied in the sintering of HA compacts by Nath *et al*. (2006); Bose *et al*. (2010), Ramesh *et al*. (2008); Hassan *et al*. (2016). In this chapter, the influences of microwave sintering (MS) on the sintering behavior of the microwave dried HA will be discussed.

6.1.1 XRD Analysis of CPS and MWS Sintered HA

The XRD profiles of HA samples sintered at different temperatures by CPS and MWS are represented in Figure 6.1 and Figure 6.2, respectively.

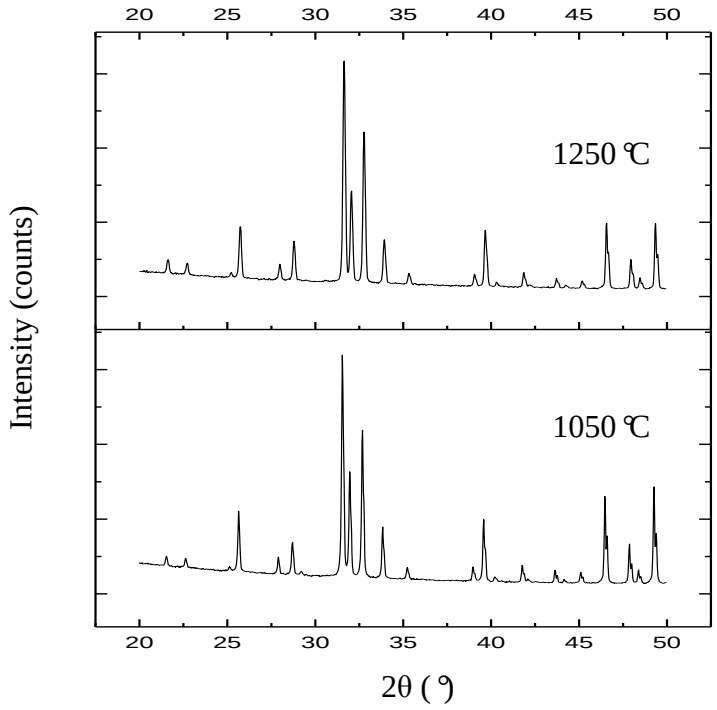

Figure 6.6.1: The XRD profiles of HA sintered by CPS at different temperatures. All peaks belong to HA phase.

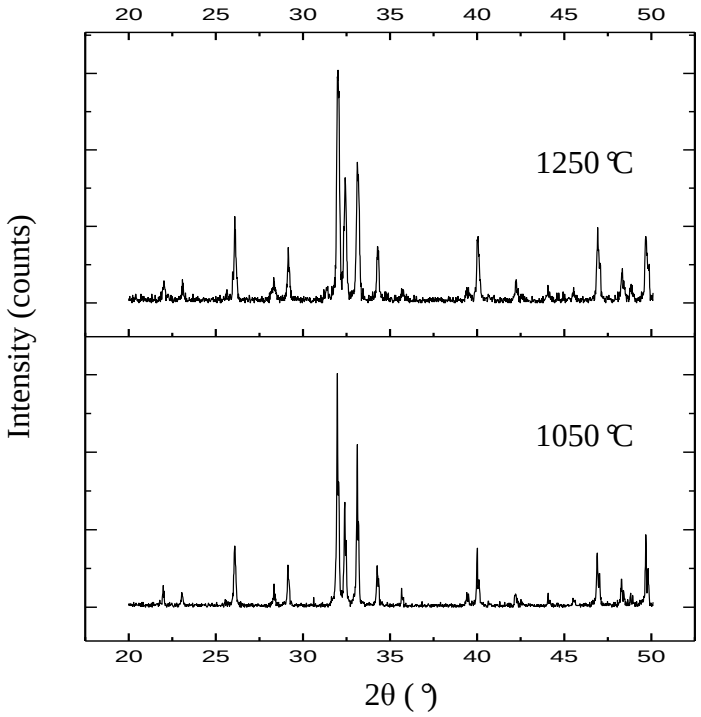

Figure 6.2: The XRD profiles of HA sintered by MWS at different temperatures. All peaks belong to HA phase.

From Figure 6.1 and Figure 6.2, it was found that HA is stable up to 1250 ℃ for both sintering methods as the only existing phase is HA. Secondary phases such as TTCP, TCP and CaO were not presented in the compacts suggesting that the phase stability of HA was not disrupted by microwave sintering. Further to that, no peak shifting was observed from XRD profiles regardless of sintering method indicated that dehydroxylation of HA did not occurred. These results were in good agreement with those reported by Nath *et al*. (2006), Ramesh *et al*. (2007) and Thuault *et al*. (2014) who reported that the phase stability of HA was preserved up to 1250 ℃. However, these results are in contradiction with the findings obtained by Harabi *et al*. (2010). The authors compared the phase stability of CPS and MWS sintered HA. They found that HA phase of CPS-HA was stable up to 1150 ℃ and then decomposed to β-TCP at 1200 ℃ while MWS-HA started to decompose into TCP when subjected to microwave sintering at 1050 ℃ and the percentage of TCP phase increased from 46% to 61% when

sintering temperature increased to 1100 ℃. Finally, the MWS-HA was found to transform into 85% TTCP and 10% α-TCP with remaining 5% as HA phase. The author suggested that this phenomenon was attributed to the higher heating efficiency of microwave heating compared to the conventional sintering (Harabi *et al*., 2010) which speed up the decomposition rate of HA into secondary phases.

6.1.2 Bulk Density of CPS and MWS Sintered HA

The effects of CPS and MWS on the densification of HA are illustrated in Figure 6.3.

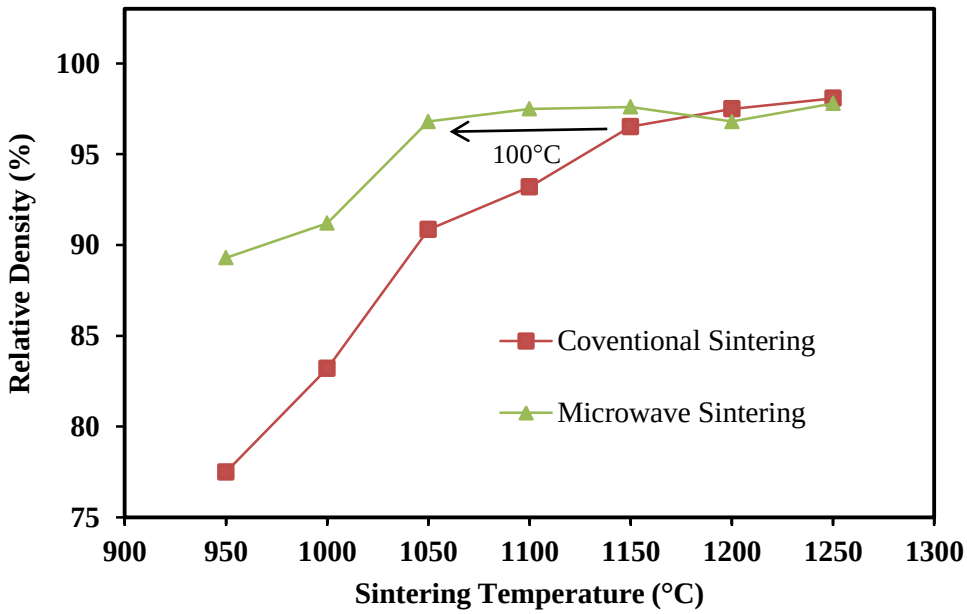

Figure 6.3: The effect of sintering temperature on the density of HA sintered by conventional sintering and microwave sintering technique.

Generally, both HA samples sintered by conventional and microwave sintering exhibited similar trend where relative density increase with increasing temperature but at different densification rates. At low temperature range (below 1150 ℃), the density of MWS-HA was significantly higher than the CPS-HA. The densification curves were shifted downward nearly 100 ℃ at the lower sintering temperature (< 1150 ℃) with difference decrease as higher temperature were reached as shown in Figure 6.3. At low temperature of 950 ℃, ~89% densified MWS-HA was obtained and the relative density

increased to ~96.8% at 1050 ℃. Further sintering lead to highly densified MWS-HA; exhibited >97% of theoretical density when sintering temperature increased to temperature above 1100 ℃. The maximum relative density of ~98% was achieved for MWS-HA sintered at 1250 ℃. In contrast, the CPS-HA displayed a relatively lower relative density value of 77.5% at 950 ℃ compared to MWS-HA (~89.3%). CPS-HA could only achieve relative density above 97% at high sintering temperature of 1200 ℃. Apart from that, at sintering temperatures above 1200 ℃, the densities of both HA compacts appeared to be similar.

From the results, the densification rate of MWS-HA was remarkably higher than CPS-HA especially at low temperature range. This high sintering rates was caused by the high diffusion rate induced by the microwave field that interact directly to the crystals in the ceramics without the need of heat transfer from surface to the core of the ceramics. This direct interaction between microwave and the material cause volumetric heating and hence the sintering and densification can occur at much lower temperatures with shorter sintering time and lower energy consumption (Demirskyi *et al*., 2011). The enhanced densification of MWS-HA at low sintering temperature compared to CPS have been widely reported (Ehsani *et al*., 2013; Thuault *et al*., 2014; Bose *et al*., 2010; Mangkonsu *et al*., 2016). Nonetheless, Ramesh *et al*. (2008) reported that the densification of CPS-HA was higher than MWS-HA throughout the sintering regime of 1000 ℃ - 1300 ℃. This contradiction could be due to the different microwave power setting of the microwave furnace.

Overall, the high densification rate of MWS-HA is favorable as highly dense HA could be obtained at low temperature which reduces the risk of decomposition and the time consumed for the sintering process was greatly reduced. For example, in order to achieve high relative density of >97%, the CPS-HA samples need to be sintered to

1200 ℃ in a conventional pressureless furnace for a total sintering time (inclusive of sintering, soaking and cooling to the room temperature) of 1290 minutes. On the contrary, highly dense MWS-HA (~97%) could be achieved at 1050 ℃ albeit the total microwave sintering time consumed was only 185 minutes which is about 7 times shorter than that of conventional sintering. Hence, the beneficial effect of microwave sintering in enhancing densification of HA can be realized.

6.1.3 Microstructural Evolution and Grain Size

The SEM micrographs of the MWS-HA and CPS-HA sintered at 950 ℃, 1000 ℃, 1050 ℃, 1100 ℃ and 1250 ℃ are presented in Figure 6.4 – 6.8.

It can be noted that densification of HA pellets had not really started when subjected to conventional sintering at 950 ℃ and 1000 ℃ as shown in Figure 6.4 (a) and Figure 6.5 (a) respectively. The samples were hardly densified as no proper grains were formed and many pores were observed. This corresponds to a relative density of ~77.5% and ~83.2%. On the other hand, it could be observed that final stage of sintering has started when MWS-HA sintered at 950 ℃ as interconnected pores started to form grain and grain outline can be seen from Figure 6.4 (b). From Figure 6.5 (b), as temperature goes up to 1000 ℃, MWS-HA sample which had remnant porosity (~8.8%) exhibited microstructure where some areas are fully densified while some nano-pores remained. It is worth mentioning that MWS-HA sintered at 1000 ℃ showed uniform fine grained microstructure and the grain size was found to be in nanometer range.

At 1050 ℃, MWS-HA (Figure 6.6 (b)) displayed almost dense microstructure that corresponds to the relative density of ~97% with a few extremely small pores (7 nm – 10nm) existed as indicated by the arrows. In contrast, CPS-HA demonstrated larger pores that varied in size (20 nm – 35 nm) as shown in Figure 6.6 (a), correlate well with

its lower density value of ~90.85%. This indicated that the densification of MWS-HA was at final stage at 1050 ℃ but not the case for CPS-HA.

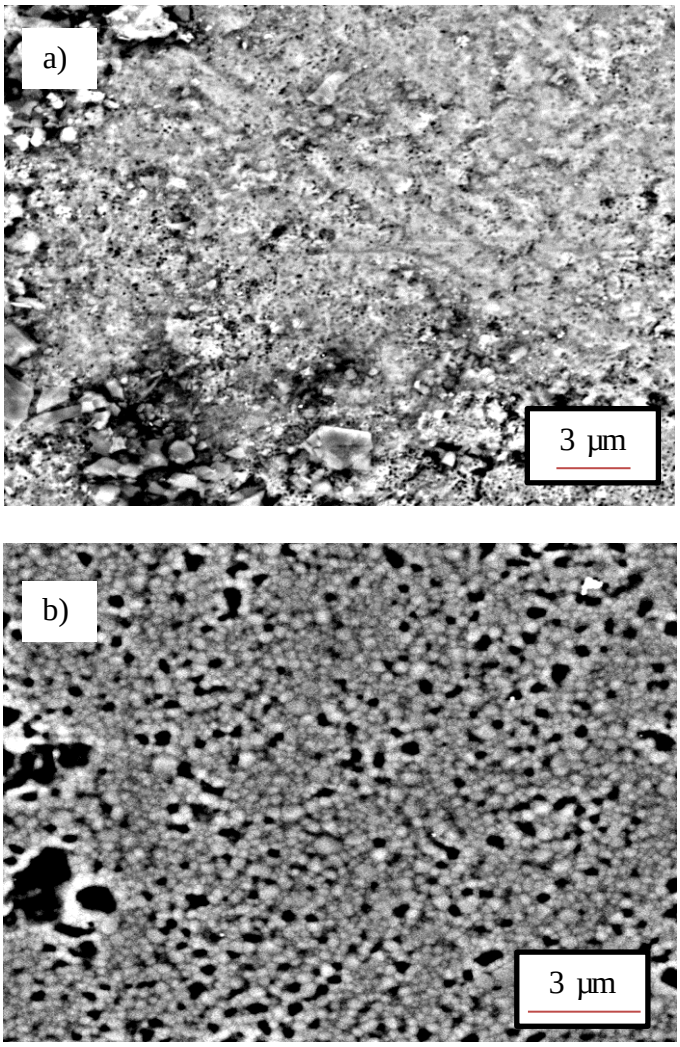

Figure 6.4: SEM images of HA sintered by (a) conventional sintering and (b) microwave sintering at 950 ℃.

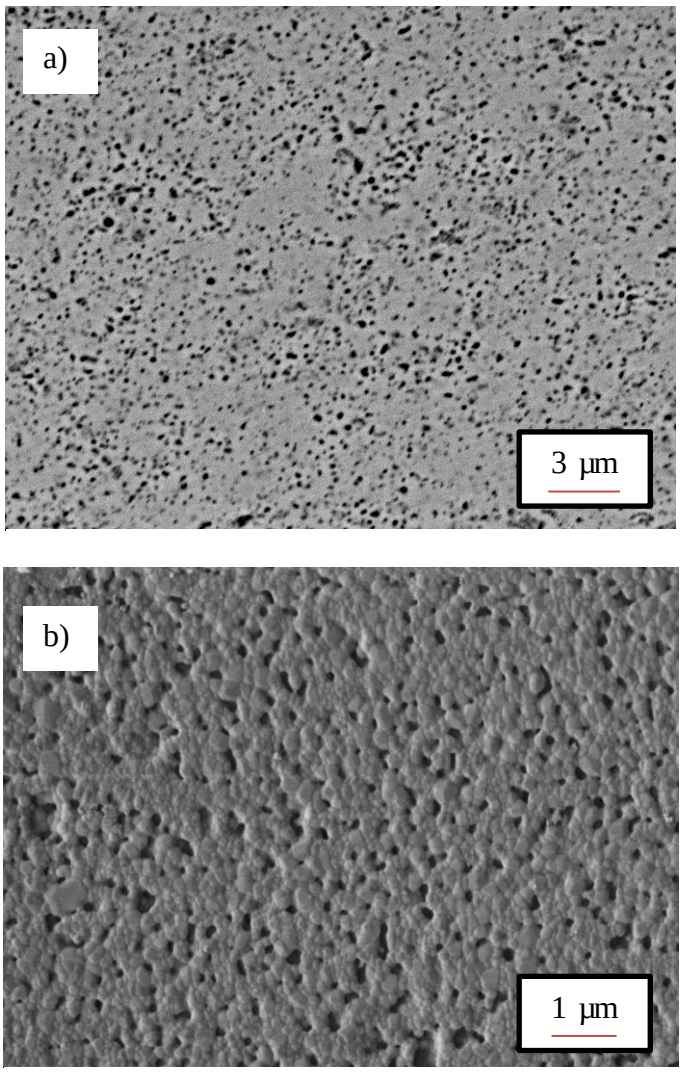

Figure 6.5: SEM images of HA sintered by (a) conventional sintering and (b) microwave sintering at 1000 ℃.

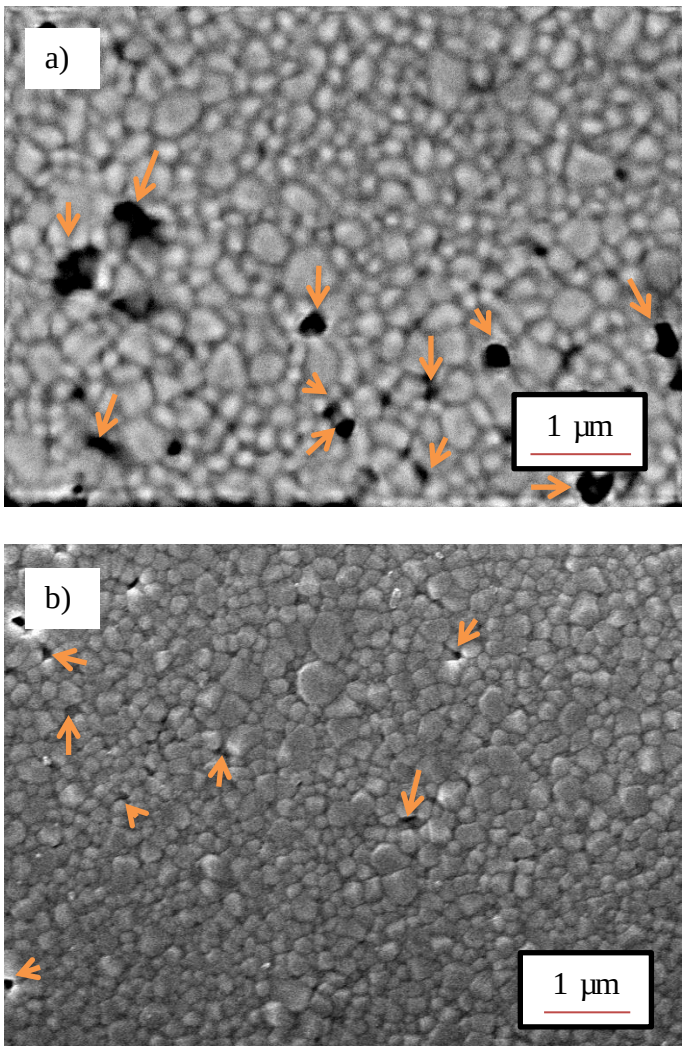

Figure 6.6: SEM images of HA sintered by (a) conventional sintering and (b) microwave sintering at 1050 ℃.

However, as the sintering temperature was increased beyond 1100 ℃, all the CPS-HA exhibited very little porosity as shown in Figure 6.7 (a) and Figure 6.8 (a). The SEM micrographs correlated well with the measured density (Figure 6.3) for all the samples sintered at high temperature regardless of sintering method as almost full densification was accomplished when compacts sintered ≥ 1100 ℃.

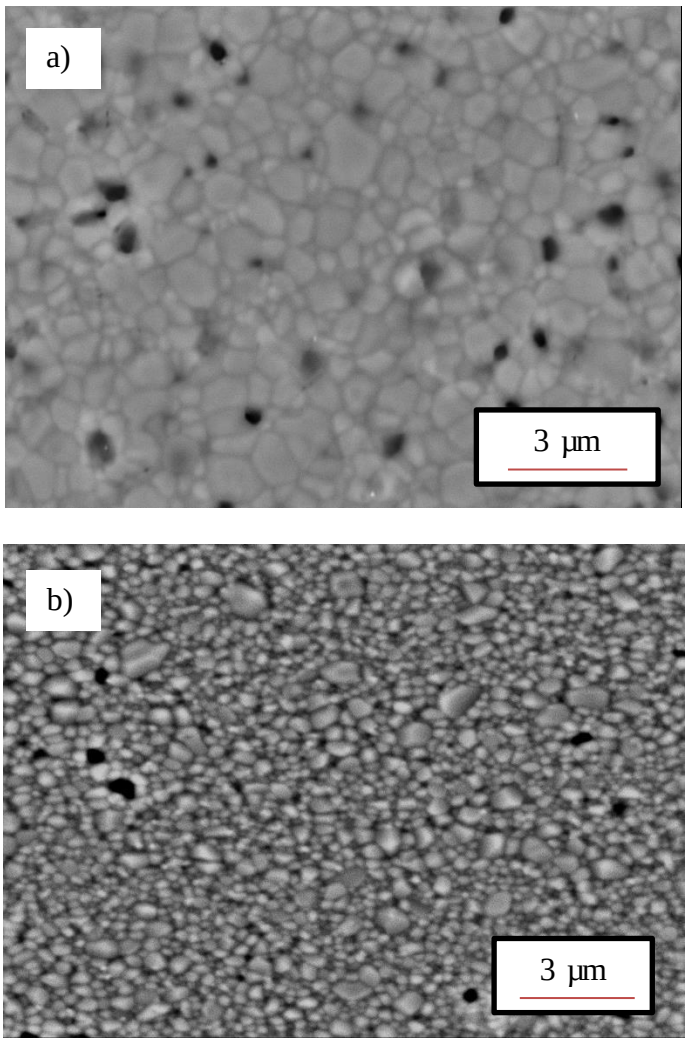

Figure 6.7: SEM images of HA sintered by (a) conventional sintering and (b) microwave sintering at 1100 ℃.

At high temperature of 1250 ℃, both MWS-HA and CPS-HA exhibited fully dense microstructures which consisted of varying grain sizes and low level of porosity as shown in Figure 6.8. Significant grain growth was observed for all the HA samples sintered at 1250 ℃ with some individual grains grown up to 4 – 6 µm in size. This growth in grain size due to the increase of sintering temperature was commonly observed in HA as reported by previous literatures (Layrolle *et al*., 1998; Mostafa, 2005; Mobaspherpour *et al*., 2007).

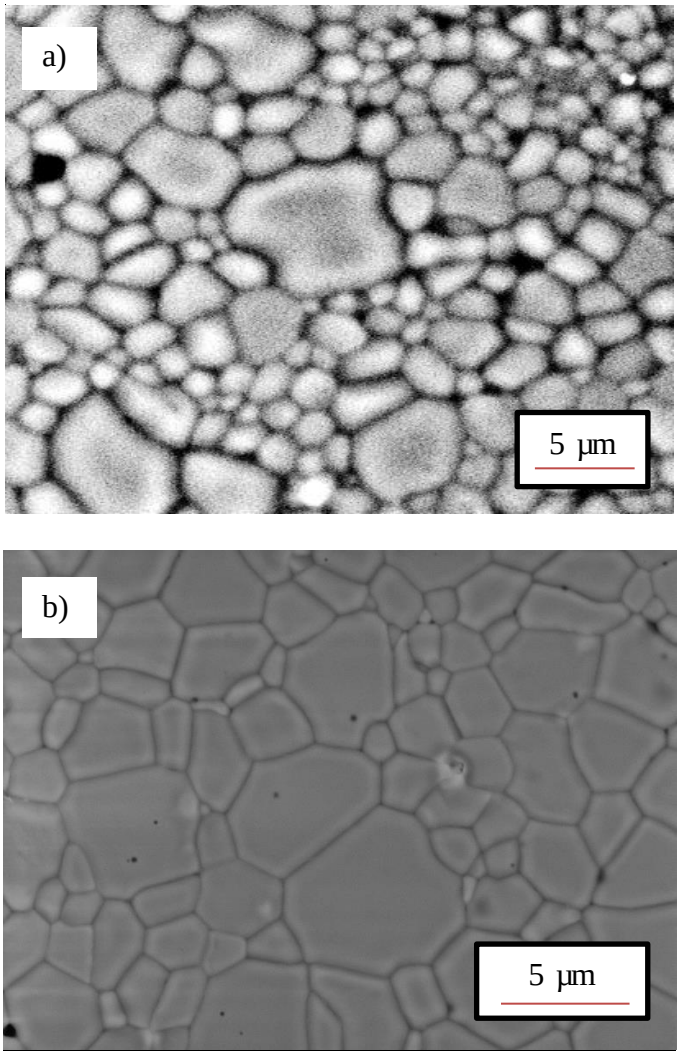

Figure 6.8: SEM images of HA sintered by (a) conventional sintering and (b) microwave sintering at 1250 ℃.

In general, the mean grain size of MWS-HA increased slowly from nanolevel (300 nm) to microlevel (~4.33 µm) with increasing temperature from 950 ℃ to 1250 ℃. As for CPS-HA, the grain size couldn't be measured at low 950 ℃ and 1000 ℃ as grains were hardly seen. The average grain size of the sample conventionally sintered at 1050 ℃ was 500 nm and increasing temperature to 1250 ℃, the grain size increased to 4.45 µm. Figure 6.9 represents the average grain size of HA sintered by microwave sintering and conventional sintering as a function of the sintering temperature. In both MWS-HA and CPS-HA, the grain size increase as the sintering temperature increases.

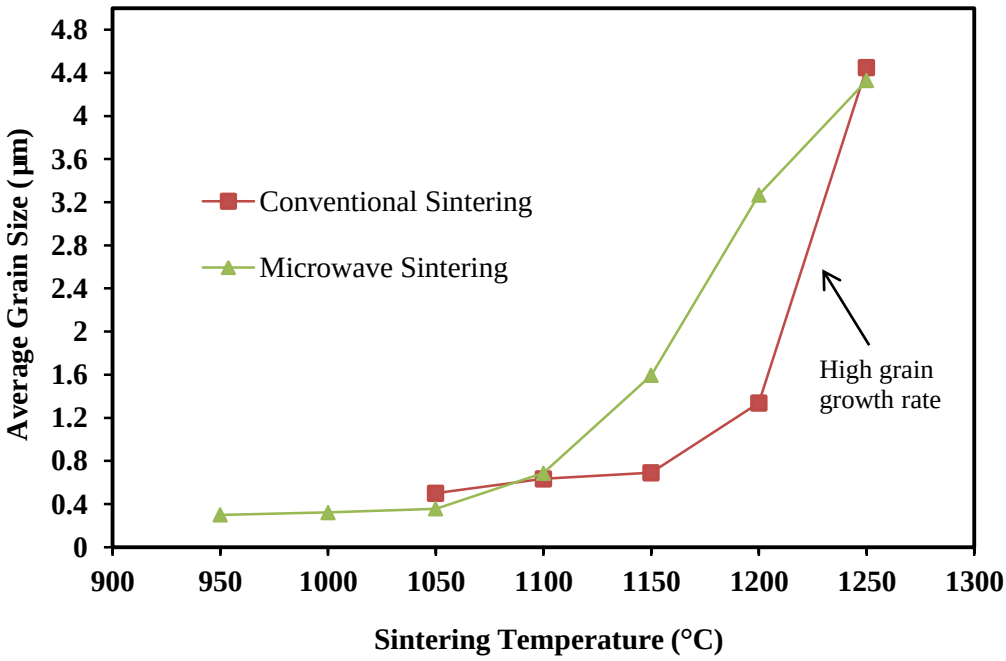

Figure 6.9: The effect of sintering temperatures on the average grain size of HA samples sintered by (a) conventional sintering and (b) microwave sintering.

It is interesting to discover that the rate of grain growth of microwave sintered HA is very slow at temperatures ranging from 950 ℃ - 1100 ℃. However, as temperature increased further, the grain size for MWS-HA increased rapidly. The grain size of the MWS-HA increased slowly from ~300 nm (950 ℃) to ~688 nm (1100 ℃) and then increased rapidly by a factor of ~2.7 from ~1.60 µm to ~4.33 µm as temperature increased from 1150 ℃ to 1250 ℃. In comparison, the grain growth rate of CPS-HA was higher than MWS-HA as evidence of the steep slope shown in Figure 6.9. The grain size of CPS-HA increased by a factor of about 6.4 from ~691 nm to ~4.45 µm at sintering temperature of 1150 ℃ and 1250 ℃, respectively. The increasing trend of grain size against sintering temperature was in good agreement with the trend reported by (Akao *et al*., 1981; Ramesh *et al*., 2007; Muralithran & Ramesh, 2000; Ramesh *et al*., 2008). The drastic grain growth of HA was observed at 1250 ℃ regardless of sintering methods. In conventional sintering, the grain enlargement of HA was associated with the surplus activation energy supplied to the HA due to elevated sintering temperature.

Current research shows that the efficacy of microwave sintering in preventing grain coarsening is profound at low temperature but not at high sintering temperature. Excessive grain growth with non-uniform grain size distribution was observed from MWS-HA sintered at 1250 ℃ as shown in Figure 6.8 (b). At high microwave sintering temperature, a large amount of microwave was absorbed by HA and leads to localized heating which resulted in excessive grain growth (Vijayan & Varma, 2002; Bykov *et al*., 1999). As the temperature increase, there is risk of getting non-uniform heating profile in the samples which contribute to the localized heating in different spots of the sample. Hence, there are some "hot spots" where heating is much more rapid than the other spots that caused the heterogeneous heating. Therefore, some of the MWS-HA grains are large and some of the grain retained in ultrafine size as shown in Figure 6.8 (b).

In short, the results showed that microwave sintering is effective in preventing grain growth while maintaining high density throughout the sintering regime and nano grain size was maintained up to 1100 ℃. In microwave sintering, the high heating rate of MWS-HA lower the sintering time exposure and leads to the suppression of the surface diffusion. Hence, the exaggerated grain growth was restricted. The smaller grain size of MWS-HA is vital because smaller grain size would generally yield HA with enhanced mechanical properties compared to HA containing large grain.

6.1.4 Vickers Hardness and Fracture Toughness of CPS and MWS Sintered HA

The variation of the Vickers hardness of both conventional and microwave sintered HA at various temperatures are shown in presented in Figure 6.10. In general, the hardness of HA samples regardless of sintering method revealed similar trends with increasing sintering temperature up to certain value at particular temperature and then decrease with further heating. The results showed that the hardness values of MWS-HA are higher than CPS-HA at lower temperature range (950 ℃ - 1100 ℃). However,

similar hardness values were recorded for both MWS-HA and CPS-HA sintered at 1150 ℃. Upon 1150 ℃, the hardness values of CPS-HA are higher than MWS-HA.

At 950 ℃, both MWS-HA and CPS-HA recorded lowest hardness values of 4.09 GPa and 2.89 GPa, respectively. As sintering temperature increased, the hardness value of MWS-HA increased and marked the maximum value of ~4.8 GPa at 1150 ℃. However, when microwave sintering was carried out >1150 ℃, the hardness started to decline linearly to ~4.4 GPa at 1200 ℃ and ~3.87 GPa at 1250 ℃. In contrast, the hardness of CPS-HA start to rise sharply from 3.01 GPa at 1000 ℃ to a maximum of ~5.04 GPa at 1200 ℃. Similar to MWS-HA, the CPS-HA showed a decline in hardness value as sintering proceed to 1250 ℃.

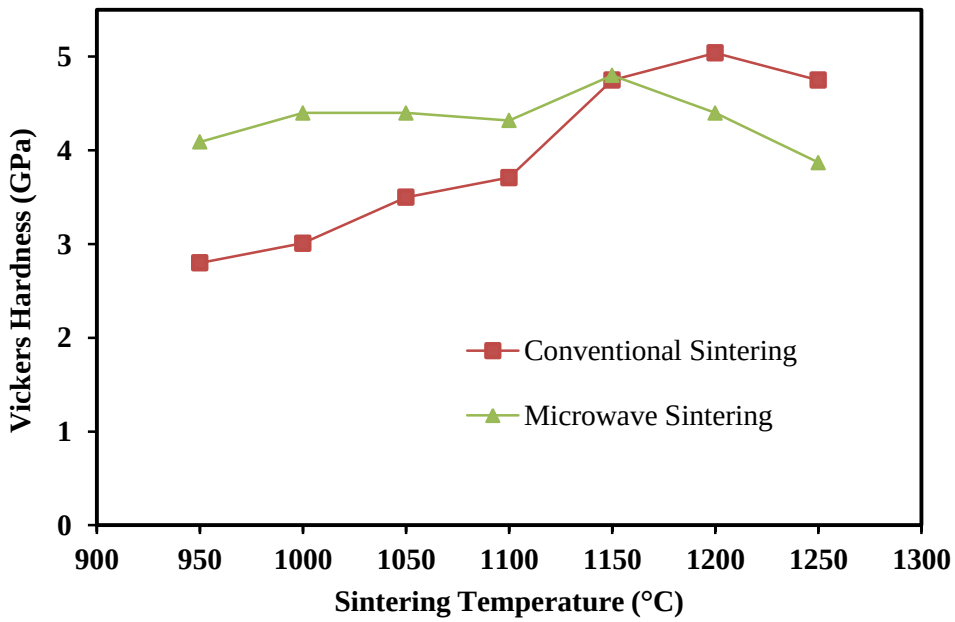

Figure 6.10: The effect of sintering temperature on the hardness of HA sintered by conventional sintering and microwave sintering technique.

In addition, the hardness of sintered HA was found to depend on the bulk density and average grain size and these relationships are plotted in Figure 6.11. Figure 6.11 clearly reflected that increase in relative density of CPS-HA from 77.5% at 950 ℃ to 97.5% at 1200 ℃ enhance the hardness of samples from 2.8 GPa to 5.04 GPa. Similarly,

improved hardness value was found when the sintering temperature increased from 950 ℃ to 1150 ℃, in accordance with the increment in relative density from 89.3% to 97.6%. However, when the temperature exceeds certain point (>1200 ℃ for CPS-HA and >1150 ℃ for MWS-HA), it was found that the change in hardness was not in accordance to the change in bulk density as the hardness value decline even the density increased. This deterioration in hardness value was the result of the large grain size obtained. For example, the hardness of CPS-HA declines from 5.04 GPa (1200 ℃) to 4.75 GPa (1250 ℃) when the grain size increase from ~1.34 μm to ~4.45 μm while big grain size of ~4.33 μm correspond to the low hardness of 3.87 GPa of MWS-HA sintered at 1250 ℃ whereas small grain size of ~1.6 μm correspond to 4.8 GPa for MWS-HA sintered at 1150 ℃.

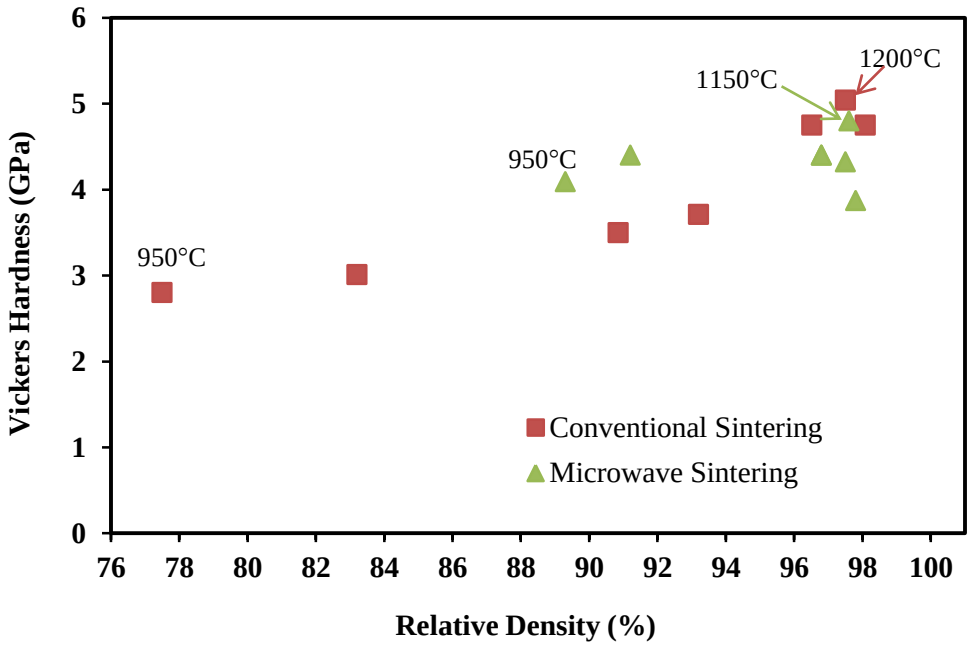

Figure 6.11: Vickers hardness dependence on the relative density of HA sintered by conventional sintering and microwave sintering technique.

The effects of sintering temperature on the fracture toughness of MWS-HA and CPS-HA are shown in Figure 6.11. The fracture toughness of CPS-HA sintered at 950 ℃ and 1000 ℃ was not measure due to the porous surface of those HA compacts. The graph

(Figure 6.12) showed that HA compact sintered by microwave sintering exhibited similar trend to the Vickers hardness trend, i.e. toughness value increase with increasing temperature and met a plateau at certain temperature and decrease thereafter. The fracture toughness value of MWS-HA increased greatly from 1.1 MPa.m$^{1/2}$ at 950 ℃ to 1.85 MPa.m$^{1/2}$ at 1050 ℃. Further sintering above 1050 ℃ showed sign of deterioration as the toughness values decrease almost linearly with increasing sintering temperature from 1.85 MPa.m$^{1/2}$ to 0.88 MPa.m$^{1/2}$ at 1250 ℃. In comparison, the fracture toughness of HA samples sintered via conventional sintering perked at 1150 ℃, recording a value of 1.16 MPa.m$^{1/2}$ and decline to a minimum value of 0.81 MPa.m$^{1/2}$ when sintered at 1250 ℃.

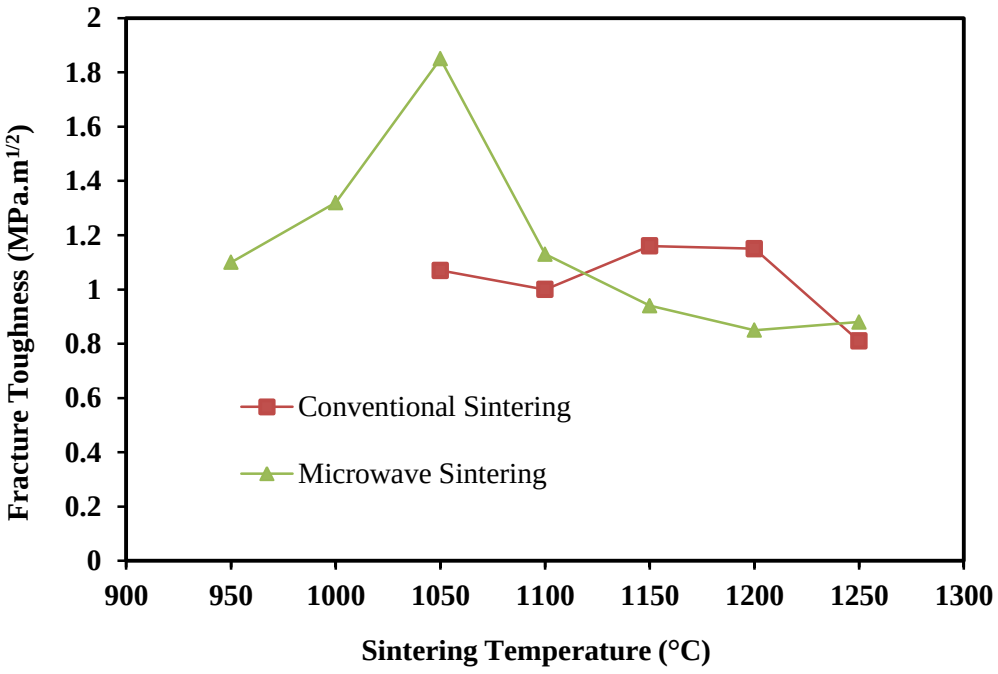

Figure 6.12: The effect of sintering temperature on the fracture toughness of HA sintered by conventional sintering and microwave sintering technique.

The fracture toughness value of the MWS-HA sintered at 1050 ℃ was significantly higher than the values reported in the literature for synthetic HA samples sintered via microwave sintering as shown in Table 6.1. Sintered dense HA was usually reported to

have low fracture toughness values less than 1 MPa.m$^{1/2}$ (Tan *et al*., 2011) which limit its use in load bearing applications. Hence, the high fracture toughness HA obtained in current research is encouraging. In conventional sintering, grain growth mechanism dominant in the early stage of sintering and followed by the densification mechanism and hence the risk of getting large grain HA is high. Nevertheless, sample was rapidly sintered to temperature region where densification predominate the grain coarsening mechanism in microwave sintering. Therefore, the grain growth can be minimized while retaining high densification during the microwave sintering of HA as evidence from current study, i.e. MWS-HA recorded relative density ~97% while maintaining nano grain size of 356 nm lead to a great enhancement of fracture toughness (1.85 MPa.m$^{1/2}$) at 1050 ℃. Therefore, it is inferred that the high fracture toughness value could be attributed to the combine effects of improved sinterability and restricted grain growth of HA during microwave sintering.

Table 6.1: A comparison of optimum fracture toughness values of current study to the available literatures (Ramesh *et al*., 2008; Kutty *et al*., 2015; Thuault *et al*., 2014).

	Sintering Temperature (°C)	**Fracture Toughness (MPa.m$^{1/2}$)**
Current Study	1050	1.85
Ramesh *et al*. (2008)	1050	1.45
Kutty *et al*. (2015)	1000	1.75
Thuault *et al*. (2014)	900	1.36

The dependence of fracture toughness on both relative density and grain size is plotted in Figure 6.13. From Figure 6.13, it is postulated that the fracture toughness of HA increase as relative density increases below a critical grain size (~356 nm in current

study). Beyond the critical grain size, the fracture toughness appeared to be governed by grain size in the trend that fracture toughness decreases with increasing grain size.

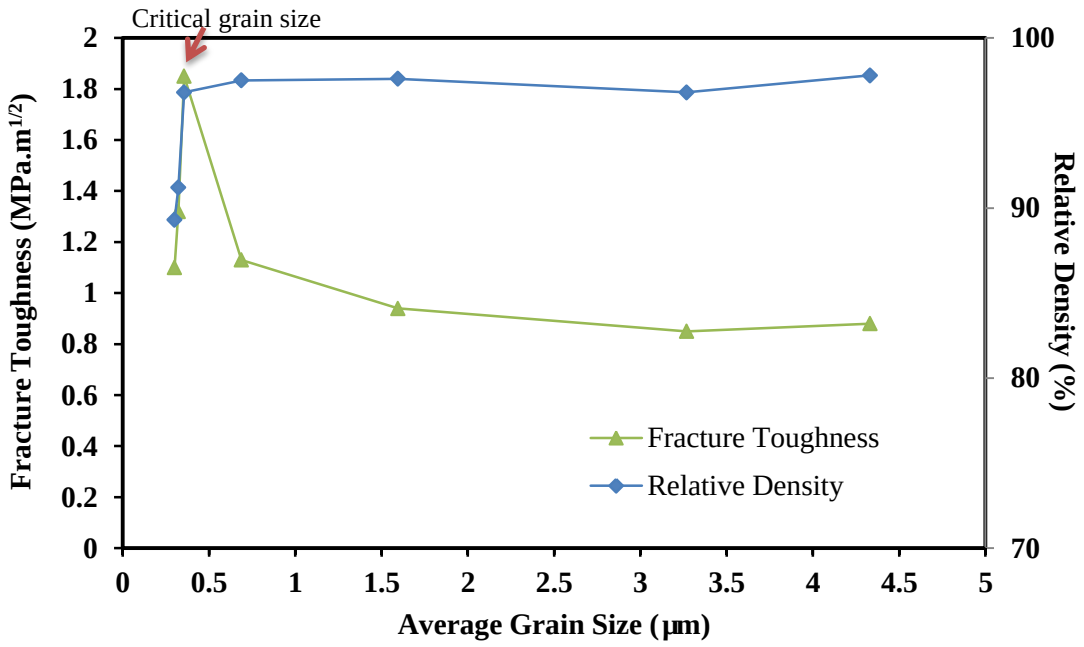

Figure 6.13: The variation of fracture toughness and relative density of HA sintered by microwave sintering technique.

Small grain size was desirable to produce high toughness HA (Kamalanathan *et al.*, 2014) as suggested by Hall-Petch equation, $\sigma_f = \sigma_0 + kd^{-1/2}$, where σ_f is the fracture strength, d is the grain size, k and σ_0 are constants, the strength decreases with increasing grain size. The strength of the materials depends on the ability to restrict the motion of dislocations and the grain boundaries serve as barriers to limit the dislocation movement. At the grain boundary, the dislocations are blocked. As shown in Figure 6.14, the pile up created driving force to push the dislocation towards the nearby grain. The bigger the grain, the bigger the pile up and therefore the bigger the driving force and hence, a small load is sufficiently to push the dislocation to the adjacent grain. By reducing the grain size, there are less pile ups creating less driving force, requiring a larger stress to move the dislocation to next grain.

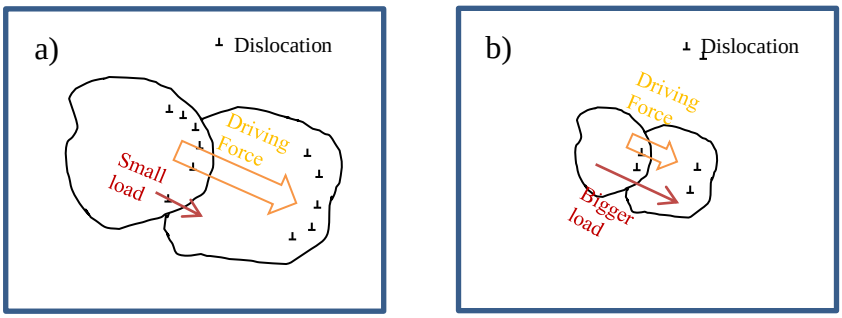

Figure 6.14: The schematic diagram of the dislocation pile up in (a) large grains and (b) small grains.

In short, small grain size microstructure provided large numbers of grain boundaries per unit volume which resulting in a smaller number of pile ups in grain (boundaries limit the dislocation movement) and in turn increase the strength of sample. This correlates well with the current study where the optimum fracture toughness of 1.85 MPa.$m^{1/2}$ obtained from HA microwave sintered at 1050 ℃ corresponds to the extremely small grain size of ~356 nm.

In summary, the results obtained suggest that microwave sintering is a promising sintering technique to produce highly dense HA ceramics with fine grained microstructure, high phase stability and enhanced mechanical properties.

6.2 Effect of Zinc Oxide (ZnO) addition on the Sinterability of HA

In this section, the effects ZnO addition on the mechanical properties of hydroxyapatite will be presented. The hydroxyapatite powder used in this work was prepared by the wet chemical precipitation method via microwave drying. Different amount of ZnO powder was added into the HA powder based on ball milling method as described in Chapter 4. The green compacts were then cold isostatic pressed at 200 MPa followed by pressureless sintering at temperatures range between 1100 ℃ to 1300 ℃.

6.2.1 XRD Analysis of Undoped and ZnO-doped HA Powder

The XRD signatures of the ZnO-doped as well as the undoped HA powders were present in Figure 6.15. The analysis shows that all the powders produced only peaks corresponded to the stoichiometric HA as shown in Figure 6.15. This result proved that the presence of ZnO had negligible effect on the HA phase stability which is consistent with the findings of other researchers (Gross *et al*., 2013; Deepa *et al*., 2013). However, it was found that ZnO-doped HA powders have higher intensity than the pure HA as indicated by the sharper and narrower peaks.

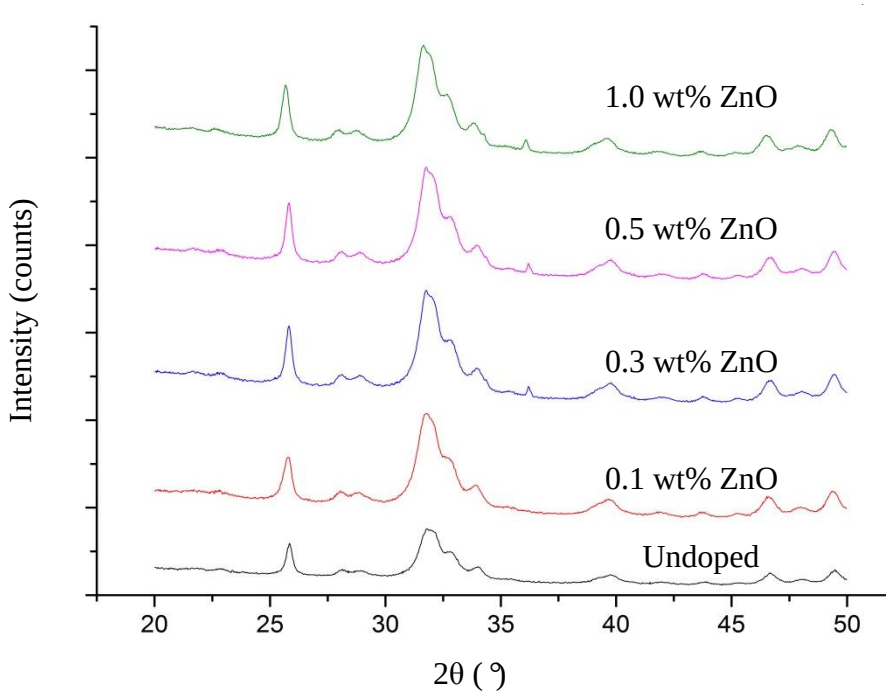

Figure 6.15: The XRD profiles of undoped HA powders and HA powders containing 0.1 wt%, 0.3 wt%, 0.5 wt% and 1 wt% ZnO, respectively.

6.2.2 XRD Analysis of Undoped and ZnO-doped Sintered HA

XRD spectrum (Figure 6.16) proved that all the samples sintered at high temperature of 1300 ℃ were pure HA regardless of the amount of ZnO addition.

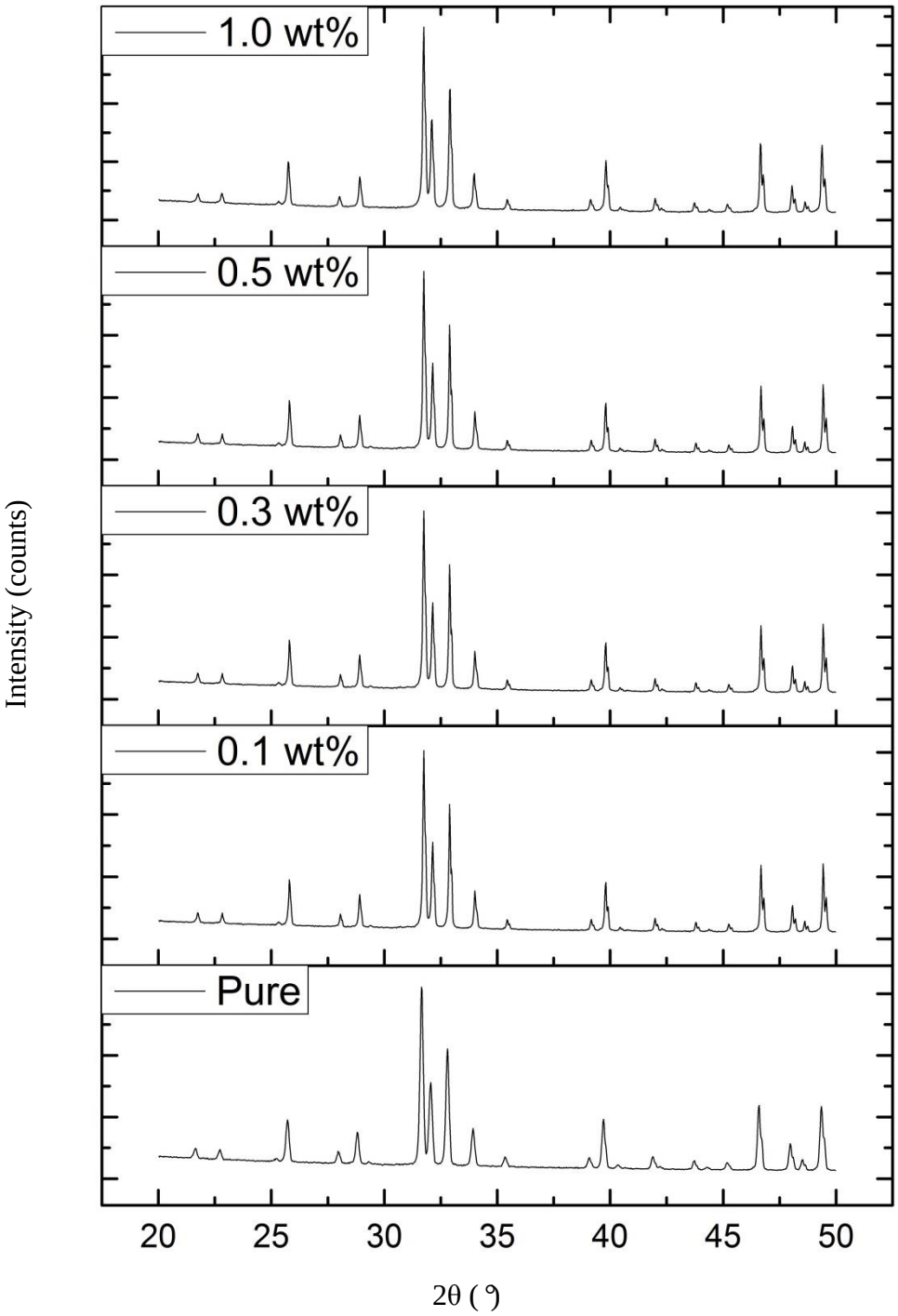

Figure 6.16: XRD patterns of HA samples sintered at 1300 ℃ for undoped HA and HA containing 0.1 wt%, 0.3 wt%, 0.5 wt% ZnO and 1 wt% ZnO, respectively.

This result revealed that the presence of ZnO and high sintering temperature had negligible effects on the sintered HA phase stability. This is inconsistent with the study reported by Bodhak *et al*. (2011), Buys *et al*. (1995) and Finoli *et al*. (2010) who observed that high sintering temperature of 1200 ℃ and above could affect the HA phase stability. Bodhak *et al*. (2011) reported that the inclusion of ZnO destabilize the HA phase and the decomposition of ZnO-doped HA started at about 1200 ℃ where strong β-TCP peaks were detected. The decomposition could be due to the nature of the starting HA powders but not the inclusion of ZnO as the authors used commercially available HA powders in their experiment. Buys *et al*. (1995) and Finoli *et al*. (2010) on the other hand reported that thermal decomposition of pure HA into TCP and CaO started at about 1200 ℃ and the presence of TCP would deteriorate the mechanical properties of HA (Royer *et al*., 1993; Wang & Chaki, 1993) while CaO would hinder the biological performance of HA (Ślósarczyk & Piekarczyk, 1999).

6.2.3 Bulk Density of Undoped and ZnO-doped Sintered HA

The densification curves of undoped and ZnO-doped HA as a function of sintering temperatures are shown in Figure 6.17. The relative density increased with increasing sintering temperature for pure HA throughout the sintering regime. However, for ZnO-doped HA regardless of dopants amount, the bulk density increase with increasing temperature and met a plateau at about 1250 ℃. From Figure 6.17, it is noticeable that ZnO-doped HA samples have demonstrated higher densification that pure HA as all the doped samples attained high relative density > 98% at 1200 ℃ while pure HA could obtain only ~97.5% of the theoretical density at the similar temperature. On the other hand, sintering study showed that 1250 ℃ is optimum sintering temperature in densifying Zn-doped HA as all the doped samples attained the highest relative density at 1250 ℃ except for pure HA. Pure HA attained highest density of ~98.43% at 1300 ℃.

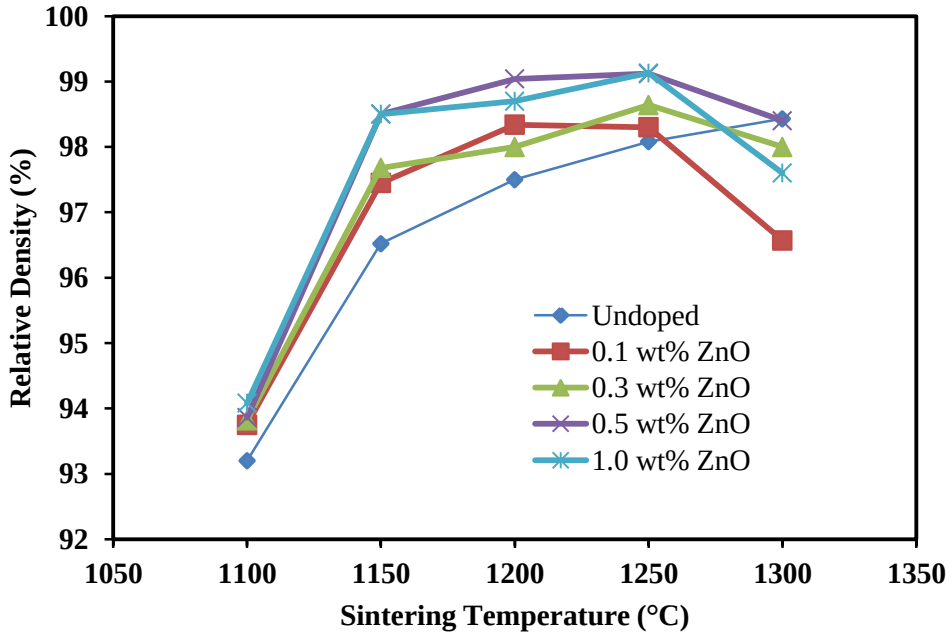

Figure 6.17: Relative density variation as a function of sintering temperatures for HA with different amount of ZnO addition.

Besides, it also appeared that higher ZnO amount is beneficial for the densification of HA especially at high temperature of 1250 ℃ as shown in Figure 6.17. Higher content of ZnO appeared to be advantageous to the densification of HA since the 1.0 wt% ZnO-doped HA attained the highest relative density of ~99.13%; followed by 0.5 wt% ZnO-doped HA (99.12%), 0.3 wt% (98.64%) ,0.1 wt% ZnO-doped HA (98.3 %) and the undoped HA achieved only 98.08% of relative density at 1250 ℃. The inclusion of ZnO improved the mass transport along the grain boundaries and thus lead to higher final densities. Moreover, zinc oxide was found to be beneficial in enhancing the densification of HA when compared to other sintering additives such as silver, iron and titania (Bhattacharjee *et al*., 2011; Kramer *et al*., 2013; Wang & Chaki, 1994).

6.2.4 Microstructure Analysis of Undoped and ZnO-doped Sintered HA

Figure 6.18 shows the representative microstructures of the ZnO-doped HA and undoped HA sintered at 1150 ℃. SEM observation in Figure 6.18 (a) showed that small pores were detected (indicated by arrows) on undoped HA and this is in agreement with

the slightly lower relative density of 96.5% at sintered at 1150 ℃. In contrast, Figure 6.18 (b) and Figure 6.18 (c) displayed dense microstructure which confirmed that the 0.1 wt% and 0.3 wt% ZnO-doped HA ceramic obtained higher density of ~97.5% which correlated well with the bulk density analysis in Figure 6.16. Besides, it could be seen that undoped HA had slightly smaller grain size (0.69 μm) than the 0.1 wt% and 0.3 wt% ZnO-doped HA, recorded grain size of 0.74 μm and 0.73 μm, respectively.

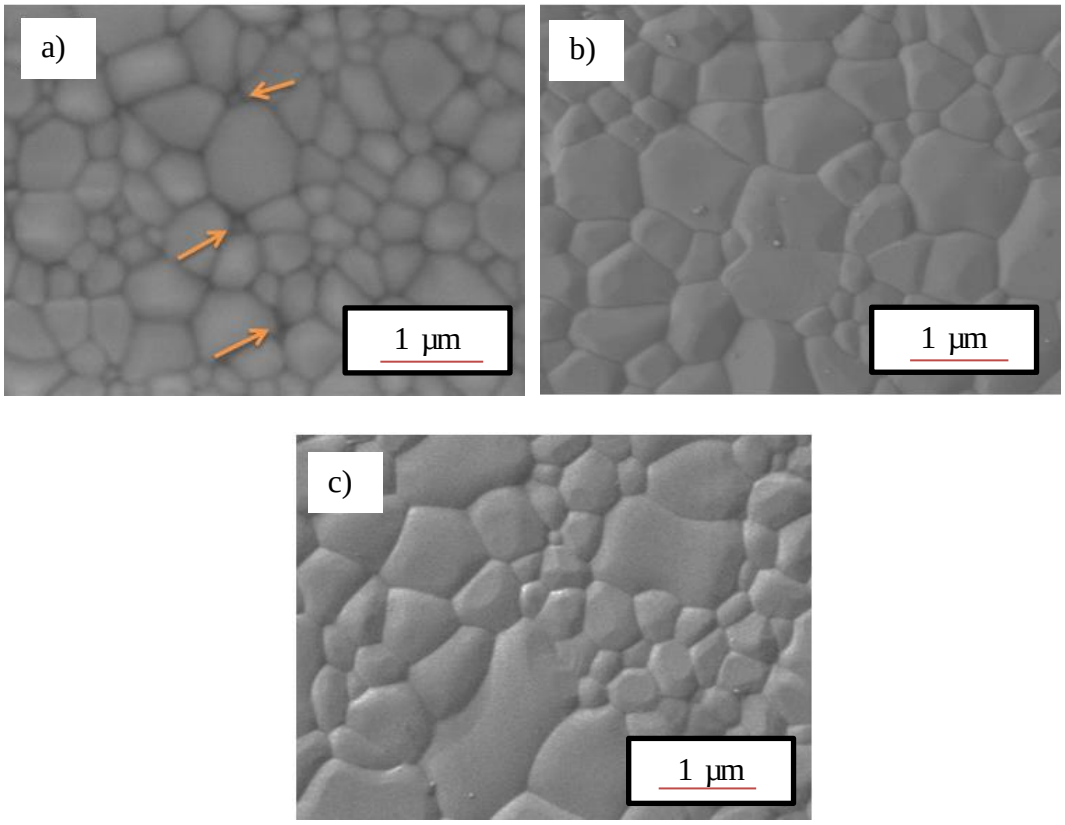

Figure 6.18: SEM analysis of HA samples sintered at 1150 ℃ for (a) undoped HA (b) 0.1 wt% ZnO-doped HA and (c) 0.3 wt% ZnO-doped HA.

The SEM micrographs of 0.5 wt% and 1.0 wt% ZnO-doped HA sintered at 1150 ℃ are shown in Figure 6.19 and Figure 6.20, respectively. It was found that high ZnO addition is beneficial in enhancing the density of HA while suppressing the grain growth as fully dense microstructure with small grains were found as shown in Figure 6.19 and Figure 6.20. 0.5 wt% ZnO-doped HA obtained smallest grain size of 0.51 μm

while 1.0 wt% recorded grain size of 0.59 µm. From Figure 6.19, some tiny bright particles were found in the 0.5 wt% ZnO-doped HA matrix and EDX analysis confirmed that the tiny bright particles were ZnO. They were found randomly dispersed on the HA matrix where some located intragranularly while some intergranularly situated at the grain boundaries and also at the triple junction.

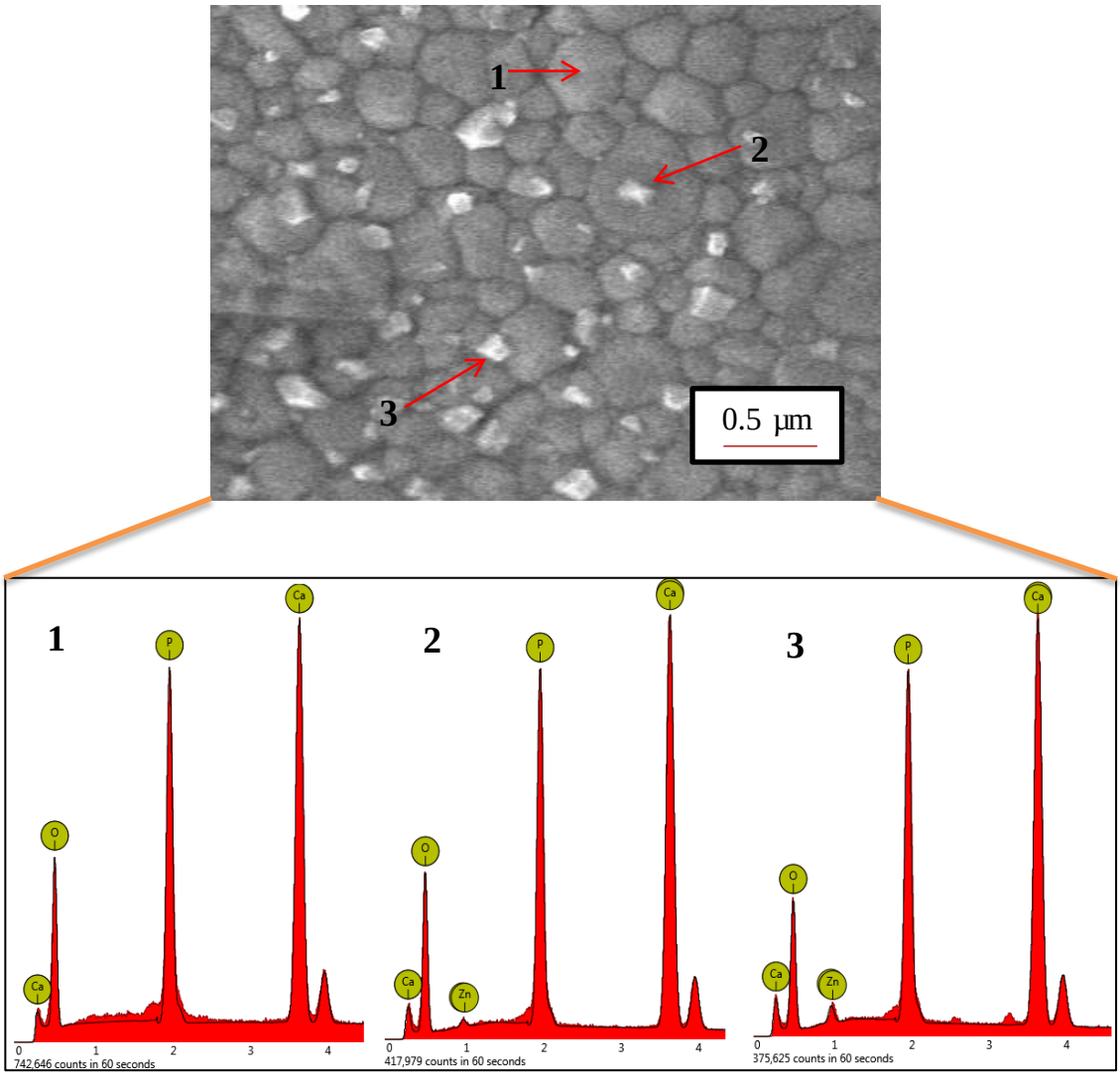

Figure 6.19: SEM analysis of 0.5 wt% ZnO-doped HA samples sintered at 1150 ℃ (inset as EDX spectrum).

Besides, Figure 6.20 proved that 1.0 wt % ZnO-doped HA contained ZnO particles in the matrix as confirmed by EDX analysis. However, the ZnO was found to be in cluster as shown in Figure 6.20. This could be due to the fact that higher amount of ZnO addition are more difficult to be dispersed homogenously, caused some of the ZnO remain as cluster within the HA matrix. In contrast, the tiny bright particles (ZnO) were not detected on the 0.1 wt% and 0.3 wt% ZnO-doped HA as indicated in Figure 6.18 (b) and (c), respectively.

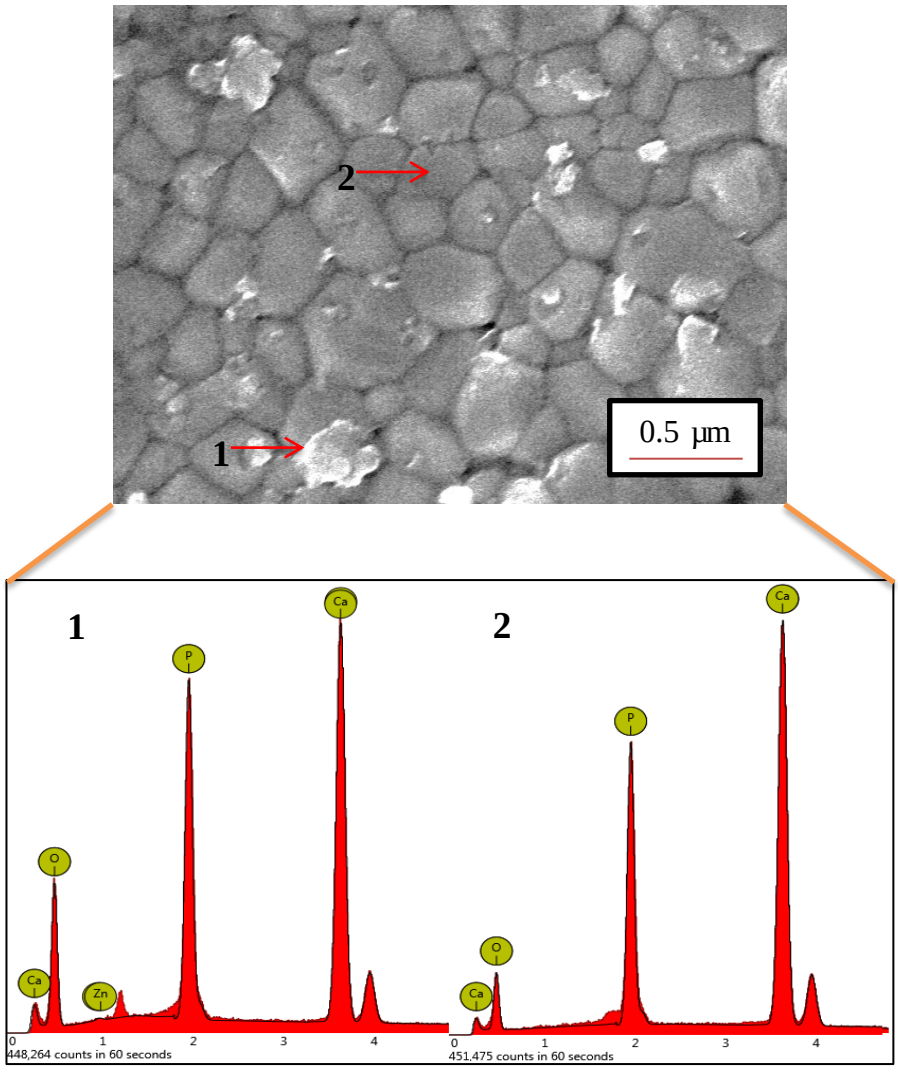

Figure 6.20: SEM analysis of 1.0 wt% ZnO-doped HA samples sintered at 1150 ℃ (inset as EDX spectrum).

The comparison of the grain size of all the HA sintered at 1150 ℃ is summarized in Table 6.2. From Table 6.2, the grain size of 0.1 wt% and 0.3 wt% ZnO-doped HA was found to be slightly bigger than undoped HA, proved that 0.1 wt% and 0.3 wt% of ZnO addition are not sufficient to inhibit the grain growth of HA. This was evidence from the SEM in Figure 6.18 (b) and (c) where no ZnO particles were detected in the samples. 0.5 wt% ZnO-doped HA was found to obtained smallest grain size, proved that 0.5 wt% ZnO addition can hinder the grain growth of HA. The intragranularly and intergranularly seated ZnO slow down the grain boundary diffusion/migration by preventing the HA grains to contact with each other freely. Hence, the diffusions of atoms along the grain boundaries between HA grains and also between the HA and ZnO grains were slow down, and the grain growth could be restricted. As ZnO content increased to 1.0 wt%, the grain growth inhibition was found to be less effective compared to 0.5 wt% ZnO addition. This could be attributed to inhomogenous dispersion of ZnO on the HA matrix as shown in Figure 6.20.

Table 6.2: Grain size of undoped and ZnO-doped HA sintered at 1150 ℃.

ZnO content (wt%)	Grain Size (μm)
Undoped	0.6911
0.1	0.7429
0.3	0.7323
0.5	0.5090
1.0	0.5946

When sintering was carried out at 1300 ℃, the grain size increased for all the samples regardless of dopant addition as shown in Figure 6.21. Pure HA showed the most significant grain growth as the grain size increased to 6.9 μm. 0.1 wt%, 0.3 wt%, 0.5 wt% and 1.0 wt% ZnO-doped HA recorded grain size of 4.4 μm, 2.74 μm, 2.15 μm and 3.23 μm, respectively. The results indicated that 0.5 wt% can inhibit grain growth effectively

even at high sintering temperature of 1300 ℃ as it exhibited smallest grain size amongst all the HA samples. It is worth mentioning that the 1.0 wt% ZnO-doped HA exhibited microstructure of extremely large grain that accompanied by small grains as shown in Figure 6.21 (e). This is due to the agglomeration of ZnO cluster on the HA matrix as the agglomerates can act as seeds for abnormal grain growth due to different densification rate (Mouzon *et al*., 2008).

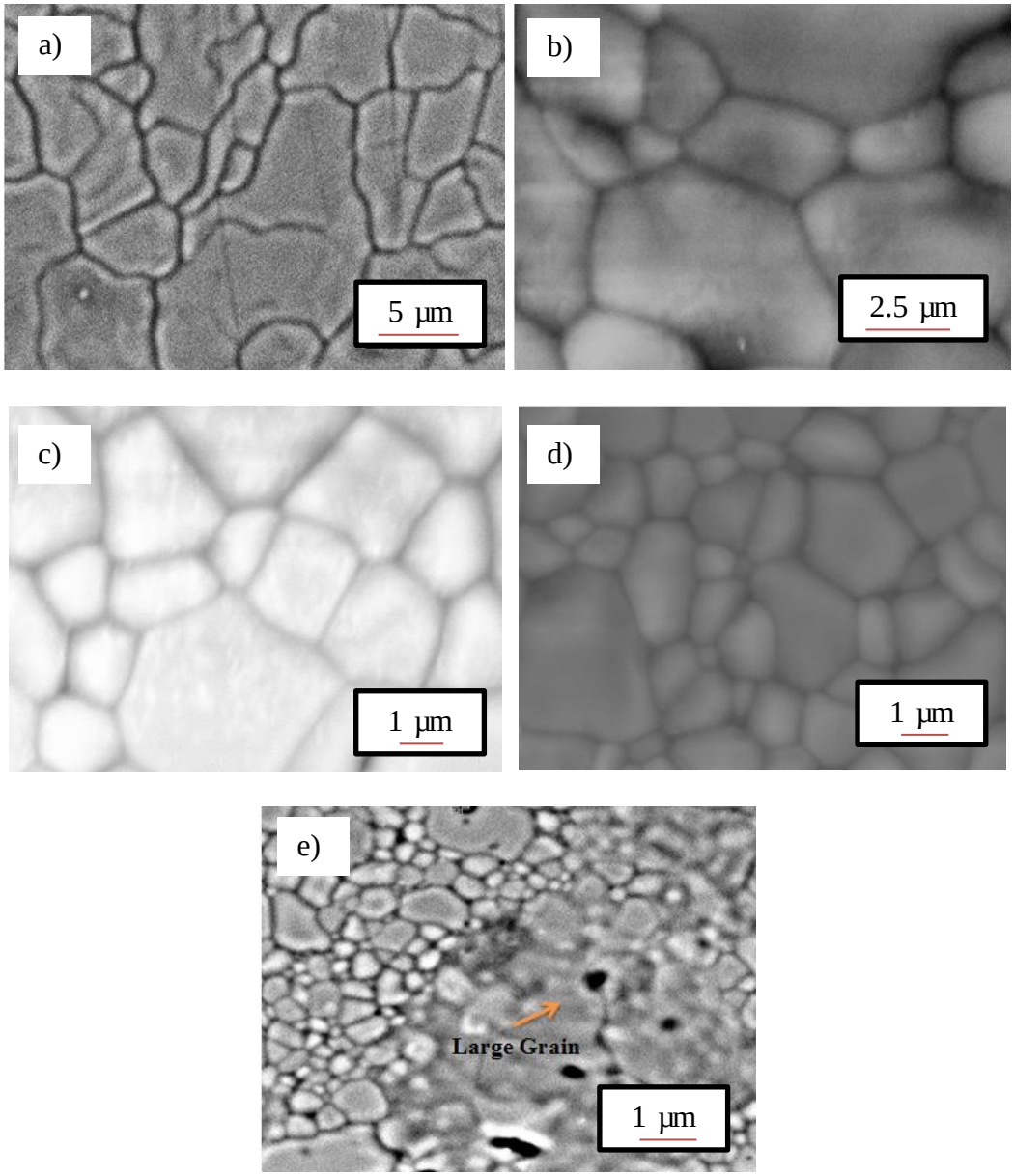

Figure 6.21: SEM analysis of HA samples sintered at 1300 ℃ for (a) undoped HA (b) 0.1 wt% ZnO-doped HA, (c) 0.3 wt% ZnO-doped HA, (d) 0.5 wt% ZnO-doped HA and (e) 1 wt% ZnO-doped HA.

For current work, the average grain size of the undoped and ZnO-doped HA increase with increasing temperature as shown in Figure 6.22. This growth in grain size due to elevated temperature was also observed by Layrolle *et al*. (1998) and Prokopieve & Sevostianov (2006). From the graph, the undoped HA showed a higher rate of grain growth compared to the ZnO-doped HA. It can be seen that upon 1200 ℃, the grain size of undoped HA increased by a factor of 5 when the temperature increased from 1200 ℃ to 1300 ℃. As for 0.5 wt% ZnO-doped HA, the grain size increased gradually from 0.73 µm (1200 ℃) to 2.15 µm (1200 ℃).

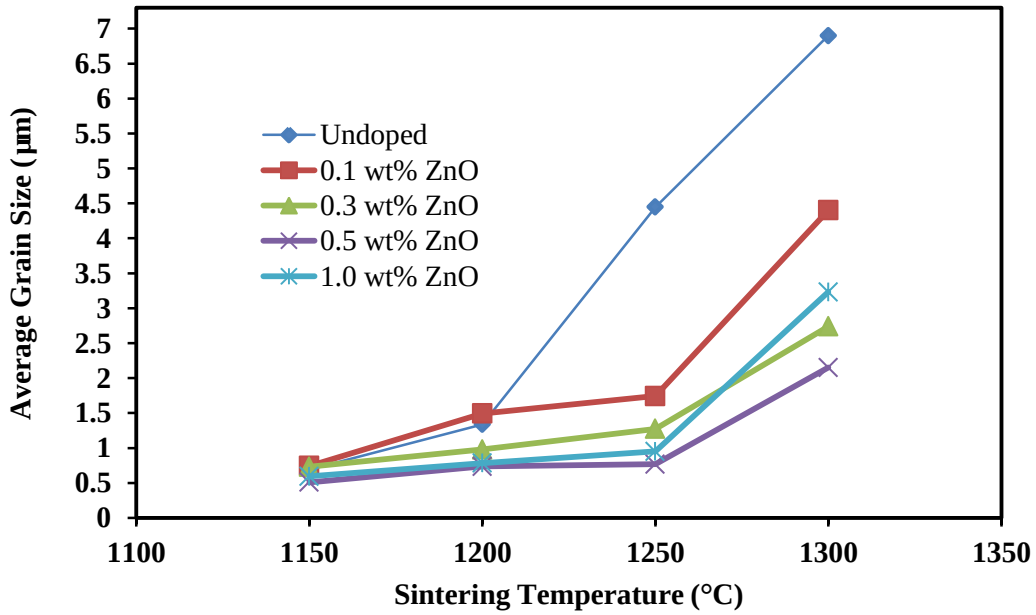

Figure 6.22: Effect of sintering temperature and ZnO addition on the average grain size of HA.

6.2.5 Vickers Hardness and Fracture Toughness of Undoped and ZnO-doped Sintered HA

The effects of ZnO addition and sintering temperature on the Vickers hardness of sintered HA are shown in Figure 6.23. A general observation which can be made from Figure 6.23 is that the measured hardness of all the undoped and ZnO-doped HA revealed a similar trend where the hardness increases with increasing temperature,

consequently reaching the maximum hardness value at certain temperature; followed by a decrease with further increase of sintering temperature. For instance, the hardness of 0.5 wt% ZnO-doped HA perked at 1150 ℃ (5.63 GPa) and decrease drastically to 4.28 GPa at sintering temperature of 1300 ℃. On the other hand, the maximum hardness was obtained at higher sintering temperature (1200 ℃) by undoped, 0.1 wt%, 0.3 wt% and 1.0 wt% ZnO-doped HA; recording value of 5.04 GPa, 5.12 GPa, 5.3 GPa and 5.37 GPa, respectively. Subsequent sintering caused deterioration or constant hardness values ranging from 4.22 GPa to 4. 8 GPa as shown in Figure 6.23.

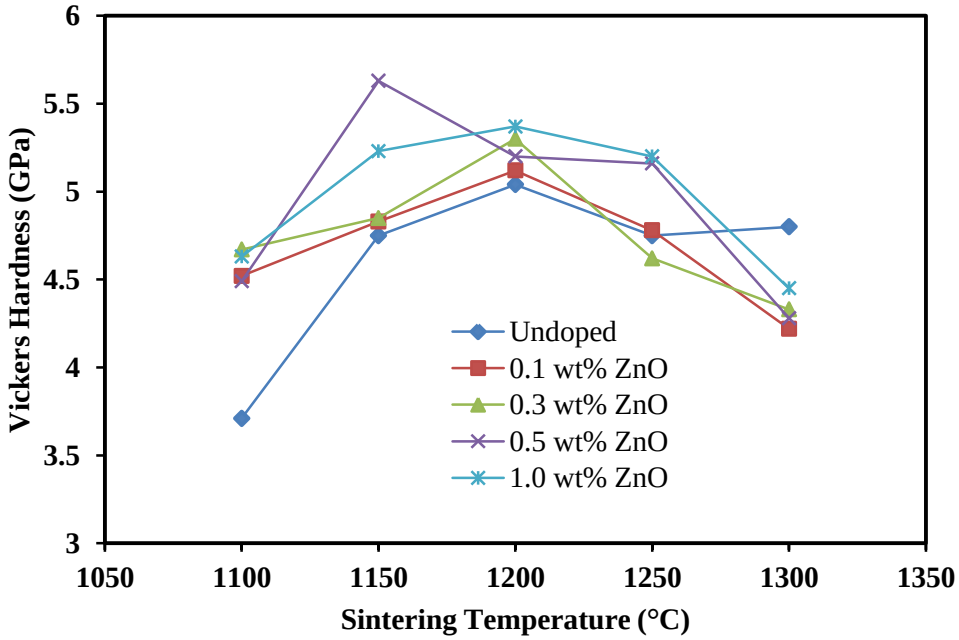

Figure 6.23: Effect of sintering temperature and ZnO addition on the Vickers hardness of HA.

The beneficial effect of ZnO in improving the hardness of HA has been revealed. It could be perceived that at temperature from 1100 ℃ to 1200 ℃, all the ZnO-doped HA samples demonstrated hardness superior to that of undoped HA. The maximum hardness achieved for all undoped and ZnO-doped HA is summarized in Table 6.3. In short, the addition of 0.5 wt% was found to be most effective as the sample obtained highest hardness values among all the samples as shown in Table 6.3.

The enhancement of hardness obtained from the 0.5 wt% ZnO-doped HA was due to the smaller grain size. Figure 6.24 shows the hardness of undoped and ZnO-doped HA ceramics as a function of the inverse square root of grain size. The values in the graph was reasonably fitted with a line (R^2 = 0.9264), which means that this dependence followed the Hall-Petch relationship (Wang *et al*., 2009) where hardness increased with decreasing grain size. The enhancement in the hardness of HA due to the smaller grain size was also observed by Veljovic *et al*. (2009), Ramesh *et al*., (2008) and Tekeli *et al*. (2006) as they stated that smaller grain size give more grain boundaries as per unit volume which acts as obstacle for plastic deformation.

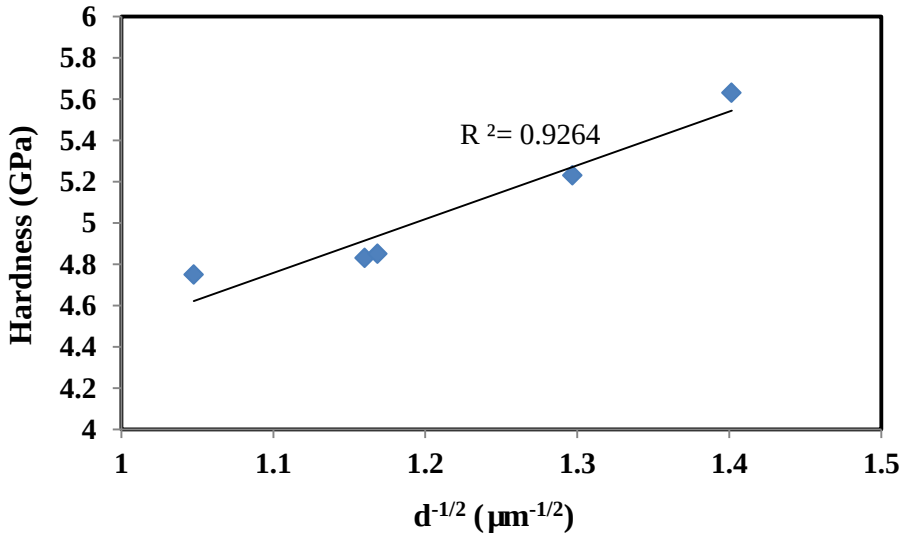

Figure 6.24: The dependence of the hardness of undoped and ZnO-doped HA on the inverse square root of grain size.

Table 6.3: A comparison of optimum Vickers hardness between undoped and ZnO-doped HA.

ZnO content (wt%)	Maximum Vickers Hardness (GPa)
Undoped	5.04
0.1	5.12
0.3	5.37
0.5	5.63
1.0	5.37

The fracture toughness variation with respect to the sintering temperature for undoped and ZnO-doped HA is shown in Figure 6.25. At low temperature of 1100 ℃, low fracture toughness values (0.97 – 1.06 MPam$^{1/2}$) were recorded for all the sintered samples which could be attributed to the weak grain boundaries of the HA matrix at low temperature (Champion, 2013). For undoped HA, no obvious trend or relationship could be observed between fracture toughness and sintering temperature (Figure 6.25) as fracture toughness fluctuated with temperatures.

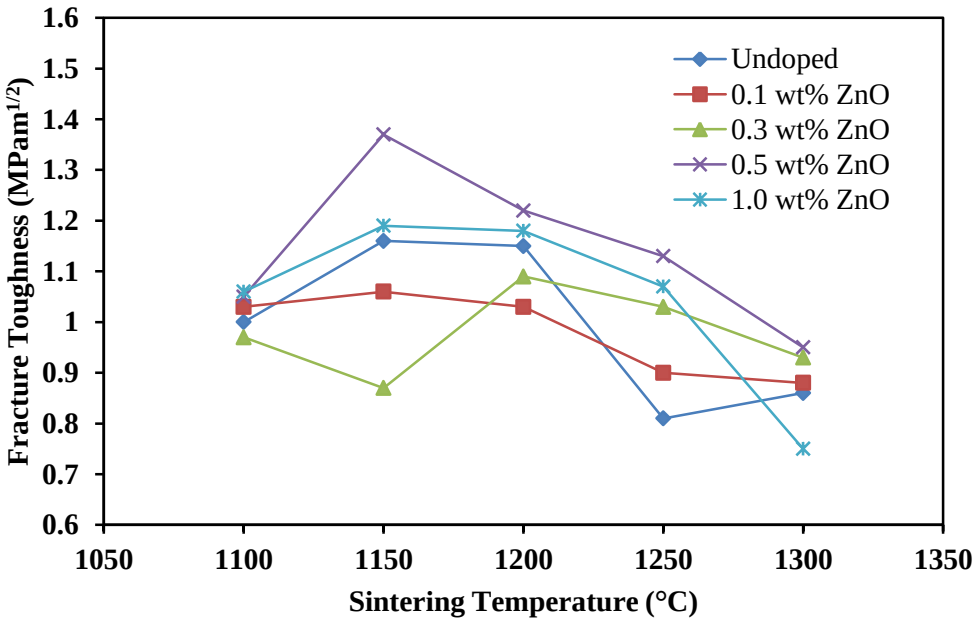

Figure 6.25: Effect of sintering temperature and ZnO addition on the fracture toughness of HA.

Further analysis indicated that the fracture toughness variation of all the ZnO-doped HA samples exhibited similar trend to the variation of Vickers hardness (Figure 6.23) as fracture toughness met a plateau at certain temperature and thereby decrease with increasing temperature. For example, the fracture toughness of 0.5 wt% ZnO-doped HA peaked at a maximum value (1.37 MPam$^{1/2}$) when sintered at 1150 ℃ and decreased almost linearly with increasing temperature (>1150 ℃). Similarly, 0.1 wt% and 1.0 wt% ZnO-doped HA obtained maximum fracture toughness value of 1.06 MPam$^{1/2}$ and 1.19

$MPam^{1/2}$ respectively at 1150 ℃ and then decrease. On the other hand, 0.3 wt% ZnO-doped HA obtain its maximum toughness value of 1.09 $MPam^{1/2}$ at 1200 ℃ and decreased with further sintering.

From Figure 6.25, low fracture toughness values were recorded for all the samples sintered at 1300 ℃. According to Buys *et al*. (1995), the decline in mechanical properties of HA are expected at higher temperatures above 1200 ℃ mainly due to HA decomposition to TCP and CaO. The volume changes associated with the formation of these new secondary phases creates internal strain within the HA matrix. This was not the case in the present work since HA decomposition was not detected for all the ZnO-doped HA sintered at 1300 ℃ and the drastic drop of fracture toughness observed could be associated to the increment in average grain size as shown in Figure 6.21. These large grains are believed to provide an easy path for crack propagation and hence lower fracture toughness (Ramesh *et al*., 2011).

6.2.6 Toughening Mechanism

The previous section has shown that 0.5 wt% ZnO-doped HA demonstrated the most enhanced hardness and fracture toughness as compared to other HA samples. Hence, the cracking behavior introduced by the Vickers indentation of the 1150 ℃ sintered 0.5 wt% ZnO-doped HA (Figure 6.27) was compared to the pure HA (Figure 6.26). As shown in Figure 6.26, pure HA tends to propagate cracks in straight line where the deflection angle is barely observed due to the absence ZnO particles as obstacles. The overall path of crack propagation was completely linear, predominantly transgranular fracture mode. In contrast, the crack path of the 0.5 wt% ZnO-doped HA has significant crack deflection with a mixture of transgranular and intergranular fracture mode as shown in Figure 6.27. The toughening mechanism of 0.5 wt% ZnO-doped HA can be summarized as the combine effects of crack deflection and crack bridging as shown in the magnified

image in Figure 6.28 and Figure 6.29, respectively. As for crack deflection (Figure 6.28), the crack cross the HA grains transgranularly and hit the intragranularly seated ZnO. This caused the crack to be deflected to the grain boundaries and continue to propagate intergranularly within the HA and ZnO grain boundaries. The high deflection angle of crack resulted in torturous crack path where higher fracture energy is needed for the crack to propagate. According to the following equation stated by Jang *et al*. (1996):

$$K_{IC} \alpha \gamma_f^{\frac{1}{2}} \quad (6.1)$$

The fracture toughness (K_{IC}) was directly proportional to the square root of fracture energy (γ_f), the higher fracture energy resulted from the crack deflection contributed to the enhanced toughening in the 0.5 wt % ZnO-doped HA. This toughening via crack deflection has been reported elsewhere (Faber & Evans, 1983; Wang & Shaw, 2009). The magnified image in Figure 6.29 showed the presence of crack bridging. The ZnO particulate bridges the two surface of crack, providing stress to counteract the applied stress and hence delay the crack propagation. The crack bridging and crack deflections as a result of ZnO addition were schematically depicted in Figure 6.30 (a) and Figure 6.30 (b).

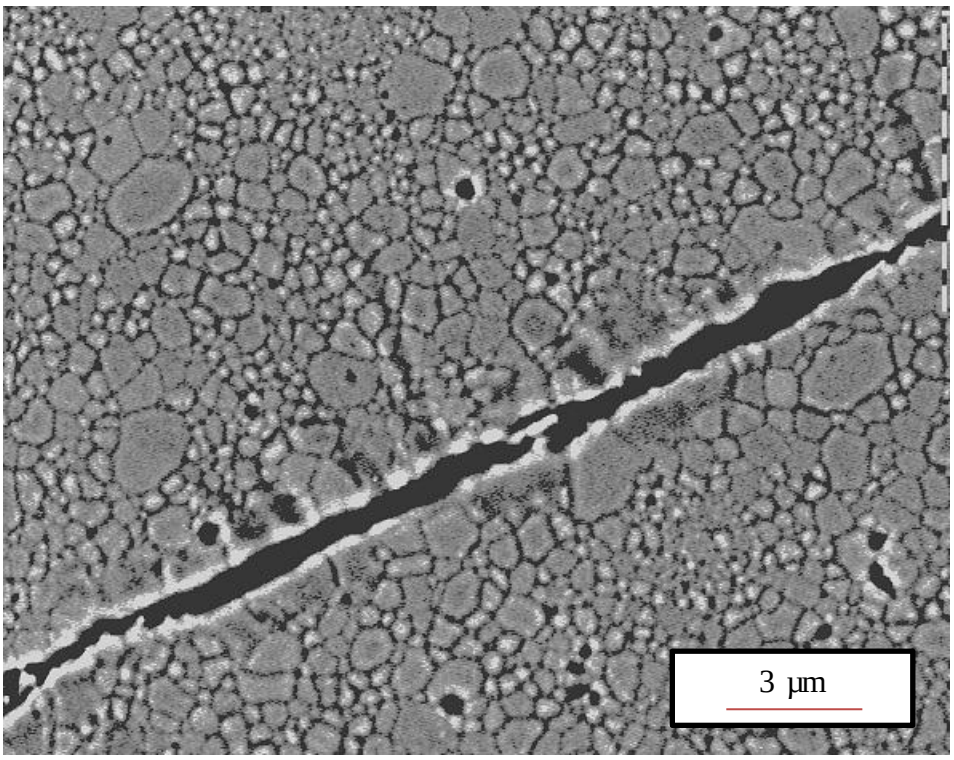

Figure 6.26: SEM micrograph of the indentation crack paths of pure HA sintered at 1150 ℃.

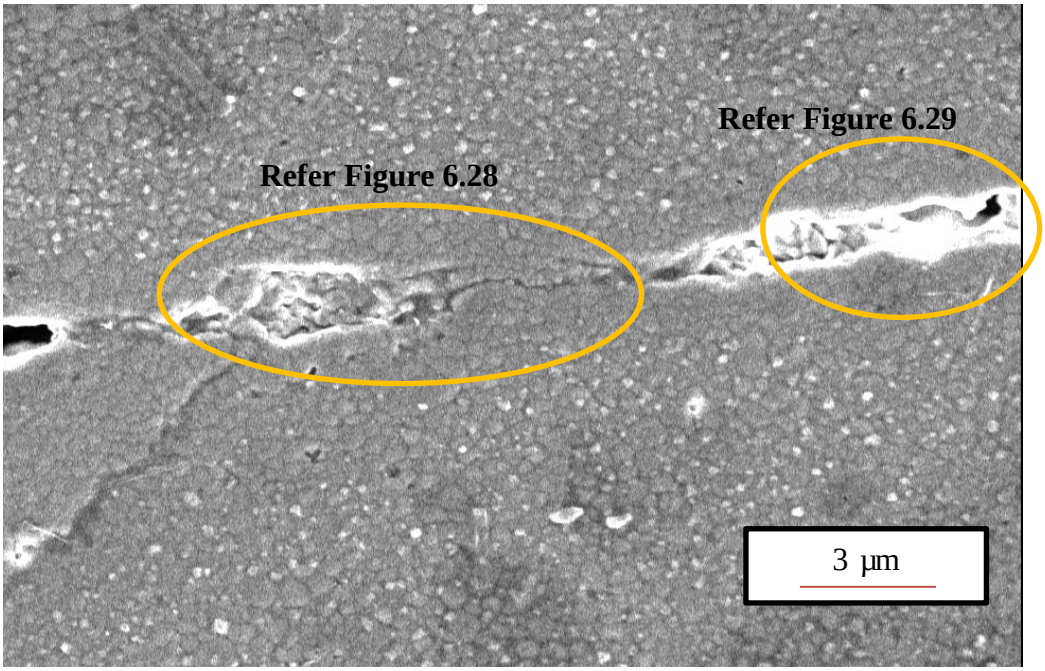

Figure 6.27: SEM micrograph of indentation crack paths of 0.5 wt% ZnO-doped HA sintered at 1150 ℃.

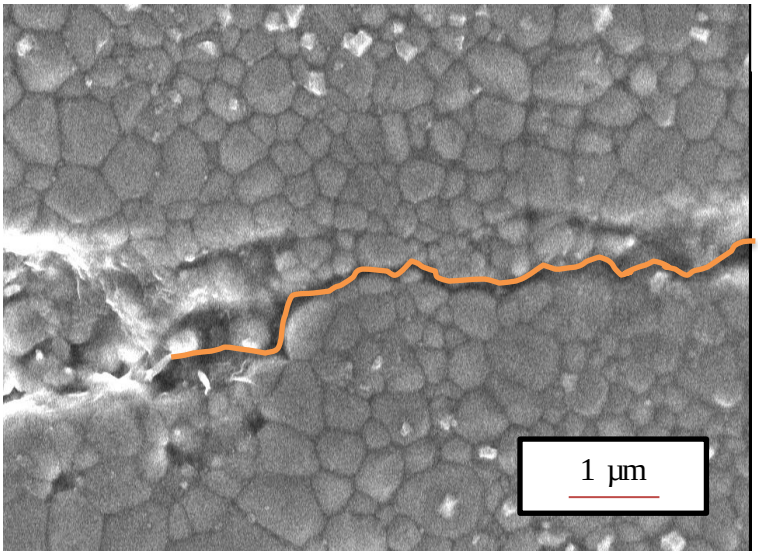

Figure 6.28: A close up view of the crack paths of Figure 6.27 indicated the crack deflection.

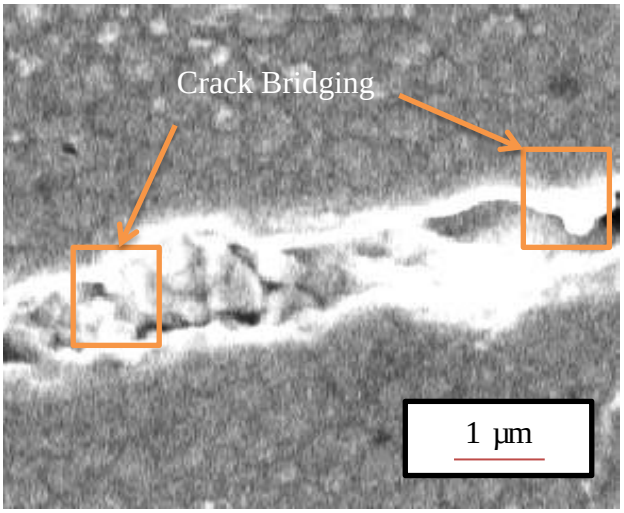

Figure 6.29: A close up view of the crack paths of Figure 6.27 indicated the crack bridging.

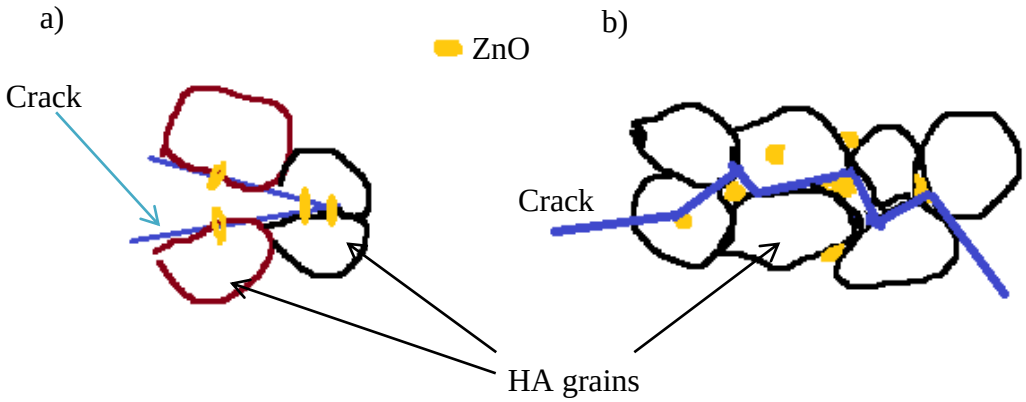

Figure 6.30: A schematic diagram of the proposed toughening mechanism: (a) crack bridging and (b) crack deflection.

In summary, the inclusion of ZnO into HA matrix is beneficial in terms of sinterability and mechanical properties without disrupting the phase stability of HA. 0.5 wt% ZnO-doped HA sintered at 1150 ℃ was found to exhibit the highest hardness of 5.63 GPa and fracture toughness of 1.37 $MPam^{1/2}$.The higher mechanical properties of 0.5 wt% ZnO-doped HA compared to other samples were attributed to the effectiveness of 0.5 wt% ZnO in suppressing the grain coarsening. Moreover, the high fracture toughness value recorded in the present work is very promising as other researchers who doped HA with different additives such as zirconia, titanium oxide, alumina and bismuth oxide (Bhattacharjee *et al*., 2011; Kim *et al*., 2003; Champion *et al*., 1996; Ramesh *et al*., 2011) obtained fracture toughness less than 1.24 $MPam^{1/2}$. Further to that, zinc oxide was proved to improve the biological properties of calcium phosphate (Bandyopadhyay *et al*., 2006; Yu *et al*., 2014; Ishikawa *et al*., 2002; Ito *et al*., 2000), making it a potential candidate for clinical applications.

CHAPTER 7: CONCLUSIONS AND FURTHER WORK

7.1 Conclusions

This study was carried out to evaluate the sinterability of HA powders synthesized via three different drying methods, i.e. oven drying (OD-HA), microwave drying (MD-HA) and freeze drying (FD-HA). Then, the effect of microwave sintering on the HA powder were evaluated and explained. The beneficial effect of adding ZnO on the sintering behaviour of HA particularly on the fracture toughness has also been evaluated. The following conclusions can be drawn from this present work.

1. Single phase pure HA powder were successfully synthesized by wet chemical method via oven drying, microwave drying and freeze drying as proved by XRD analysis and FTIR analysis.

2. EDX analysis showed that FD-HA had Ca/P ratio of 1.77, closer to the stoichiometry HA (Ca/P = 1.67) compared to MD-HA (Ca/P =1.85) and OD-HA (Ca/P = 1.90). However, it was found that the Ca/P ratio did not affect the phase stability of the HA powder as all the three drying methods produced pure HA.

3. FE-SEM micrographs proved that MD-HA and FD-HA consisted of small to large size agglomerates that made of HA particles in nanosize while OD-HA consisted of extremely large agglomerates.

4. It was found that both FD-HA and OD-HA demonstrated needle like morphology with specific surface area of ~ 97 m^2/g. In comparison, MD-HA was in nanorod morphology accompanied with higher specific surface area of ~ 111 m^2/g.

5. Microwave drying significantly reduced the time of HA synthesis and it was found that MD-HA exhibited higher thermal stability that OD-HA. MD-HA showed no sign of decomposition into tri-calcium phosphate, tetra tri-calcium phosphate and calcium oxide despite sintering at a high temperature of 1350 ℃. However, β-TCP peaks were detected from the OD-HA sintered at 1350 ℃. On the other hand, peak shifting was detected from the XRD profiles of FD-HA indicating the possibility of dehydroxylation.

6. MD-HA was found to be slightly more sinteractive than FD-HA and OD-HA particularly at low temperature range below 1150 ℃. The enhancement in the sinterability of synthesized HA at low temperature could be attributed to the nanorod morphology, homogenous distribution and the high specific surface area of MD-HA particles.

7. All the synthesized HA achieved a final sintered density of 96.5% to 98% of theoretical density at 1150 ℃ - 1300 ℃ regardless of drying methods.

8. All the HA recorded increasing grain size value as the sintering temperature increased. MD-HA sample demonstrated slower grain growth rate typically at 1050 ℃ - 1200 ℃ compared to FD-HA and OD-HA. However, as the temperature increased to 1350 ℃, MD-HA recorded the highest grain size of 10.85 μm compared to FD-HA (8.9 μm) and OD-HA (9.3 μm).

9. Throughout the sintering regime, it was found that the drying methods had minimal effects on the hardness of HA. All the HA samples exhibited similar trend whereby hardness increased to a maximum hardness value at certain temperature (i.e. 1150 ℃ for FD-HA and OD-HA and 1200 ℃ for MD-HA) and thereafter declined with further sintering. FD-HA and OD-HA recorded

maximum hardness values of 5.3 GPa and 5.12 GPa, respectively, at 1150 ℃ while MD-HA recorded the maximum hardness of 5.04 GPa at 1200 ℃.

10. MD-HA possessed better fracture toughness when compared to both FD-HA and MD-HA throughout the sintering regime. The MD-HA achieved maximum fracture toughness of 1.16 $MPam^{1/2}$ at 1150 ℃. In comparison, both FD-HA and OD-HA could only achieved toughness values of 1.13 $MPam^{1/2}$ and 1 $MPam^{1/2}$, respectively at the similar temperature. The low fracture toughness value of OD-HA could be attributed to the inhomogenous grain distributions as indicated by the SEM analysis.

11. Further investigation indicated that the fracture toughness of sintered HA samples is dependent on the grain size of sintered HA where fracture toughness increase with a decrease in grain size. Hence, the MD-HA that recorded the smallest grain size of 0.691 μm at 1150 ℃ recorded higher fracture toughness compared to FD-HA (1.023 μm) and OD-HA (0.974 μm) at the similar temperature.

12. The effects of microwave sintering (MWS) on the sinterability of MD-HA were investigated in terms of phase stability, sintered bulk densities, microstructure and grain size, hardness and fracture toughness. The study revealed that microwave sintering plays an important role in enhancing the densification and mechanical properties of HA and dense microwave sintered HA was produced at low temperature of 1050 ℃.

13. The study revealed that microwave sintering did not disrupt the phase stability of HA. Secondary phases such as TTCP, TCP and CaO were not presented in the compacts throughout the sintering range. Further to that, no peak shifting was

observed from XRD profiles regardless of sintering method indicated that dehydroxylation of HA did not occurred.

14. Both HA samples sintered by conventional pressureless sintering (CPS) and microwave sintering (MWS) exhibited similar trend where relative density increase with increasing temperature but at different densification rates. At low temperature range (below 1150 ℃), the density of MWS-HA was significantly higher than the CPS-HA. At low temperature of 950 ℃, ~89% densified MWS-HA was obtained and further sintering lead to highly densified MWS-HA; exhibited >97% of theoretical density when sintering temperature increased to temperature above 1100 ℃. In contrast, the CPS-HA displayed a relatively lower relative density value of 77.5% at 950 ℃ and CPS-HA could only achieve relative density above 97% at high sintering temperature of 1200 ℃.

15. In both MWS-HA and CPS-HA, the grain size increase as the sintering temperature increases. The mean grain size of MWS-HA increased slowly from nanolevel (300 nm) to microlevel (~4.33 μm) with increasing temperature from 950 ℃ to 1250 ℃. As for CPS-HA, the grain size couldn't be measured at low 950 ℃ and 1000 ℃ as grains were hardly seen. Then, the grain size of CPS-HA increased by a factor of about 6.4 from ~691 nm to ~4.45 μm at sintering temperature of 1150 ℃ and 1250 ℃, respectively.

16. The results showed that microwave sintering is effective in preventing grain growth while maintaining high density throughout the sintering regime and nano grain size was maintained up to 1100 ℃.

17. The results showed that the hardness values of MWS-HA are higher than CPS-HA at lower temperature range (950 ℃ - 1100 ℃). However, similar hardness

values were recorded for both MWS-HA and CPS-HA sintered at 1150 ℃. Upon 1150 ℃, the hardness values of CPS-HA are higher than MWS-HA.

18. The results proved that microwave sintering has significantly enhance the fracture toughness of the HA. Fracture toughness value as high as 1.85 MPa.$m^{1/2}$ was obtained from MWS-HA sintered at low temperature of 1050 ℃ as compared to 1.16 MPa.$m^{1/2}$ of CPS-HA sintered 1150 ℃.

19. The enhancement in the fracture toughness of microwave sintered HA was due to the combine effects of improved densification and restricted grain growth of HA during microwave sintering.

20. ZnO doping carried out in the current work had negligible effects on the phase stability of HA powders. The XRD traces indicated that the sintering of ZnO-doped HA (up to 1.0 wt% ZnO) did not result in the formation of secondary phases throughout the sintering range employed, thus indicating that the addition of ZnO did not interrupt the thermal stability of HA phase.

21. The bulk density variation of all the composition (undoped, 0.1 wt%, 0.3 wt%, 0.5 wt%, 1.0 wt% of ZnO) possessed similar increasing trend with increasing sintering temperature. Higher content of ZnO appeared to be advantageous to the densification of HA since the 1.0 wt% ZnO-doped HA attained the highest relative density of ~99.13%; followed by 0.5 wt% ZnO-doped HA (99.12%), 0.3 wt% (98.64%) ,0.1 wt% ZnO-doped HA (98.3 %) and the undoped HA achieved only 98.08% of relative density at 1250 ℃.

22. The beneficial effect of ZnO especially for the 0.5 wt% addition in enhancing the mechanical properties (hardness and fracture toughness) of HA has been revealed. The highest hardness value of 5.63 GPa was obtained for HA doped

with 0.5 wt% ZnO sintered at 1150 ℃. In addition, at the similar temperature, the 0.5 wt% ZnO-doped HA sample achieved the highest fracture toughness of 1.37 $MPam^{1/2}$. In contrast, undoped HA could only attained hardness of 4.75 GPa and 1.16 $MPam^{1/2}$ at the similar sintering temperature of 1150 ℃.

23. The improvement in the hardness of 0.5 wt% ZnO-doped HA compared to undoped HA is associated with a decreased in the grain size of the HA sintered body; correlated well with the Hall-Petch relationship. The smaller grain size gives more grain boundaries as per unit volume which acts as obstacle for plastic deformation.

24. The introduction of ZnO as dopants into the HA matrix is believed to change the transgranular fracture mode of the pure HA into the mix mode of transgranular and intergranular fracture. The ZnO seated intragranularly and intergranularly in the HA matrix deflected the crack, resulted in torturous crack path where higher fracture energy is needed for further crack propagation. As fracture toughness is directly proportional to the fracture energy, the fracture toughness of ZnO-doped HA was increased. Besides, the ZnO particles were found to bridge the two surfaces of cracks, delaying the crack propagation which in turn increased the fracture toughness of the sintered HA.

In conclusion, the objectives of the research were achieved as a rapid microwave drying method was incorporated to accelerate the synthesis process of HA without compromising the properties of HA. On the other hand, microwave sintering and the addition of ZnO were beneficial in enhancing the mechanical properties of HA, particularly on fracture toughness. A high fracture toughness of 1.85 $MPam^{1/2}$ was successfully obtained by sintering microwave dried HA pellets in microwave furnace at 1050 ℃.

7.2 Further Work

Following are some suggestions for further work to be done:

1. Raman spectroscopy studies would provide a more insightful detail on the dehydroxylation phenomenon and the relation to the XRD peak shifting of the current work.

2. The biocompatibility of the HA sintered samples can be examined using the simulated body fluid (SBF). The surface morphological changes of the HA samples upon immersion in the SBF could be determined by the scanning electron microscopy.

3. The use of more sophisticated equipment such as transmission electron microscope (TEM) could be used to investigate the microstructure of the sintered HA compacts as the resulting microstructure of sintered HA could affect the mechanical properties of HA.

4. Other powder consolidation techniques such as two step sintering, spark plasma sintering, hot pressing and hot isostatic pressing could be applied to produce HA with high density and high mechanical properties. Besides, a comparison of the sinterability of ZnO-doped HA obtained from these advanced sintering techniques could be interesting.

5. The influences of other sintering additives such as magnesium oxide, titanium oxide, zirconia, alumina etc on the mechanical properties of sintered HA should also be investigated.

REFERENCES

Abd Rahman, H., Rahmat, N., and Shariff, M. (2009). Microwave drying effects on the properties of alumina-zeolite foam.

Afshar, A., Ghorbani, M., Ehsani, N., Saeri, M., and Sorrell, C. (2003). Some important factors in the wet precipitation process of hydroxyapatite. *Materials & Design, 24*(3): 197-202.

Agrawal, D. (2006). Microwave sintering of ceramics, composites and metallic materials, and melting of glasses. *Transactions of the Indian ceramic society, 65*(3): 129-144.

Agrawal, D.K. (1998). Microwave processing of ceramics. *Current Opinion in Solid State and Materials Science, 3*(5): 480-485.

Akao, M., Aoki, H., and Kato, K. (1981). Mechanical properties of sintered hydroxyapatite for prosthetic applications. *Journal of Materials Science, 16*(3): 809-812.

Akao, M., Sakatsume, M., Aoki, H., Takagi, T., and Sasaki, S. (1993). In vitro mineralization in bovine tooth germ cell cultured with sintered hydroxyapatite. *Journal of Materials Science: Materials in Medicine, 4*(6): 569-574.

Akkaya, B. (2013). Porous and spherical hydroxyapatite microcomposites for immunoglobulin g adsorption. *Journal of Applied Polymer Science, 130*(4): 2764-2771.

Alobeedallah, H., Ellis, J.L., Rohanizadeh, R., Coster, H., and Dehghani, F. (2011). Preparation of nanostructured hydroxyapatite in organic solvents for clinical applications. *Trends Biomater. Artif. Organs, 25*: 12-19.

Aminzare, M., Eskandari, A., Baroonian, M., Berenov, A., Hesabi, Z.R., Taheri, M., and Sadrnezhaad, S. (2013). Hydroxyapatite nanocomposites: Synthesis, sintering and mechanical properties. *Ceramics International, 39*(3): 2197-2206.

Andres-Verges, M., Fernandez-Gonzalez, C., and Martinez-Gallego, M. (1998). Hydrothermal synthesis of calcium deficient hydroxyapatites with controlled size and homogeneous morphology. *Journal of the European Ceramic Society, 18*(9): 1245-1250.

Angelescu, N., Ungureanu, D.N., Catangiu, A., Bratu, V., and Anghelina, F.V. (2011). Synthesis and characterization of hydroxyapatite powders obtained by wet chemical method. *Metalurgia International, 16*(4): 125-128.

Arias, J., García-Sanz, F., Mayor, M., Chiussi, S., Pou, J., Leon, B., and Pérez-Amor, M. (1998). Physicochemical properties of calcium phosphate coatings produced by pulsed laser deposition at different water vapour pressures. *Biomaterials, 19*(10): 883-888.

Ashokan, A., Menon, D., Nair, S., and Koyakutty, M. (2010). A molecular receptor targeted, hydroxyapatite nanocrystal based multi-modal contrast agent. *Biomaterials, 31*(9): 2606-2616.

ASTM, E. (1999). 384-99: Standard test method for microindentation hardness of materials. *West Conshohocken, PA: American Standard for Testing Materials International*.

ASTM, E. (2004). 112-96: Standard test methods for determining average grain size. *West Conshocken, Annual Book of ASTM Standards. West Conshohocken, PA, USA*.

Atong, D., Ratanadecho, P., and Vongpradubchai, S. (2006). Drying of a slip casting for tableware product using microwave continuous belt dryer. *Drying technology, 24*(5): 589-594.

Balamurugan, A., Michel, J., Faure, J., Benhayoune, H., Wortham, L., Sockalingum, G., Banchet, V., Bouthors, S., Laurent-Maquin, D., and Balossier, G. (2006). Synthesis and structural analysis of sol gel derived stoichiometric monophasic hydroxyapatite. *Ceramics- Silikaty, 50*(1): 27-31.

Bandyopadhyay, A., Bernard, S., Xue, W., and Bose, S. (2006). Calcium phosphate-based resorbable ceramics: Influence of mgo, zno, and sio2 dopants. *Journal of the American Ceramic Society, 89*(9): 2675-2688.

Bandyopadhyay, A., Withey, E.A., Moore, J., and Bose, S. (2007). Influence of zno doping in calcium phosphate ceramics. *Materials Science and Engineering: C, 27*(1): 14-17.

Banerjee, A., Bandyopadhyay, A., and Bose, S. (2007). Hydroxyapatite nanopowders: Synthesis, densification and cell–materials interaction. *Materials Science and Engineering: C, 27*(4): 729-735.

Barralet, J., Best, S., and Bonfield, W. (1995). *Preparation and sintering of carbonate hydroxyapatite.* Paper presented at the Br. Ceram. Proc.

Bertrand, G., Roy, P., Filiatre, C., and Coddet, C. (2005). Spray-dried ceramic powders: A quantitative correlation between slurry characteristics and shapes of the granules. *Chemical Engineering Science, 60*(1): 95-102.

Best, S., Porter, A., Thian, E., and Huang, J. (2008). Bioceramics: Past, present and for the future. *Journal of the European Ceramic Society, 28*(7): 1319-1327.

Bettger, W.J., and O'Dell, B.L. (1993). Physiological roles of zinc in the plasma membrane of mammalian cells. *The Journal of Nutritional Biochemistry, 4*(4): 194-207.

Bhattacharjee, P., Begam, H., and Chanda, A. (2011). Development and physical, chemical and mechanical characterization of doped hydroxyapatite. *International Journal of Scientific & Engineering Research, 2*(4): 1-8.

Bianco, A., Cacciotti, I., Lombardi, M., Montanaro, L., and Gusmano, G. (2007). Thermal stability and sintering behaviour of hydroxyapatite nanopowders. *Journal of thermal analysis and calorimetry, 88*(1): 237-243.

Bildstein, L., Hillaireau, H., Desmaele, D., Lepêtre-Mouelhi, S., Dubernet, C., and Couvreur, P. (2009). Freeze-drying of squalenoylated nucleoside analogue nanoparticles. *International journal of pharmaceutics, 381*(2): 140-145.

Binner, J., Annapoorani, K., Paul, A., Santacruz, I., and Vaidhyanathan, B. (2008). Dense nanostructured zirconia by two stage conventional/hybrid microwave sintering. *Journal of the European Ceramic Society, 28*(5): 973-977.

Bodhak, S., Bose, S., and Bandyopadhyay, A. (2011). Influence of mgo, sro, and zno dopants on electro-thermal polarization behavior and in vitro biological properties of hydroxyapatite ceramics. *Journal of the American Ceramic Society, 94*(4): 1281-1288.

Bortzmeyer, D. (1995). Dry pressing of ceramic powders *Ceramic processing* (pp. 102-146): Springer.

Bose, S., Dasgupta, S., Tarafder, S., and Bandyopadhyay, A. (2010). Microwave-processed nanocrystalline hydroxyapatite: Simultaneous enhancement of mechanical and biological properties. *Acta biomaterialia, 6*(9): 3782-3790.

Boutinguiza, M., Pou, J., Comesaña, R., Lusquiños, F., De Carlos, A., and León, B. (2012). Biological hydroxyapatite obtained from fish bones. *Materials Science and Engineering: C, 32*(3): 478-486.

Bouyer, E., Gitzhofer, F., and Boulos, M. (2000). Morphological study of hydroxyapatite nanocrystal suspension. *Journal of Materials Science: Materials in Medicine, 11*(8): 523-531.

Brundavanam, S., Poinern, G.E.J., and Fawcett, D. (2015). Synthesis of a hydroxyapatite nanopowder via ultrasound irradiation from calcium hydroxide powders for potential biomedical applications. *Nanoscience and Nanoengineering, 3*(1): 1-7.

Buys, A., Sorrell, C., Brandwood, A., and Milthorpe, B. (1995). Hydroxyapatite sintering characteristics: Correlation with powder morphology bv high-resolution microscopy. *Journal of materials science letters, 14*(10): 744-747.

Bykov, Y., Eremeev, A., Egorov, S., Ivanov, V., Kotov, Y., Khrustov, V., and Sorokin, A. (1999). Sintering of nanostructural titanium oxide using millimeter-wave radiation. *NanoStructured Materials, 12*(1): 115-118.

Cao, J.M., Feng, J., Deng, S.G., Chang, X., Wang, J., Liu, J.S., Lu, P., Lu, H.X., Zheng, M.B., and Zhang, F. (2005). Microwave-assisted solid-state synthesis of hydroxyapatite nanorods at room temperature. *Journal of materials science, 40*(23): 6311-6313.

Cao, W., and Hench, L.L. (1996). Bioactive materials. *Ceramics international, 22*(6): 493-507.

Catros, S., Guillemot, F., Lebraud, E., Chanseau, C., Perez, S., Bareille, R., Amédée, J., and Fricain, J.-C. (2010). Physico-chemical and biological properties of a nano-hydroxyapatite powder synthesized at room temperature. *Irbm, 31*(4): 226-233.

Chai, C.S., Gross, K.A., and Ben-Nissan, B. (1998). Critical ageing of hydroxyapatite sol–gel solutions. *Biomaterials, 19*(24): 2291-2296.

CHAIKINA, M. (1997). Mechanochemical synthesis of phosphates and apatites-new way of preparation of complex materials. *Phosphorus Research Bulletin, 7*(0): 35-38.

Chaki, T., and Wang, P. (1994). Densification and strengthening of silver-reinforced hydroxyapatite-matrix composite prepared by sintering. *Journal of Materials Science: Materials in Medicine, 5*(8): 533-542.

Champion, E. (2013). Sintering of calcium phosphate bioceramics. *Acta biomaterialia, 9*(4): 5855-5875.

Champion, E., Gautier, S., and Bernache-Assollant, D. (1996). Characterization of hot pressed al2o3-platelet reinforced hydroxyapatite composites. *Journal of Materials Science: Materials in Medicine, 7*(2): 125-130.

Chanda, A., Dasgupta, S., Bose, S., and Bandyopadhyay, A. (2009). Microwave sintering of calcium phosphate ceramics. *Materials Science and Engineering: C, 29*(4): 1144-1149.

Chen, B., Zhang, T., Zhang, J., Lin, Q., and Jiang, D. (2008). Microstructure and mechanical properties of hydroxyapatite obtained by gel-casting process. *Ceramics International, 34*(2): 359-364.

Chen, C.-W., Riman, R.E., TenHuisen, K.S., and Brown, K. (2004). Mechanochemical–hydrothermal synthesis of hydroxyapatite from nonionic surfactant emulsion precursors. *Journal of crystal growth, 270*(3): 615-623.

Chen, D., Jiang, C., Sun, H., Feng, B., Lu, X., Weng, J., and Wang, J. (2014). Sintering study of ito using a zno-doped and microwave hybrid sintering approach. *Journal of Asian Ceramic Societies, 2*(1): 57-63.

Chen, F., Huang, P., Zhu, Y.-J., Wu, J., and Cui, D.-X. (2012). Multifunctional eu 3+/gd 3+ dual-doped calcium phosphate vesicle-like nanospheres for sustained drug release and imaging. *Biomaterials, 33*(27): 6447-6455.

Chen, G., and Wang, W. (2007). Role of freeze drying in nanotechnology. *Drying Technology, 25*(1): 29-35.

Chen, I.-W., and Wang, X.-H. (2000). Sintering dense nanocrystalline ceramics without final-stage grain growth. *Nature, 404*(6774): 168-171.

Chen, J., Wang, Y., Chen, X., Ren, L., Lai, C., He, W., and Zhang, Q. (2011). A simple sol-gel technique for synthesis of nanostructured hydroxyapatite, tricalcium phosphate and biphasic powders. *Materials Letters, 65*(12): 1923-1926.

Chen, Q., Zhu, C., and Thouas, G. (2012). Progress and challenges in biomaterials used for bone tissue engineering: Bioactive glasses and elastomeric composites. *Progress in Biomaterials, 1*(1): 1-22. doi: 10.1186/2194-0517-1-2

Cheng, J., Agrawal, D., Roy, R., and Jayan, P. (2000). Continuous microwave sintering of alumina abrasive grits. *Journal of materials processing technology, 108*(1): 26-29.

Chesnaud, A., Bogicevic, C., Karolak, F., Estournès, C., and Dezanneau, G. (2007). Preparation of transparent oxyapatite ceramics by combined use of freeze-drying and spark-plasma sintering. *Chemical Communications*(15): 1550-1552.

Chesnaud, A., Bogicevic, C., Karolak, F., Estournès, C., and Dezanneau, G. (2007). Preparation of transparent oxyapatite ceramics by combined use of freeze-drying and spark-plasma sintering. *Chemical Communications*(15): 1550-1552.

Cho, J.S., and Kang, Y.C. (2008). Nano-sized hydroxyapatite powders prepared by flame spray pyrolysis. *Journal of Alloys and Compounds, 464*(1): 282-287.

Chou, L., Marek, B., and Wagner, W. (1999). Effects of hydroxylapatite coating crystallinity on biosolubility, cell attachment efficiency and proliferation in vitro. *Biomaterials, 20*(10): 977-985.

Chu, C., Xue, X., Zhu, J., and Yin, Z. (2006). In vivo study on biocompatibility and bonding strength of ti/ti–20vol.% ha/ti–40vol.% ha functionally graded biomaterial with bone tissues in the rabbit. *Materials Science and Engineering: A, 429*(1): 18-24.

Chu, M.Y., Rahaman, M.N., Jonghe, L.C., and Brook, R.J. (1991). Effect of heating rate on sintering and coarsening. *Journal of the American Ceramic Society, 74*(6): 1217-1225.

Clark, D.E., and Sutton, W.H. (1996). Microwave processing of materials. *Annual Review of Materials Science, 26*(1): 299-331.

Coreño A, J., Coreño A, O., Cruz R, J., and Rodríguez C, C. (2005). Mechanochemical synthesis of nanocrystalline carbonate-substituted hydroxyapatite. *Optical Materials, 27*(7): 1281-1285.

Cuccu, A., Montinaro, S., Orrù, R., Cao, G., Bellucci, D., Sola, A., and Cannillo, V. (2015). Consolidation of different hydroxyapatite powders by sps: Optimization of the sintering conditions and characterization of the obtained bulk products. *Ceramics International, 41*(1): 725-736.

Darimont, G., Cloots, R., Heinen, E., Seidel, L., and Legrand, R. (2002). In vivo behaviour of hydroxyapatite coatings on titanium implants: A quantitative study in the rabbit. *Biomaterials, 23*(12): 2569-2575.

Das, S., Mukhopadhyay, A., Datta, S., and Basu, D. (2009). Prospects of microwave processing: An overview. *Bulletin of Materials Science, 32*(1): 1-13.

De Groot, K., Geesink, R., Klein, C., and Serekian, P. (1987). Plasma sprayed coatings of hydroxylapatite. *Journal of biomedical materials research, 21*(12): 1375-1381.

De Groot, K., Klein, C., Wolke, J.d., and de Blieck-Hogervorst, J. (1990). Chemistry of calcium phosphate bioceramics. *Handbook of bioactive ceramics, 2*: 3-16.

Decareau, R.V. (1985). Microwaves in the food processing industry. *Food science and technology (USA)*.

Deepa, C., BEGUM, N., and Aravindan, S. (2013). Preparation and antimicrobial observations of zinc doped nanohydroxyapatite. *Наносистемы: физика, химия, математика, 4*(3).

Del Regno, G.E. (2006). Susceptor for hybrid microwave sintering system, hybrid microwave sintering system including same and method for sintering ceramic members using the hybrid microwave sintering system.

Demirskyi, D., Agrawal, D., and Ragulya, A. (2011). Neck growth kinetics during microwave sintering of nickel powder. *Journal of Alloys and Compounds, 509*(5): 1790-1795.

Descamps, M., Boilet, L., Moreau, G., Tricoteaux, A., Lu, J., Leriche, A., Lardot, V., and Cambier, F. (2013). Processing and properties of biphasic calcium phosphates bioceramics obtained by pressureless sintering and hot isostatic pressing. *Journal of the European Ceramic Society, 33*(7): 1263-1270.

Donadel, K., Laranjeira, M., Gonçalves, V.L., Fávere, V.T., De Lima, J.C., and Prates, L.H. (2005). Hydroxyapatites produced by wet-chemical methods. *Journal of the American Ceramic Society, 88*(8): 2230-2235.

Dorantes-Alvarez, L., Barbosa-Cánovas, G.V., and Gutiérrez-López, G. (2000). Blanching of fruits and vegetables using microwaves. *Innovations in food processing*: 149-162.

Doremus, R. (1992). Bioceramics. *Journal of Materials Science, 27*(2): 285-297.

Dorozhkin, S.V. (2009). Calcium orthophosphate cements and concretes. *Materials, 2*(1): 221-291.

Dorozhkin, S.V. (2010). Calcium orthophosphates as bioceramics: State of the art. *Journal of functional biomaterials, 1*(1): 22-107.

Ehsani, N., Sorrell, C., and Ruys, A. (2013). Microwave hybrid processing of hydroxyapatite. *J Biomim Biomater Tissue Eng, 18*(108): 2.

Elliott, J.C., Mackie, P., and Young, R. (1973). Monoclinic hydroxyapatite. *Science, 180*(4090): 1055-1057.

Eshtiagh-Hosseini, H., Housaindokht, M.R., and Chahkandi, M. (2007). Effects of parameters of sol–gel process on the phase evolution of sol–gel-derived hydroxyapatite. *Materials Chemistry and Physics, 106*(2): 310-316.

Faber, K., and Evans, A. (1983). Crack deflection processes—i. Theory. *Acta Metallurgica, 31*(4): 565-576.

Fang, Y., Agrawal, D.K., Roy, D.M., and Roy, R. (1994). Microwave sintering of hydroxyapatite ceramics. *Journal of materials research, 9*(01): 180-187.

Fang, Y., Cheng, J., and Agrawal, D.K. (2004). Effect of powder reactivity on microwave sintering of alumina. *Materials Letters, 58*(3): 498-501.

Fanovich, M., and Lopez, J.P. (1998). Influence of temperature and additives on the microstructure and sintering behaviour of hydroxyapatites with different ca/p ratios. *Journal of Materials Science: Materials in Medicine, 9*(1): 53-60.

Fathi, M., Hanifi, A., and Mortazavi, V. (2008). Preparation and bioactivity evaluation of bone-like hydroxyapatite nanopowder. *Journal of materials processing technology, 202*(1): 536-542.

Fathi, M., and Zahrani, E.M. (2009). Mechanical alloying synthesis and bioactivity evaluation of nanocrystalline fluoridated hydroxyapatite. *Journal of Crystal Growth, 311*(5): 1392-1403.

Feng, P., Wei, P., Shuai, C., and Peng, S. (2014). Characterization of mechanical and biological properties of 3-d scaffolds reinforced with zinc oxide for bone tissue engineering. *PloS one, 9*(1): e87755.

Ferraz, M., Monteiro, F., and Manuel, C. (2004). Hydroxyapatite nanoparticles: A review of preparation methodologies. *Journal of Applied Biomaterials and Biomechanics, 2*(2): 74-80.

Finoli, A., McKeel, D., Gerlach, J., and Nettleship, I. (2010). Phase transformation behaviour of hydroxyapatite foams subject to heat treatmentthis work was presented at the materials science and technology (ms&t'09) conference symposium: Next generation biomaterials, pittsburgh, pa, 25–29 october 2009. *Biomedical Materials, 5*(1): 015004.

Fuentes, G., Hernández, Y., Campos, Y., López, N., Rojas, M., Peón, E., Almirall, A., and Delgado, J. (2008). Composition influence on properties of acrylic composites loaded with synthetic hydroxyapatite. *Latin American applied research, 38*(2): 105.

Gatti, A., Zaffe, D., and Poli, G. (1990). Behaviour of tricalcium phosphate and hydroxyapatite granules in sheep bone defects. *Biomaterials, 11*(7): 513-517.

Gibson, I., Ke, S., Best, S., and Bonfield, W. (2001). Effect of powder characteristics on the sinterability of hydroxyapatite powders. *Journal of Materials Science: Materials in Medicine, 12*(2): 163-171.

Girija, E., Kumar, G.S., Thamizhavel, A., Yokogawa, Y., and Kalkura, S.N. (2012). Role of material processing on the thermal stability and sinterability of nanocrystalline hydroxyapatite. *Powder Technology, 225*: 190-195.

Göller, G., and Oktar, F.N. (2002). Sintering effects on mechanical properties of biologically derived dentine hydroxyapatite. *Materials Letters, 56*(3): 142-147.

Gomes, J.F., Granadeiro, C.C., Silva, M.A., Hoyos, M., Silva, R., and Vieira, T. (2008). An investigation of the synthesis parameters of the reaction of hydroxyapatite precipitation in aqueous media. *International Journal of Chemical Reactor Engineering, 6*(1).

Grant, E., and Halstead, B.J. (1998). Dielectric parameters relevant to microwave dielectric heating. *Chemical Society Reviews, 27*(3): 213-224.

Gross, K., Komarovska, L., and Viksna, A. (2013). Efficient zinc incorporation into hydroxyapatite through crystallization of an amorphous phase could extend the properties of zinc apatites. *Journal of the Australian Ceramic Society Volume, 49*(2): 129-135.

Groza, J., and Dowding, R. (1996). Nanoparticulate materials densification. *Nanostructured materials, 7*(7): 749-768.

Groza, J.R. (2007). Nanocrystalline powder consolidation methods. *Nanostructured Materials: Processing, Properties and Applications*: 173-217.

Gu, Y., Loh, N., Khor, K., Tor, S., and Cheang, P. (2002). Spark plasma sintering of hydroxyapatite powders. *Biomaterials, 23*(1): 37-43.

Gunnewiek, R.F., and Kiminami, R.H. (2014). Effect of heating rate on microwave sintering of nanocrystalline zinc oxide. *Ceramics International, 40*(7): 10667-10675.

Guo, X., and Xiao, P. (2006). Effects of solvents on properties of nanocrystalline hydroxyapatite produced from hydrothermal process. *Journal of the European Ceramic Society, 26*(15): 3383-3391.

Guo, X., Xiao, P., Liu, J., and Shen, Z. (2005). Fabrication of nanostructured hydroxyapatite via hydrothermal synthesis and spark plasma sintering. *Journal of the American Ceramic Society, 88*(4): 1026-1029.

Han, J.-K., Song, H.-Y., Saito, F., and Lee, B.-T. (2006). Synthesis of high purity nano-sized hydroxyapatite powder by microwave-hydrothermal method. *Materials chemistry and physics, 99*(2): 235-239.

Han, Y., Li, S., Wang, X., and Chen, X. (2004). Synthesis and sintering of nanocrystalline hydroxyapatite powders by citric acid sol–gel combustion method. *Materials Research Bulletin, 39*(1): 25-32.

Harabi, A., Belamri, D., Karboua, N., and Mezahi, F.-Z. (2010). Sintering of bioceramics using a modified domestic microwave oven: Natural hydroxyapatite sintering. *Journal of thermal analysis and calorimetry, 104*(1): 383-388.

Hart, J.N., Menzies, D., Cheng, Y.-B., Simon, G.P., and Spiccia, L. (2007). A comparison of microwave and conventional heat treatments of nanocrystalline tio 2. *Solar energy materials and solar cells, 91*(1): 6-16.

Hassan, M.N., Mahmoud, M.M., Link, G., El-Fattah, A.A., and Kandil, S. (2016). Sintering of naturally derived hydroxyapatite using high frequency microwave processing. *Journal of Alloys and Compounds, 682*: 107-114.

Hayek, E., and Stadlmann, W. (1955). Preparation of pure hydroxyapatite for adsorption uses. *Angew. Chem, 67*: 327.

He, J., Peng, Z., Fu, Z., Wang, C., and Fu, X. (2012). Effect of zno doping on microstructural and electrical properties of sno 2–ta 2 o 5 based varistors. *Journal of Alloys and Compounds, 528*: 79-83.

Hench, L.L. (1991). Bioceramics: From concept to clinic. *Journal of the American Ceramic Society, 74*(7): 1487-1510.

Hench, L.L. (1998). Bioceramics. *Journal of the American Ceramic Society, 81*(7): 1705-1728. doi: 10.1111/j.1151-2916.1998.tb02540.x

Hernández-Sierra, J.F., Ruiz, F., Pena, D.C.C., Martínez-Gutiérrez, F., Martínez, A.E., Guillén, A.d.J.P., Tapia-Pérez, H., and Castañón, G.M. (2008). The antimicrobial sensitivity of streptococcus mutans to nanoparticles of silver, zinc oxide, and gold. *Nanomedicine: Nanotechnology, Biology and Medicine, 4*(3): 237-240.

Hing, K.A. (2005). Bioceramic bone graft substitutes: Influence of porosity and chemistry. *International journal of applied ceramic technology, 2*(3): 184-199.

Hino, T., Shimabayashi, S., Ohnishi, N., Fujisaki, M., Mori, H., Watanabe, O., Kawashima, K., and Nagao, K. (2000). Development of a new type nozzle and spray-drier for industrial production of fine powders. *European journal of pharmaceutics and biopharmaceutics, 49*(1): 79-85.

Hoepfner, T.P., and Case, E. (2003). The influence of the microstructure on the hardness of sintered hydroxyapatite. *Ceramics International, 29*(6): 699-706.

Honarmandi, P., Honarmandi, P., Shokuhfar, A., Nasiri-Tabrizi, B., and Ebrahimi-Kahrizsangi, R. (2010). Milling media effects on synthesis, morphology and structural characteristics of single crystal hydroxyapatite nanoparticles. *Advances in Applied Ceramics, 109*(2): 117-122.

Hsieh, M.-F., Perng, L.-H., Chin, T.-S., and Perng, H.-G. (2001). Phase purity of sol–gel-derived hydroxyapatite ceramic. *Biomaterials, 22*(19): 2601-2607.

Hsu, T.-C., and Chiou, J.-S. (2011). Vacuum drying for ultrafine alumina powders. *Drying Technology, 29*(5): 566-572.

Huang, Z., Gotoh, M., and Hirose, Y. (2009). Improving sinterability of ceramics using hybrid microwave heating. *journal of materials processing technology, 209*(5): 2446-2452.

Inthong, S., Tunkasiri, T., Eitssayeam, S., Pengpat, K., and Rujijanagul, G. (2013). Physical properties and bioactivity of nanocrystalline hydroxyapatite synthesized by a co-precipitation route. *Ceramics International, 39*: S533-S536.

Ioiţescu, A., Vlase, G., Vlase, T., Ilia, G., and Doca, N. (2009). Synthesis and characterization of hydroxyapatite obtained from different organic precursors by sol–gel method. *Journal of thermal analysis and calorimetry, 96*(3): 937-942.

Ishikawa, K., Miyamoto, Y., Yuasa, T., Ito, A., Nagayama, M., and Suzuki, K. (2002). Fabrication of zn containing apatite cement and its initial evaluation using human osteoblastic cells. *Biomaterials, 23*(2): 423-428.

Iskandar, F., Gradon, L., and Okuyama, K. (2003). Control of the morphology of nanostructured particles prepared by the spray drying of a nanoparticle sol. *Journal of Colloid and Interface Science, 265*(2): 296-303.

Itatani, K., Tsugawa, T., Umeda, T., Musha, Y., Davies, I.J., and Koda, S. (2010). Preparation of submicrometer-sized porous spherical hydroxyapatite agglomerates by ultrasonic spray pyrolysis technique. *Journal of the Ceramic Society of Japan, 118*(1378): 462-466.

Ito, A., Ojima, K., Naito, H., Ichinose, N., and Tateishi, T. (2000). Preparation, solubility, and cytocompatibility of zinc-releasing calcium phosphate ceramics. *Journal of biomedical materials research, 50*(2): 178-183.

Jallot, E., Nedelec, J.-M., Grimault, A.S., Chassot, E., Grandjean-Laquerriere, A., Laquerriere, P., and Laurent-Maquin, D. (2005). Stem and edxs characterisation of physico-chemical reactions at the periphery of sol–gel derived zn-substituted hydroxyapatites during interactions with biological fluids. *Colloids and surfaces B: Biointerfaces, 42*(3): 205-210.

Jamuna-Thevi, K., Zakaria, F., Othman, R., and Muhamad, S. (2009). Development of macroporous calcium phosphate scaffold processed via microwave rapid drying. *Materials Science and Engineering: C, 29*(5): 1732-1740.

Jang, B.-K., Enoki, M., Kishi, T., Lee, S.-H., and Oh, H.-K. (1996). Fracture behaviour and toughening of alumina-based composites fabricated by microstructural control *Fracture mechanics of ceramics* (pp. 371-382): Springer.

Jarcho, M., Bolen, C., Thomas, M., Bobick, J., Kay, J., and Doremus, R.H. (1976). Hydroxylapatite synthesis and characterization in dense polycrystalline form. *Journal of Materials Science, 11*(11): 2027-2035.

Jarudilokkul, S., Tanthapanichakoon, W., and Boonamnuayvittaya, V. (2007). Synthesis of hydroxyapatite nanoparticles using an emulsion liquid membrane system. *Colloids and Surfaces A: Physicochemical and Engineering Aspects, 296*(1): 149-153.

Jayaswal, G.P., Dange, S., and Khalikar, A. (2010). Bioceramic in dental implants: A review. *The Journal of Indian Prosthodontic Society, 10*(1): 8-12.

Jha, L., Best, S., Knowles, J., Rehman, I., D SANTOS, J., and Bonfield, W. (1997). Preparation and characterization of fluoride-substituted apatites. *Journal of materials science: materials in Medicine, 8*(4): 185-191.

Jha, L., Best, S., Knowles, J., Rehman, I., D SANTOS, J., and Bonfield, W. (1997). Preparation and characterization of fluoride-substituted apatites. *Journal of materials science: materials in Medicine, 8*(4): 185-191.

Jillavenkatesa, A., and Condrate Sr, R. (1998). Sol–gel processing of hydroxyapatite. *Journal of materials science, 33*(16): 4111-4119.

Kamalanathan, P., Ramesh, S., Bang, L., Niakan, A., Tan, C., Purbolaksono, J., Chandran, H., and Teng, W. (2014). Synthesis and sintering of hydroxyapatite derived from eggshells as a calcium precursor. *Ceramics International, 40*(10): 16349-16359.

Katti, K.S. (2004). Biomaterials in total joint replacement. *Colloids and Surfaces B: Biointerfaces, 39*(3): 133-142.

Kawamura, H., Ito, A., Miyakawa, S., Layrolle, P., Ojima, K., Ichinose, N., and Tateishi, T. (2000). Stimulatory effect of zinc-releasing calcium phosphate implant on bone formation in rabbit femora. *Journal of biomedical materials research, 50*(2): 184-190.

Kieswetter, K., Bauer, T., Brown, S., Van Lente, F., and Merritt, K. (1994). Characterization of calcium phosphate powders by esca and edxa. *Biomaterials, 15*(3): 183-188.

Kijima, T., and Tsutsumi, M. (1979). Preparation and thermal properties of dense polycrystalline oxyhydroxyapatite. *Journal of the American Ceramic Society, 62*(9-10): 455-460.

Kim, H.-M., Himeno, T., Kokubo, T., and Nakamura, T. (2005). Process and kinetics of bonelike apatite formation on sintered hydroxyapatite in a simulated body fluid. *Biomaterials, 26*(21): 4366-4373.

Kim, H.W., Kong, Y.M., Koh, Y.H., Kim, H.E., Kim, H.M., and Ko, J.S. (2003). Pressureless sintering and mechanical and biological properties of fluor-hydroxyapatite composites with zirconia. *Journal of the American Ceramic Society, 86*(12): 2019-2026.

Kim, I.-S., and Kumta, P.N. (2004). Sol–gel synthesis and characterization of nanostructured hydroxyapatite powder. *Materials Science and Engineering: B, 111*(2): 232-236.

Kong, L., Ma, J., and Boey, F. (2002). Nanosized hydroxyapatite powders derived from coprecipitation process. *Journal of materials science, 37*(6): 1131-1134.

Kothapalli, C., Wei, M., Vasiliev, A., and Shaw, M. (2004). Influence of temperature and concentration on the sintering behavior and mechanical properties of hydroxyapatite. *Acta Materialia, 52*(19): 5655-5663.

Koutsopoulos, S. (2002). Synthesis and characterization of hydroxyapatite crystals: A review study on the analytical methods. *Journal of biomedical materials research, 62*(4): 600-612.

Kozlova, D., Chernousova, S., Knuschke, T., Buer, J., Westendorf, A.M., and Epple, M. (2012). Cell targeting by antibody-functionalized calcium phosphate nanoparticles. *Journal of Materials Chemistry, 22*(2): 396-404.

Kramer, E., Zilm, M., and Wei, M. (2013). A comparative study of the sintering behavior of pure and iron-substituted hydroxyapatite. *Bioceramics Development and Applications, 2013*.

Kumar, R., Prakash, K., Cheang, P., and Khor, K. (2004). Temperature driven morphological changes of chemically precipitated hydroxyapatite nanoparticles. *Langmuir, 20*(13): 5196-5200.

Kumta, P.N., Sfeir, C., Lee, D.-H., Olton, D., and Choi, D. (2005). Nanostructured calcium phosphates for biomedical applications: Novel synthesis and characterization. *Acta Biomaterialia, 1*(1): 65-83.

Kurapova, O.Y., Konakov, V., Golubev, S., Ushakov, V., and Archakov, I.Y. (2012). Cryochemical methods for manufacturing nanosized ceramics and ceramic precursor powders with low agglomeration degree: A review. *Rev. Adv. Mater. Sci, 32*: 112-132.

Kutty, M.G., Bhaduri, S.B., Zhou, H., and Yaghoubi, A. (2015). In situ measurement of shrinkage and temperature profile in microwave-and conventionally-sintered hydroxyapatite bioceramic. *Materials Letters, 161*: 375-378.

Kutty, M.G., and Singh, R. (2001). The effects of zirconia additions on the sintering behaviour and phase stability of hydroxyapatite ceramics. *Pertanika Journal of Science & Technology, 9*(2): 229-238.

Kutz, M. (2002). Handbook of materials selection.

Landi, E., Tampieri, A., Celotti, G., and Sprio, S. (2000). Densification behaviour and mechanisms of synthetic hydroxyapatites. *Journal of the European Ceramic Society, 20*(14): 2377-2387.

Lasri, J., Ramesh, P.D., and Schächter, L. (2000). Energy conversion during microwave sintering of a multiphase ceramic surrounded by a susceptor. *Journal of the American Ceramic Society, 83*(6): 1465-1468.

Lau, E. (1997). *Osteoporosis in asia: Crossing the frontiers*: World Scientific.

Layrolle, P., Ito, A., and Tateishi, T. (1998). Sol-gel synthesis of amorphous calcium phosphate and sintering into microporous hydroxyapatite bioceramics. *Journal of the American Ceramic Society, 81*(6): 1421-1428.

Lazić, S., Zec, S., Miljević, N., and Milonjić, S. (2001). The effect of temperature on the properties of hydroxyapatite precipitated from calcium hydroxide and phosphoric acid. *Thermochimica Acta, 374*(1): 13-22.

Lefeuvre, S. (1981). Microwave drying of porous materials. *Physics in Technology, 12*(4): 155.

LeGeros, R.Z., and LeGeros, J.P. (1993). Dense hydroxyapatite. *Advanced series in ceramics, 1*: 139-180.

Lemons, J.E. (1996). Ceramics: Past, present, and future. *Bone, 19*(1): S121-S128.

Leparoux, S., Vaucher, S., and Beffort, O. (2003). Assessment of microwave heating for sintering of al/sic and for in-situ synthesis of tic. *Advanced Engineering Materials, 5*(6): 449-453.

Li, J., Chen, Y.-C., Tseng, Y.-C., Mozumdar, S., and Huang, L. (2010). Biodegradable calcium phosphate nanoparticle with lipid coating for systemic sirna delivery. *Journal of controlled release, 142*(3): 416-421.

Li, P., and de Groot, K. (1994). Better bioactive ceramics through sol-gel process. *Journal of Sol-Gel Science and Technology, 2*(1-3): 797-801.

Li, Z., Wang, P., and Wu, Z. (2005). Preparation of nanosized hydroxyapatite particles at low temperatures. *Journal of materials science, 40*(24): 6589-6591.

Lidström, P., Tierney, J., Wathey, B., and Westman, J. (2001). Microwave assisted organic synthesis—a review. *Tetrahedron, 57*(45): 9225-9283.

Lin, K., Chang, J., Cheng, R., and Ruan, M. (2007). Hydrothermal microemulsion synthesis of stoichiometric single crystal hydroxyapatite nanorods with mono-dispersion and narrow-size distribution. *Materials Letters, 61*(8): 1683-1687.

Lin, K., Chen, L., and Chang, J. (2012). Fabrication of dense hydroxyapatite nanobioceramics with enhanced mechanical properties via two-step sintering process. *International Journal of Applied Ceramic Technology, 9*(3): 479-485. doi: 10.1111/j.1744-7402.2011.02654.x

Lin, K., Liu, P., Wei, L., Zou, Z., Zhang, W., Qian, Y., Shen, Y., and Chang, J. (2013). Strontium substituted hydroxyapatite porous microspheres: Surfactant-free hydrothermal synthesis, enhanced biological response and sustained drug release. *Chemical engineering journal, 222*: 49-59.

Liu, D.-M., Troczynski, T., and Tseng, W.J. (2001). Water-based sol–gel synthesis of hydroxyapatite: Process development. *Biomaterials, 22*(13): 1721-1730.

Liu, D.-M., Yang, Q., Troczynski, T., and Tseng, W.J. (2002). Structural evolution of sol–gel-derived hydroxyapatite. *Biomaterials, 23*(7): 1679-1687.

Liu, H., Chin, T., Lai, L., Chiu, S., Chung, K., Chang, C., and Lui, M. (1997). Hydroxyapatite synthesized by a simplified hydrothermal method. *Ceramics International, 23*(1): 19-25.

Liu, H., Yazici, H., Ergun, C., Webster, T.J., and Bermek, H. (2008). An in vitro evaluation of the ca/p ratio for the cytocompatibility of nano-to-micron particulate calcium phosphates for bone regeneration. *Acta Biomaterialia, 4*(5): 1472-1479.

Liu, H.-S., Chin, T.S., Lai, L., Chiu, S., Chung, K., Chang, C., and Lui, M. (1997). Hydroxyapatite synthesized by a simplified hydrothermal method. *Ceramics International, 23*(1): 19-25.

Liu, Y., Schoenaers, J., De Groot, K., De Wijn, J., and Schepers, E. (2000). Bone healing in porous implants: A histological and histometrical comparative study on sheep. *Journal of Materials Science: Materials in Medicine, 11*(11): 711-717.

Liu, Y., Wang, X.-P., Zhou, D.-F., Ning, D.-Z., Zhang, G.-M., and Meng, J. (2014). Effect of zno addition on the sintering and electrical properties of ceria-based electrolyte materials. *Advances in Energy Engineering, 2*: 61-66.

Loo, S.C.J., Siew, Y.E., Ho, S., Boey, F.Y.C., and Ma, J. (2008). Synthesis and hydrothermal treatment of nanostructured hydroxyapatite of controllable sizes. *Journal of Materials Science: Materials in Medicine, 19*(3): 1389-1397.

Loty, C., Sautier, J.M., Boulekbache, H., Kokubo, T., Kim, H.M., and Forest, N. (2000). In vitro bone formation on a bone-like apatite layer prepared by a biomimetic process on a bioactive glass–ceramic. *Journal of biomedical materials research, 49*(4): 423-434.

Lu, H., Qu, Z., and Zhou, Y. (1998). Preparation and mechanical properties of dense polycrystalline hydroxyapatite through freeze-drying. *Journal of Materials Science: Materials in Medicine, 9*(10): 583-587.

Lu, K. (2008). Sintering of nanoceramics. *International Materials Reviews, 53*(1): 21-38.

Luo, Z., Cui, F., and Li, W. (1999). Low-temperature crystallization of calcium phosphate coatings synthesized by ion-beam-assisted deposition. *Journal of biomedical materials research, 46*(1): 80-86.

Manafi, S., and Rahimipour, M.R. (2011). Synthesis of nanocrystalline hydroxyapatite nanorods via hydrothermal conditions. *Chemical Engineering & Technology, 34*(6): 972-976.

Mandal, B.B., and Kundu, S.C. (2009). Osteogenic and adipogenic differentiation of rat bone marrow cells on non-mulberry and mulberry silk gland fibroin 3d scaffolds. *Biomaterials, 30*(28): 5019-5030.

Mangkonsu, C., Kunio, I., Bunhan, L., Otman, R., and Noor, A.-F.M. (2016). The effect of microwave sintering on the microstructure and properties of calcium phosphate ceramic. *Procedia Chemistry, 19*: 498-504.

Manso, M., Jimenez, C., Morant, C., Herrero, P., and Martınez-Duart, J. (2000). Electrodeposition of hydroxyapatite coatings in basic conditions. *Biomaterials, 21*(17): 1755-1761.

Markovic, M., Fowler, B.O., and Tung, M.S. (2004). Preparation and comprehensive characterization of a calcium hydroxyapatite reference material. *Journal of Research of the National Institute of Standards and Technology, 109*(6): 553-568.

Mazaheri, M., Haghighatzadeh, M., Zahedi, A., and Sadrnezhaad, S. (2009). Effect of a novel sintering process on mechanical properties of hydroxyapatite ceramics. *Journal of alloys and compounds, 471*(1): 180-184.

Mazaheri, M., Simchi, A., and Golestani-Fard, F. (2008). Densification and grain growth of nanocrystalline 3y-tzp during two-step sintering. *Journal of the European Ceramic Society, 28*(15): 2933-2939.

Mendelson, M.I. (1969). Average grain size in polycrystalline ceramics. *Journal of the American Ceramic Society, 52*(8): 443-446.

Mobasherpour, I., Heshajin, M.S., Kazemzadeh, A., and Zakeri, M. (2007). Synthesis of nanocrystalline hydroxyapatite by using precipitation method. *Journal of Alloys and Compounds, 430*(1): 330-333.

Mochales, C., El Briak-BenAbdeslam, H., Ginebra, M.P., Terol, A., Planell, J.A., and Boudeville, P. (2004). Dry mechanochemical synthesis of hydroxyapatites from dcpd and cao: Influence of instrumental parameters on the reaction kinetics. *Biomaterials, 25*(7): 1151-1158.

Moller, M., and Linn, H. (2001). Microwave drying of refractory materials. *CN Refractories, 5*: 79-80.

Monma, H., and Kamiya, T. (1987). Preparation of hydroxyapatite by the hydrolysis of brushite. *Journal of materials science, 22*(12): 4247-4250.

Monmaturapoj, N. (2008). Nano-size hydroxyapatite powders preparation by wet-chemical precipitation route. *Journal of Metals, Materials and Minerals, 18*(1): 15-20.

Monmaturapoj, N., and Yatongchai, C. (2010). Effect of sintering on microstructure and properties of hydroxyapatite produced by different synthesizing methods. *Journal of Metals, Materials and Minerals, 20*(2): 53-61.

Moonga, B.S., and Dempster, D.W. (1995). Zinc is a potent inhibitor of osteoclastic bone resorption in vitro. *Journal of Bone and Mineral Research, 10*(3): 453-457.

Morrison, C.J., Gagnon, P., and Cramer, S.M. (2011). Purification of monomeric mab from associated aggregates using selective desorption chromatography in hydroxyapatite systems. *Biotechnology and bioengineering, 108*(4): 813-821.

Morrissey, R., Rodr ǵuez-Lorenzo, L.M., and Gross, K.A. (2005). Influence of ferrous iron incorporation on the structure of hydroxyapatite. *Journal of Materials Science: Materials in Medicine, 16*(5): 387-392. doi: 10.1007/s10856-005-6976-5

Mostafa, N.Y. (2005). Characterization, thermal stability and sintering of hydroxyapatite powders prepared by different routes. *Materials chemistry and physics, 94*(2): 333-341.

Mouzon, J., Lindbäck, T., and Odén, M. (2008). Influence of agglomeration on the transparency of yttria ceramics. *Journal of the American Ceramic Society, 91*(10): 3380-3387.

Mungu á, N., V ázquez, C.G., and Barba, C.P. (2005). Stoichiometric hydroxyapatite obtained by precipitation and sol gel processes. *Revista mexicana de fisica, 51*(3): 284-293.

Muralithran, G., and Ramesh, S. (2000). The effects of sintering temperature on the properties of hydroxyapatite. *Ceramics International, 26*(2): 221-230.

Murtaza, Q., Stokes, J., and Ardhaoui, M. (2012). Experimental analysis of spray dryer used in hydroxyapatite thermal spray powder. *Journal of thermal spray technology, 21*(5): 963-974.

Murugan, R., and Ramakrishna, S. (2005). Aqueous mediated synthesis of bioresorbable nanocrystalline hydroxyapatite. *Journal of Crystal Growth, 274*(1): 209-213.

Myoui, A., Tamai, N., Nishikawa, M., Yoshikawa, H., Araki, N., Nakase, T., and Akita, A. (2003). Three-dimensionally engineered hydroxyapatite ceramics with interconnected pores as a bone substitute and tissue engineering scaffold. *Biomater Orthop, 13*: 287-300.

Nasiri-Tabrizi, B., Honarmandi, P., Ebrahimi-Kahrizsangi, R., and Honarmandi, P. (2009). Synthesis of nanosize single-crystal hydroxyapatite via mechanochemical method. *Materials Letters, 63*(5): 543-546.

Nath, S., Basu, B., and Sinha, A. (2006). A comparative study of conventional sintering with microwave sintering of hydroxyapatite synthesized by chemical route. *Trends in Biomaterials & Artificial Organs, 19*(2): 93-98.

Nejati, E., Firouzdor, V., Eslaminejad, M., and Bagheri, F. (2009). Needle-like nano hydroxyapatite/poly (l-lactide acid) composite scaffold for bone tissue engineering application. *Materials Science and Engineering: C, 29*(3): 942-949.

Niakan, A., Ramesh, S., Ganesan, P., Tan, C., Purbolaksono, J., Chandran, H., and Teng, W. (2015). Sintering behaviour of natural porous hydroxyapatite derived from bovine bone. *Ceramics International, 41*(2): 3024-3029.

Niihara, K., Morena, R., and Hasselman, D. (1982). Evaluation ofk ic of brittle solids by the indentation method with low crack-to-indent ratios. *Journal of Materials Science Letters, 1*(1): 13-16.

Nihara, K. (1985). Indentation microfracture of ceramics- its application and problems. *CERAM. JAP. Ceram. Jap., 20*(1): 12.

Nilsson, M., Wang, J.-S., Wielanek, L., Tanner, K., and Lidgren, L. (2004). Biodegradation and biocompatability of a calcium sulphate-hydroxyapatite bone substitute. *Bone & Joint Journal, 86*(1): 120-125.

Norhidayu, D., Sopyan, I., and Ramesh, S. (2008). *Development of zinc doped hydroxyapatite for bone implant applications.* Paper presented at the International Conference on Construction and Building Technology.

Oghbaei, M., and Mirzaee, O. (2010). Microwave versus conventional sintering: A review of fundamentals, advantages and applications. *Journal of Alloys and Compounds, 494*(1): 175-189.

Oguchi, H., Ishikawa, K., Mizoue, K., Seto, K., and Eguchi, G. (1995). Long-term histological evaluation of hydroxyapatite ceramics in humans. *Biomaterials, 16*(1): 33-38.

Oh, S., Oh, N., Appleford, M., and Ong, J.L. (2006). Bioceramics for tissue engineering applications—a review. *Am J Biochem Biotechnol, 2*(2): 49-56.

Okabayashi, R., Nakamura, M., Okabayashi, T., Tanaka, Y., Nagai, A., and Yamashita, K. (2009). Efficacy of polarized hydroxyapatite and silk fibroin composite dressing gel on epidermal recovery from full-thickness skin wounds. *Journal of Biomedical Materials Research Part B: Applied Biomaterials, 90*(2): 641-646.

Okamoto, M., Dohi, Y., Ohgushi, H., Shimaoka, H., Ikeuchi, M., Matsushima, A., Yonemasu, K., and Hosoi, H. (2006). Influence of the porosity of hydroxyapatite ceramics on in vitro and in vivo bone formation by cultured rat bone marrow stromal cells. *Journal of materials science: Materials in medicine, 17*(4): 327-336.

Oktar, F.N., Agathopoulos, S., Ozyegin, L.S., Gunduz, O., Demirkol, N., Bozkurt, Y., and Salman, S. (2007). Mechanical properties of bovine hydroxyapatite (bha) composites doped with sio2, mgo, al2o3, and zro2. *Journal of Materials Science: Materials in Medicine, 18*(11): 2137-2143.

Okumura, M., Ohgushi, H., and Tamai, S. (1991). Bonding osteogenesis in coralline hydroxyapatite combined with bone marrow cells. *Biomaterials, 12*(4): 411-416.

Orefice, R.L., Hench, L.L., and Brennan, A.B. (2000). In vitro bioactivity of polymer matrices reinforced with a bioactive glass phase. *Journal of the Brazilian Chemical Society, 11*(1): 78-85.

Orlovskii, V., Komlev, V., and Barinov, S. (2002). Hydroxyapatite and hydroxyapatite-based ceramics. *Inorganic Materials, 38*(10): 973-984.

Osaka, A., Miura, Y., Takeuchi, K., Asada, M., and Takahashi, K. (1991). Calcium apatite prepared from calcium hydroxide and orthophosphoric acid. *Journal of Materials Science: Materials in Medicine, 2*(1): 51-55.

Otsuka, M., Matsuda, Y., Hsu, J., Fox, J.L., and Higuchi, W.I. (1994). Mechanochemical synthesis of bioactive material: Effect of environmental conditions on the phase transformation of calcium phosphates during grinding. *Bio-medical materials and engineering, 4*(5): 357-362.

Pang, Y., and Bao, X. (2003). Influence of temperature, ripening time and calcination on the morphology and crystallinity of hydroxyapatite nanoparticles. *Journal of the European Ceramic Society, 23*(10): 1697-1704.

Patel, N., Gibson, I., Ke, S., Best, S., and Bonfield, W. (2001). Calcining influence on the powder properties of hydroxyapatite. *Journal of Materials Science: Materials in Medicine, 12*(2): 181-188.

Pattanayak, D.K., Dash, R., Prasad, R., Rao, B., and Mohan, T.R. (2007). Synthesis and sintered properties evaluation of calcium phosphate ceramics. *Materials Science and Engineering: C, 27*(4): 684-690.

Pham, T.T.T., Nguyen, T.P., Pham, T.N., Vu, T.P., Thai, H., and Dinh, T.M.T. (2013). Impact of physical and chemical parameters on the hydroxyapatite nanopowder synthesized by chemical precipitation method. *Advances in Natural Sciences: Nanoscience and Nanotechnology, 4*(3): 035014.

Pramanik, S., Agarwal, A.K., and Rai, K. (2005). Development of high strength hydroxyapatite for hard tissue replacement. *Trends in Biomaterials and Artificial Organs, 19*(1): 46-51.

Pramanik, S., Agarwal, A.K., Rai, K., and Garg, A. (2007). Development of high strength hydroxyapatite by solid-state-sintering process. *Ceramics International, 33*(3): 419-426.

Prasad, S.E. (1990). A review of: "Introduction to the principles of ceramic processing" james s. Reed john wiley & sons, new york, ny 485 pages, hardcover, 1988. *Materials and Manufacturing Processes, 5*(1): 133-134. doi: 10.1080/10426919008953237

Pratihar, S.K., Garg, M., Mehra, S., and Bhattacharyya, S. (2006). Phase evolution and sintering kinetics of hydroxyapatite synthesized by solution combustion technique. *Journal of Materials Science: Materials in Medicine, 17*(6): 501-507.

Pretto, M., Costa, A.L., Landi, E., Tampieri, A., and Galassi, C. (2003). Dispersing behavior of hydroxyapatite powders produced by wet-chemical synthesis. *Journal of the American Ceramic Society, 86*(9): 1534-1539.

Prokopiev, O., and Sevostianov, I. (2006). Dependence of the mechanical properties of sintered hydroxyapatite on the sintering temperature. *Materials Science and Engineering: A, 431*(1): 218-227.

Pushpakanth, S., Srinivasan, B., Sreedhar, B., and Sastry, T. (2008). An in situ approach to prepare nanorods of titania–hydroxyapatite (tio 2–hap) nanocomposite by microwave hydrothermal technique. *Materials Chemistry and Physics, 107*(2): 492-498.

Qi, Y., Anlage, S.M., Zheng, H., and Ramesh, R. (2007). Local dielectric measurements of batio 3–cofe 2 o 4 nanocomposites through microwave microscopy. *Journal of materials research, 22*(05): 1193-1199.

Rajabi-Zamani, A., Behnamghader, A., and Kazemzadeh, A. (2008). Synthesis of nanocrystalline carbonated hydroxyapatite powder via nonalkoxide sol–gel method. *Materials Science and Engineering: C*, *28*(8): 1326-1329.

Ramesh, S. (2004). A method for manufacturing hydroxyapatite bioceramic. *Malaysia Patent*.

Ramesh, S., Aw, K., Tolouei, R., Amiriyan, M., Tan, C., Hamdi, M., Purbolaksono, J., Hassan, M., and Teng, W. (2013). Sintering properties of hydroxyapatite powders prepared using different methods. *Ceramics International*, *39*(1): 111-119.

Ramesh, S., Natasha, A., Tan, C., Bang, L., Ching, C., and Chandran, H. (2016). Direct conversion of eggshell to hydroxyapatite ceramic by a sintering method. *Ceramics International*, *42*(6): 7824-7829.

Ramesh, S., Tan, C., Bhaduri, S., Teng, W., and Sopyan, I. (2008). Densification behaviour of nanocrystalline hydroxyapatite bioceramics. *Journal of materials processing technology*, *206*(1): 221-230.

Ramesh, S., Tan, C., Bhaduri, S., and Teng, W. (2007a). Rapid densification of nanocrystalline hydroxyapatite for biomedical applications. *Ceramics international*, *33*(7): 1363-1367.

Ramesh, S., Tan, C., Peralta, C., and Teng, W. (2007b). The effect of manganese oxide on the sinterability of hydroxyapatite. *Science and Technology of Advanced materials*, *8*(4): 257-263.

Ramesh, S., Tan, C.Y., Yeo, W., Tolouei, R., Amiriyan, M., Sopyan, I., and Teng, W.D. (2011). Effects of bismuth oxide on the sinterability of hydroxyapatite. *Ceramics International*, *37*(2): 599-606.

Rao, R.R., and Kannan, T. (1999). Synthesis and sintering of hydroxyapatite in presence of oxide additives. *Transactions of the Indian Ceramic Society*, *58*(3): 64-68.

Rapacz-Kmita, A., Paluszkiewicz, C., Ślósarczyk, A., and Paszkiewicz, Z. (2005). Ftir and xrd investigations on the thermal stability of hydroxyapatite during hot pressing and pressureless sintering processes. *Journal of molecular structure*, *744*: 653-656.

Raynaud, S., Champion, E., Bernache-Assollant, D., and Thomas, P. (2002). Calcium phosphate apatites with variable ca/p atomic ratio i. Synthesis, characterisation and thermal stability of powders. *Biomaterials*, *23*(4): 1065-1072.

Reeds, J. (1988). Introduction of the principles of ceramic processing.

Rhee, S.-H. (2002). Synthesis of hydroxyapatite via mechanochemical treatment. *Biomaterials*, *23*(4): 1147-1152.

Rodríguez, J.J., Barbosa-Cánovas, G.V., Gutiérrez-López, G.F., Dorantes-Álvarez, L., Yeom, H.W., and Zhang, Q.H. (2003). An update on some key alternative food processing technologies: Microwave, pulsed electric field, high hydrostatic

pressure, irradiation and ultrasound. *Food science and food biotechnology*: 279-312.

Rodr ǵuez-Lorenzo, L.M., Vallet-Reg ί M., Ferreira, J.M.F., Ginebra, M.P., Aparicio, C., and Planell, J.A. (2002). Hydroxyapatite ceramic bodies with tailored mechanical properties for different applications. *Journal of Biomedical Materials Research, 60*(1): 159-166. doi: 10.1002/jbm.1286

Rodríguez-Ruiz, I., Delgado-López, J.M., Durán-Olivencia, M.A., Iafisco, M., Tampieri, A., Colangelo, D., Prat, M., and Gómez-Morales, J. (2013). Ph-responsive delivery of doxorubicin from citrate–apatite nanocrystals with tailored carbonate content. *Langmuir, 29*(26): 8213-8221.

Royer, A., Viguie, J.C., Heughebaert, M., and Heughebaert, J.C. (1993). Stoichiometry of hydroxyapatite: Influence on the flexural strength. *Journal of Materials Science: Materials in Medicine, 4*(1): 76-82. doi: 10.1007/BF00122982

Ruys, A., Brandwood, A., Milthorpe, B., Dickson, M., Zeigler, K., and Sorrell, C. (1995). The effects of sintering atmosphere on the chemical compatibility of hydroxyapatite and particulate additives at 1200 c. *Journal of materials science: materials in medicine, 6*(5): 297-301.

Ruys, A., Wei, M., Sorrell, C., Dickson, M., Brandwood, A., and Milthorpe, B. (1995). Sintering effects on the strength of hydroxyapatite. *Biomaterials, 16*(5): 409-415.

Sadat-Shojai, M., Khorasani, M.-T., Dinpanah-Khoshdargi, E., and Jamshidi, A. (2013). Synthesis methods for nanosized hydroxyapatite with diverse structures. *Acta biomaterialia, 9*(8): 7591-7621.

Saeri, M., Afshar, A., Ghorbani, M., Ehsani, N., and Sorrell, C. (2003). The wet precipitation process of hydroxyapatite. *Materials Letters, 57*(24): 4064-4069.

Saiz, E., Gremillard, L., Menendez, G., Miranda, P., Gryn, K., and Tomsia, A.P. (2007). Preparation of porous hydroxyapatite scaffolds. *Materials Science and Engineering: C, 27*(3): 546-550.

Salma, K., Berzina-Cimdina, L., and Borodajenko, N. (2010). Calcium phosphate bioceramics prepared from wet chemically precipitated powders. *Processing and Application of Ceramics, 4*(1): 45-51.

Saluja, V., Amorij, J., Kapteyn, J., de Boer, A., Frijlink, H., and Hinrichs, W. (2010). A comparison between spray drying and spray freeze drying to produce an influenza subunit vaccine powder for inhalation. *Journal of Controlled Release, 144*(2): 127-133.

Samuel, L.K.L., Tan, C.Y., Singh, R., Yap, B., Tolouei, R., and Amiriyan, M. (2012). Effects of ramp rates with short holding time on the sinterability of hydroxyapatite. *Advanced Materials Research, 545*: 229-234.

Sanosh, K., Chu, M.-C., Balakrishnan, A., Kim, T., and Cho, S.-J. (2010). Pressureless sintering of nanocrystalline hydroxyapatite at different temperatures. *Metals and Materials International, 16*(4): 605-611.

Santhosh, S., and Prabu, S.B. (2012). Characterization of nano-hydroxyapatite synthesized from sea shells through wet chemical method. *International Journal of Nanoscience, 11*(05): 1250031.

Santhosh, S., and Prabu, S.B. (2013). Thermal stability of nano hydroxyapatite synthesized from sea shells through wet chemical synthesis. *Materials Letters, 97*: 121-124.

Santos, M.H., Oliveira, M.d., Souza, L.P.d.F., Mansur, H.S., and Vasconcelos, W.L. (2004). Synthesis control and characterization of hydroxyapatite prepared by wet precipitation process. *Materials Research, 7*(4): 625-630.

Sasikumar, S., and Vijayaraghavan, R. (2010). Synthesis and characterization of bioceramic calcium phosphates by rapid combustion synthesis. *Journal of Materials Science & Technology, 26*(12): 1114-1118.

Satapathy, L. (1997). Cold isostatic pressing of advanced ceramics. *Interceram, 46*(1): 37-40.

Savary, E., Marinel, S., Colder, H., Harnois, C., Lefevre, F., and Retoux, R. (2011). Microwave sintering of nano-sized zno synthesized by a liquid route. *Powder Technology, 208*(2): 521-525.

Savary, E., Marinel, S., Colder, H., Harnois, C., Lefevre, F., and Retoux, R. (2011). Microwave sintering of nano-sized zno synthesized by a liquid route. *Powder technology, 208*(2): 521-525.

Shih, W.-J., Chen, Y.-F., Wang, M.-C., and Hon, M.-H. (2004). Crystal growth and morphology of the nano-sized hydroxyapatite powders synthesized from cahpo 4 · 2h 2 o and caco 3 by hydrolysis method. *Journal of crystal growth, 270*(1): 211-218.

Shih, W.-J., Wang, J.-W., Wang, M.-C., and Hon, M.-H. (2006). A study on the phase transformation of the nanosized hydroxyapatite synthesized by hydrolysis using in situ high temperature x-ray diffraction. *Materials Science and Engineering: C, 26*(8): 1434-1438.

Shirai, T., Yasuoka, M., Hotta, Y., and Watari, K. (2006). Rapid microwave drying for slip cast bodies. *Nippon seramikkusu kyokai gakujutsu ronbunshi, 114*(2): 217-219.

Shirkhanzadeh, M. (1994). X-ray diffraction and fourier transform infrared analysis of nanophase apatite coatings prepared by electrocrystallization. *Nanostructured materials, 4*(6): 677-684.

Shlyakhtin, O., Oh, Y.-J., and Tretyakov, Y.D. (2000). Preparation of dense la 0.7 ca 0.3 mno 3 ceramics from freeze-dried precursors. *Journal of the European Ceramic Society, 20*(12): 2047-2054.

Shyju, D. (2010). Effect of microwave drying in improving granule characteristics in tablets.

Siddharthan, A., Seshadri, S., and Kumar, T.S. (2006). Influence of microwave power on nanosized hydroxyapatite particles. *Scripta materialia, 55*(2): 175-178.

Silva, C., Pinheiro, A., De Oliveira, R., Goes, J., Aranha, N., De Oliveira, L., and Sombra, A. (2004). Properties and in vivo investigation of nanocrystalline hydroxyapatite obtained by mechanical alloying. *Materials Science and Engineering: C, 24*(4): 549-554.

Silva, C., Pinheiro, A., Miranda, M., Góes, J., and Sombra, A. (2003). Structural properties of hydroxyapatite obtained by mechanosynthesis. *Solid State Sciences, 5*(4): 553-558.

Singh, S., Gupta, D., Jain, V., and Sharma, A.K. (2015). Microwave processing of materials and applications in manufacturing industries: A review. *Materials and Manufacturing Processes, 30*(1): 1-29.

Sinha, A., Ingle, A., Munim, K., Vaidya, S., Sharma, B., and Bhisey, A. (2001). Development of calcium phosphate based bioceramics. *Bulletin of Materials Science, 24*(6): 653-657.

Sires, B.S., and Benda, P.M. (2000). Osteogenesis in a human hydroxyapatite orbital implant 5.5 years after implantation. *American journal of ophthalmology, 130*(3): 368-369.

Ślósarczyk, A., and Piekarczyk, J. (1999). Ceramic materials on the basis of hydroxyapatite and tricalcium phosphate. *Ceramics International, 25*(6): 561-565. doi: http://dx.doi.org/10.1016/S0272-8842(98)00019-4

Smičiklas, I., Onjia, A., and Raičević, S. (2005). Experimental design approach in the synthesis of hydroxyapatite by neutralization method. *Separation and purification technology, 44*(2): 97-102.

Song, J., Liu, Y., Zhang, Y., and Jiao, L. (2011). Mechanical properties of hydroxyapatite ceramics sintered from powders with different morphologies. *Materials Science and Engineering: A, 528*(16–17): 5421-5427. doi: http://dx.doi.org/10.1016/j.msea.2011.03.078

Sooksaen, P., Jumpanoi, N., Suttiphan, P., and Kimchaiyong, E. (2010). Crystallization of nano-sized hydroxyapatite via wet chemical process under strong alkaline conditions. *Sci J UBU, 1*: 20-27.

Srogi, K. (2006). A review: Application of microwave techniques for environmental analytical chemistry. *Analytical Letters, 39*(7): 1261-1288.

Stanley, R., and Nesaraj, A.S. (2014). Effect of surfactants on the wet chemical synthesis of silica nanoparticles. *International Journal of Applied Science and Engineering 12 (1)*: 9-21.

Stea, S., Visentin, M., Savarino, L., Ciapetti, G., Donati, M., Moroni, A., Caja, V., and Pizzoferrato, A. (1995). Microhardness of bone at the interface with ceramic-coated metal implants. *Journal of biomedical materials research, 29*(6): 695-699.

Strumillo, C., and Kudra, T. (1986). Drying: Principles, science and design. *Gordon and Breach Science Publishers, New York, 42*.

Suchanek, W., Yashima, M., Kakihana, M., and Yoshimura, M. (1997). Hydroxyapatite ceramics with selected sintering additives. *Biomaterials, 18*(13): 923-933.

Suchanek, W., and Yoshimura, M. (1998). Processing and properties of hydroxyapatite-based biomaterials for use as hard tissue replacement implants. *Journal of Materials Research, 13*(01): 94-117.

Suchanek, W.L., Shuk, P., Byrappa, K., Riman, R.E., TenHuisen, K.S., and Janas, V.F. (2002). Mechanochemical–hydrothermal synthesis of carbonated apatite powders at room temperature. *Biomaterials, 23*(3): 699-710.

Sun, E., Datta, A., and Lobo, S. (1994). Composition-based prediction of dielectric properties of foods. *The Journal of microwave power and electromagnetic energy: a publication of the International Microwave Power Institute, 30*(4): 205-212.

Sun, R., Li, M., Lu, Y., and Wang, A. (2006). Immersion behavior of hydroxyapatite (ha) powders before and after sintering. *Materials characterization, 56*(3): 250-254.

Sundaram, J., Durance, T.D., and Wang, R. (2008). Porous scaffold of gelatin–starch with nanohydroxyapatite composite processed via novel microwave vacuum drying. *Acta biomaterialia, 4*(4): 932-942.

Sung, Y.-M., Lee, J.-C., and Yang, J.-W. (2004). Crystallization and sintering characteristics of chemically precipitated hydroxyapatite nanopowder. *Journal of Crystal Growth, 262*(1): 467-472.

Sutton, W.H. (1989). Microwave processing of ceramic materials. *American Ceramic Society Bulletin, 68*(2): 376-386.

Tampieri, A., Celotti, G., Sprio, S., and Mingazzini, C. (2000). Characteristics of synthetic hydroxyapatites and attempts to improve their thermal stability. *Materials chemistry and physics, 64*(1): 54-61.

Tan, C., Tolouei, R., Ramesh, S., Yap, B., and Amiriyan, M. (2011). *Calcination effects on the sinterability of hydroxyapatite bioceramics.* Paper presented at the 5th Kuala Lumpur International Conference on Biomedical Engineering 2011.

Taquet, N., Pironon, J., De Donato, P., Lucas, H., and Barres, O. (2013). Efficiency of combined ftir and raman spectrometry for online quantification of soil gases: Application to the monitoring of carbon dioxide storage sites. *International Journal of Greenhouse Gas Control, 12*: 359-371.

Tas, A.C. (2000). Combustion synthesis of calcium phosphate bioceramic powders. *Journal of the European ceramic society, 20*(14): 2389-2394.

Tatsuo, S., Kohsuke, O., Kanako, S., and Ken-Ichi, M. (1993). The effect of aging on the healing of hydroxylapatite implants. *Journal of oral and maxillofacial surgery, 51*(1): 51-56.

Teh, Y., Tan, C., Ramesh, S., Purbolaksono, J., Tan, Y., Chandran, H., Teng, W., and Yap, B. (2014). Effect of calcination on the sintering behaviour of hydroxyapatite. *Ceramics-Silikáty, 58*(4): 320-325.

Tekeli, S. (2006). The flexural strength, fracture toughness, hardness and densification behaviour of various amount of al 2 o 3-doped 8yscz/al 2 o 3 composites used as an electrolyte for solid oxide fuel cell. *Materials & design, 27*(3): 230-235.

Thamaraiselvi, T., Prabakaran, K., and Rajeswari, S. (2006). Synthesis of hydroxyapatite that mimic bone minerology. *Trends Biomater. Artif. Organs, 19*(2): 81-83.

Thangamani, N., Chinnakali, K., and Gnanam, F. (2002). The effect of powder processing on densification, microstructure and mechanical properties of hydroxyapatite. *Ceramics international, 28*(4): 355-362.

Thuault, A., Savary, E., Hornez, J.-C., Moreau, G., Descamps, M., Marinel, S., and Leriche, A. (2014). Improvement of the hydroxyapatite mechanical properties by direct microwave sintering in single mode cavity. *Journal of the European Ceramic Society, 34*(7): 1865-1871.

Tian, T., Jiang, D., Zhang, J., and Lin, Q. (2008). Synthesis of si-substituted hydroxyapatite by a wet mechanochemical method. *Materials Science and Engineering: C, 28*(1): 57-63.

Tolouei, R., Ramesh, S., Tan, C.Y., Satgunam, M., and Amiriyan, M. (2012). *Manufacturing of high toughness hydroxyapatite produced by wet chemical method.* Paper presented at the Applied Mechanics and Materials.

Tolouei, R., Tan, C., Amiriyan, M., and Teng, W. (2011). Sintering effects on the densification of nanocrystalline hydroxyapatite. *Int J Automot Mech Eng (IJAME), 3*: 249-255.

Tonanon, N., Wareenin, Y., Siyasukh, A., Tanthapanichakoon, W., Nishihara, H., Mukai, S.R., and Tamon, H. (2006). Preparation of resorcinol formaldehyde (rf) carbon gels: Use of ultrasonic irradiation followed by microwave drying. *Journal of non-crystalline solids, 352*(52): 5683-5686.

Uhlmann, D.R., Bowen, H.K., and Kingery, W. (1976). Introduction to ceramics.

Uysal, I., Severcan, F., Tezcaner, A., and Evis, Z. (2014). Co-doping of hydroxyapatite with zinc and fluoride improves mechanical and biological properties of hydroxyapatite. *Progress in Natural Science: Materials International, 24*(4): 340-349.

Vaidhyanathan, B., and Rao, K. (1996). Rapid microwave assisted synthesis of hydroxyapatite. *Bulletin of Materials Science, 19*(6): 1163-1165.

Vallet-Regi, M., and Gonz á lez-Calbet, J.M. (2004). Calcium phosphates as substitution of bone tissues. *Progress in Solid State Chemistry, 32*(1): 1-31.

Van Blitterswijk, C., Grote, J., Kuypers, W., Blok-van Hoek, C., and Daems, W.T. (1985). Bioreactions at the tissue/hydroxyapatite interface. *Biomaterials, 6*(4): 243-251.

Van Dijk, H., Hattu, N., and Prijs, K. (1981). Preparation, microstructure and mechanical properties of dense polycrystalline hydroxy apatite. *Journal of materials science, 16*(6): 1592-1598.

Van Landuyt, P., Li, F., Keustermans, J., Streydio, J., Delannay, F., and Munting, E. (1995). The influence of high sintering temperatures on the mechanical properties of hydroxylapatite. *Journal of Materials Science: Materials in Medicine, 6*(1): 8-13.

Veljović, D., Jokić, B., Petrović, R., Palcevskis, E., Dindune, A., Mihailescu, I., and Janaćković, D. (2009). Processing of dense nanostructured hap ceramics by sintering and hot pressing. *Ceramics International, 35*(4): 1407-1413.

Venkatesh, M., and Raghavan, G. (2004). An overview of microwave processing and dielectric properties of agri-food materials. *Biosystems Engineering, 88*(1): 1-18.

Verwilghen, C., Rio, S., Nzihou, A., Gauthier, D., Flamant, G., and Sharrock, P.J. (2007). Preparation of high specific surface area hydroxyapatite for environmental applications. *Journal of materials science, 42*(15): 6062-6066.

Vijayan, S., and Varma, H. (2002). Microwave sintering of nanosized hydroxyapatite powder compacts. *Materials letters, 56*(5): 827-831.

Vollmer, M. (2004). Physics of the microwave oven. *Physics Education, 39*(1): 74.

Wang, A., Liu, D., Yin, H., Wu, H., Wada, Y., Ren, M., Jiang, T., Cheng, X., and Xu, Y. (2007). Size-controlled synthesis of hydroxyapatite nanorods by chemical precipitation in the presence of organic modifiers. *Materials Science and Engineering: C, 27*(4): 865-869.

Wang, A.-j., Lu, Y.-p., Zhu, R.-f., Li, S.-t., and Ma, X.-l. (2009). Effect of process parameters on the performance of spray dried hydroxyapatite microspheres. *Powder Technology, 191*(1): 1-6.

Wang, C.T., Lin, L.S., and Yang, S.J. (1992). Preparation of mgal2o4 spinel powders via freeze-drying of alkoxide precursors. *Journal of the American Ceramic Society, 75*(8): 2240-2243.

Wang, D., Chen, C., Liu, X., and Lei, T. (2007). Effects of sol–gel processing parameters on the phases and microstructures of ha films. *Colloids and Surfaces B: Biointerfaces, 57*(2): 237-242.

Wang, J., and Shaw, L.L. (2007). Morphology-enhanced low-temperature sintering of nanocrystalline hydroxyapatite. *Advanced Materials, 19*(17): 2364-2369.

Wang, J., and Shaw, L.L. (2009). Nanocrystalline hydroxyapatite with simultaneous enhancements in hardness and toughness. *Biomaterials, 30*(34): 6565-6572. doi: http://dx.doi.org/10.1016/j.biomaterials.2009.08.048

Wang, L., and Lloyd, I.K. (1991). Sinterability of calcined freeze-dried alumina powders. *Journal of the American Ceramic Society, 74*(11): 2934-2936.

Wang, P., Li, C., Gong, H., Jiang, X., Wang, H., and Li, K. (2010). Effects of synthesis conditions on the morphology of hydroxyapatite nanoparticles produced by wet chemical process. *Powder Technology, 203*(2): 315-321.

Wang, P.E., and Chaki, T. (1993). Sintering behaviour and mechanical properties of hydroxyapatite and dicalcium phosphate. *Journal of Materials Science: Materials in Medicine, 4*(2): 150-158.

Wang, T., Dorner-Reisel, A., and Müller, E. (2004). Thermogravimetric and thermokinetic investigation of the dehydroxylation of a hydroxyapatite powder. *Journal of the European Ceramic Society, 24*(4): 693-698.

Wang, X., Fan, H., Xiao, Y., and Zhang, X. (2006). Fabrication and characterization of porous hydroxyapatite/β-tricalcium phosphate ceramics by microwave sintering. *Materials Letters, 60*(4): 455-458.

Webster, T.J., Ergun, C., Doremus, R.H., Siegel, R.W., and Bizios, R. (2000). Enhanced functions of osteoblasts on nanophase ceramics. *Biomaterials, 21*(17): 1803-1810.

Williams, D.F. (2008). On the mechanisms of biocompatibility. *Biomaterials, 29*(20): 2941-2953.

Wilson, O.C., and Hull, J.R. (2008). Surface modification of nanophase hydroxyapatite with chitosan. *Materials Science and Engineering: C, 28*(3): 434-437.

Wong, M., Eulenberger, J., Schenk, R., and Hunziker, E. (1995). Effect of surface topology on the osseointegration of implant materials in trabecular bone. *Journal of biomedical materials research, 29*(12): 1567-1575.

Wu, L., Dou, Y., Lin, K., Zhai, W., Cui, W., and Chang, J. (2011). Hierarchically structured nanocrystalline hydroxyapatite assembled hollow fibers as a promising protein delivery system. *Chemical Communications, 47*(42): 11674-11676.

Wu, S.-C., Tsou, H.-K., Hsu, H.-C., Hsu, S.-K., Liou, S.-P., and Ho, W.-F. (2013). A hydrothermal synthesis of eggshell and fruit waste extract to produce nanosized hydroxyapatite. *Ceramics International, 39*(7): 8183-8188.

Xia, L., Lin, K., Jiang, X., Xu, Y., Zhang, M., Chang, J., and Zhang, Z. (2013). Enhanced osteogenesis through nano-structured surface design of macroporous

hydroxyapatite bioceramic scaffolds via activation of erk and p38 mapk signaling pathways. *Journal of Materials Chemistry B, 1*(40): 5403-5416.

Xu, J., Khor, K.A., and Kumar, R. (2007). Physicochemical differences after densifying radio frequency plasma sprayed hydroxyapatite powders using spark plasma and conventional sintering techniques. *Materials Science and Engineering: A, 457*(1): 24-32.

Xue, W., Tao, S., Liu, X., Zheng, X., and Ding, C. (2004). In vivo evaluation of plasma sprayed hydroxyapatite coatings having different crystallinity. *Biomaterials, 25*(3): 415-421.

Yamaguchi, M., Oishi, H., and Suketa, Y. (1987). Stimulatory effect of zinc on bone formation in tissue culture. *Biochemical pharmacology, 36*(22): 4007-4012.

Yang, J.H., Kim, K.H., You, C.K., Rautray, T.R., and Kwon, T.Y. (2011). Synthesis of spherical hydroxyapatite granules with interconnected pore channels using camphene emulsion. *Journal of Biomedical Materials Research Part B: Applied Biomaterials, 99*(1): 150-157.

Yang, Y., Ong, J.L., and Tian, J. (2002). Rapid sintering of hydroxyapatite by microwave processing. *Journal of materials science letters, 21*(1): 67-69.

Yang, Y.-C., and Chang, E. (2005). Measurements of residual stresses in plasma-sprayed hydroxyapatite coatings on titanium alloy. *Surface and Coatings Technology, 190*(1): 122-131.

Yeong, K., Wang, J., and Ng, S. (2001). Mechanochemical synthesis of nanocrystalline hydroxyapatite from cao and cahpo 4. *Biomaterials, 22*(20): 2705-2712.

Yongsawatdigul, J., and Gunasekaran, S. (1996). Microwave-vacuum drying of cranberries: Part i. Energy use and efficiency. *Journal of Food Processing and Preservation, 20*(2): 121-143.

Yoruc, A.B.H., and Koca, Y. (2009). Double step stirring: A novel method for precipitation of nano-sized hydroxyapatite powder. *Digest J. Nanomater. Biostructures, 4*: 73-81.

Yoshimura, M., and Byrappa, K. (2008). Hydrothermal processing of materials: Past, present and future. *Journal of Materials Science, 43*(7): 2085-2103.

Yu, J., Wang, G., and Cheng, B. (2010). Effects of microwave drying on the microstructure and photocatalytic activity of bimodal mesoporous tio 2 powders. *Journal of Physics and Chemistry of Solids, 71*(4): 523-526.

Yu, J., Zhang, W., Li, Y., Wang, G., Yang, L., Jin, J., Chen, Q., and Huang, M. (2014). Synthesis, characterization, antimicrobial activity and mechanism of a novel hydroxyapatite whisker/nano zinc oxide biomaterial. *Biomedical Materials, 10*(1): 015001.

Yu, K.-C., Chen, C.-C., and Wu, P.-C. (2011). Research on application and rehydration rate of vacuum freeze drying of rice. *Journal of Applied Sciences, 11*(3): 535-541.

Yu, Q., Dave, R.N., Zhu, C., Quevedo, J.A., and Pfeffer, R. (2005). Enhanced fluidization of nanoparticles in an oscillating magnetic field. *AIChE Journal, 51*(7): 1971-1979.

Yubao, L., De Groot, K., De Wijn, J., Klein, C., and Meer, S. (1994). Morphology and composition of nanograde calcium phosphate needle-like crystals formed by simple hydrothermal treatment. *Journal of materials science: Materials in Medicine, 5*(6-7): 326-331.

Zhang, G., Chen, J., Yang, S., Yu, Q., Wang, Z., and Zhang, Q. (2011). Preparation of amino-acid-regulated hydroxyapatite particles by hydrothermal method. *Materials Letters, 65*(3): 572-574.

Zhang, H., and Cooper, A.I. (2005). Synthesis and applications of emulsion-templated porous materials. *Soft Matter, 1*(2): 107-113.

Zhang, X., and Vecchio, K.S. (2007). Hydrothermal synthesis of hydroxyapatite rods. *Journal of Crystal Growth, 308*(1): 133-140.

Zhang, Y., and Yokogawa, Y. (2008). Effect of drying conditions during synthesis on the properties of hydroxyapatite powders. *Journal of Materials Science: Materials in Medicine, 19*(2): 623-628.

Zhao, H., Dong, W., Zheng, Y., Liu, A., Yao, J., Li, C., Tang, W., Chen, B., Wang, G., and Shi, Z. (2011). The structural and biological properties of hydroxyapatite-modified titanate nanowire scaffolds. *Biomaterials, 32*(25): 5837-5846.

Zhou, H., and Lee, J. (2011). Nanoscale hydroxyapatite particles for bone tissue engineering. *Acta Biomaterialia, 7*(7): 2769-2781.

Zhou, J., Zhang, X., Chen, J., Zeng, S., and De Groot, K. (1993). High temperature characteristics of synthetic hydroxyapatite. *Journal of materials science: materials in medicine, 4*(1): 83-85.

Zhu, R., Yu, R., Yao, J., Wang, D., and Ke, J. (2008). Morphology control of hydroxyapatite through hydrothermal process. *Journal of alloys and Compounds, 457*(1): 555-559.

Ziegler, A., McNaney, J., Hoffmann, M., and Ritchie, R. (2005). On the effect of local grain-boundary chemistry on the macroscopic mechanical properties of a high-purity y2o3-al2o3-containing silicon nitride ceramic: Role of oxygen. *Journal of the American Ceramic Society, 88*(7): 1900-1908.

Zlotorzynski, A. (1995). The application of microwave radiation to analytical and environmental chemistry. *Critical Reviews in Analytical Chemistry, 25*(1): 43-76.

LIST OF PUBLICATIONS AND PAPERS PRESENTED

Journals

1. **The Effects of Calcium-to-Phosphorus Ratio on the Densification and Mechanical Properties of Hydroxyapatite Ceramic**; (2015) *International Journal of Applied Ceramic Technology*, Vol. 12 (1), 223-227

2. **Effect of Calcination on the Sintering Behaviour of Hydroxyapatite** (2014) *Ceramics Silikaty*, Vol. 58 (4), 320-325

3. **The Effect of Sintering Ramp Rate on the Sinterability of Forsterite Ceramics** (2014) *Materials Research Innovations*, Vol. 18, S6-61-64

4. **Sinterability of Forsterite Prepared via Solid State Reaction** (2015) *International Journal of Applied Ceramic Technology,* Vol. 12(2), 437-442

5. **Effect of Attritor Milling on Synthesis and Sintering of Forsterite Ceramics** (2016) *International Journal of Applied Ceramic Technology,* Vol. 13(4), 726-735

6. **Study on the Effects of Milling Time and Sintering Temperature on the Sinterability of Forsterite (Mg_2SiO_4)** (2015) *Journal of Ceramic Society of Japan,* Vol. 123, 1032-1037

Proceedings

1. **The Effect of Zinc Oxide on the Sinterability of Hydroxyapatite**, *Proceedings of the International Conference on Applied System Innovation (ICASI 2016)*

2. **The Effect of Microwave Drying on the Sinterability of Hydroxyapatite**, *Proceedings of the World Congress on Mechanical, Chemical, and Material Engineering (MCM 2015)*

3. **Wet Chemical Synthesis of Hydroxyapatite Powder via Microwave Drying**. *Proceedings of the AUD/SEED-NET Regional Conference on Materials Engineering (2014)*

4. **Synthesis and Characterization of Nano-Hydroxyapatite via Rapid Microwave Drying**, *Proceedings of the 4th Nano Today Conference (2015)*

5. **The Effect of Heat Treatment Time on the Formation of Forsterite** . *Proceedings of the 7th International Conference on Bioinformatics and Biomedical Technology (ICBBT 2015)*

Awards

1. *First Paper Award* *in the International Conference on Applied System Innovation (ICASI 2016)).* **The Effect of Zinc Oxide on the Sinterability of Hydroxyapatite**

APPENDIX A

INSTRUMENTATION

Figure A-1: Drying Oven

Figure A-2: Microwave Oven

Figure A-3: Freeze Dryer

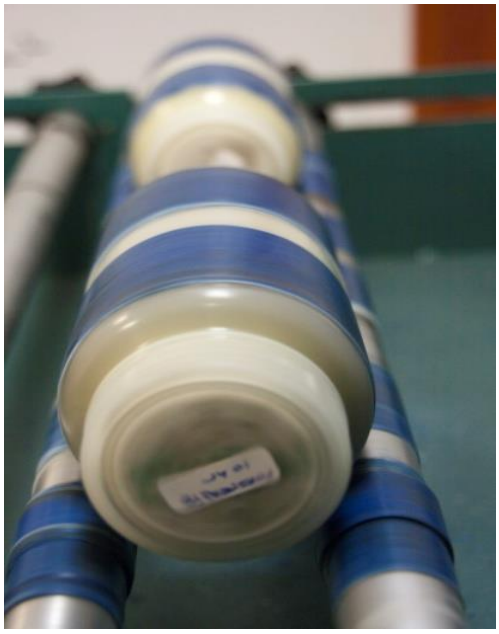

Figure A-4: Table Top Ball Milling

Figure A-5: Ultrasonic Bath Machine

Figure A-6: Uniaxial Press

Figure A-7: Cold Isostatic Press

Figure A-8: Convetional Sintering Furnace

Figure A-9: Microwave Sintering Furnace

Figure A-10: Grinding and Polishing Machine

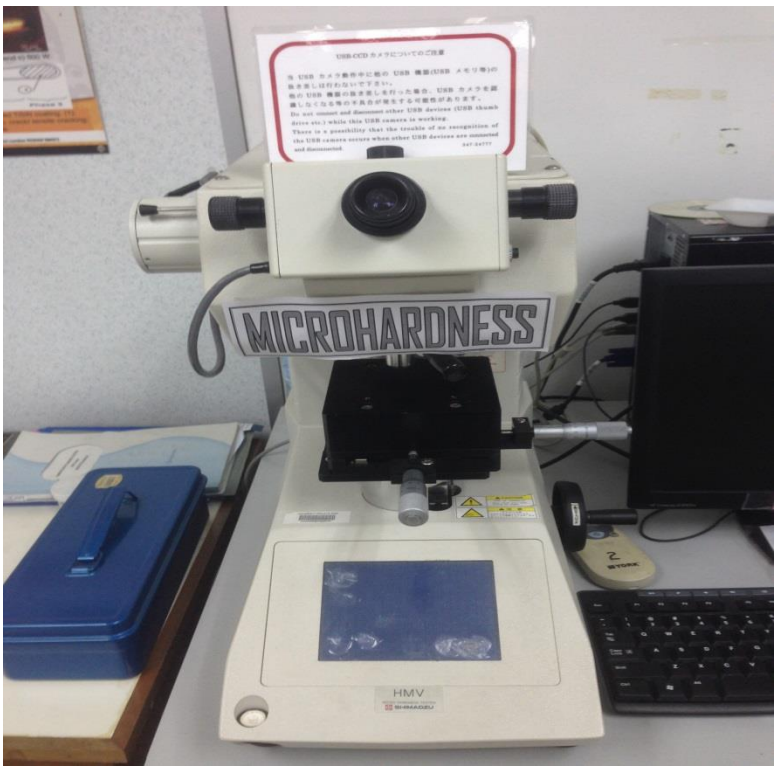

Figure A-11: Vickers Hardness Indenter

Figure A-12: XRD Machine

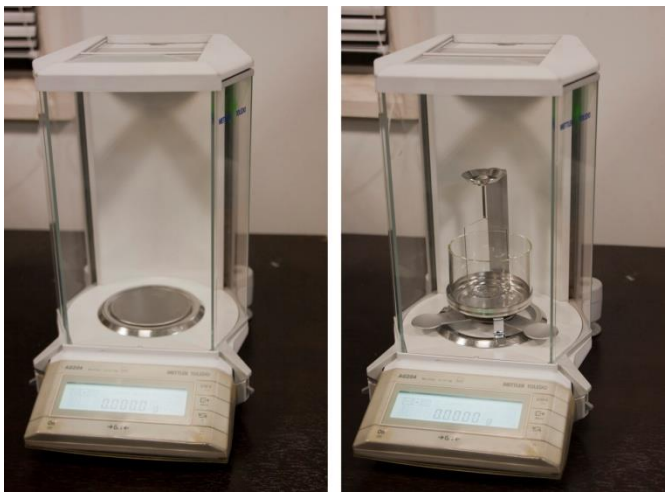

Figure A-13: Densi Meter

APPENDIX B

WATER DENSITY TABLE

As a Function of Water Temperature

(Source: Operating Instruction, *Density Determination Kit*, Mettler-Toledo, Switzerland, Manual No. P706039, pp. 14)

T/°C	0.0	0.1	0.2	0.3	0.4	0.5	0.6	0.7	0.8	0.9
10.	0.99973	0.99972	0.99971	0.99970	0.99969	0.99968	0.99967	0.99966	0.99965	0.99964
11.	0.99963	0.99962	0.99961	0.99960	0.99959	0.99958	0.99957	0.99956	0.99955	0.99954
12.	0.99953	0.99951	0.99950	0.99949	0.99948	0.99947	0.99946	0.99944	0.99943	0.99942
13.	0.99941	0.99939	0.99938	0.99937	0.99935	0.99934	0.99933	0.99931	0.99930	0.99929
14.	0.99927	0.99926	0.99924	0.99923	0.99922	0.99920	0.99919	0.99917	0.99916	0.99914
15.	0.99913	0.99911	0.99910	0.99908	0.99907	0.99905	0.99904	0.99902	0.99900	0.99899
16.	0.99897	0.99896	0.99894	0.99892	0.99891	0.99889	0.99887	0.99885	0.99884	0.99882
17.	0.99880	0.99879	0.99877	0.99875	0.99873	0.99871	0.99870	0.99868	0.99866	0.99864
18.	0.99862	0.99860	0.99859	0.99857	0.99855	0.99853	0.99851	0.99849	0.99847	0.99845
19.	0.99843	0.99841	0.99839	0.99837	0.99835	0.99833	0.99831	0.99829	0.99827	0.99825
20.	0.99823	0.99821	0.99819	0.99817	0.99815	0.99813	0.99811	0.99808	0.99806	0.99804
21.	0.99802	0.99800	0.99798	0.99795	0.99793	0.99791	0.99789	0.99786	0.99784	0.99782
22.	0.99780	0.99777	0.99775	0.99773	0.99771	0.99768	0.99766	0.99764	0.99761	0.99759
23.	0.99756	0.99754	0.99752	0.99749	0.99747	0.99744	0.99742	0.99740	0.99737	0.99735
24.	0.99732	0.99730	0.99727	0.99725	0.99722	0.99720	0.99717	0.99715	0.99712	0.99710
25.	0.99707	0.99704	0.99702	0.99699	0.99697	0.99694	0.99691	0.99689	0.99686	0.99684
26.	0.99681	0.99678	0.99676	0.99673	0.99670	0.99668	0.99665	0.99662	0.99659	0.99657
27.	0.99654	0.99651	0.99648	0.99646	0.99643	0.99640	0.99637	0.99634	0.99632	0.99629
28.	0.99626	0.99623	0.99620	0.99617	0.99614	0.99612	0.99609	0.99606	0.99603	0.99600
29.	0.99597	0.99594	0.99591	0.99588	0.99585	0.99582	0.99579	0.99576	0.99573	0.99570
30.	0.99567	0.99564	0.99561	0.99558	0.99555	0.99552	0.99549	0.99546	0.99543	0.99540

Figure B-1: Water Density Table

APPENDIX C

JCPDS FILES

Name and formula

Reference code:	01-074-0565
Mineral name:	Hydroxylapatite
Compound name:	Calcium Hydroxide Phosphate
Empirical formula:	$Ca_{10}H_2O_{26}P_6$
Chemical formula:	$Ca_{10}(PO_4)_6(OH)_2$

Crystallographic parameters

Crystal system:	Hexagonal
Space group:	P63/m
Space group number:	176
a (Å):	9.4240
b (Å):	9.4240
c (Å):	6.8790
Alpha (°):	90.0000
Beta (°):	90.0000
Gamma (°):	120.0000
Calculated density (g/cm^3):	3.15
Measured density (g/cm^3):	3.08
Volume of cell (10^6 pm^3):	529.09
Z:	1.00
RIR:	1.06

Subfiles and quality

Subfiles:	ICSD Pattern Inorganic Mineral
Quality:	Calculated (C)

Comments

Creation Date:	1/1/1970
Modification Date:	1/1/1970
ICSD Collection Code:	026204
Test from ICSD:	Calc. density unusual but tolerable
Sample Source or Locality:	Specimen from Holly Springs, Georgia, USA
Additional Patterns:	See PDF 00-009-0432, 01-072-1243 and 01-074-0566

Significant Precision in Crystal Structural Details: Holly Springs Hydroxyapatite.

References

Primary reference:	*Calculated from ICSD using POWD-12++*, (1997)
Structure:	Sudarsanan, K., Young, R.A., *Acta Crystallogr., Sec. B*, **25**, 1534, (1969)

Peak list

No.	h	k	l	d [A]	2Theta[deg]	I [%]
1	1	0	0	8.16142	10.832	17.3
2	1	0	1	5.25985	16.842	4.6
3	1	1	0	4.71200	18.817	2.3
4	2	0	0	4.08071	21.762	6.4
5	1	1	1	3.88745	22.858	6.0
6	2	0	1	3.50965	25.357	2.4
7	0	0	2	3.43950	25.883	35.3
8	1	0	2	3.16953	28.131	8.8
9	2	1	0	3.08473	28.921	16.0
10	2	1	1	2.81468	31.766	100.0
11	1	1	2	2.77811	32.195	52.0
12	3	0	0	2.72047	32.897	60.9
13	2	0	2	2.62992	34.063	20.8
14	3	0	1	2.52983	35.455	4.0
15	2	2	0	2.35600	38.168	0.2
16	2	1	2	2.29645	39.197	4.9
17	1	3	0	2.26357	39.791	20.0
18	2	2	1	2.22890	40.436	1.7
19	1	0	3	2.20753	40.845	0.3
20	1	3	1	2.15016	41.986	5.5
21	3	0	2	2.13372	42.325	1.1
22	1	1	3	2.06183	43.876	4.5
23	4	0	0	2.04036	44.362	1.1
24	2	0	3	1.99902	45.330	3.4
25	4	0	1	1.95612	46.381	0.7
26	2	2	2	1.94372	46.694	28.1
27	1	3	2	1.89084	48.081	12.3
28	2	3	0	1.87236	48.586	4.1
29	2	1	3	1.84027	49.490	31.2
30	3	2	1	1.80663	50.475	16.0
31	1	4	0	1.78097	51.255	11.6
32	4	0	2	1.75482	52.075	11.8
33	0	0	4	1.71975	53.220	13.9
34	1	0	4	1.68280	54.484	1.0
35	3	2	2	1.64449	55.863	5.9
36	5	0	0	1.63228	56.318	0.2
37	3	1	3	1.61089	57.134	3.7
38	5	0	1	1.58819	58.027	1.5
39	2	0	4	1.58477	58.164	1.1
40	4	1	2	1.58153	58.295	1.1
41	3	3	0	1.57067	58.737	0.8
42	2	4	0	1.54236	59.925	4.3
43	3	3	1	1.53126	60.404	3.2
44	2	4	1	1.50500	61.571	3.2
45	1	2	4	1.50209	61.704	5.2
46	5	0	2	1.47465	62.982	7.9
47	5	1	0	1.46583	63.404	1.6
48	3	0	4	1.45365	63.998	7.5
49	3	2	3	1.45028	64.165	9.3
50	5	1	1	1.43365	65.000	7.0
51	1	4	3	1.40655	66.412	2.1
52	2	2	4	1.38906	67.359	0.1
53	3	1	4	1.36936	68.461	0.4
54	6	0	0	1.36024	68.985	0.2
55	1	0	5	1.35666	69.193	0.2
56	5	1	2	1.34848	69.673	2.0
57	4	3	0	1.34173	70.075	0.4
58	6	0	1	1.33440	70.517	0.1

59	5	0	3	1.32977	70.799	0.2
60	1	1	5	1.32066	71.362	0.4
61	4	3	1	1.31691	71.596	3.6
62	5	2	0	1.30687	72.232	2.8
63	2	0	5	1.30370	72.436	1.6
64	3	3	3	1.29582	72.947	0.3
65	5	2	1	1.28391	73.735	2.0
66	2	4	3	1.27979	74.012	3.7
67	2	3	4	1.26657	74.916	1.4
68	6	0	2	1.26491	75.031	1.2
69	2	1	5	1.25649	75.622	4.6
70	3	4	2	1.24999	76.085	2.4
71	6	1	0	1.24461	76.473	1.8
72	1	4	4	1.23712	77.021	5.0
73	5	1	3	1.23504	77.174	4.5
74	3	0	5	1.22773	77.720	0.2
75	1	6	1	1.22472	77.947	0.9
76	2	5	2	1.22166	78.179	5.7
77	2	2	5	1.18807	80.837	0.3
78	5	0	4	1.18391	81.180	0.5
79	4	4	0	1.17800	81.673	1.8
80	1	3	5	1.17567	81.870	1.2
81	1	6	2	1.17034	82.323	0.6
82	7	0	0	1.16592	82.704	0.7
83	4	4	1	1.16110	83.123	1.0
84	3	3	4	1.15976	83.240	1.0
85	4	3	3	1.15805	83.391	3.6
86	2	4	4	1.14822	84.268	3.4
87	0	0	6	1.14650	84.423	1.7
88	4	0	5	1.14070	84.953	0.2
89	5	2	3	1.13541	85.443	1.7
90	2	6	0	1.13179	85.782	1.0
91	5	1	4	1.11558	87.338	2.4
92	4	4	2	1.11400	87.494	4.1
93	2	3	5	1.10868	88.021	2.5
94	3	5	2	1.10420	88.471	5.8
95	1	6	3	1.09386	89.530	0.3

Structure

No.	Name	Elem.	X	Y	Z	Biso	sof	Wyck.
1	H1	H	0.00000	0.00000	0.06080	0.5000	0.5000	4e
2	O1	O	0.00000	0.00000	0.19500	0.5000	0.5000	4e
3	CA1	Ca	0.24680	0.25340	0.25000	0.5000	1.0000	6h
4	CA2	Ca	0.33333	0.66667	0.00150	0.5000	1.0000	4f
5	P1	P	0.39870	0.03020	0.25000	0.5000	1.0000	6h
6	O2	O	0.34370	0.08580	0.07020	0.5000	1.0000	12i
7	O3	O	0.58730	0.12220	0.25000	0.5000	1.0000	6h
8	O4	O	0.15640	0.48480	0.25000	0.5000	1.0000	6h

Stick Pattern

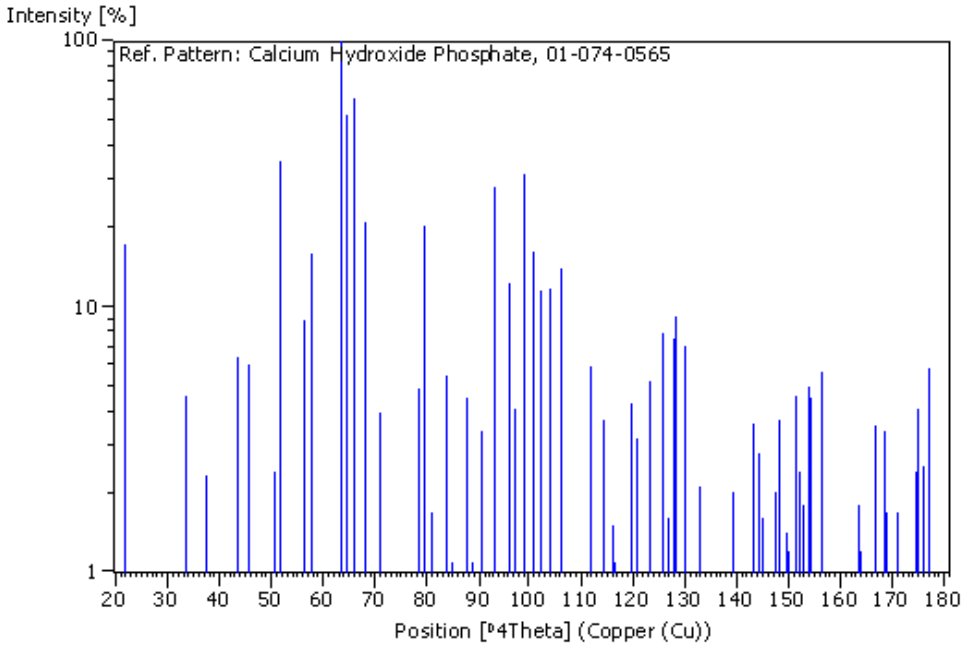

Figure C-1: JCPDS No. 74-566 for HA

Name and formula

Reference code:	00-009-0345
Compound name:	Calcium Phosphate
Empirical formula:	$Ca_2O_7P_2$
Chemical formula:	$Ca_2P_2O_7$

Crystallographic parameters

Crystal system:	Orthorhombic
a (Å):	8.5240
b (Å):	12.6460
c (Å):	5.3090
Alpha (°):	90.0000
Beta (°):	90.0000
Gamma (°):	90.0000
Calculated density (g/cm^3):	2.95
Measured density (g/cm^3):	2.93
Volume of cell (10^6 pm^3):	572.28
Z:	4.00
RIR:	-

Subfiles and quality

Subfiles:	Common Phase Forensic Inorganic
Quality:	Indexed (I)

Comments

Creation Date:	1/1/1970
Modification Date:	1/1/1970
Optical Data:	A=1.584, B=1.599, Q=1.605, Sign=-, 2V=50°
Melting Point:	1363°
Sample Preparation:	Sample obtained by heating $CaHPO_4 \cdot 2H_2O$. Transition point 1140° (Hill, Ibid.)
Additional Patterns:	To replace 00-001-0667.

References

Primary reference:	de Wolff, P., Technisch Physische Dienst, Delft, The Netherlands., *ICDD Grant-in-Aid*
Optical data:	Hill, Faust, Reynolds., *Am. J. Sci.*, **242**, 457, (1944)

Peak list

No.	h	k	l	d [A]	2Theta[deg]	I [%]
1	1	1	0	7.06000	12.528	25.0
2	0	2	0	6.31000	14.024	10.0

3	1	2	0	5.08000	17.443	2.0
4	0	1	1	4.90000	18.089	40.0
5	1	0	1	4.50000	19.713	6.0
6	2	0	0	4.26000	20.835	30.0
7	1	3	0	3.78000	23.517	35.0
8	1	2	1	3.67000	24.232	10.0
9	2	2	0	3.53000	25.208	35.0
10	2	0	1	3.32000	26.832	50.0
11	0	3	1	3.30000	26.998	100.0
12	2	1	1	3.21000	27.769	95.0
13	0	4	0	3.16000	28.218	10.0
14	1	3	1	3.08000	28.967	55.0
15	2	3	0	2.99600	29.797	12.0
16	1	4	0	2.96400	30.127	1.0
17	2	2	1	2.94300	30.347	6.0
18	3	1	0	2.77100	32.280	30.0
19	0	0	2	2.65500	33.732	45.0
20	2	3	1	2.61000	34.331	12.0
21	3	2	0	2.59000	34.605	45.0
22	2	4	0	2.53900	35.322	10.0
23	3	0	1	2.50600	35.803	6.0
24	1	1	2	2.48600	36.101	6.0
25	3	1	1	2.45800	36.527	30.0
26	1	5	0	2.42400	37.058	25.0
27	1	2	2	2.35400	38.201	14.0
28	3	2	1	2.32900	38.628	14.0
29	0	5	1	2.28600	39.384	6.0
30	2	0	2	2.25300	39.985	8.0
31	2	1	2	2.21900	40.625	6.0
32	1	5	1	2.20600	40.875	4.0
33	1	3	2	2.17300	41.524	1.0
34	3	3	1	2.15400	41.907	6.0
35	2	2	2	2.12200	42.570	4.0
36	0	6	0	2.10800	42.867	14.0
37	4	1	0	2.10200	42.995	30.0
38	1	6	0	2.04600	44.233	20.0
39	2	3	2	1.98800	45.595	70.0
40	1	4	2	1.97700	45.863	2.0
41	3	4	1	1.96300	46.209	2.0
42	4	1	1	1.95300	46.459	1.0
43	3	0	2	1.94000	46.789	1.0
44	1	6	1	1.91000	47.569	6.0
45	4	2	1	1.88800	48.158	18.0
46	3	2	2	1.85500	49.071	6.0
47	2	4	2	1.83400	49.671	18.0
48	1	5	2	1.79000	50.978	16.0
49	2	6	1	1.78000	51.285	25.0
50	3	3	2	1.76400	51.784	6.0
51	0	1	3	1.75200	52.166	1.0
52	1	0	3	1.73200	52.814	4.0
53	0	7	1	1.71100	53.514	10.0
54	1	7	1	1.67700	54.688	10.0
55	2	7	0	1.66300	55.187	4.0
56	4	1	2	1.64700	55.770	4.0
57	2	0	3	1.63500	56.216	20.0
58	0	3	3	1.63100	56.366	8.0
59	5	0	1	1.62300	56.669	10.0
60	5	1	1	1.61100	57.129	10.0
61	4	2	2	1.60700	57.285	4.0
62	2	7	1	1.58600	58.115	6.0

63	0	8	0	1.58100	58.316	4.0
64	5	2	1	1.57300	58.642	8.0
65	4	5	1	1.55700	59.304	1.0
66	2	6	2	1.54100	59.983	6.0
67	2	3	3	1.52400	60.722	8.0
68	5	4	0	1.50000	61.799	10.0
69	0	7	2	1.49300	62.121	6.0

Stick Pattern

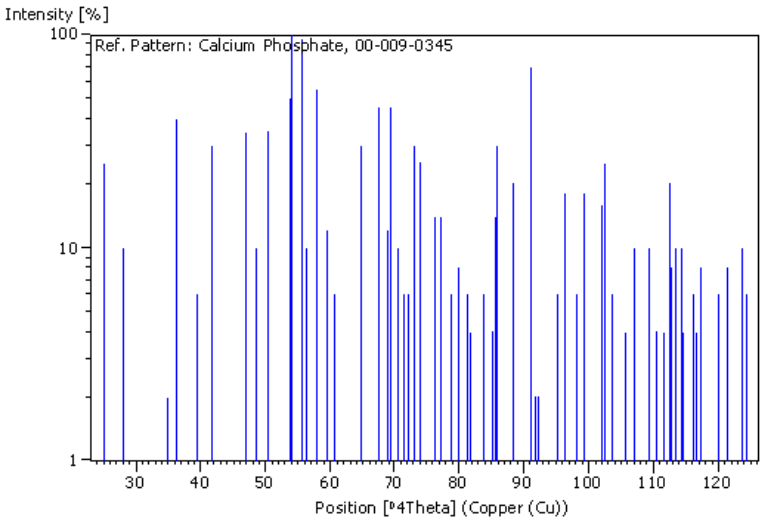

Figure C-2: JCPDS No. 9-345 for α-TCP

Name and formula

Reference code:	00-009-0169
Mineral name:	Whitlockite, syn
Compound name:	Calcium Phosphate
Empirical formula:	$Ca_3O_8P_2$
Chemical formula:	$Ca_3(PO_4)_2$

Crystallographic parameters

Crystal system:	Rhombohedral
Space group:	R-3c
Space group number:	167
a (Å):	10.4290
b (Å):	10.4290
c (Å):	37.3800
Alpha (°):	90.0000
Beta (°):	90.0000
Gamma (°):	120.0000
Calculated density (g/cm^3):	3.07
Measured density (g/cm^3):	3.12
Volume of cell (10^6 pm^3):	3520.91
Z:	21.00
RIR:	-

Subfiles and quality

Subfiles:	Common Phase Corrosion Educational pattern Forensic Inorganic Mineral
Quality:	Indexed (I)

Comments

Color:	Colorless, white, gray, yellow
Creation Date:	1/1/1970
Modification Date:	1/1/1970
Color:	Colorless, white, gray, yellow
Optical Data:	A=1.626, B=1.629, Sign=-
Sample Source or Locality:	Sample obtained by heating a commercial sample
Structures:	Nearly isostructural with cerite
Additional Patterns:	Validated by calculated pattern 00-042-0577
Additional Patterns:	See ICSD 6191 (PDF 01-070-2065).

References

Primary reference:	de Wolff, P., Technisch Physische Dienst, Delft, The Netherlands., *ICDD Grant-in-* (1957)
Structure:	Calvo, C., Gopal, R., *Am. Mineral.*, **60**, 120, (1975)
Optical data:	*Dana's System of Mineralogy, 7th Ed.*, **II**, 684, (1951)

Peak list

No.	h	k	l	d [A]	2Theta[deg]	I [%]
1	0	1	2	8.15000	10.847	12.0
2	1	0	4	6.49000	13.633	16.0
3	0	0	6	6.22000	14.228	6.0
4	1	1	0	5.21000	17.005	20.0
5	1	1	3	4.80000	18.469	2.0
6	2	0	2	4.39000	20.212	8.0
7	0	1	8	4.15000	21.394	4.0
8	0	2	4	4.06000	21.874	16.0
9	1	1	6	4.00000	22.206	4.0
10	1	0	10	3.45000	25.803	25.0
11	2	1	1	3.40000	26.189	4.0
12	1	2	2	3.36000	26.507	10.0
13	1	1	9	3.25000	27.421	8.0
14	2	1	4	3.21000	27.769	55.0
15	1	2	5	3.11000	28.681	2.0
16	3	0	0	3.01000	29.655	16.0
17	0	2	10	2.88000	31.027	100.0
18	1	2	8	2.75700	32.449	20.0
19	3	0	6	2.71000	33.027	10.0
20	1	1	12	2.67400	33.485	8.0
21	2	2	0	2.60700	34.372	65.0
22	0	1	14	2.56200	34.995	6.0
23	2	2	3	2.55300	35.122	8.0
24	2	1	10	2.52000	35.598	12.0
25	1	3	1	2.49900	35.907	6.0
26	1	2	11	2.40700	37.329	10.0
27	3	1	5	2.37500	37.851	6.0
28	1	0	16	2.26300	39.801	10.0
29	1	1	15	2.24900	40.059	4.0
30	0	4	2	2.24100	40.209	2.0
31	4	0	4	2.19500	41.089	14.0
32	3	0	12	2.16500	41.685	12.0
33	1	2	14	2.10300	42.974	4.0
34	0	0	18	2.07600	43.561	8.0
35	3	2	1	2.06800	43.738	4.0
36	2	3	2	2.06100	43.894	6.0
37	0	4	8	2.03300	44.531	10.0
38	3	2	4	2.02300	44.763	6.0
39	3	1	11	2.01700	44.903	4.0
40	2	2	12	2.00000	45.306	8.0
41	4	1	0	1.97000	46.035	2.0
42	4	1	3	1.94600	46.636	4.0
43	4	0	10	1.93300	46.969	20.0
44	2	3	8	1.89500	47.969	16.0
45	4	1	6	1.87900	48.404	14.0
46	0	1	20	1.83000	49.787	12.0
47	3	2	10	1.81200	50.315	6.0
48	5	0	2	1.79800	50.735	6.0
49	4	1	9	1.78100	51.254	6.0
50	0	5	4	1.77400	51.471	8.0
51	3	3	0	1.73800	52.618	4.0

52	2	0	20	1.72800	52.946	25.0
53	3	0	18	1.71100	53.514	8.0
54	5	0	8	1.68500	54.407	8.0
55	4	1	12	1.66500	55.116	4.0
56	2	3	14	1.63700	56.141	6.0
57	2	2	18	1.62500	56.593	6.0
58	4	2	8	1.60300	57.441	6.0
59	5	1	4	1.60000	57.559	4.0
60	5	1	7	1.55200	59.515	12.0
61	1	5	8	1.53200	60.372	4.0
62	2	1	22	1.52000	60.899	4.0
63	6	0	0	1.50500	61.571	4.0
64	1	5	11	1.46500	63.445	6.0
65	0	4	20	1.44000	64.678	4.0
66	0	5	16	1.42900	65.238	4.0
67	3	4	8	1.41400	66.017	4.0
68	5	2	6	1.40900	66.282	6.0
69	1	5	14	1.38700	67.473	4.0

Stick Pattern

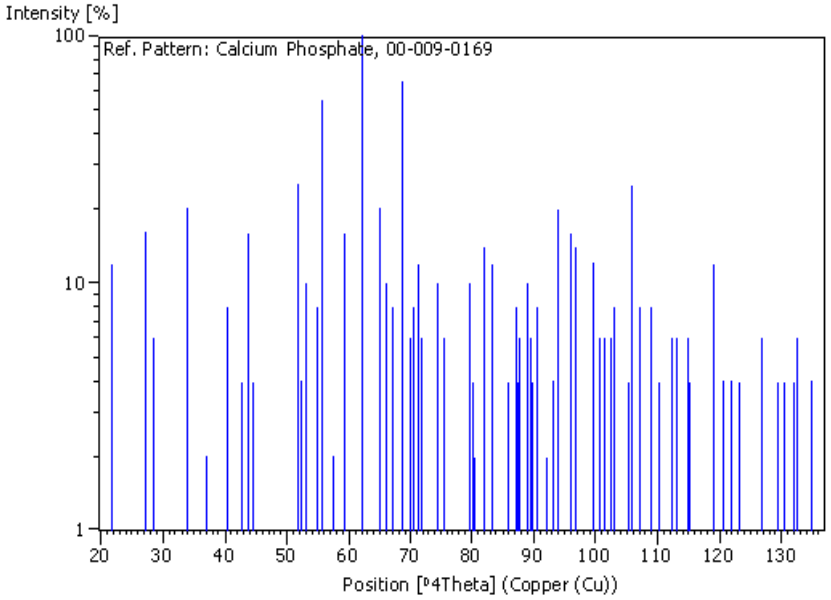

Figure C-3: JCPDS No. 9-169 for β-TCP

Name and formula

Reference code: 00-011-0232

Compound name: Calcium Phosphate

Empirical formula: $Ca_4O_9P_2$
Chemical formula: $Ca_4P_2O_9$

Crystallographic parameters

Crystal system: Unknown

RIR: -

Status, subfiles and quality

Status: Marked as deleted by ICDD
Subfiles: Inorganic
Quality: Low precision (O)

Comments

Creation Date: 1/1/1970
Modification Date: 1/1/1970
Deleted Or Rejected By: Deleted by 25-1137.

References

Primary reference: Sarver, J., Dept. Cer. Tech., Penn State Univ., University Park, PA., USA., *Private Communication*, (1958)

Peak list

No.	h	k	l	d [A]	2Theta[deg]	I [%]
1				4.06000	21.874	15.0
2				3.85000	23.083	5.0
3				3.66000	24.299	10.0
4				3.49000	25.502	25.0
5				3.44000	25.879	40.0
6				3.28000	27.165	5.0
7				3.24000	27.507	10.0
8				3.18000	28.037	20.0
9				3.06000	29.160	20.0
10				3.04000	29.356	30.0
11				2.98000	29.961	55.0
12				2.86000	31.249	25.0
13				2.80000	31.937	100.0
14				2.77000	32.292	70.0
15				2.71000	33.027	65.0
16				2.62000	34.196	20.0
17				2.60000	34.467	10.0

18	2.52000	35.598	10.0
19	2.47000	36.343	10.0
20	2.31500	38.871	10.0
21	2.28700	39.366	10.0
22	2.25000	40.041	20.0
23	2.20100	40.972	5.0
24	2.16600	41.664	5.0
25	1.97300	45.961	10.0
26	1.93700	46.866	35.0
27	1.90300	47.755	10.0
28	1.88400	48.267	10.0
29	1.86300	48.846	10.0
30	1.83800	49.555	25.0
31	1.81400	50.256	5.0
32	1.80100	50.644	15.0
33	1.79700	50.765	15.0
34	1.77400	51.471	10.0
35	1.74900	52.262	20.0
36	1.72200	53.145	10.0
37	1.70700	53.649	10.0
38	1.70100	53.854	10.0

Stick Pattern

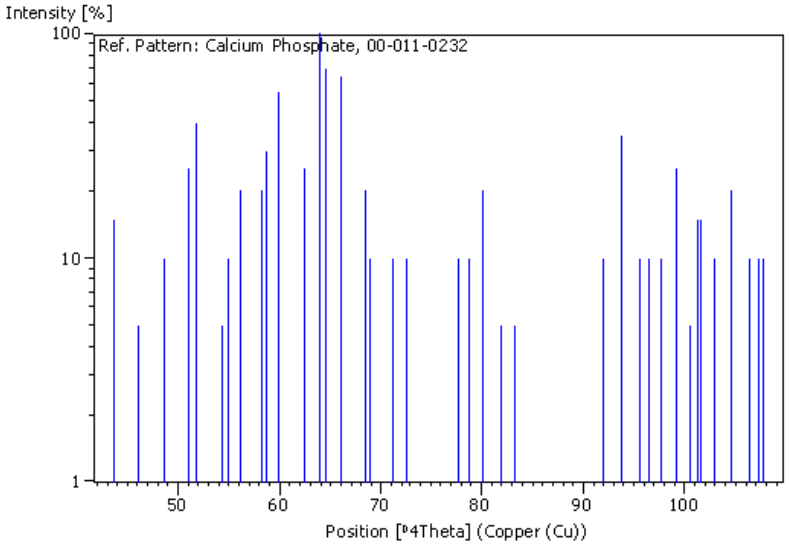

Figure C-4: JCPDS No. 11-232 for TTCP

Name and formula

Reference code:	00-048-1467
Compound name:	Calcium Oxide
Empirical formula:	CaO
Chemical formula:	CaO

Crystallographic parameters

Crystal system:	Cubic
Space group:	Fm-3m
Space group number:	225
a (Å):	4.8106
b (Å):	4.8106
c (Å):	4.8106
Alpha (°):	90.0000
Beta (°):	90.0000
Gamma (°):	90.0000
Calculated density (g/cm^3):	3.35
Volume of cell (10^6 pm^3):	111.33
Z:	4.00
RIR:	4.45

Subfiles and quality

Subfiles:	Alloy, metal or intermetalic Inorganic Pharmaceutical Superconducting Material
Quality:	Calculated (C)

Comments

Creation Date:	1/1/1970
Modification Date:	1/1/1970
Additional Patterns:	See also 00-037-1497.

References

Primary reference:	Reardon, B., Hubbard, C., TM-11948., *Oak Ridge Natl. Lab. Rep. ORNL (U.S.)*, (1992)
Unit cell:	McMurdie, H., *Powder Diffraction*, **1**, 265, (1986)

Peak list

No.	h	k	l	d [A]	2Theta[deg]	I [%]
1	1	1	1	2.77771	32.200	40.0
2	2	0	0	2.40506	37.360	100.0
3	2	2	0	1.70081	53.860	51.0
4	3	1	1	1.45038	64.160	17.0

5	2	2	2	1.38868	67.380	14.0
6	4	0	0	1.20263	79.660	5.0
7	3	3	1	1.10362	88.530	7.0
8	4	2	0	1.07566	91.470	14.0
9	4	2	2	0.98196	103.340	11.0
10	5	1	1	0.92578	112.621	7.0
11	4	4	0	0.85042	129.859	5.0
12	5	3	1	0.81313	142.642	15.0
13	4	4	2	0.80176	147.793	19.0

Stick Pattern

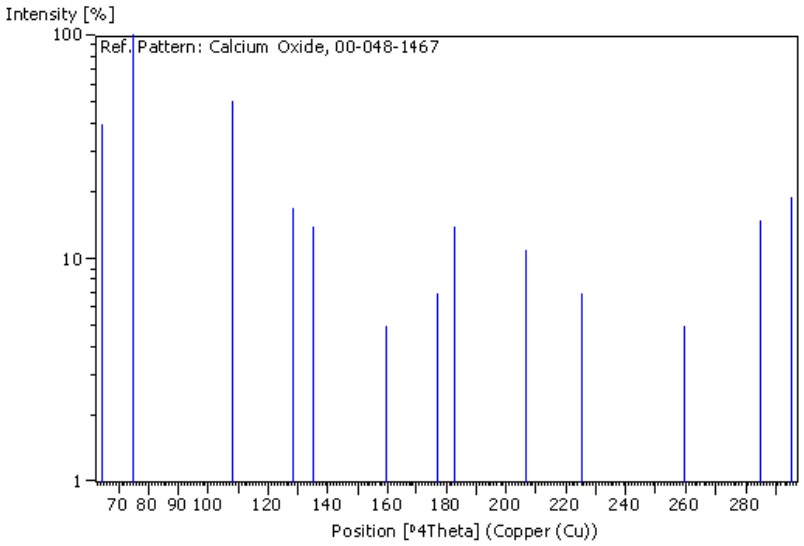

Figure C-5: JCPDS No. 48-1467 for CaO